Hidden Patterns of Ray-Finned Fish Evolution: Bridging Paleontology and Neuroanatomy

by

Rodrigo Tinoco Figueroa

A dissertation submitted in partial fulfillment
of the requirements for the degree of
Doctor of Philosophy
(Earth and Environmental Sciences)
in the University of Michigan
2024

Doctoral Committee:

Professor Matt Friedman, Chair
Emeritus Professor Daniel Fisher
Associate Professor Hernán López-Fernández
Professor Jeffrey Wilson Mantilla
Associate Professor Selena Smith

Rodrigo T. Figueroa

rtfiguer@umich.edu

ORCID iD: 0000-0001-9862-904X

Dedication

I dedicate this dissertation to the beauty of human curiosity and the desire to grasp the natural world and all its wonders.

"E uma das condições necessárias a pensar certo é não estarmos demasiado certos de nossas certezas"

-Paulo Freire, 1996

Acknowledgements

This dissertation was funded by the Department of Earth and Environmental Sciences of the University of Michigan, the Scott Turner Student Research Grant Award, the University of Michigan Rackham Graduate School Predoctoral Fellowship, the Society of Systematic Biologists Graduate Student Research Award the Center for Latin American and Caribbean Studies Tinker Field Work Grant, the National Science Foundation and the European Synchrotron Radiation Facility.

I would like to thank the numerous institutions, museum curators and collection managers that kindly ceded specimens or permitted my visit to their collection throughout this PhD. These include the Centro Paleontologico da Universidade do Contestado (CENPALEO), Museu de Ciências da Terra (MCT/CPRM), The University of Michigan Museum of Paleontology (UMMP), the University of Michigan Museum of Zoology (UMMZ), the New Mexico Museum of Natural History and Science (NMMNHS), the University of Stockholm, the Melbourne Museum and the University of Louisville Department of Biology. I would like to especially thank the several curators and collection managers who made this research possible, including Luiz Carlos Weinschutz (CENPALEO), Rafael Costa da Silva (MCT), Randall Singer (UMMZ), Hernán López-Fernández (UMMZ), Adam Routney (UMMP), Matt Friedman (UMMP).

None of the field work associated with my PhD would have been possible without the collaboration of local researchers, geologists and field assistants involved in research across the Paraná and Parnaíba basins in Brazil. It would be impossible to name everyone that played a role and helped me during field work but there are several I would like to extend a special thank you. Juan Carlos Cisneros, Luiz Carlos Weinschütz, Artur, Seu Vilson (and his 'kombi'), João Ricetti, Ethan Shirley, Kenneth Angielczyk, Jorg Frobisch, Jason Pardo, Selena Martinez, Roger Smith, Maria Eduarda Elesbão, and Amanda Atenas.

I am not sure I would have made it this far without the comments, advice and several meetings I had with my dissertation committee: Hernán López-Fernández, Jeff Wilson, Dan Fisher and Selena Smith. Your comments and suggestions were paramount for my dissertation and my development as a researcher throughout the past five years.

I would like to thank several researchers that have participated in my development as a researcher in the past couple of years and some who even became good friends. I am grateful to have worked with you and hope to keep on collaborating with all of you. Sam Giles and Matt Kolmann, thank you for all the great exchanges and all the fish talks the past couple of years!

Matt, I am very thankful for working with you and learning so much from you these past 10 years since we started discussing my shark fin spines fragments from the Devonian of Brazil all the way to now. We have been through a lot, good memories, some drama, travels, conferences, French tacos, caipirinhas… I would never have reached this point if it wasn't for your support both as an advisor and as a friend. I am certain there is still a lot we will go through as friends and fish nerds in the upcoming years. Thank you so much!

Eu preciso agradecer também a todos meus amigos no Brasil, que mesmo tão distantes fisicamente sempre estão ao meu lado. As vezes as longas distâncias atrapalham um pouco, mas sempre demos um jeito. Meus grandes amigos que a UniRio me deu, Beatriz Marinho Hormanseder, Helena Machado e Renato da Hora Loureiro. Também queria agradecer ao Igor Lourenço Lopes, que mesmo não estando mais conosco a tanto tempo, ainda me inspira a seguir meus sonhos dia após dia. Muitos outros amigos também foram importantíssimos para mim nesses últimos anos, nem que seja só por suportarem minhas reclamações sobre os EUA e Ann Arbor. Dentre esses, não poderia deixar de agradecer a Mariana Brasil, que desde o ensino médio (tirando a época que "me mudei pra Austrália") está sempre ao meu lado. Muito obrigado a todos vocês e por favor nunca desapareçam da minha vida!

Também preciso agradecer a todos os Brasileiros que me acolheram aqui em Michigan e me deram um gostinho especial desse lugar tão distante de casa. Em especial Matheus, Thiago e Natalia. Sem vocês esses últimos dois anos de doutorado teriam me endoidado de vez!

As it became tradition for me, I like to acknowledge local shops and bars that provided good food, drinks and memories throughout my career, so I must acknowledge a few of the Ann Arbor restaurants and bars. Hop Cat has a special place for me as it not only was the first bar I went to after starting my PhD but also has been the most present throughout these years. Many good (and bad) memories. In fact, many of the words of this dissertation were written and many of the figures were planned during the happy hour. I also need to thank Frita Batidos for being the only place in Ann Arbor to offer good caipirinhas and where people pronounce my name correctly. I would like to thank Pizza House for providing excellent cups for scanning fossil and extant fishes. Although not local, I must acknowledge Culver's for the many value baskets consumed before and after work in the field or at RMC.

These past five years were definitely messy, and they would have been much more if it wasn't for the company and understanding of the friends I have lived with in both 'paleohouse' and 'geohut'. Who would have known that moving in with paleo colleagues, Alessio Capobianco, James Salisbury, Kierstin Rosenbach and Kelly Matsunaga, I briefly met the year prior would be the best decision I took during this PhD? I cannot imagine how I would have survived pandemic time away from my family and country without the company of some of you. From sharing the frustrations of grad school to sharing beers on the porch in front of the police station, my first years living in Ann Arbor were only bearable because of all of you. Of course I also have to add here my good friend Aaron Kurt who I am very thankful to have met while living at the 'paleohouse'. Then comes 'geohut' and the tumultuous final years of graduate school. Mike Machesky, Jeronimo Moralez Toledo, Cecilia Howard and Tessa Casselman, I also think we had a great time, and I am happy to have so many memories with all of you and of course Uhura Howard and Minerva Casselman. So yeah, for all of you that had to live with me these past years, thank you so much for putting up with me and for being my friends and guides through foreign lands.

I also must thank the many close friends that I made during this PhD journey and who shared the office space with me, unfortunately for all of you. Ethan Shirley, James Andrews, Hadeel Saad, Sanaa El Sayed, Lindsey DeHaan, Tariq Abdul Karem, Ted/Teddy/Theodore

Matel, Rafael Rivero-Vega, Fabian Hardy, Brielle Canares and Lynnea Jackson. I know I bothered all of you a lot these past years and at times made you lose your focus on work, but I hope it wasn't too much or too annoying, just a little bit. Thank you for being there with me, never punching me in the face, and more than that, thank you for helping me go through this dissertation. Hope we all keep in touch even after I leave Ann Arbor and looking forward to bumping into you and bothering you elsewhere. Please don't work too much and keep the chaotic vibe of the office after I leave! Cheers!

I cannot name everyone in the department, there are too many of you, but I wanted to make sure all of you feel acknowledged here. From those of you I had classes with, taught with or just had beers with. This department was very good for me and has taught me a lot personally and professionally. Hopefully I also retributed this somehow and left a positive impact.

Quem diria que eu conheceria uma pessoa tão especial por simples acaso durante uma viagem de campo com o departamento! Elis Maria Gomes Santana, você se tornou um dos pilares mais fortes da minha vida e eu só tenho a agradecer pela sorte de te ter em minha vida desde o ano passado. Tão pouco tempo juntos, mas já temos tantas histórias e tantas memórias que eu guardo com muito amor no fundo do meu coração. Obrigado por ser uma luz em minha vida e me fazer lembrar que o amor vale a pena e que a vida é muito mais legal quando é compartilhada com alguém especial. Tenho muito orgulho de você e mal posso esperar para ver o que ainda vamos viver juntos!

Mi querida familia en Costa Rica, tengo mucho que agradecer por todo el amor y apoyo que ustedes tan amablemente pusieron en mí. Yo jamás me tornaría la persona que soy hoy si no fuera por ser parte de la Familia Figueroa. La curiosidad y la pasión por la naturaleza que todos ustedes tienes fue la semilla que planto en mi corazón el deseo de estudiar la naturaleza. Los paseos por el patio en Esparza, los campamentos abajo de los almendros y el arbolito de Tambor, las gran remadas por los manglares de Mata de Limón y Tivives, las pescas de plateadas y búsqueda de fósiles en el Rio Esparza. Si hoy puedo decir que soy un paleontólogo es por todo lo que ustedes me enseñaron sobre amar y buscar conocer la naturaleza. También tengo que agradecer por nombre a muchos de ustedes, Pacho, Federico, Álvaro, Vicky, Mario, abuela

Maria, Mario, Adolfo, Dalia, Manuela, tío Chalo, Alvarito, José Aníbal, Arturo, Vanessa, Thelmita, Felipito. En especial, tengo que agradecer con todo mi corazón a mi tía Estrella por ser la persona con el corazón más grande que he visto en toda mi vida. Que cuido de mi cuando era chiquito, cuido de abuela por tantos años y ahora que amablemente cuida de mi papá. ¡Muchas gracias por todo mi tía, te amo mucho!

Dida e Douglas, vocês são muito especiais para mim. Sei que convivemos muito pouco desde que me mudei para os EUA mas vocês seguem sempre em um lugar especial em meu coração. Muito obrigado por serem sempre tão bons comigo e tão companheiros nos momentos bons e nos ruins também. Tenho muita sorte em ter vocês na minha família e no meu coração.

Pai, eu não sei nem como te agradecer. Sei que você não vai poder ler essa mensagem, mas espero que de alguma forma você se sinta muito amado e agradecido por mim. Desde que eu era pequeno você sempre me apoiou e me influenciou a amar fósseis a natureza e o mar. Tantas memórias brincando com meus bichinhos de plástico, você me ensinando a mergulhar e a pescar, te ver assistindo Star Trek até pegar no sono, e por aí vai... Tivemos muitos momentos altos e baixos e sinto muita saudade de conversar com você. Eu te amo muito e obrigado por tudo.

Mãe, eu tenho muita sorte em ter você como mãe e como amiga. Sei que muitas vezes quando eu era pequeno eu não entendia muito do que você fazia por mim, mas hoje eu só tenho a agradecer por você ter me ajudado a ser a pessoa que eu sou hoje. Não só como cientista e pessoa persistente, mas também como alguém que sabe o que quer e faz o possível para alcançar seus objetivos. Nunca vou me esquecer dos momentos que vivemos juntos, tanto os bons quanto os ruins, e tudo que aprendi contigo. Aprendi que mesmo entrando no lago pode ser apenas um pingo, aprendi que sempre posso ganhar de você em jogo de tabuleiro, e mais do que tudo aprendi contigo que a vida é cheia de altos e baixos, mas não vale a pena focar nos baixos. Me inspiro muito em você. Te amo.

Table of Contents

List of Tables

List of Figures

List of Appendices

Abstract

The fossil record of ray-finned fishes dates back to more than 400 million years and the clade is remarkably diverse in extant settings. However, there is still little understanding of the early evolution of the clade. The apparent lack of morphological disparity in Paleozoic forms has been challenging for a precise placement of early fossils within the ray-finned fish tree, both with respect to each other and to living groups. In this dissertation I expand on the knowledge of the evolution of ray-finned fishes based on poorly understood aspects of their morphological diversity, phylogeny and geographic distribution. Focus is given to describing important aspects of endocranial and soft tissue anatomy that can directly link fossil and living taxa in an ecomorphological and phylogenetic framework.

I first describe important new Paleozoic ray-finned fish taxa from poorly sampled high-latitude localities in the southern hemisphere in chapters 2 and 3. In these chapters I present in detail the anatomy of new taxa and discuss the implications of the observed morphologies for our understanding of early ray-finned fish evolution. Additionally, I discuss the importance of poorly explored axes of morphological diversity of stem ray-finned fishes, with emphasis on endocranial anatomy of Permo-Carboniferous taxa. By joining description of taxa from poorly known high-latitude localities with the description and comparison of hidden aspects of endocranial anatomy across early ray finned fishes, chapters 2 and 3 provide a starting point for future biogeographic and phylogenetic work on Paleozoic actinopteygians.

In Chapters 4 and 5 I provide a detailed account of soft tissue preservation in Paleozoic ray-finned fish fossils, with special emphasis on aspects of their neuroanatomy. This represents the first description of three-dimensional soft-tissue fossilization in Paleozoic ray-finned fishes and the oldest evidence of morphological disparity in vertebrate fossil brains. The results of these two chapters summarize important morphological variation in fossil brains and other associated soft tissues, providing a tentative reconstruction of the early evolution of the ray-finned fish brain.

In Chapter 6 I expand on the knowledge of morphological diversity of living ray-finned fish brains and endocasts through the application of diffusible iodine contrast enhanced micro-tomography (dice-CT) of more than 70 living ray-finned fish taxa. Through a new landmark scheme, volumetric comparisons and general description of morphological variation in living ray-finned fish brains I expand on the knowledge of ecomorphological diversity of the ray-finned fish brain, as well as providing a new morphological map for living ray-finned fish endocasts which can be directly compared to extinct counterparts.

With the results presented in this dissertation I expect to provide a new framework for future research on fossil and living ray-finned fishes where the description of endocranial and soft tissue anatomy of both fossil and living taxa will play a major role in drawing more robust assessments on the phylogenetic relationship of early ray-finned fishes as well as more accurate reconstructions of neuroanatomical evolution through time and space.

Chapter 1 Introduction

The study of ray-finned fish fossils has been a topic of interest for paleontologists since the early days of the field (Bemis 2016). Given the extensive nature of the ray-finned fish fossil record, it provides important information on evolutionary patterns across time and space as well as information regarding the effects of environmental change on vertebrate faunas (Friedman and Sallan 2012; Friedman 2022). However, despite the ample work on ray-finned fish paleontology there are still many questions that remains unanswered due to gaps in the sampling or poor understanding of phylogenetic relationships of fossil taxa, especially within the late Paleozoic (~359–251 Mya). Exploring these gaps in knowledge is a fundamental next step towards a better understanding of the evolutionary history of fishes. In the following sections I will explore some of these knowledge gaps and describe sampling and descriptive strategies to study extinct and extant ray-finned fishes.

1.1 The obscure record of high-latitude Paleozoic vertebrates

There were important diversification events for several vertebrate lineages during the Paleozoic. Not only related to the emergence of gnathostome anatomical innovations—such as jaws and pelvic fins (Coates 2003; Anderson et al. 2011; Zhu et al. 2012a; Mansuit et al. 2021; Jones et al. 2023)—but also key diversification events (Wen-Jin and Min 2007; Friedman and Sallan 2012; Sallan 2014; Friedman 2015; Henderson et al. 2022b; Giles et al. 2023) and the rise of all major lineages of crown gnathostomes (Friedman and Sallan 2012; Brazeau and Friedman 2015). However, our knowledge of fish faunas from the Paleozoic is virtually restricted to localities in North America, Europe and Asia (Janvier and Maisey 2010; Figueroa and Machado 2018; Henderson et al. 2022a). The record of fossil fishes in South America and Africa are mostly understudied and represent an almost insignificant portion of sampled taxa worldwide (Henderson et al. 2022a). As paleogeographic reconstructions indicate, most of North America, Eurasia and Australia were concentrated at the paleotropical latitudes (Hinsbergen et al. 2015),

raising questions on how well the early evolutionary history of fishes can be reconstructed given this biased sampling.

The Early and Middle Devonian invertebrate faunas from southern South America appear highly distinct from those from eastern Gondwana, Euramerica and Siberia (Melo 1988; Boucot et al. 2001). This unique invertebrate fauna in shallow marine deposits from southern South America defines biogeographic region, the Malvinokaffric or Malvinoxhosan Realm (Boucot et al. 1969; Boucot 1988; Penn-Clarke 2019; Penn-Clarke and Harper 2023). Malvinoxhosan assemblages predominate high-latitude localities within Gondwana up to the late Middle Devonian when marine transgressions and immigration of taxa from Euramerican faunas started to merge with the taxonomic composition of Malvinoxhosan faunas (Melo 1988; Sanchez et al. 1991; Boucot et al. 2001; Bosetti et al. 2012; Horodyski et al. 2014; Penn-Clarke and Harper 2023). However, despite our good understanding of faunal composition and turnover for invertebrates, we still lack a comprehensive understanding of coeval vertebrate faunas (Janvier 2007; Figueroa and Machado 2017, 2018; Figueroa et al. 2021). This is likely due to the fragmentary nature of most vertebrate occurrences from the Devonian of South America and Africa—especially prior to the Late Devonian (Anderson et al. 1999; Murray 2000; Figueroa and Machado 2018), with a few exceptions (Janvier and Suárez-Riglos 1986). Nevertheless, these uncommon fossils indicate that, as with invertebrates, the taxonomic composition of vertebrate assemblages within the Malvinoxhosan realm differs from that of paleotropical localities. This is evidenced by a predominance of chondrichthyans to the detriment of placoderms and osteichthyans at these high paleolatitudes (Janvier 2007; Figueroa and Machado 2017, 2018). This differs from Late Devonian faunas from northern South America (in Colombia, Venezuela, and northern Brazil) where taxonomic composition is much similar to that of Middle-Late Devonian localities from paleotropical localities (Janvier and Melo 1987; Janvier and Villarroel 2000; Young and Moody 2003; Janvier 2007; Rezende et al. 2021). Additional evidence of the uniqueness of circumpolar vertebrate faunas in the Devonian comes from endemic and anatomically distinctive taxa such as the stem chondrichthyans †*Pucapampella rodrigae*, the enigmatic †*Ramirosuarezia boliviana* (Janvier and Suárez-Riglos 1986; Pradel et al. 2009a) and the predatory ray-finned fish †*Austelliscus ferox* (see Chapter 2; Figueroa et al. (2021)).

Major glaciation events in the southern hemisphere throughout most of the Carboniferous severely impacted depositional rates and faunal composition at high latitudes (Caputo 1985;

Eyles et al. 1993; Cagliari et al. 2016; Fallgatter and Paim 2019; Rosa et al. 2019; Mouro et al. 2020). Thus, most of the Carboniferous vertebrate record in South America and Africa is restricted to the latest Carboniferous or to fragmentary and microvertebrate remains at lower paleolatitudes (Murray 2000; Figueroa and Machado 2018). Some of these microvertebrate remains from the Pennsylvanian Itaituba Formation in northern Brazil highlight South American connections to Euramerican faunas (Duffin et al. 1996; Richter et al. 1999; Moutinho et al. 2016; Figueroa and Machado 2018). Better-preserved and articulated fishes are found in interglacial deposits of southern South America with putative latest Carboniferous-early Permian age such as the San Gregorio Formation in Uruguay and the Campo Mourão Formation in Brazil (Mones 1986; Cione et al. 2010; Mouro et al. 2020; Saldanha et al. 2022). Currently described ray-finned fishes from these deposits show similar morphology to other Carboniferous faunas from North America and Europe, but a precise phylogenetic placement for these fossils is not possible given the lack of endocranial remains (e.g. neurocranium, hyobranchial apparatus and vertebral column) for most named taxa. Similar material is also known from South Africa in the lower Carboniferous Witteberg Series as well as the Beaufort Group going into the Permian (Gardiner 1962; Bender 1999; Evans 1999; Murray 2000).

There are several vertebrate-rich Permian localities spread across South America, but mostly within Brazil and Bolivia (Janvier 1992; Figueroa and Gallo 2017; Figueroa and Machado 2018). Sparse vertebrate remains are known from the Permian of Argentina (Cione et al. 2010), Chile (Richter and Breitkreuz 1997), and Uruguay (Mones 1986). In Brazil, both Paraná and Parnaíba basins contain rich vertebrate-bearing deposits, with fish remains being well-known in the middle–late Permian Passa Dois group of the Paraná Basin (Dunkle and Schaeffer 1956; Vega-Dias et al. 2000; Richter 2002, 2007; Figueiredo and Carvalho 2004; Toledo and Bertini 2005; Mutter and Richter 2007; Dias 2012; Chahud and Petri 2013; Figueroa et al. 2017) and the early Permian Pedra de Fogo Formation for the Parnaíba Basin (Cox and Hutchinson 1991; Alves 2010; Figueroa and Gallo 2017; Figueroa and Machado 2018; Figueroa et al. 2019; Richter et al. 2022). In Bolivia fish remains are known mostly from the early Permian Copacabana Formation (Janvier 1992; Figueroa and Machado 2018). It is interesting to note that by the Permian there are already well-established faunal connections between South America and Africa and between South America and North America, based on vertebrate material (Cisneros et al. 2015; Rodrigues et al. 2023). While these connections and faunal

comparisons are easily done with chondrichthyan material, the poor understanding of Permian ray-finned fishes from South America does not allow for in-depth comparisons. Morphological diversity is clearly present—evidenced by deep-bodied forms (e.g. †*Paranaichthys*; Dias (2012)), large piscivorous taxa (e.g. †*Brazilichthys*; Cox and Hutchinson (1991)) and more generalized early actinopterygians (e.g. †*Roslerichthys*; Figueiredo and Carvalho (2004))—but the poor sampling of Permian fish localities in South America remains a challenge for both taxonomic and biogeographic studies.

1.2 The early evolutionary history of ray-finned fishes

Ray-finned fishes are the most diverse lineage of vertebrates in contemporary aquatic settings, with a long phylogenetic history (Nelson et al. 2016). Estimates point to a Silurian (~443.8–419.2 Ma) divergence between ray-finned fishes and lobe-finned fishes, but the oldest unequivocal ray-finned fish fossils are Early Devonian in age (Friedman 2015; Lu et al. 2016; Figueroa et al. 2021). Early in their evolutionary history ray-finned fishes were seemingly morphologically conservative and species-poor, but by the early Carboniferous (~346 Ma) there is already evidence of increase in morphological diversity, which seems to have, at least partially, emerged before the end-Devonian mass extinction (Henderson et al. 2022b; Giles et al. 2023). Despite this forementioned diversity, the phylogenetic position of many late Paleozoic taxa is still poorly supported and the relationship of many Paleozoic clades to the actinopterygian crown remains uncertain. Despite the established Paleozoic origin of crown ray-finned fishes, the affinities of late Paleozoic taxa to the crown are still poorly established (Giles et al. 2017). Thus, there are long ghost lineages leading to crown ray-finned fish diversity, which hinders interpretations of diversification patterns and rates of evolution within this group. In the following section I describe early ray-finned fish diversity and phylogenetic placement based on the available literature.

1.2.1 The first ray-finned fishes

The Devonian marks the appearance of the first definitive ray-finned fish fossils (Friedman 2015), although Silurian taxa have occasionally been interpreted as stem ray-finned

fishes (Schultze and Cumbaa 2001; Schultze 2016). This paucity of Early Devonian ray-finned fishes contrasts with the abundant lobe-finned fish record during the same interval (Brazeau and Friedman 2015; Friedman 2015; Lu et al. 2016). †*Meemannia eos*, remains the only unequivocal ray-finned fish known from the Early Devonian (Lu et al. 2016), although it was originally interpreted as a stem sarcopterygian (Zhu et al. 2010). Other taxa of disputed affinities such as †*Dialipina* and †*Ligulalepis* are generally recovered in the osteichthyan stem in more recent analyses (Davis et al. 2012; Giles et al. 2015a; Friedman 2015; Lu et al. 2016; Figueroa et al. 2019; Giles et al. 2023). Towards the Middle Devonian ray-finned fishes become more common and widely distributed, but articulated, and especially three-dimensional remains are still rare (Friedman 2015; Figueroa et al. 2021; Giles et al. 2023). Middle and Late Devonian forms such as †*Howqualepis*, †*Moythomasia*, and †*Mimipiscis* tend to be recovered as a monophyletic group of 'Devonian forms' whereas †*Meemannia* and †*Cheirolepis* form a grade stemward to these 'Devonian forms' (Giles et al. 2015b, 2017; Figueroa et al. 2019; Stack and Gottfried 2021; Giles et al. 2023). Late Devonian taxa such as †*Tegeolepis* are occasionally recovered crownward of other Devonian taxa (see Chapter 2; Figueroa et al. (2021)).

The phylogenetic relationship of early ray-finned fishes of Devonian age is poorly understood, not only due to the scarcity of their fossil record but also given the lack of well-described three-dimensional fossils showing both endoskeletal and dermal anatomy in detail. A few exceptions—and thus the models of our understanding of Devonian actinopterygian morphologies—include the classical monograph on †*Mimipiscis* and †*Moythomasia* (Gardiner 1984) and more recently described taxa (e.g. †*Raynerius splendens*, †*Palaeoneiros clackorum*) made possible by the advancement of micro-computed tomography (Giles et al. 2015b, 2023). The inclusion of these well-preserved taxa and new endocranial characters have provided better support for phylogenetic resolution of stem actinopterygians (Giles et al. 2023). Nevertheless, questions remain on how many ray-finned fish lineages diversified during the Devonian and how many survived the end-Devonian mass extinction (Figueroa et al. 2021; Giles et al. 2023).

1.2.2 The Permo-Carboniferous: a cryptic diversification of ray-finned fishes

The Permo-Carboniferous represents an important interval in ray-finned fish evolutionary history. It is during this interval that actinopterygians start to display new body-shapes and

diverse feeding adaptations (Friedman 2015). Part of the success of ray-finned fishes in post-Devonian settings might be related to empty niches left by placoderms and many sarcopterygians that disappeared after the end-Devonian mass extinction (Sallan and Coates 2010; Friedman and Sallan 2012; Henderson et al. 2022b). By the Pennsylvanian, ray-finned fishes already represent a major component of aquatic vertebrate biotas not only in terms of number of species—or fossil occurrences—but also in terms of ecomorphological diversity (Friedman 2015; Friedman et al. 2018; Figueroa and Andrews 2022; Henderson et al. 2022b). Ray-finned fishes are rivaled by chondrichthyans, which also experienced an expansion of ecomorphological diversity through the Carboniferous (Friedman and Sallan 2012). Nevertheless, this diversity remains little explored. Consequently, the phylogenetic relationships of late Paleozoic ray-finned fishes remain weakly supported and numerous competing hypotheses have been made (Watson 1925; Rayner 1952; Gardiner and Schaeffer 1989; Poplin and Véran 1996; Coates 1998; Friedman and Blom 2006; Sallan 2014; Giles et al. 2015b; Lu et al. 2016; Giles et al. 2017; Wilson et al. 2018; Figueroa et al. 2019; Stack and Gottfried 2021; Caron et al. 2023; Giles et al. 2023).

Part of the issue underlying the phylogenetic relationships of late Paleozoic ray-finned fishes comes from the lack of endocranial data for most of known taxonomic diversity. With the exception of a handful of well-preserved three-dimensional specimens most of the Paleozoic actinopterygian record is composed of flattened specimens (Cloutier and Arratia 2004; Mickle 2012; Friedman 2015, 2022; Henderson et al. 2022b). Because of this preservation pattern, current morphological phylogenetic matrices remain highly biased towards characters from the external dermal skull, squamation and body shape, which can be easily observed in the majority of specimens but have recently been shown to have little phylogenetic value at a broad scale (Friedman 2015; Giles et al. 2017, 2023). Some features of the endoskeleton such as braincase ossifications and branchial elements are more readily comparable across a broad set of taxa, and thus might provide better phylogenetic constraints. In recent years tomographic data from a handful of specimens have shed light on some outstanding hypotheses on early ray-finned fish phylogenetics (Giles and Friedman 2014; Giles et al. 2015b, 2017, 2018; Figueroa et al. 2019; Argyriou et al. 2022; Giles et al. 2023). However, these do not suffice for a sample capable of stabilizing the placement of rogue taxa—and lineages—which have historically been problematic (Gardiner 1967, 1984; Patterson 1982; Coates 1998; Cloutier and Arratia 2004; Gardiner et al. 2005; Sallan 2014).

Throughout the late Paleozoic, several ray-finned fish morphotypes can be recognized and many of these have been proposed as taxonomic groups. A few common putative families include Rhadinichthydae, Elonichthyidae, Acrolepidae, Haplolepidae, Platysomidae, among others (Schaeffer 1956; Gardiner and Schaeffer 1989; Gardiner et al. 2005; Figueiredo and Gallo da Silva 2006). Problems arise as, given the limited systematic assessment of most of these families, taxa are allocated to groups based on common features (e.g. large fangs, blunt snout, oblique suspensoium). Thus, many of these classical early ray-finned fish families need in-depth reviews to assess not only their validity but also their relationship to other groups of early actinopterygians and to the actinopterygian crown. Recent work has demonstrated hidden aspects of early ray-finned fish morphological (and functional) diversity which could help shed light on the interrelationships of early ray-finned fishes (Friedman et al. 2018; Figueroa and Andrews 2022).

Molecular analyses reconstruct the origin of crown ray-finned fishes well within the late Paleozoic (Near et al. 2012; Betancur-R et al. 2013; Near and Thacker 2024), but this does not directly reflect the composition of late Paleozoic ray-finned fish faunas. Although a handful of Paleozoic taxa have been consistently recovered as being close to or within the ray-finned fish crown (Friedman 2015; Giles et al. 2018; Wilson et al. 2018; Argyriou et al. 2022; Caron et al. 2023), it is during the Triassic that undisputed crown ray-finned fishes become prominent. This apparent lack of crown ray-finned fishes in the Paleozoic is likely a phylogenetic issue rather than sampling, given the plasticity of phylogenetic hypotheses for stem ray-finned fishes. Thus, a better understanding of the internal anatomy of established taxa might be the key for building a more robust phylogenetic framework for early ray-finned fishes. Exceptional fossils, such as those showing anatomical details of soft-tissue anatomy might reveal hidden aspects of morphological diversity and phylogenetic relationships for this hyper-diverse clade.

1.3 Soft-tissue preservation in the fossil record

1.3.1 What is really missing from fossils?

The vast majority of fossilized remains consist of hard parts such as shells, carapaces, teeth, and bones (Clements and Gabbott 2022). However, under the correct pre- and post-

diagenetic settings in some rare cases it is possible to preserve tissues (or facsimiles thereof) that would otherwise be lost during pre-burial decay or during diagenesis (Allison and Briggs 1993; Martin 1999; Parry et al. 2018; Clements and Gabbott 2022). These unique fossils, generally associated with fossil *Konservat-Lagerstätte*, provide novel information regarding obscure parts of the fossil record, such as the evolution of soft-bodied organisms or variation in organ morphology, pigmentation and behavior (Aldridge and Theron 1993; Lindgren et al. 2012, 2013; Ma et al. 2012; Cunningham et al. 2014; Parry et al. 2018; Klug et al. 2021; Clements and Gabbott 2022; Wang et al. 2022). Soft-tissue preservation can be used to draw a better picture of past biotas and environments, which would be impossible to reach with hard parts alone (Parry et al. 2018; Clements and Gabbott 2022). Through the Phanerozoic there are multiple examples of fossil *Lagerstätte* with varying types of soft-tissue preservation for both invertebrates and vertebrates (Allison and Briggs 1993). Nevertheless, the rarity of some of these remains still pose a challenge to a more holistic interpretation of the available soft-tissue evidence (Allison and Briggs 1993; Clements and Gabbott 2022).

For fishes, there are several unique localities that yield numerous types of soft-tissue preservation of different elements of the body, including: eyes, skin, pigmentation, muscles, heart, brain and other internal organs (Alvarado-Ortega et al. 2007; Maldanis et al. 2016; Osés et al. 2017; Frey et al. 2020; Rossi et al. 2022; Trinajstic et al. 2022b). Although the fossil record of fishes is geographically widespread, there are only around 57 Phanerozoic localities that have been reported to bear some degree of soft-tissue preservation (Fig. 1.1; Appendix A) and many of these still lack appropriate studies on the taphonomic processes involved. In terms of lithology, it seems that exceptional preservation in two dimensions is more common in limestone deposits whereas three-dimensional preservation is more common in concretions (McCoy 2014; Saleh et al. 2023), generally of sideritic composition.

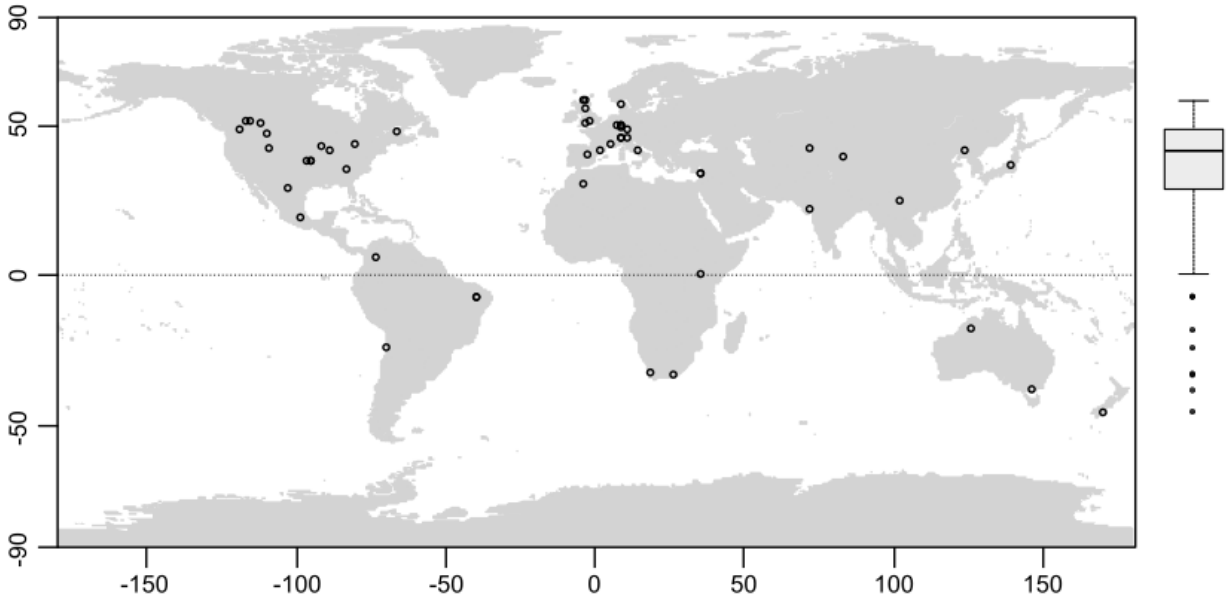

Figure 0.1 – Geographic distribution of soft-tissue preservation in the fish fossil record. Boxplot on the right side of the map summarizes the latitudinal diversity, highlighting the lack of localities in the southern hemisphere.

1.3.2 Exceptional fossils

Soft-tissue preservation in the fossil record goes much beyond mere oddities, as they provide information on extinct organisms pertaining to their anatomy, physiology and behavior (Clements and Gabbott 2022). However, despite the enormous potential of exceptionally preserved fossils, accurate interpretation of these remains depends on a range of disciplines from taphonomy to comparative anatomy. It is not unusual that interpretations of soft tissues in the fossil record become disputed. For example, nervous tissues in flattened Cambrian arthropods have been proposed to be biased by bacterial activity (Liu et al. 2018). Other examples include interpretations of pigment cells (Lindgren et al. 2012; Slater et al. 2020) and systematic analysis of soft-bodied chordates (Sansom et al. 2011). Thus, it is paramount to pay attention to depositional settings and diagenetic processes involved in the fossilization of these exceptional fossils to minimize the risk of misinterpretation.

Three-dimensional soft-tissue preservation is still poorly known in the fossil record, with only a handful of examples. In fishes, there are examples of cardiovascular tissue in the Cretaceous pachyrhizodontid †*Rhacolepis buccalis* (Maldanis et al. 2016), multiple internal organs of an arthrodire placoderm and the symmoriform chondrichthyan †*Ferromirum* (Frey et

al. 2020; Trinajstic et al. 2022b) and nervous tissue of the iniopterygian †*Iniopera* and the stem ray-finned fish †*Coccocephalus* (Pradel et al (2009b), Figueroa et al (2023); Chapters 4-5). Given the rarity of three-dimensional fossil soft tissue preservation in vertebrates, the processes responsible are still poorly understood. Hypotheses on the modes of preservation of these tissues tend to be related to an anoxic microenvironment forming around—or within—the carcass after burial (Figueroa et al. 2023; Muscente et al. 2023; Saleh et al. 2023). Isolated taphonomic experiments with vertebrate carcasses have given support for these hypotheses, but observed variation in soft-tissue preservation between and within strata and units is still not adequately explained. In the following chapters (Chapter 4-5; Appendices D-E) I will briefly hypothesize on different pathways for three-dimensional soft tissue preservation in fishes, with an emphasis on nervous tissues within the neurocranium.

1.4 The brain of ray-finned fishes

Ray-finned fishes comprise roughly half of living vertebrate diversity (Nelson et al. 2016) and occupy a myriad of environments performing complex and intricate behaviors as vast as those of their sarcopterygian counterparts (including tetrapods). Given that the brain is responsible for controlling major aspects of vertebrate function, from movement of the body to social interactions and internal organ function, it is particularly important to understand patterns of brain morphological variation across this hyperdiverse group. Nevertheless, detailed knowledge on ray-finned fish neuroanatomy is restricted to a handful of taxa (e.g. zebrafishes, salmonids, cyprinids, mormyrids), which does not represent the morphological and ecological disparity of the group. Ray-finned fishes provide a unique model for understanding pathways to phenotypic plasticity, morphological and ecological diversity from neuroanatomy (Hall and Tropepe 2020). By comparing neuroanatomical adaptations of ray-finned fishes to tetrapods we might be able to better understand if vertebrates adopt similar neuroanatomical adaptations to perform similar functions or if similar function can be achieved with distinct neuroanatomical adaptations in closely related vertebrate lineages.

1.4.1 The unique brain of ray-finned fishes

The long evolutionary history of ray-finned fishes, coupled with their hyperdiverse crown, results in a wide range of morphological variation between major ray-finned fish lineages: Cladistia, Chondrostei, Holostei, and Teleostei (Nieuwenhuys 1982; Nieuwenhuys et al. 1998). The most well-known unique neuroanatomical feature of ray-finned fishes is the presence of the so-called 'everted' telencephalon. The telencephalic pallial cell masses found medially in other vertebrates seem to be lateral and exposed to the surface in ray-finned fishes (Nieuwenhuys 2009), leading to the hypothesis that in this group the development of the telencephalon from the embryonic prosencephalon occurs in a unique manner: instead of bulging to form a central cavity (telencephalic ventricle) it would evert its medial layers to the outside, similar to the opening of a flower (Braford 2009; Nieuwenhuys 2009). More recent work has pointed out a much more complex eversion process, based on studies of the zebrafish dorsomedial pallial amygdala and telencephalic tela choroidea (Mueller 2022). Indeed, a better understanding of the development of the tela choroidea (and choroid plexus) of vertebrates might be key for understanding the process of telencephalic eversion in ray-finned fishes.

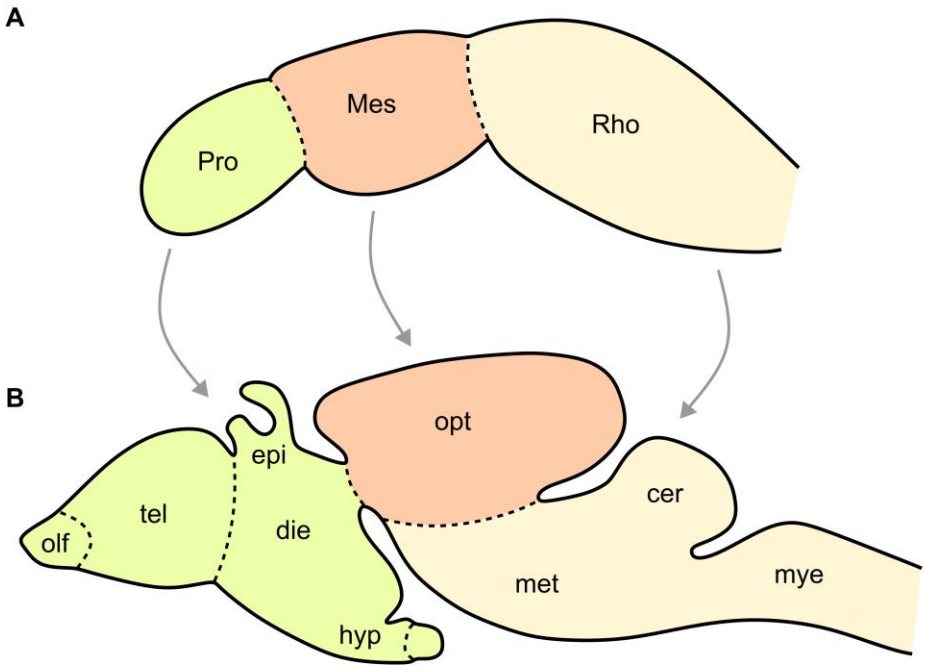

Figure 0.2 – Schematic representation of brain and development of main brain regions from an embryo (A) to a juvenile (B) hypothesized vertebrate. cer, cerebellum, die, diencephalon, epi, epiphysis, hyp, hypophysis, Mes, mesencephalon, met, metencephalon, mye, myelencephalon, olf, olfactory bulb, opt, optic tectum, Pro, prosencephalon, Rho, rhombencephalon, tel, telencephalon.

The diencephalon of ray-finned fishes is positioned between the telencephalon anterodorsally and the optic tectum posteriorly. According to Braford (2008) the diencephalon of ray-finned fishes can be divided into three thalamic subdivisions: the dorsal thalamus, ventral thalamus and a posterior tubercular thalamus. The actinopterygian diencephalon strongly differs in structure from that of other vertebrates in bearing numerous adaptations, such as a preglomerular complex and hypothalamic inferior lobes (Schmidt 2020; Ishikawa et al. 2022). Within the diencephalon, maybe the most notable structure is the hypothalamus, of which there are three regions, the periventricular area, the tuberal lobes, and the inferior lobes. There is visible variation in the morphology of the hypothalamus across ray-finned fishes, but it remains poorly described in the literature (Schmidt 2020). For example, the hypothalamus inferior lobes are absent in cladistians (e.g. *Polypterus*) but present in all other living ray-finned fishes, with indications it would be independent from the inferior lobes of chondrichthyans (Schmidt 2020). The epithalamus of teleosts can be divided into habenular nuclei, epiphysis and saccus dorsalis, with the function of the habenula being still obscure (Meek and Nieuwenhuys 1998) and the epiphysis being

primordially associated with photoreception (Hoffman 1970; Meek and Nieuwenhuys 1998). A few teleosts exhibit a corpuscular structure anteroventral to the habenular nuclei, the nucleus rostralis, which seems to be associated to the epithalamus and associated with visual input processing (Saidel and Butler 1997; Saidel 2013). The epiphyseal complex is a plastic structure within vertebrates (Hoffman 1970), but there is little literature on the morphological variation within ray-finned fishes.

The rhombencephalon is the most complex and interconnected part of the vertebrate brain, bearing the origin for most of the cranial nerves and communicating the rostral portion of the brain to the spinal cord (Butler and Hodos 1996; Nieuwenhuys et al. 1998). From the undifferentiated rhombencephalon two main regions form, the metencephalon and the myelencephalon, respectively. The metencephalon gives rise to the cerebellum and associated structures, while the myelencephalon roughly corresponds to the medulla oblongata (Butler and Hodos 1996). Given the complexity of this major brain region, it is beyond the scope to list all subdivisions and the complex functions executed by the rhombencephalon. Rather, the focus will be on describing important morphological variation of these structures across ray-finned fishes.

The cerebellum is a highly complex structure of the vertebrate brain, both in morphological and functional aspects, representing a major axis of morphological variation among vertebrates (Butler and Hodos 1996; Nieuwenhuys et al. 1998; Murakami and Sugahara 2021; Ikenaga et al. 2022). The cerebellum performs a variety of functions, generally associated with integrating and coordinating sensory and motor input from different regions of the nervous system (Butler and Hodos 1996). Among the principal inferred functions of the cerebellum are balancing, coordination, and smoothing of motor activity (Butler and Hodos 1996). In ray-finned fishes however, there are a variety of morphofunctional adaptations of the cerebellum and other rhombencephalic regions. Ray-finned fishes exhibit a variety of cerebellar-like structures that seem to be highly connected to the cerebellum, such as the torus longitudinalis, the crista cerebellaris and the electrosensing lateral line lobe (Butler and Hodos 1996; Nieuwenhuys et al. 1998; Murakami and Sugahara 2021; Ikenaga et al. 2022). The best known is the electrosensory adaptations of mormyrids and gymnotiforms associated with hypertrophy of the cerebellar-like structures and well-developed electroreceptive lateral line lobes (Butler and Hodos 1996; Bell et al. 2008; Meek et al. 2008). In many of these fishes, the cerebellum represents most of the volume of the brain, overlaying more rostral regions of the brain (Nieuwenhuys et al. 1998; Meek et al.

2008; Sukhum et al. 2016; Schumacher and Carlson 2022; Gebhardt and Hofmann 2023). Unfortunately, the variation of the morphology of the ray-finned fish cerebellum is still poorly understood, apart from a handful of lineages, but variation in the distribution of proliferative zones of granule neurons in the ray-finned fish brain (Butts et al. 2014) hints at a high potential for morphofunctional variation in the cerebellum across the whole lineage, but especially within teleosts.

1.4.2 Brain morphology: Ecology or phylogeny?

Vertebrate brain anatomy has long been considered to capture information about organismal behavior and ecology (Edinger 1964; Striedter and Northcutt 2019). Total brain size as well as size of brain regions have been proposed to correlate with ecology and behavior at both intraspecific (Gonda et al. 2013; Rizzato and Bichuette 2024) and interspecific levels (Kotrschal et al. 1998; Schumacher and Carlson 2022; Gebhardt and Hofmann 2023). However, the complex organization and interconnection of different brain regions presents a challenge when trying to understand correlations between size (e.g. volume, surface area) and ecological function. There is a wide range of studies relating brain morphology to ecology in ray-finned fishes, most of which have used qualitative and comparative approaches between closely-related species (Evans 1931; Northcutt and Wullimann 1988; Gebhardt and Hofmann 2023). Volumetric approaches to ray-finned fish brain ecomorphology are common, and have led to competing results on whether brain morphology (in terms of relative volume) can be correlated with ecology and behavior (see Kotrschal et al. (1998) for a detailed review of studies on ray-finned fish brain morphology and ecology).

Cyprinids are a classic example used in brain ecomorphology of ray-finned fishes due to their abundance in northern hemisphere freshwater systems and wide range of morphological adaptations that can be directly related to ecology and behavior, such as barbels, pharyngeal jaws, sucking and tactile lips (Kotrschal and Palzenberger 1992; Nelson et al. 2016). These studies found correlations between gross anatomy and volume of brain regions to broad ecological niches, where areas of the brain related to functionally important aspects of their ecology would be enlarged in respect to closely related species that adopted a different life strategy (Kotrschal and Palzenberger

1992; Kotrschal et al. 1998). Similar patterns have been observed in gadids, flatfishes, and cichlids (Evans 1936, 1940; Finger 1988; Kotrschal et al. 1998).

There is ample evidence of intraspecific variation in brain size in respect to numerous ecological parameters. For example, it has been demonstrated that dissolved oxygen availability relates to variation in brain size of some African cichlids and mormyrids (Chapman and Hulen 2001; Chapman et al. 2008; Crispo and Chapman 2010), whereas behavior and reproductive strategies also seem to relate to variation in brain size (and proportions) in several taxa, such as cichlids, salmonids and sticklebacks (Shumway 2008; Kolm et al. 2009; Park and Bell 2010). Thus, it is not imprudent to extrapolate that variation in brain size and proportions between different brain regions might also correlate to environmental preferences and ecology across species. However, most literature on interspecific brain size variation concerns birds and mammals (Healy and Rowe 2006; Gonda et al. 2013). Given the lack of available information on brain size variation with respect to environmental and ecomorphological differences within ray-finned fishes, it is not currently possible to determine whether brain size is a good predictor for ecology in this clade, and studies exploring interspecific brain size variation should take into account potential biases caused by intraspecific variation and brain plasticity.

Apart from relative size of brain regions among closely related taxa, brain anatomy can be informative of ecological adaptations on a large macroevolutionary scale (Kotrschal et al. 1998; Schumacher and Carlson 2022). Morphological and sensory innovations are bound with differentiation of brain regions. One example is hypertrophy of the hindbrain, especially the corpus cerebelli, in mormyrids (Sukhum et al. 2016; Schumacher and Carlson 2022) or the enlarged oculomotor nucleus of *Astroscopus* (Dahlgren 1927; Leonard and Willis 1979), both of which have specialized electrossensing tissues. However, within a broad phylogenetic bracket (i.e. across all ray-finned fishes) it becomes challenging to determine whether brain morphology is better explained by phylogenetic relationship or differences in ecology of the sampled species.

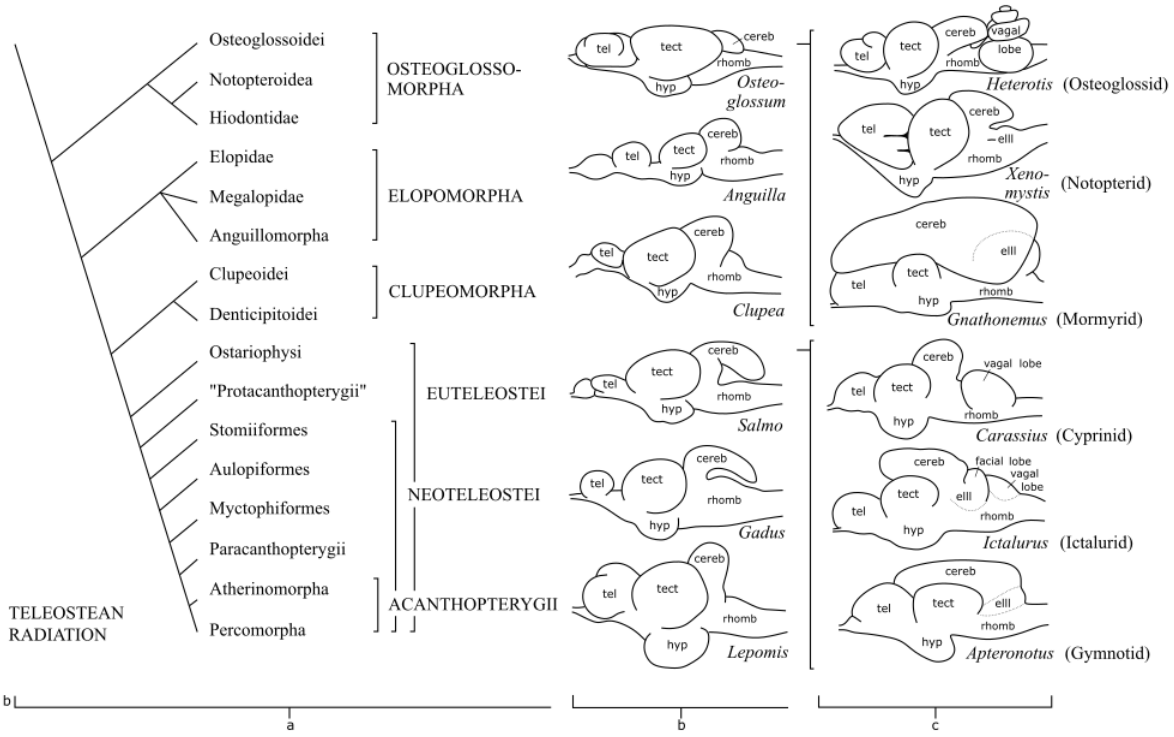

Figure 0.3 - Variation in teleost brain gross-morphology adapted from Meek & Nieuwenhuys (1998) noting the variation in proportions of different brain regions and variation in post-cerebellum lobes presence/absence.

Despite modern phylogenetic comparative methods and morphometric analysis being able to infer phylogenetic signal as well as potential correlations with specified traits, there is currently not enough information on ray-finned fish neuroanatomical diversity to test such hypotheses with confidence. The ray-finned fish brain is highly complex and is comparable to that of tetrapods (Vernier 2017). Nevertheless, there is little information on the impact of phylogenetic relationship on brain shape and size. Only a handful of studies have dealt with exploring patterns of brain diversity in a phylogenetic context within ray-finned fishes, and these have focused on volumetric approaches or estimations of brain/body size ratios (Iglesias et al. 2015; Schumacher and Carlson 2022; Gebhardt and Hofmann 2023). Thus, an important step toward a better understanding of the relation between ray-finned fish neuroanatomy and ecomorphology and phylogeny is a more robust sampling of extant species dispersed across the ray-finned fish tree as well as ecological variation in closely related taxa.

1.4.3 Brain and endocast

Another question regarding brain morphology is that of encephalization, which can be defined as an increase in brain size without a corresponding increase in body size (Jerison 1973). Teleosts seem to have constrained encephalization (Striedter and Northcutt 2019), meaning that brain-body ratios are consistent across taxa of varying body sizes. A few exceptions include changes in encephalization with depth in marine fishes (Iglesias et al. 2015) and the hypertrophied mormyrid hindbrain mentioned above (Schumacher and Carlson 2022). Encephalization and covariation of brain and neurocranium seem to play an important role in shaping brain anatomy in fishes, and examples demonstrate developmental and morphological constraints to brain shape within the neurocranium (Striedter and Northcutt 2006; Conith et al. 2022; Kozol et al. 2023).

The internal space within the neurocranium (endocast) represents the space available for the brain to occupy (Balanoff and Bever 2017). In several vertebrate lineages (e.g. archosaurs and mammals) it has been demonstrated that endocast shape is a good predictor of brain shape (Neubauer 2014; Watanabe et al. 2019a). Thus, for some lineages, fossil endocasts represent a good proxy for reconstructing the brains of extinct species (Clement et al. 2016; Balanoff and Bever 2017). However, the relationship between endocast shape and brain shape is less clear in other clades (Clement et al. 2015; Allemand et al. 2022). For ray-finned fishes there is little evidence that endocasts are good predictors of brain size and shape, although endocasts have been useful for understanding the interrelationships of extinct taxa (Moodie 1915; Coates 1999; Giles and Friedman 2014) there is little evidence that endocasts are good predictors of brain size and shape within this clade. This has been highlighted by the discovery of fossilized brains in a stem ray-finned fishes showing little resemblance between brain and endocast (see Chapters 4–5; Figueroa et al. (2023, 2024)).

Moreover, although extant ray-finned fishes show a wide range of neurocranial morphologies (Schaeffer 1971; Friedman and Giles 2016; Knapp et al. 2023), there is virtually no information regarding their endocast morphology. Part of this knowledge gap is probably related to the nature of some teleost neurocrania and inner ears, which can sometimes be only partially ossified, precluding identification of endocranial shape in skeletonized specimens commonly used for descriptive work. Given the known diversity of ray-finned fish brains and neurocrania it would not be unreasonable to hypothesize that a comparable morphological diversity could be found in their endocasts. This is especially plausible considering evidence of covariation between brain and endocrania in selected ray-finned fish lineages such as cichlids (Conith et al. 2022). However,

without a better sampling it remains impossible to determine the morphological diversity of teleost endocasts and the relation between endocast and brain morphology within this clade and in relation to non-teleost taxa.

1.4.4 How independent are different brain regions?

Vertebrate brain development is conservative in the sense that its organization in neuromeres (units resulting from the specification of the neural tube) is consistent from agnathans to mammals (Redies and Puelles 2001; Northcutt 2002; Kiecker and Lumsden 2005). Thus, it is important to consider which developmental paths might have led to the high disparity among brain morphologies in vertebrates as a whole and within vertebrate clades.

It has long been hypothesized that the vertebrate brain is highly modular (Leise 1990), meaning that different regions of the brain can evolve independently, which would help explain the high disparity in brain morphologies. However, studies on mammals have demonstrated that development of different brain regions is associated with size of the brain and indicate that modularity might be restricted when dealing with closely related taxa (Finlay and Darlington 1995; Barton and Harvey 2000; Rowe et al. 2011). On the other hand, brain regions seem to be highly modular when considering large macroevolutionary scales and anatomical and behavioral innovations, such as the example above on mormyrid fishes (Schumacher and Carlson 2022).

The modularity of the vertebrate brain can be thus used to explain the high disparity in brain morphologies found in the group. However, when coupled with our poor understanding of neuroanatomical diversity in teleosts, it precludes us from understanding patterns of brain evolution across the ray-finned fish tree. If a brain region can change independently from the rest of the brain, it might be highly affected by clade-specific life-strategies, and thus brain morphology might better represent ecology than phylogenetic relationships. Since the brain is an expensive tissue to develop and maintain it can be expected that phenotypic plasticity of the brain to be restricted to modifications with adaptive value (Gonda et al. 2013).

1.4.5 Summary

In this dissertation I will integrate data on fossil and living species to better understand the early evolution of ray-finned fishes dating back to the Devonian. Focus will be given to describing fossil taxa from poorly sampled high-latitude localities in South America as well as exceptional soft-tissue preservation of brains and other organs that allow direct comparison to living clades. Finally, I will discuss our understanding of living ray-finned fish brains and provide insight into the neuroanatomical diversity of ray-finned fishes.

Chapter 2 The Oldest Devonian Circumpolar Ray-Finned Fish?

Note: The contents of this chapter have been published[1].

Abstract: Actinopterygians (ray-finned fishes) are the most diverse group of living fishes but have a sparse Devonian fossil record restricted to low paleolatitudes. Here we report a new actinopterygian from the Paraná Basin of Brazil, which occupied a circumpolar position in the Palaeozoic. Available geological evidence supports a Middle Devonian or older age for this taxon, which shares features of the mandibular symphysis with the latest Devonian *Tegeolepis*. A phylogenetic analysis resolves these two as sister taxa. This new record expands the paleogeographic distribution of Devonian ray-fins and suggests that gaps in their fossil record might be filled by exploring poorly sampled high-latitude localities within the Malvinokaffric Realm.

Keywords: Devonian, Actinopterygii, Malvinokaffric, Osteichthyes, Brazil, paleopolar

[1]Figueroa, R.T., Weinschütz, L.C. and Friedman, M. 2021. The oldest Devonian circumpolar ray-finned fish? *Biology Letters*, 17(3): 20200766

2.1 Background

Osteichthyans (bony fishes) diversified during the Devonian (ca. 419-359 Ma) "Age of Fishes" (Wen-Jin and Min 2007). Taxonomic and palaeobiogeographic imbalance characterizes the Devonian osteichthyan record. Despite modest diversity in modern aquatic settings, lobe-finned fishes (Sarcopterygii) were the dominant Devonian osteichthyan group gauged by morphological disparity (Anderson et al. 2011), taxonomic richness (Sallan and Coates 2010), and abundance of individuals in many settings (Trewin 1986) (but see (Long and Trinajstic 2010)). By contrast,

ray-finned fishes have nearly non-existent Early Devonian (Lu et al. 2016) and scarce Middle Devonian (Sallan and Coates 2010) fossil records that give little indication of their major role in post-Devonian aquatic ecosystems (Sallan and Coates 2010; Friedman and Sallan 2012; Friedman 2015). Sites at low palaeolatitudes yield the majority of Early-Middle Devonian osteichthyans (Brazeau and Friedman 2015). Fishes from high palaeolatitude deposits of that age include acanthodians, chondrichthyans, and placoderms (Janvier and Maisey 2010; Richter et al. 2017), with bony fishes only well represented in the Late Devonian (Gess and Whitfield 2020). This mirrors the taxonomically depauperate Early to Middle Devonian invertebrate communities from southern high latitudes characterizing the Malvinokaffric Realm, a central feature of Devonian biogeography (Boucot et al. 2001; Dowding and Ebach 2018, 2019).

Here we report a new ray-finned fish of probable Middle Devonian age that challenges these signature features of the early bony fish record. First, with a distinctive morphology resembling latest Devonian actinopterygians, it highlights unanticipated disparity among earlier ray-finned fishes. Second, the new form derives from a Brazilian palaeopolar site, making it the first candidate for an identifiable Malvinokaffric bony fish. This discovery prompts reconsideration of divergence times within Devonian actinopterygian phylogeny, along with the possibility that important events in the early history of the group took place outside of regions yielding abundant osteichthyans.

2.2 Methods

2.2.1 Specimen visualization

The specimen (Museu de Ciências da Terra, Rio de Janeiro, Brazil, MCT890-P) was scanned with a GE Phoenix v|tome|x m scanner in the Museu de Zoologia, Universidade de São Paulo. We also scanned a dentary of *Tegeolepis clarki* (Cleveland Museum of Natural History, Cleveland, USA, CMNH 8124) with a Nikon XT H 225 ST scanner at the University of Michigan. Details of these scans and those of published specimens are in Supplementary Material 1.

μCT data were segmented with Mimics 19.0 (Materialise, Leuven, Belgium). Resulting .ply files were edited in Meshlab (Cignoni et al. 2008) and rendered in Blender (Garwood and

Dunlop 2014) (blender.org). 3D models and μCT data are deposited in Dryad (10.5061/dryad.b8gtht7b7).

2.2.2 Phylogenetic analysis

We included MCT890-P in the matrix of Giles et al. (Giles et al. 2017), which focuses on ray-finned fishes but contains 11 early sarcopterygians and two stem osteichthyans. We excluded *Brachydegma*, which is under revision by one of us (MF) and others, and included a new character (concavity on the ventral margin of the dentary: 0=absent; 1=present).

Parsimony analysis was conducted in PAUP 4.0 (Cummings 2014) using a heuristic search, with 100 replicates under the TBR branch swapping methodology. Maxtrees was initially set to 1,000 with automatic increase, with nchuck=10,000 and chuckscore=1. We enforced constraints among non-osteichthyans as in Giles et al. (Giles et al. 2017): (*Dicksonosteus* (*Entelognathus* (*Acanthodes*, *Cladodoides*, *Ozarcus*) Osteichthyes))). A Nexus dataset is in Apendix B or through Dryad (https://doi.org/10.5061/dryad.b8gtht7b7).

Bayesian analysis was conducted using the MkV model implemented in MrBayes 3.2.5 (Ronquist et al. 2012; Wright and Hillis 2014). Number of substitution types was set to 1, constraining all rates to be equal. The analysis was run until maximum standard deviation between the two samples approached 0.05, sampling every 500 generations over a total of 10 million generations. The first 10% of sampled trees were discarded as burn-in. See Appendix B for script.

2.2.3 Estimation of Total Length (TL)

We estimated TL for MCT890-P by using the proportion of dentary length anterior to the adductor fossa relative to TL for eight Devonian actinopterygians, reflecting a range of possible proportions (Appendix B).

2.3 Systematic Paleontology

Osteichthyes Huxley, 1880

Actinopterygii Cope, 1887

Austelliscus ferox Figueroa et al., 2021

Etymology: Generic name references the high palaeolatitude locality (*austelli*, from the Latin meaning ‘the southern portion’), combined with the Latin suffix for ‘fish’ (*iscus*). Species epithet alludes to the large teeth of the specimen (*ferox*, from the Latin meaning ‘ferocious’).

Generic Diagnosis: Actinopterygian with robust, conical. anteriorly oriented teeth on the dentary, except for the symphysis where teeth point posteriorly; symphysis reflexed posteriorly; jaw ramus constricted posterior to the symphysis. Differs from *Tegeolepis* in having: large oval replacement sockets in the lingual tooth row (rather than circular); lingual and labial tooth series converge posteriorly (rather than remaining well separated); more substantial post-symphyseal constriction of the dentary; external surface of dentary ornamented with rounded tubercles anteroventrally and vermiform ornamentation posteriorly (rather than having only sparse tubercles and ridges).

Specific Diagnosis: As for genus.

Holotype: MCT890-P, mold of an incomplete left dentary in part and counterpart.

Locality and Horizon: Data for MCT890-P indicates collection near Ponta Grossa, Paraná, Brazil, but no specific locality. Host matrix comprises bioturbated yellowish siltstone with parallel lamination and lenticulation. It contains a lingulid brachiopod indicative of a marine setting (Appendix B), narrow burrows oriented parallel to bedding with rare interconnecting vertical tubes (cf. *Thalassinoides* (Ekdale 1985)), and multiple undulating horizontal burrows (cf. *Phycosiphon* (Sedorko et al. 2017)).

Candidate deposits in Ponta Grossa are exclusively Palaeozoic and lie within the Apucarana sub-basin of the Paraná Basin (Fig. 2.1a-b). The upper Silurian-Lower Devonian (Pridoli-Lochkovian) Furnas Formation is the oldest, and comprises sandstones, shales and mudstones representing a fluvial or coastal setting (Grahn et al. 2010; Sedorko et al. 2017). This

disagrees with the associated matrix, and seems unlikely on biostratigraphic grounds. The youngest rocks belong to the upper Carboniferous-lower Permian (Gzhelian-Cisuralian) Itararé Group, which consists of glacial deposits (e.g., siltstones and varvitic shales cut by glacial channels) likewise inconsistent with MCT890-P . This leaves the Devonian (Pragian-Frasnian) Ponta Grossa Formation, the upper parts of which are sometimes recognized as the São Domingos Formation, as the most probable candidate (Grahn et al. 2013). The Ponta Grossa Formation consists of shallow marine siltstones, mudstones, and shales that are grey to yellow in color (Grahn et al. 2013). Its uppermost sequence (sequence F of Grahn et al. (2013)) is not exposed in the eastern part of the Paraná Basin (Rostirolla et al. 2007; Grahn et al. 2013), suggesting MCT890-P is early Givetian or older in age (~387 Ma; Supplementary Material 1). Lithological composition of the sample is similar to that described for older sequences with bioturbated fine-grained yellowish sediments, rich in invertebrate fossils (sequences B and C of Grahan et al. (2013)). The top of these sequences is within the GS Western Gondwanan Spore Zone (Grahn et al. 2013). This is correlated with the AP Western European Spore Zone and the *costatus* Conodont Zone (Melo and Loboziak 2003), the top of which is Eifelian with an estimated age of ~389 Ma (Becker et al. 2012). Presence of tuberous trace fossils (see Appendix B) is consistent with Sedorko et al. (2018) Facies 5, representing inner-shelf deposits at or near the storm wave base. We conclude that MCT890-P is likely from the Ponta Grossa Formation and thus Devonian. Lithological composition, geographic locality, and known availability of outcrop imply an early Givetian or older age, but more precise determination is not possible.

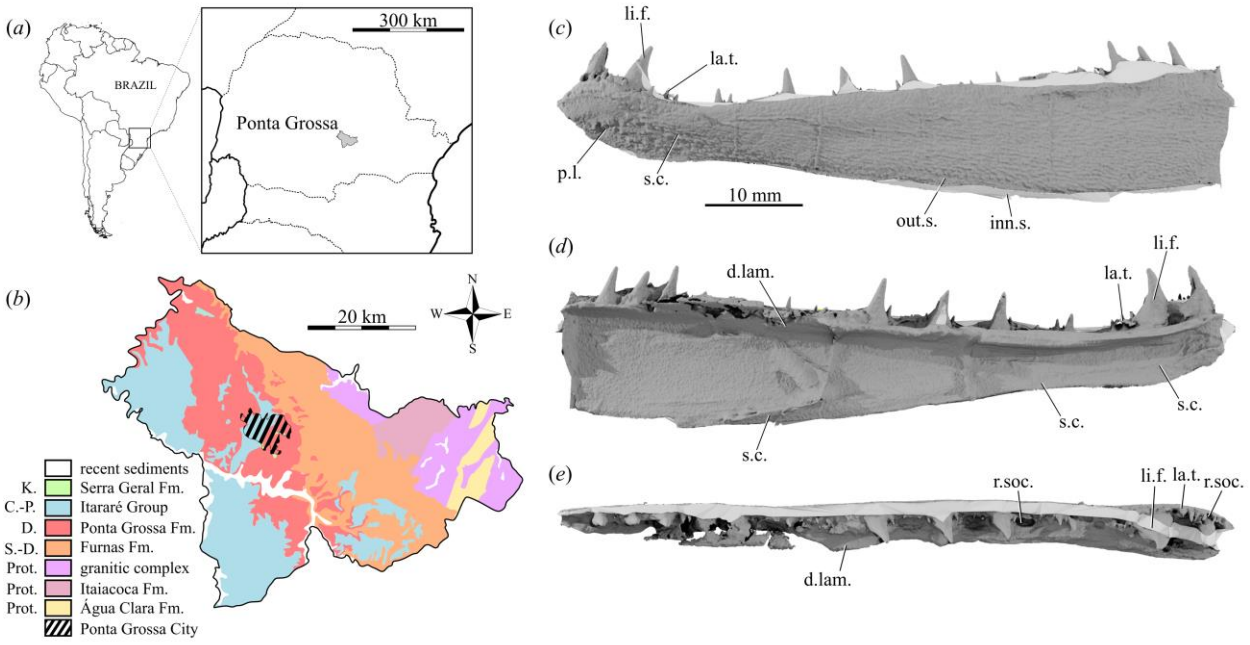

Figure 2.1 – Locality and specimen. (a) Maps of South America, the Brazilian state of Paraná, and Ponta Grossa municipality with (b) geology from Bosetti (Bosetti 2004). *Austelliscus ferox*, holotype MCT890-P, virtual cast of left dentary in (c) lateral, (d) medial, and (e) dorsal views. Light grey represents infilled gap between part and counterpart. Abbreviations: d.lam., dorsal lamina; inn.s., inner surface of the dentary; la.t., labial teeth; li.f., lingual fangs; out.s., outer surface of the dentary; p.l, pitline; r.soc, replacement sockets, s.c., sensory canal.

Description: The isolated left dentary of *Austelliscus* measures 70 mm in length but is missing its posterior end (Fig. 1c-e). Teeth are present along the entire dorsal margin, indicating the bone is broken at or before the anterior margin of the adductor fossa.

The dentary is slender in comparison to most other Devonian actinopterygians (Fig. 2.2 a- b) and tapers anteriorly to a region posterior to the symphysis, at which point it expands and changes orientation. Along with a strong constriction to the jaw ramus posterior to the symphyseal region, this gives the distal tip of the jaw a reflexed geometry. The overall shape of the dentary most closely resembles that of *Tegeolepis*. No other bones are present, but a notch in the posteroventral margin of the dentary implies a slender anterior extension of an infradentary. The jaw lacks an articulation surface for additional infradentaries anterior to this notch, indicating that the dentary formed the bulk of the ventral mandibular margin as in other actinopterygians (Gardiner 1984).

Ornament on the lateral surface consists of small, rounded tubercles anteroventrally andshort, wavy ridges elsewhere (Fig. 2.1 c-e). Smaller tubercles are also found near the ventral

margin, and occasionally coalesce with the more dorsal ridges. A small crescent-shaped pit line is present below the symphysis.

There are two rows of well-developed teeth: a lingual series of proportionally large fangs and a labial series of smaller conical teeth. The presence of acrodin caps cannot be confirmed. The lingual series includes large oval replacement sockets, while the labial row has small, closely spaced circular sockets near the symphysis. Posteriorly, the lingual and labial tooth rows converge, nearly forming a single series. The tips of the anteriormost lingual fangs are reclined posteriorly, but all others are gently inclined anteriorly. The bases of the lingual fangs are partially obscured by the external lamina of the dentary in lateral view. This lamina is expanded at the symphysis.

In mesial view, a shelf-like lamina supports the lingual fangs. The lamina is thin but prominent posteriorly and becomes thicker but less prominent anteriorly, expanding slightly below the parasymphyseal region. A thickening extending along the inner face of the dentary near the ventral margin of the bone marks the course of the mandibular canal posteriorly, and anteriorly near the symphysis.

We estimate a total length for *Austelliscus* of 500-700 mm. This makes *Austelliscus* among the largest of Devonian actinopterygians, only regularly exceeded in size by *Tegeolepis* (Fig. 2.2 a-b; Appendix B).

2.4 Phylogenetic results

Austelliscus was scored for 13 of 266 characters in our matrix. Parsimony analysis places *Austelliscus* as the sister taxon of the Fammenian *Tegeolepis*, but this clade collapses at one extra step (Bremer support = 1). This clade falls within a polytomy of Devonian actinopterygians crownward of the early diverging *Meemannia* and *Cheirolepis* (Fig. 2.2 c; Bremer support = 2). Presence of the mandibular canal in the dentary represents the clearest support for an actinopterygian placement of *Austelliscus*. This relates to the derived mandibular construction of ray-finned fishes, where there are few infradentaries restricted to the posterior part of the jaw and the anterior part of the mandible is dominated by the dentary (Gardiner 1984). *Austelliscus* clearly shows this arrangement, with the lower margin of much of the jaw formed by the dentary. By contrast, the infradentaries extend to the near the symphysis in other other gnathostomes that

possess these bones (e.g., the stem gnathostome *Entelognathus* (Zhu et al. 2013)), most sarcopterygians (Gardiner 1984), and the probable stem osteichthyan *Dialipina* (Schultze and Cumbaa 2001)).Within actinoperygians, *Tegeolepis* and *Austelliscus* are united by the presence of a concave ventral margin of the dentary (character 266). They also share a dentary with a conspicuously reflexed distal tip (character 81), although this feature is also found in *Howqualepis*.

The Bayesian analysis also yielded a *Tegeolepis* + *Austelliscus* clade (posterior probability = 0.92), but with reduced resolution among other Devonian actinopterygian lineages.

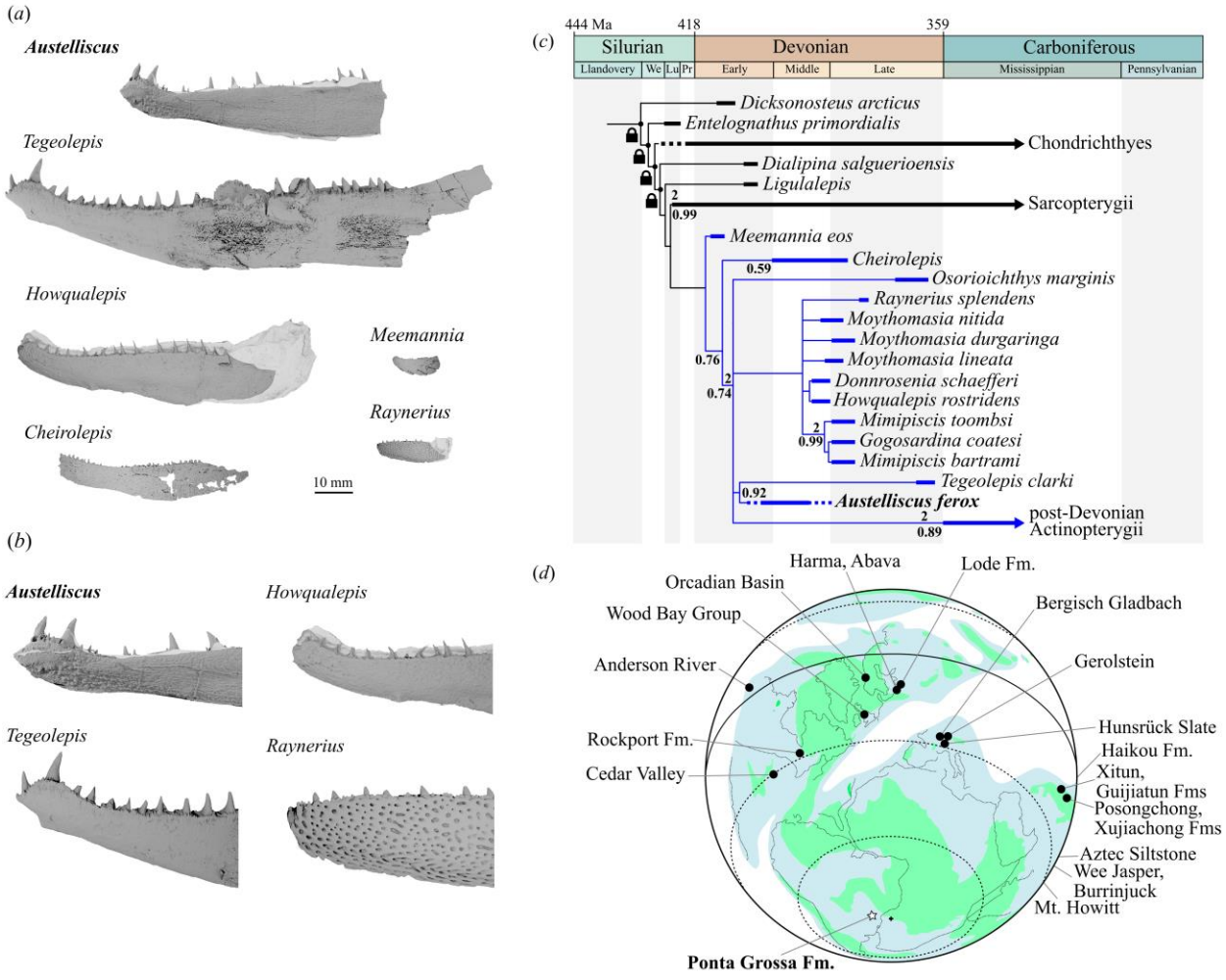

Figure 2.2 – Morphological, evolutionary, and paleobiogeographic context. (a) Lower jaws of Devonian actinopterygians in lateral view (Supplementary Material 3). Scale=10 mm. (b) Comparison of the symphyseal region of Devonian actinopterygians. Black arrows indicate the concavity on the anteroventral margin of the lower jaw (character 266). (c) Strict consensus of 92,389 most-parsimonious trees of 1,317 steps (Length = 1,316, Consistency Index = 0.222, Retention Index = 0.643) plotted against geological time. Decimal node values represent Bayesian posterior probabilities; whole numbers represent Bremer decay index. Stratigraphic ranges marked by

thick lines. Actinopterygians indicated by blue. For *Austelliscus*, dashed line gives the age range of Ponta Grossa Formation, solid line indicating probable age of the specimen. Clade uniting the species of *Cheirolepis* collapsed for clarity. Padlocks represent constrained nodes. (d) Middle Devonian paleogeographic reconstruction based on Scotese (2020) showing distribution of key bony fish assemblages of Early and Middle Devonian age.

2.5 Discussion

The divergence of sarcopterygians and actinopterygians occurred during mid–late Silurian (Zhu et al. 2009), but the oldest complete actinopterygian fossils are Middle Devonian (Pearson and Westoll 1979). Ray-fins of this age are rare compared to their sarcopterygian contemporaries (Trewin 1986), and show limited morphological and functional variety relative to both coeval lobe-finned fishes (Anderson et al. 2011) and post-Devonian ray-fins (Sallan and Friedman 2011). The handful of known Middle Devonian actinopterygians appear conservative when contrasted with sarcopterygians of this age that include eel-like coelacanths (Friedman and Coates 2006), lungfishes with diverse feeding adaptations (Campbell and Barwick 1990), and tetrapod-like elpistostegalians (Boisvert et al. 2008).

If interpretation of a Middle Devonian age is correct, even the limited material of *Austelliscus* points to greater morphological diversity among early actinopterygians than previously anticipated. Instead of being closely associated with known Middle Devonian taxa, it is consistently placed with the latest Devonian *Tegeolepis* (Dunkle and Schaeffer 1973) (Famennian; *expansa* Conodont Zone, ~361 Ma (Over 2007; Becker et al. 2012)). A probable minimum age of early Givetian suggested by available geological evidence implies the presence of several ghost lineages for actinopterygian groups that first appear in late Givetian or younger deposits. This amplifies the puzzling lack of diverse actinopterygian fossils of Early and Middle Devonian age, but the geographical context of *Austelliscus* points to a possible solution. Nearly all Devonian actinopterygians are known from a restricted set of localities concentrated in North America, Europe and Australia (Sallan and Coates 2010), which were located at low paleolatitudes. By contrast, estimated paleolatitudes for the site yielding *Austelliscus* range from 84°S to 73°S (Hinsbergen et al. 2015), placing this taxon firmly in a circumpolar setting regardless of ambiguities in age (Fig. 2.2 d). The peculiarity of high-latitude southern faunas in the Early and Middle Devonian is well established, with Malvinokaffric vertebrates represented almost exclusively by fragmentary chondrichthyan (including acanthodian) and placoderm remains from southern South America (e.g., Brazil and Bolivia) (Janvier 2007; Janvier and

Maisey 2010; Richter et al. 2017), the Falkland Islands (Maisey et al. 2002), and South Africa (Gess 2016). Even in Late Devonian high-latitude localities postdating dissolution of the Malvinokaffric realm, actinopterygians remains rare and represented mostly by fragments of little taxonomic value (Janvier and Suárez-Riglos 1986; Janvier and Melo 1987; Gess 2016; Rezende et al. 2021). *Austelliscus* hints that the little-studied circumpolar region might have been an important area for early divergences in actinopterygian evolution, potentially accounting for the sparse early record of Devonian ray-finned fishes captured by better-known sites at lower paleolatitudes.

Chapter 3 Two New Permo-Carboniferous Actinopterygians from Brazil Highlight the Endocranial Disparity of Late Paleozoic Ray-Finned Fishes

Abstract: The late Paleozoic represents an important interval for early ray-finned fish evolution, but the interrelationships of taxa from this interval remain poorly understood. This might be caused by two major problems, one geographic and one phylogenetic: the lack of well-described three-dimensional specimens outside the paleotropics (i.e. North America, Europe and parts of Asia) and the uneven character sampling used in morphological matrices of early ray-finned fishes. Here I tackle both of these problems by describing exceptionally preserved three-dimensional ray-finned fishes from the latest Carboniferous–early Permian of southern Brazil. These specimens represent two morphotypes, distinguishable on the basis of both dermal and endoskeletal characteristics, but also by differences in the geometry of the neurocranium and elements present in the hyobranchial apparatus. Comparison to other Paleozoic and early Mesozoic taxa indicate that these two taxa occupy distinct positions along the ray-finned fish stem, with one being crownward close to Triassic taxa such as *Australosomus*, and the other is more closely aligned to Carboniferous taxa such as *Kansasiella*. Additionally, I provide a brief discussion of neglected sources of morphological characters within the ray-finned fish endoskeleton, mostly within the hyobranchial apparatus and pectoral girdle. These results point to the need for revising available morphological matrices to include information from well-preserved but poorly understood modules of the ray-finned fish body that may have the potential for better constraining the relationships among early actinopterygians.

3.1 Introduction

The Permo-Carboniferous represents an important interval in ray-finned fish evolution, as it marks the appearance of a diverse set of ecomorphologies that were not present in the Devonian (Sallan 2014; Friedman 2015; Friedman and Giles 2016). This is reflected in the fossil

record as an increase in morphological and taxonomic diversity. Most of the Permo-Carboniferous taxa known to date are represented by partially articulated and flattened material. Recent work has determined that this type of preservation do not provide enough information for phylogenetic studies (Giles et al. 2017, 2023; Latimer and Giles 2018; Figueroa et al. 2019; Argyriou et al. 2022). Thus, phylogenetic analyses of early ray-finned fishes have heavily relied on characters pertaining to the external dermal skeleton with occasional well-preserved material being used to investigate further aspects of anatomy such as neurocranium (Poplin 1974; Gardiner 1984; Hamel and Poplin 2008; Giles and Friedman 2014; Lu et al. 2016; Giles et al. 2017). Only a handful of well-preserved three-dimensional fossils have been studied in detail paying attention to endocranial anatomy (Poplin 1974; Poplin and Véran 1996; Coates 1999; Hamel and Poplin 2008; Giles and Friedman 2014; Giles et al. 2015b, 2017; Wilson et al. 2018; Argyriou et al. 2022).

Neurocrania are well represented in the late Paleozoic fossil record of ray-finned fishes, these have been used to better understand their phylogenetic relationships, moving forward from simple descriptions of dermal skull bones(Giles and Friedman 2014; Giles et al. 2017; Coates and Tietjen 2018; Caron et al. 2023). In recent years, advanced imaging techniques have helped increase the number of late Paleozoic taxa for which we have a good understanding of neurocranial anatomy as well as other parts of the endoskeleton, highlighting the importance of these features for phylogenetic and ecomorphological studies (Coates and Tietjen 2018; Friedman et al. 2018; Figueroa and Andrews 2022; Caron et al. 2023; Giles et al. 2023).

Nevertheless, there are still many aspects of endoskeletal anatomy that remain largely overlooked in descriptive and phylogenetic work. For example, despite the high variation in the organization and geometry of hyobranchial elements, there is little understanding of their morphological diversity and only a handful of hyobranchial characters have been used in phylogenetic analyses. In this chapter I describe two new exceptionally preserved taxa from the Carboniferous-Permian of southern Brazil and discuss potentially overlooked characters pertaining to the ray-finned fish endoskeleton that could better refine future phylogenetic analyses.

3.2 Methods

3.2.1 Material examined

The fossil specimens described here were collected at the Lontras Shale (uppermost Campo Mourão Formation) 'campáleo' outcrop and are deposited at the paleontological collection of the Centro Paleontológico da Universidade do Contestado (CENPALEO/CP).

3.2.2 Specimen visualization

The specimens were scanned with a Nikon XT H 225 ST scanner at the CTEES facility in the Department of Earth and Environmental Sciences, University of Michigan. The CT procedure was conducted using variable parameters depending on sample size, density and intended voxel size. For details on the scanning parameters for each sample refer to Appendix XX. Segmentation of the resulting data was completed in Mimics 19.0 (Materialise, Leuven, Belgium) and further imaging of the obtained surface models (.ply) was done in Blender 4.0 (Garwood and Dunlop, 2014; blender.org).

3.2.3 Locality and horizon

The specimen was collected at the 'campáleo' outcrop in the city of Mafra, Santa Catarina State, southern Brazil. This locality exposes the uppermost portion of the Campo Mourão Formation, a unit termed the Lontras Shale (França and Potter 1991).

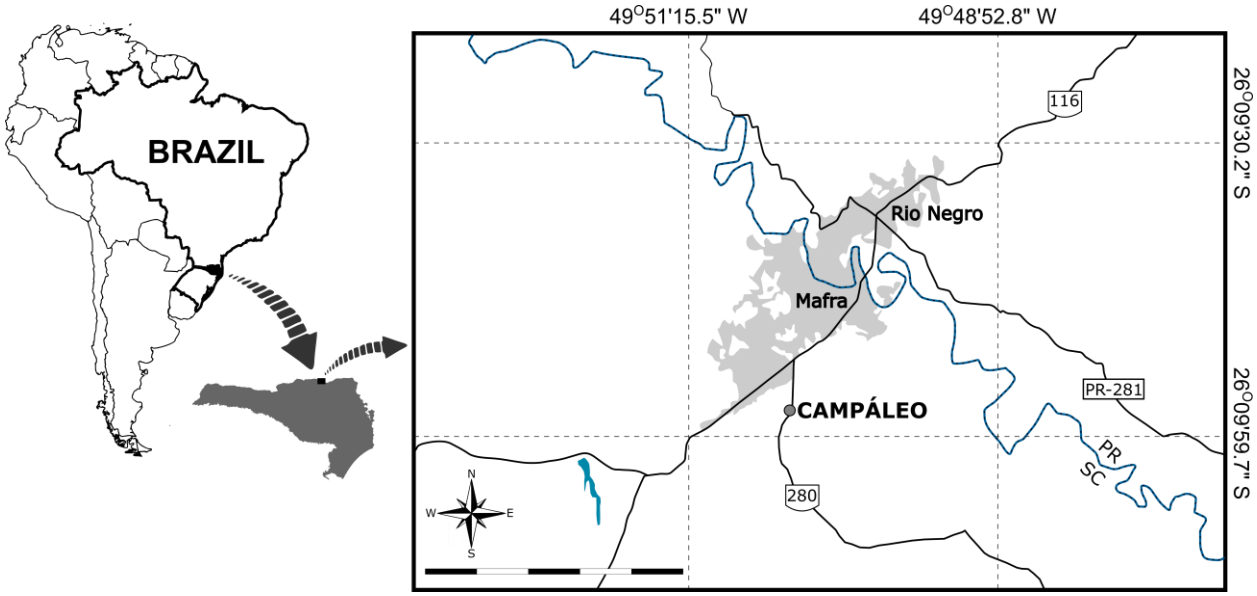

Figure 3.1 – Map of the type locality in Mafra, Santa Catarina, Brazil. Light gray shaded area represent urban development covering of the Mafra and Rio Negro cities.

The Lontras Shale consists of intercalated siltstones, varved shales, and highly fossiliferous black shales. The latter lithology is exposed at the 'campáleo' outcrop (Hamel 2005). The age of the Lontras Shale is estimated by both absolute and relative methods, giving competing results around the latest Carboniferous to early Permian. Biostratigraphic markers such as conodots and palinomorphs tend to give an early Permian (Asselian–Sakmarian) age for this unit (Holz et al. 2010; Wilner et al. 2016; Mouro et al. 2020). By contrast, radiometric dating methods give estimates of latest Carboniferous (Kasimovian–Gzhelian) age (Cagliari et al. 2016; Griffis et al. 2019a, 2019b; Valdez Buso et al. 2019; Mouro et al. 2020). In terms of paleoenvironment, there is ample evidence of glacial and peri-glacial activity within the Itararé Group of the Paraná Basin (Eyles et al. 1993; Cagliari et al. 2016; Mouro et al. 2017, 2020; Fallgatter and Paim 2019; Schemiko et al. 2023). The Lontras Shale might represent a fjord system based on the presence of mostly marine taxa (e.g. sponges, ammonoids and brachiopods) with occurrence of continental forms (e.g. insects and plants) in deep-marine shale deposits (Mouro et al. 2020; Saldanha et al. 2022). Considering the uncertainty of the age of the Lontras Shale, these strata are regarded here as late Pennsylvanian to Cisuralian in age.

3.3 Systematic Paleontology

3.3.1 Actinopterygii gen. et sp. nov. 1

Type material: CP 065 (holotype), a three-dimensionally preserved skull and anteriormost portion of the body preserved in a split concretion.
Additional specimens: CP.V 4364, CP.V 7053, CP.V 7227

Diagnosis: Actinopterygian defined by the following combination of features. Almost vertical suspensorium; elongate anterior spatulate end of the hyomandibula; two ceratohyal ossifications; one interhyal element directly below the hyomandibula; lack of a dermohyal; large curved

uncinate processes on the first and second epibranchials; braincase bearing a well-developed fossa bridgei; a median olfactory canal; elongated horizontal semicircular canal; oval enlarged anterodorsal fontanelle; small circular posterodorsal fontanelle; parasphenoid arching anterodorsally; small basipterygoid processes on parasphenoid; basipterygoid projections on the palatoquadrate; enlarged first basiventral partially roofing the aortic canal.

Description:

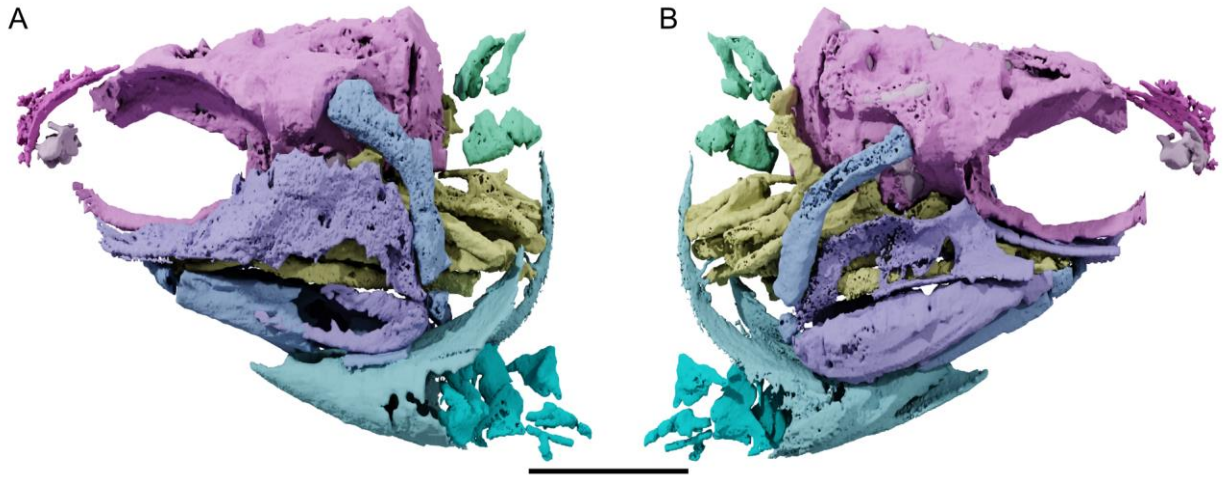

Figure 3.2 – Render of Actinopterygii gen. et sp. 1 (CP 065) in (A) left and (B) right lateral views. Scale bar = 10 mm.

3.3.1.1 Skull roof

The skull roof is poorly preserved in the holotype and is only visible through casts of the inside of the specimen. The supraorbital sensory canal that emerges from the poorly preserved snout passes through the dorsal portion of the skull roof, arching mesially above the orbit and then laterally before entering the posterior portion of the skull roof. The distal portion of the infraorbital canal is visible lateral to the supraorbital canal behind the level of the orbit. However, due to the poor preservation it is not possible to identify the bones that bear the canal along this path. The posterior margin of the skull roof seems to be lunate, probably formed by large extrascapulars. It is unclear if the skull roof bears any ornament.

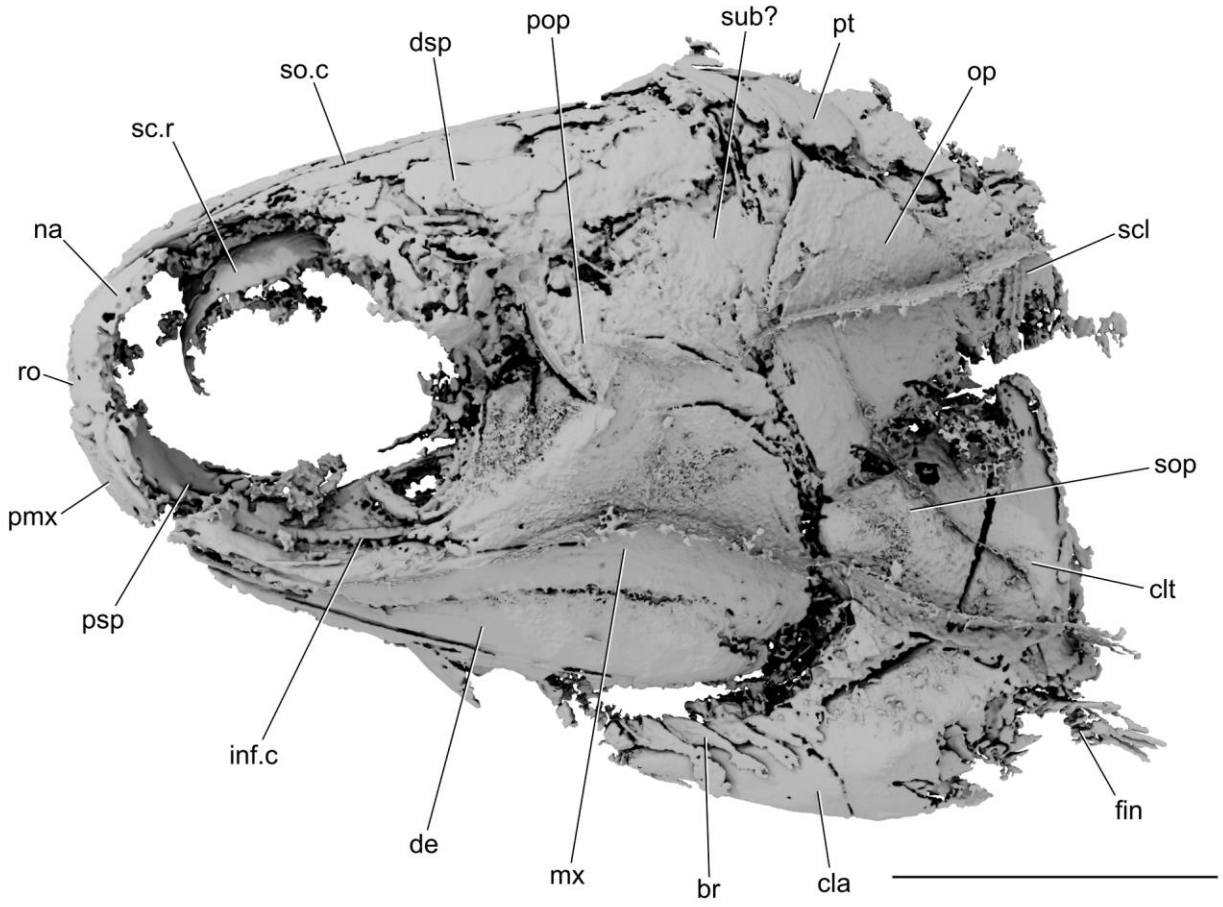

Figure 3.3 – Render of the skull of CP 5073 in left lateral view (Actinopterygii gen. et sp. nov. 1).br, branchiostegal rays, cla, clavicle, clt, cleithrum, de, dentary, dsp, dermosphenotic, inf.c, infraorbital canal, mx, maxilla, na, nasal, op, opercle, pmx, premaxilla, pop, preopercle, psp, parasphenoid, pt, postemporal, ro, rostral, sc.r, sclerotic ring, scl, supracleithrum, so.c, supraorbital canal, sop, subopercle, sub, suborbital. Scale bar = 10 mm.

CP.V 7227 reveals additional features of the skull roof. The snout is capped by a single median rostral that exhibits a triangular dorsal surface directly contacting the frontals. The median rostral is notched laterally forming the opening of the anterior nasal opening. Ventrally the median rostral contacts the premaxilla. The frontals are large and extend from the level of the anterior end of the orbit to the level of the anterior end of the preopercle, and thus forming most of the skull roof. The parietals are small and sub-quadrate, bearing a medially directed sensory canal. Part of the extrascapular series is apparent behind the parietal. Due to poor preservation it is not possible to determine the number of medial extrascapulars, but there seems to be only one, which is then flanked laterally by two small rounded lateral extrascapulars.

3.3.1.2 Jaws and palate

The dermal jaw bones of CP065 are only visible as a mold and therefore provide little information. CP 7227 preserves intact dermal jaw bones. The upper jaw has a prominent postorbital blade with a straight dorsal margin, terminating with an abrupt angle posteriorly. The sub-orbital portion of the maxilla is long and narrow, curving dorsally towards the snout. A possible pit line is visible below the orbit on the maxilla of the holotype but such a line is absent in CP 7227. The palatoquadrate is well preserved and follows the shape of the maxilla, terminating at an abrupt angle where the hyomandibula rests. The palatoquadrate seems to be formed as a single ossification given the lack of sutures, but it is not possible to determine the number of ossification centers. The palatoquadrate bears a well-developed metapterygoid process. The anterior process of the parasphenoid is separated from the palatoquadrate by a long accessory vomer that seems to be edentulous. There is a central element below the endochondral sphenoid that extends anteromedially between the two accessory vomers that seems to be part of the dermal parasphenoid. It merges with the braincase posteriorly below the orbit.

The lower jaw is straight and bears no sign of a reflexed distal tip of the dentary. In CP 5073 and CP 7227 a single row of the small, procumbent conical teeth extends along the dorsal margin of the dentary (Figure 3.7). The mandibular sensory canal line arches dorsally towards the symphysis on the dentary and the surface of the bone is ornamented with rounded tubercles. Other lower jaw ossifications (e.g. angular, articular, prearticular) are poorly preserved and no clear boundaries are visible between ossifications except the articular cotyles for the jaw joint (i.e. glenoids) are visible in CP 065. The portion that would represent the angular extends ventrally below the dentary. The adductor fossa seems to be small and defines an elongated ellipse in dorsal view. The coronoids are preserved as a single ossification making up the lingual margin of the lower jaw.

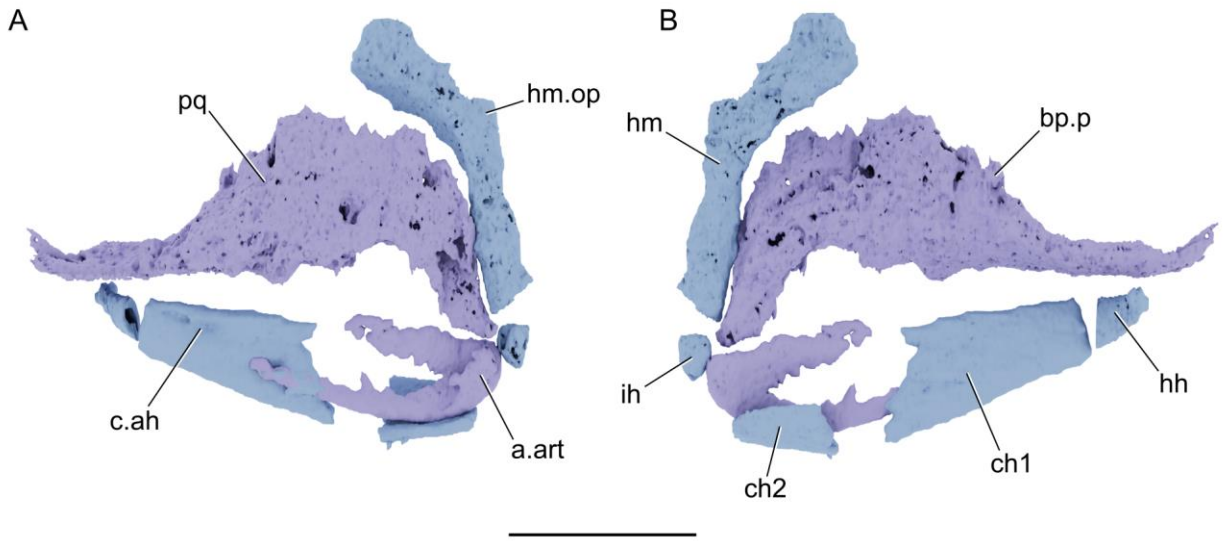

Figure 3.4 – Render of left jaws and hyoid arch of CP 065 in (A) lateral and (B) mesial views.a.art, angulo-articular, bp.p, basipterygoid process, c.ah, canal for the afferent hyoid artery, ch1, first ceratohyal, ch2, second ceratohyal, hh, hypohyal, hm, hyomandibula, hm.op, hyomandibula opercular process, ih, interhyal, pq, palatoquadrate complex. Scale bar = 10 mm.

3.3.1.3 Circumorbital series

The circumorbital series is poorly preserved and it is not possible to determine the number and shape of constituent bones, although the infraorbital and supraorbital canals are partially visible as impressions on the matrix. The jugal bone is the best-preserved element of the circumorbital series, with a lunate shape and being restricted to the posteroventral fourth of the orbital margin. There is no evidence of rami diverging from the infraorbital canal on the jugal. The remainder of the infraorbital series is poorly preserved and consists of a thin lamina of bone connecting the anterior margin of the jugal to the snout. There is no evidence of sutures in the infraorbital series. CP 7227 reveals more details of the supraorbital series. The nasal bone extends dorsally forming the anterodorsal margin of the orbit and is separated from the dermosphenotic by a thin supraorbital. The shape of the dermosphenotic is not clearly defined but there are indications of tuberculate ornament. Posteroventral to the dermosphenotic there is at least one suborbital separating the anterior border of the preopercle from the jugal.

3.3.1.4 Neurocranium

The neurocranium is partially complete with both sides preserved; the left side is more complete and shows better contrast in the CT data. The neurocranium appears to be a single ossification and shows typical proportions for late Paleozoic actinopterygians. Of the distinct regions of the neurocranium (ethmoidal, optic, and otico-occipital) the ethmoidal is the only one that is not complete, as it is only visible through the pyritized infil of the nasal capsules. The optic region is large and represents around 50% of the length of the neurocranium, formed ventrally by the ventral sphenoid and the dermal parasphenoid and dorsally by the supraorbital ridge and interorbital septum. The otico-occipital region is the most topographically complex portion of the neurocranium and starts at the level of the ventral otic fissure and terminates at the level of the foramen magnum posteriorly. The otic and occipital divisions are separated by the otico-occipital fissure.

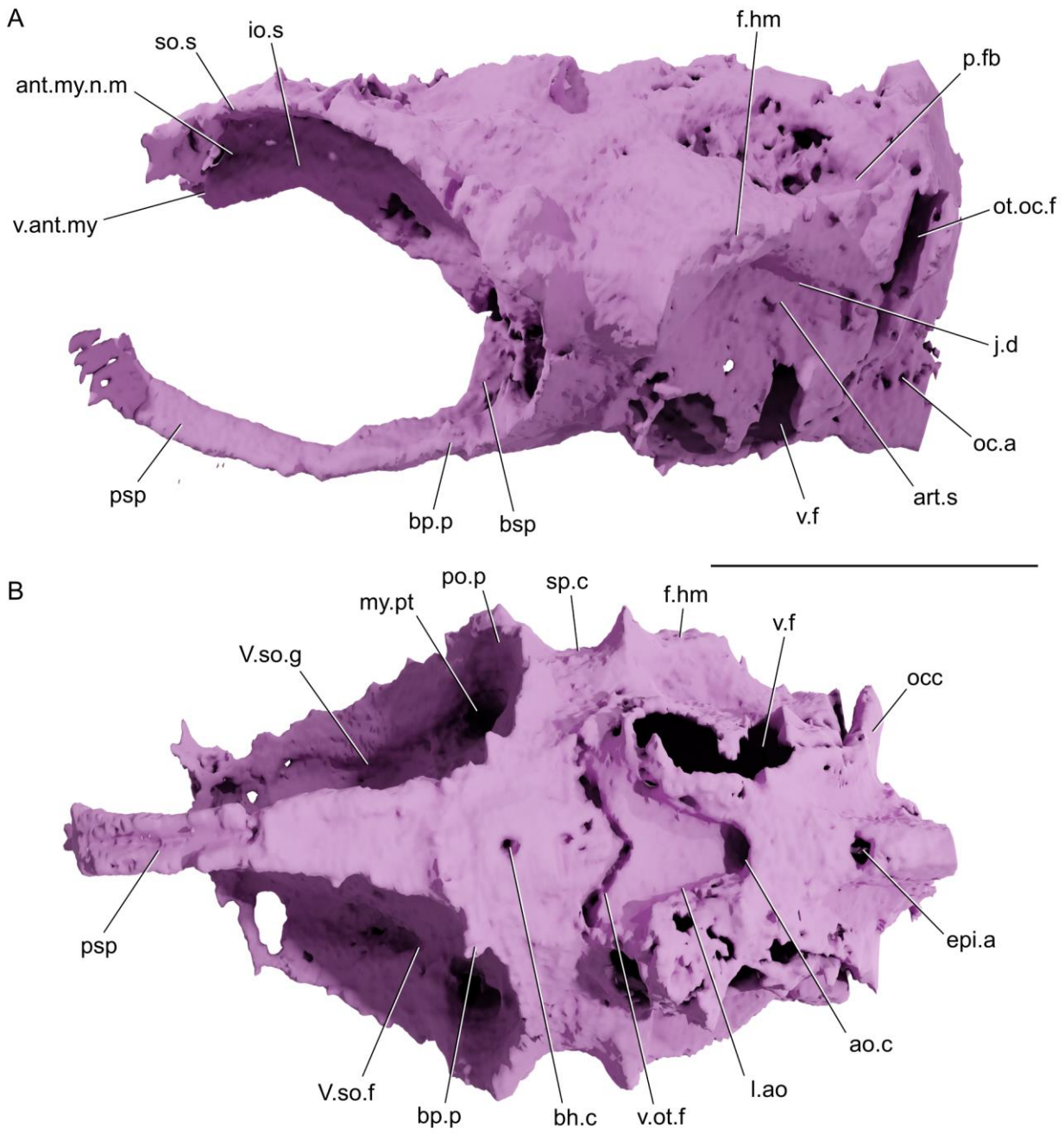

Figure 3.5 – Render of the neurocranium of the holotype (CP 065) in (A) lateral and (B) ventral views. ant.my.n.m, non-ocular anterior myodome, ao.c, aortic canal, art.s, articular surface for first suprapharyngobranchial, buccohypophyseal canal, bp.p, basipterygoid process, bsp, basisphenoid, epi.a, foramen for epibranchial arteries, f.hm, hyomandibular facet, io.s, interorbital septum, j.d, jugal depression, l.ao, canal for the lateral aortae, my.pt, myodome for the pterygoideus muscle (or adductor mandibulae, segmentum buccalis, pars sphenoidalis of XXXX), oc.a, foramen for the occipital artery, occ, occipital arch, ot.oc.f, otico-occipital fissure, p.fb, posterior fossa bridge, po.p, postorbital process, psp, parasphenoid, so.s, supraorbital shelf, sp.c, spiracular canal, v.ant.my, ventral anterior myodome, v.f, vestibular fontanelle, v.ot.f, ventral occipital fissure, V.so.f, foramen for the supraophthalmic branch of the trigeminal nerve, V.so.g, groove for the passage of the supraophthalmic branch of the trigeminal nerve. Scale bar = 10 mm.

The ethmoid region of the neurocranium is only represented by infill of the olfactory capsules and nasobasal canals. Although not completely preserved the olfactory capsules seem to have been diminutive and rounded, lying close to the anterodorsal end of the parasphenoid. These olfactory capsules communicate with the outside of the ethmoidal region of the neurocranium through nasobasal canals and the canals for the profundus nerve. A short canal is found anterior to the olfactory capsules, connecting it to the snout. This is identified as the medial nasobasal canal. Posterodorsally on the right olfactory capsule there are two canals that extend posterodorsally that likely accommodated the profundus nerve.

The long and narrow sphenoid is well-preserved, except for the articular facet for the palatoquadrate at the ethmoid region, which is only partially visible in the CT scan. The sphenoid has a long and slender anterior process with a triangular shape in transverse section. The ventral surface of the anterior process is concave, giving it a wide caret shape in cross section. There is no evidence of dentition on the ventral surface of the anterior process, but it is unclear if this is due to the resolution of the CT scan. Laterally, the anterior process of the sphenoid contacts the paired long accessory vomers that complete the dorsal roof of the mouth between the parasphenoid and the dermal ossifications of the palatoquadrate. These also seem to be edentulous. Anteriorly on the ethmoid region the anterior process seems to expand forming the articular facet for the palatoquadrate. Unfortunately it was partially compromised during preservation and is mostly obscured by matrix.

The dermal parasphenoid is preserved ventral to the sphenoid as a thin sheet of bone. The parasphenoid basipterygoid processes are reduced but a small bump is present on each side of the proximal end of the parasphenoid anterior process. These small basipterygoid processes seem to be anteroposteriorly compressed. In the holotype it is unclear if there was a dermal component to the basipterygoid process, but CP 7053 shows a clear dermal basipterygoid process in the transversal CT sections. The parasphenoid is strongly bound to the neurocranium through the ascending processes. The ascending processes are visible as thin laminas that extend on the external surface of the lateral commissure. It is not possible to determine the posterior margin of the ascending processes of the parasphenoid as they seem to fuse with the neurocranium ossification, but it bears a groove for the spiracular canal. The dorsal extent of the ascending process cannot be easily determined as it seems to coalesce with the endocranium at the level of

the postorbital processes of the neurocranium. The parasphenoid body is perforated by a small buccohypophyseal canal and terminates at the level of the ventral cranial fissure.

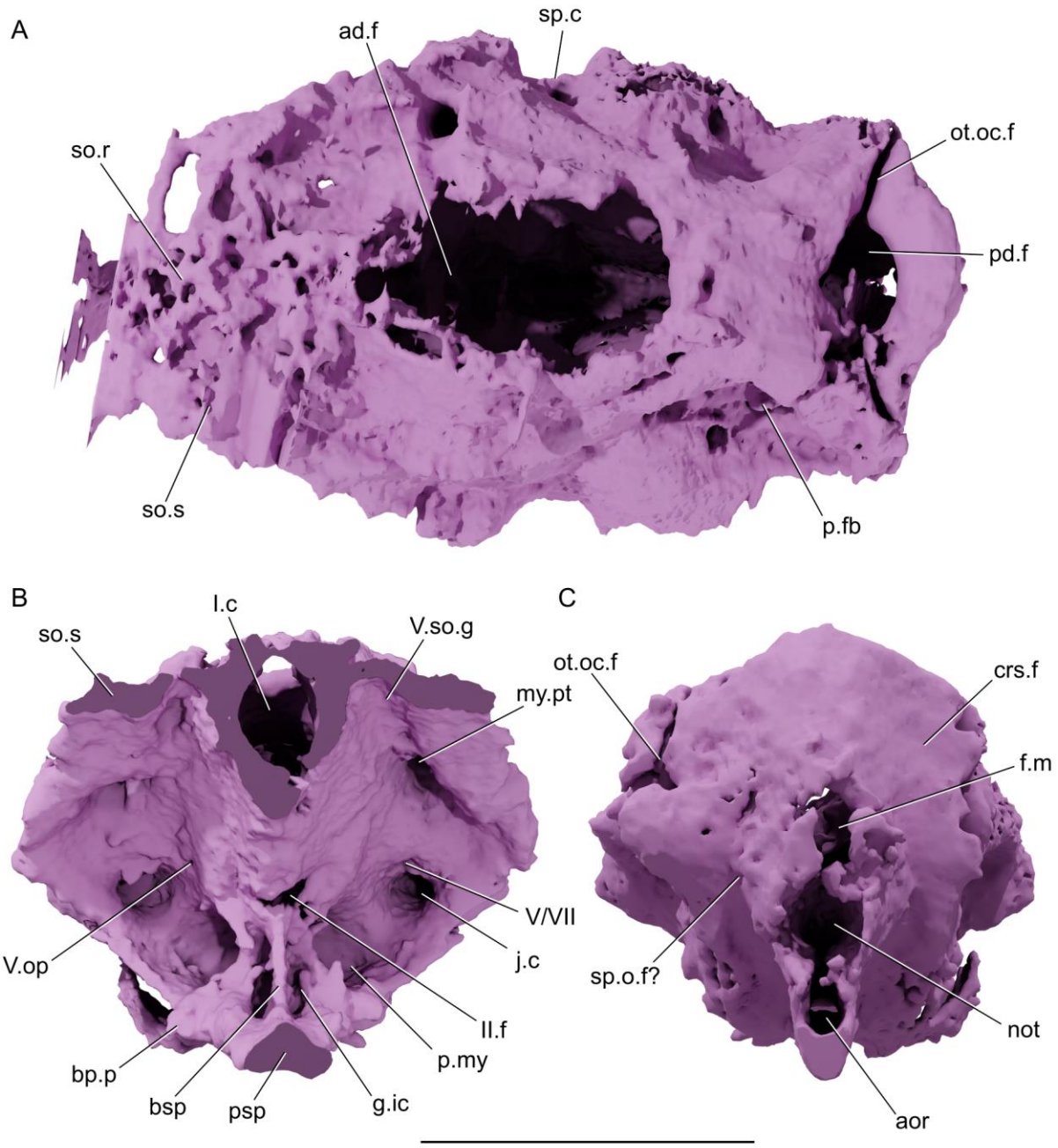

Figure 3.6 – Render of the neurocranium of the holotype (CP 065) in (A) dorsal, (B) frontal and (C) posterior views. ad.f, anterodorsal fontanelle, aor, aortic canal, bp.p, basipterygoid process, bsp, basisphenoid, crs.f, craniospinal fossa, f.m, foramen magnum, g.ic, groove for the internal carotid artery, j.c, jugal canal, my.pt, myodome for the pterygoideus muscle, not, notochord canal, ot.oc.f, otico-occipital fissure, p.fb, posterior fossa bridgei, p.my, posterior myodome, psp, parasphenoid, so.r, supraorbital ridge, so.s, supraorbital shelf, sp.c, spiracular canal, sp.o.f, foramen for the spinooccipital nerve, I.c, canal for the olfactory nerve, II.f, foramen for the optic nerve, V.op,

foramen for the ophthalmic branch of the trigeminal nerve, V.so.g, groove for the supraophthalmic branch of the trigeminal nerve, V/VII, foramina for the motor branch of the trigeminal and facial nerves. Scale bar = 10 mm.

Dorsal to the parasphenoid body there is a small, blade-like basisphenoid that extends dorsally towards the optic foramen. Laterally to the basisphenoid there are long ellipsoid notches for the internal carotid artery. A large median posterior myodome lies posterior to the basisphenoid. It does not bear a longitudinal septum separating both sides of the myodome. The myodome is short and terminates at the level of the hyomandibula articulation facet.

The orbital cavity on the optico-sphenoid region of the neurocranium is surrounded dorsally by the supraorbital shelf and posteriorly by a well-developed and robust postorbital process. Above the supraorbital shelf there is a single reduced lateral ridge that extends towards the ethmoid region of the braincase. A deep myodome lies at the junction between the supraorbital shelf and postorbital surface, corresponding to the posterior end of the groove for the supraophthalmic nerve. Given its position it is interpreted here as the myodome for the pterygoideus muscle (Allis (1922); named '*adductor mandibulae, segmentum buccalis, pars sphenoidalis*' by Datovo and Rizzato (2018)). Posteroventral to the postorbital process on the left side of the specimen there is a small depression that could represent the foramen for the spiracular canal. Dorsally at the same level there is an opening that corresponds to the spiracular fossa and canal opening. This opening is separated from the anterior fossa bridgei. The jugal canal is visible between the postorbital process and the posterior myodome, exiting posteriorly behind the well-developed and inclined hyomandibular articulation facet. Dorsal to the left jugal canal there is a foramen that due to its position, likely represents the exit of the ophthalmic branch of the trigeminal nerve (V_{oph}). Dorsal to the basisphenoid the exit for the optic nerve (II) is obstructed by matrix but partially visible. Within the ventromedial wall of the posterior myodome there is a foramen interpreted as one of the exits of the abducens nerve (VI).

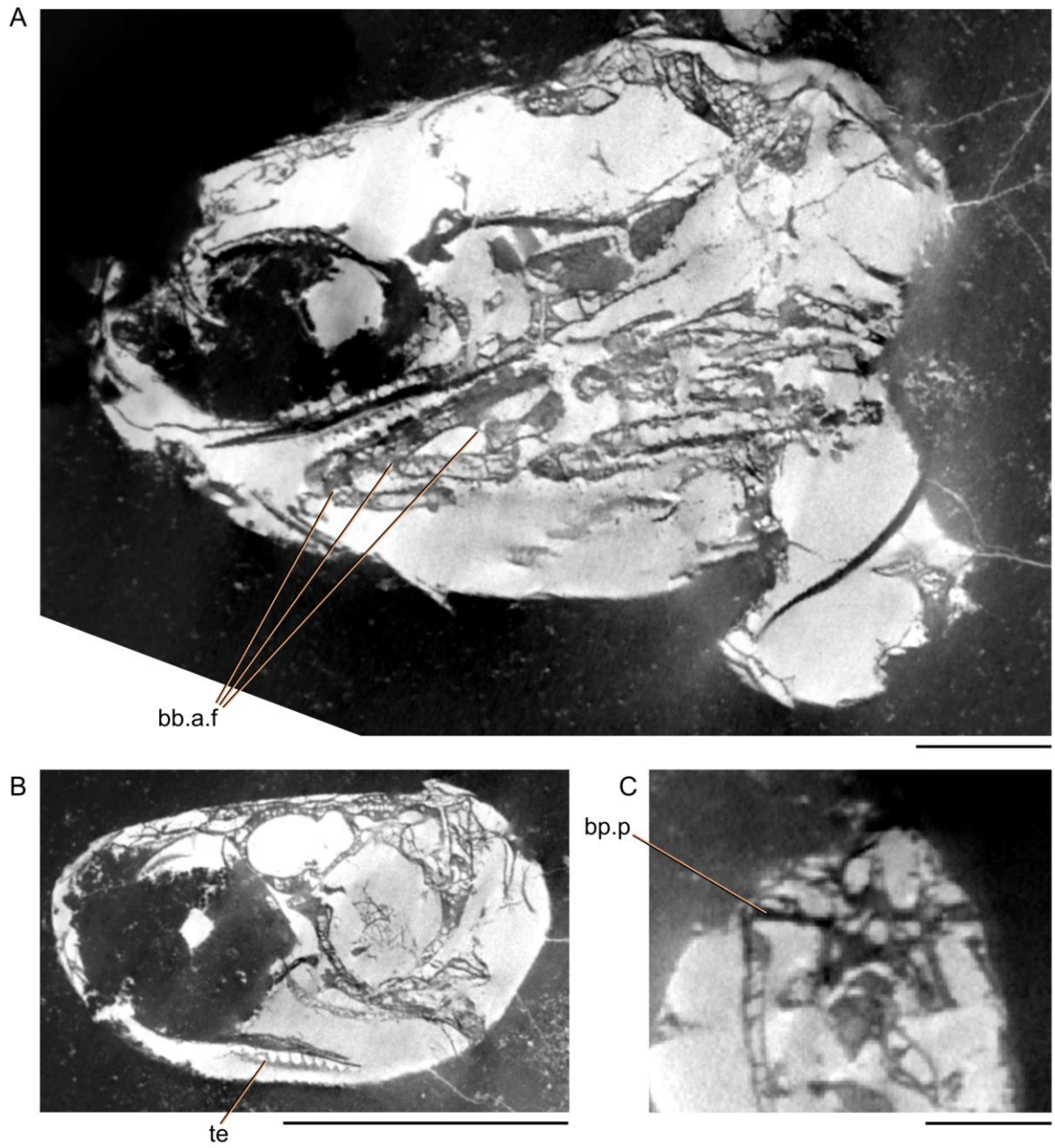

Figure 3.7 – CT sections through the skull of CP 5073. (A) Parasagittal section through the skull showing the articular facets for the hypobranchials in the basibranchials. (B) Parasagittal section through the skull showing the lower jaw dentition. (C) Transverse section through the base of the neurocranium showing the dermal component of the basipterygoid process. bb.a.f, basibranchial articulation facet for the hypobranchials, bp.p, basipterygoid process, te, teeth. Scale bar = 5 mm.

To the dorsal surface of the otico-occipital region of the braincase bears the large diamond-shaped fossa bridgei and the crista of the posterior semicircular canal. The anterodorsal fontanelle is long and ellipsoid in dorsal view. It extends from the level anterior to the basisphenoid to the level of the anterior margin of the vestibular fontanelle. The posterodorsal fontanelle is shaped as

a short ellipse with its longest axis being laterally oriented towards the margins of the otico-occipital fissure. The ventral surface of the otico-occipital region of the neurocranium is well preserved. Posterior to the rear termination of the parasphenoid at the lateral end of the ventral otic fissure there is a small groove with a foramen leading to the saccular chamber. This foramen indicates the passage of the palatine ramus of the facial nerve (VII_{pal}). The vestibular fontanelle seems to have been large but due to the poor preservation it is not possible to determine its exact shape. The vestibular fontanelle is contiguous with the otico-occipital fissure. Posteriorly on the external wall of the saccular chamber, close to the otico-occipital fissure, there is a small protuberance that could be the articulation facet for the first epibranchial. At the posterior end of the jugular depression, just in front of the margin of the otico-occipital fissure there is a structure that seems to be the remnant of the exit of the glossopharyngeal nerve (IX). There is no evidence of a discrete notch for the passage of the vagus nerve (X) through the otico-occipital fissure. The ventral surface of the aortic canal is perforated by a small, rounded foramen for the passage of the epibranchial arteries. More anteriorly the aortic canal becomes an exposed groove that splits before reaching the ventral otic fissure. On the posterior surface of the otic region the foramen magnum seems to have been small in comparison to the notochordal opening which is large and oval. The notochordal canal is deep extending up to the level of the vestibular fontanelles. More ventrally, the aortic foramen is small and round. The dorso-lateral prominence of the occipital ossification is small and slightly curved being closer to the area of insertion of the intermuscular septa than in other Paleozoic actinopterygians. The craniospinal fossa is relatively small and shallow being curved at a 45-degree angle toward the dorsal wall of the foramen magnum. The ventral margin of the craniospinal fossa is delimited by a notch that separates it from the craniospinal process.

3.3.1.5 Endocast

The endocranial cavity is well preserved with the exception of the anteriormost portion of the ethmoid region, reflecting the apparent lack of mineralization of this portion of the braincase. Due to the low contrast between bone and matrix, combined with poor preservation, most of the canals of cranial nerves do not show well in the 3D model of the endocavity space.

The forebrain region of the endocast includes the small paired olfactory bulbs that lies at the anteriormost portion of the telencephalic chamber. Anterior to the olfactory bulbs there is a

long and ventrally directed olfactory tract which would hold the passage of the olfactory nerve (I). There is no dichotomization of this canal through the extent of the preserved portion of the braincase. The telencephalic chamber is small and round. Posterodorsally to the telencephalic chamber there is a vertical expansion of the diencephalon, the epiphyseal canal, which seems to be individualized from the anterodorsal fontanelle. There is no clear boundary between the telencephalic and diencephalic regions. The forebrain region bears a ventral protrusion corresponding to the the hypophyseal region, but it seems to be incomplete.

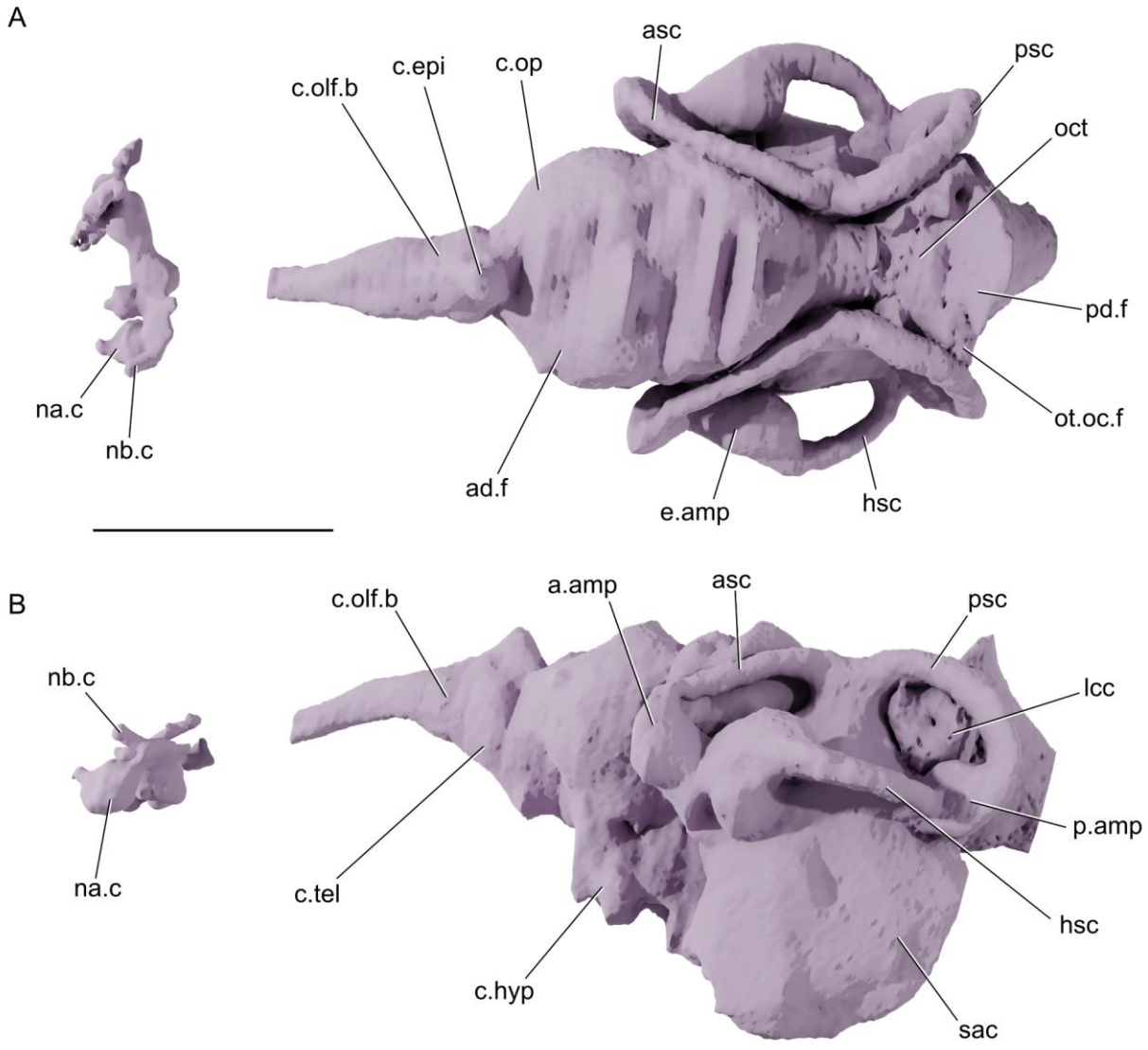

Figure 3.8 – Render of the endocast of the holotype of Actinopterygii gen. et sp. nov. (CP 065) in (A) dorsal and (B) left lateral views.a.amp, anterior ampullae, ad.f, anterodorsal fontanelle, asc, anterior semicircular canal, c.epi,

epiphyseal chamber, c.hyp, hypophyseal chamber, c.olf.b, chamber for the olfactory bulbs, c.op, chamber for the optic lobes, c.tel, telencephalic chamber, e.amp, external ampullae, hsc, horizontal semicircular canal, lcc, lateral cranial canal, na.c, nasal capsule, nb.c, nasobasal canal, oct, area octavolateralis, ot.oc.f, otico-occipital fissure, p.amp, posterior ampullae, pd.f, posterodorsal fontanelle, psc, posterior semicircular canal, sac, saccular chamber. Scale bar = 5 mm.

The dorsal portion of the mesencephalic region is well preserved, showing clearly separated bilateral lobes of the optic tectum, plus the opening of the anterodorsal fontanelle, which extends posteriorly to the auricles. The mesencephalic bulbs are large and round, showing a small protrusion on the left side where the trochlear nerve (cranial nerve IV) would pass. The floor of the mesencephalic region is poorly preserved, lacking definition on the region where the oculomotor nerve (cranial nerve III) is expected to emerge. Despite this, the anteroventral portion of the mesencephalic region shows the medial exit of the optic nerves (cranial nerve II). This tract defines an almost right angle with the long axis of the endocast. In dorsal view posterior to the mesencephalic lobes, a V-shaped margin separates the optic tectum region from the cerebellar auricle region. The auricles are elongated lobes which diverge anteriorly. The mediodorsal margin of this region is poorly defined due to the contact with the opening of the anterodorsal fontanelle. The posterior margin of the auricles is delimited by a deep invagination that separates it from the inner ear portion of the endocavity space.

The area octavolateralis is visible dorsally between the left and right cruss commune. It contacts the cerebellar auricles anteriorly and the myelencephalic lobe posteriorly. The area octavolateralis in this specimen is slender and short, concave in dorsal view. The area octavolateralis is separated from the inner ear by a deep invagination. Posteriorly on the rhombecephalic region of the endocast there is the expanded myelencephalic bulb, which is laterally expanded and transversely cut by the otico-occipital fissure. Its dorsal surface is mostly formed by the posterodorsal fontanelle. Posteriorly the rhombecephalic region is constricted towards the foramen magnum. Exits of the occipital nerves cannot be resolved in the scans.

The inner ear, including the skeletal labyrinth, is well-preserved on both sides of the specimen. The anterior semicircular canal extends from the cruss commune reaching the level of the optic tectum-auricle contact anteriorly. This canal terminates with a closed curve leading to the anterior ampulla. The anterior ampulla is flattened laterally and round in lateral view. Ventrally it contacts the commissure with the external ampulla. The horizontal (or external) semicircular canal is short and C-shaped in dorsal view. It extends from the anteriormost portion of the posterior

ampulla and terminates anterior at the external ampulla, which is oval in shape, slightly expanded mesiolaterally towards the crus commune. The external ampulla also bears a ventral rounded expansion. The posterior semicircular canal is shorter than the anterior semicircular canal and curves at its posterior end towards the posterior ampulla. The posterior ampulla is small and round in lateral view, forming the posterior end of the horizontal semicircular canal. The crus commune, representing the connection between anterior and posterior semicircular canals, is higher than the roof of the octavolateralis region of the endocast. Ventrally on the inner ear region the sacculus chamber is large and exhibits a rounded lateral surface. Ventrally it bears the passage of the vestibular fontanelle and connects to the otico-occipital cranial fissure.

3.3.1.6 Hyobranchial apparatus

The well-preserved hyoid arch consists of a hyomandibula, at least one interhyal, two ceratohyals, and a hypohyal.

The hyomandibula is dorsally oriented forming and expands dorsally towards the articulation with the braincase. There is a small but visible opercular process, which is dorsoventrally oriented. It is not possible to determine whether the hyomandibula was perforated or not. Ventral to the hyomandibula there is a subspherical ossification identified here as a single interhyal, that seems to have participated in the jaw articulation. The ceratohyal is divided in two independent ossifications. The anterior one is larger, tapering anteriorly towards the hypohyals and bears the groove for the afferent hyoid artery. The groove crosses the ceratohyal through its longest axis. The posterior ceratohyal is smaller and sub-rectangular in shape, with a grove for the afferent hyoid artery along its ventral margin. The hypohyals are shaped as flattened cones which curve anteriorly towards the central axis of the branchial skeleton.

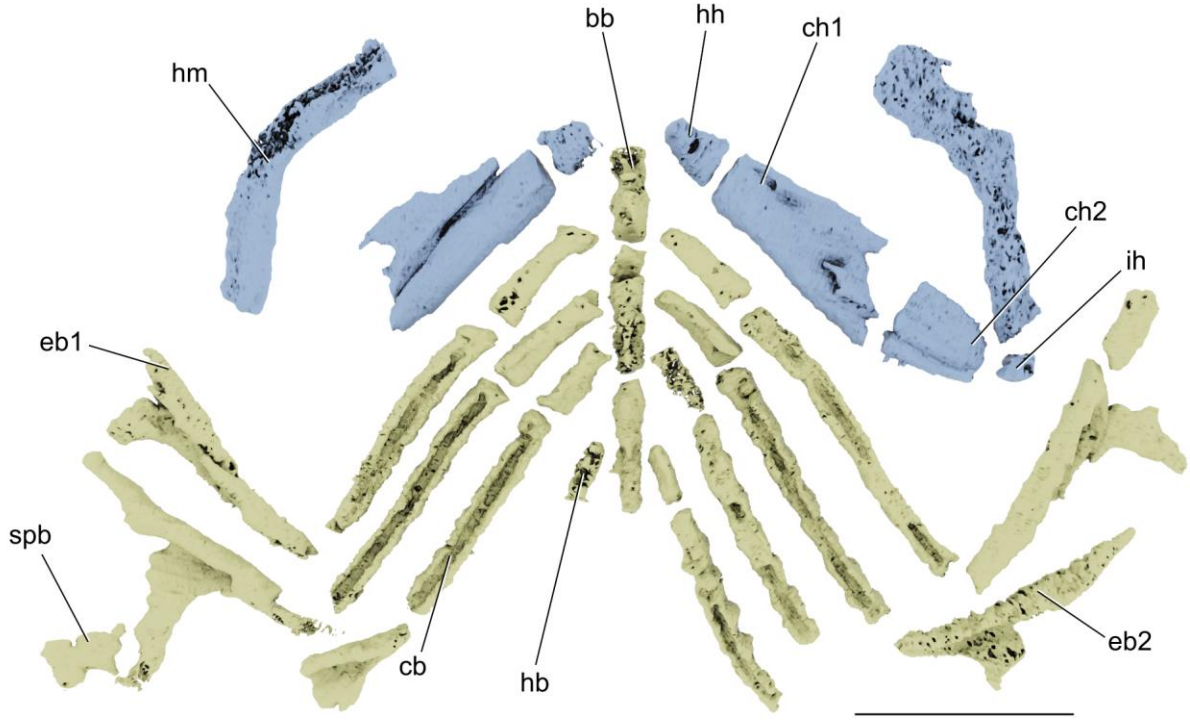

Figure 3.9 – Render of the hyobranchial apparatus of CP 065, reconstructed to interpretative position. bb, basibranchial, cb, ceratobranchial, ch, ceratohyal, eb, epibranchial, hb, hypobranchial, hh, hypohyal, hm, hyomandibula, ih, interhyal, spb, suprapharyngobranchial. Scale bar = 10 mm.

The branchial apparatus is almost complete, including basibranchials, hypobranchials, ceratobranchials and epibranchials. The basibranchial appears to consist of three individual ossificiations. The small, cylindrical anteriormost basibranchial serves as articulation for the first pair of hypobranchials posteriorly. The second basibranchial is almost twice the length of the first hypobranchial. It bears an hourglass shaped process medially on its ventral margin, probably for articulation with the second and third pair of basibranchials. The third basibranchial is of the same size as the second basibranchial, but slightly tapering posteriorly. The fourth pair of hypobranchials articulates with the ventromedial portion of the third basibranchial. There is no evidence of dentition on the basibranchials. CP 5073 clearly shows the articular facets for the hypobranchials on the ventrolateral faces of the basibranchials. The first pair of hypobranchials is cylindrical but expands anteriorly towards the articulation with the first basibranchial. The second pair of hypobranchials differs from the first pair only by lacking this anterior expansion. The third pair of hypobranchials is short and seems to have a double head—one ventral one dorsal—for articulation with the second basibranchial. The last pair of hypobranchials is reduced to small

cylinders. The ceratobranchials are long and bearing the groove for the branchial arteries ventrally. The length of the ceratobranchials decreases gradually with posterior pairs. Only the first and second pairs of epibranchials are preserved, with the third epibranchial being preserved only on the right side. The first pair is long and rod-like, bearing the groove for the branchial arteries dorsally and a large uncinate process. The second pair of epibranchials has a large uncinate process as long as the main body of the epibranchial. The second epibranchial is shorter and bears a smaller rectangular uncinate process. An anterior process on the head of the second epibranchial extends towards the ventral surface of the braincase. There is evidence of a small conical bone articulating anteriorly to the main body of the left first epibranchial. This bone is interpreted as an infrapharyngobranchial. On the right second epibranchial, dorsal to the uncinate process, there is a small plate-like bone. It is rhomboid in lateral view, tapering anterodorsally. This bone is identified as a suprapharyngobranchial.

3.3.1.7 Operculogular series

The preopercle seems to follow the contour of the underlying hyomandibula, but it is not possible to detect the passage of the preopercular sensory canal since the lateral surface of this bone is incomplete. The preopercle tapers when reaching the posterodorsal margin of the maxilla, and then bends over it expanding, forming a spatulate anterior end. In CP 7227 the well-preserved preopercle shows a large spatulate anterior end almost the same height as the maxilla and exhibits almost 90-degree curvature towards the posterior expansion. The opercle and subopercle are rhomboid and large, being almost equal in size. The dorsal margin of the opercle is straight where it contacts the skull roof. The contact between opercle and subopercle is smooth, arching dorsally at its posterior end. Bones of the opercular series are unornamented on their external faces. The branchiostegal series is not visible on the exposed surface, but a reconstructed model of the internal space of the skull region reveals a median gular anteriorly, followed by branchiostegals that become progressively longer posteriorly along the series. A small drop-shaped median gular is present. It is not possible to confirm the presence of lateral gulars.

3.3.1.8 Shoulder girdle

CP065 is represented mostly by the cephalic region, but it preserves also the anteriormost part of the post-cranium. The shoulder girdle is partially complete, showing well-developed triangular clavicles that articulate with the blade-like cleithrum. The contact between the cleithrum and clavicle is clearest on the right side of the specimen, showing the triangular margin between these two ossifications. There is no evidence of an interclavicle or the endoskeletal ossifications associated with the pectoral fin articulation (e.g. scapulocoracoid). CP 5073 shows the imprint of the dorsalmost portion of the dermal shoulder girdle, indicating the presence of a large supracleithrum bearing a deep sensory canal for the lateral line.

In CP 065 the right pectoral fin is partially preserved, as well as the endoskeletal pectoral girdle. The endoskeletal pectoral girdle is partially compressed laterally and therefore it is not possible to identify the mesocoracoid arch in the holotype. In CP 5073 the scapulocoracoid is preserved in detail, showing a large oblique supracoracoid foramen. The mesocoracoid arch is thin and relatively short in relation to the height of the scapulocoracoid. The mesial surface of the coracoid is only slightly concave, indicating a restricted ventral muscle canal. Both anterior and mesocoracoid processes of the scapulocoracoid are well-developed. In CP 065 the articulation surface for the fin radials is also partially preserved and seems to have been oriented almost dorsoventrally. The fin radials are incomplete but show the presence of a large propterygium dorsally. Due to the poor preservation it is not possible to determine if the propterygium was perforated. The propterygium is followed by two small hammer-shaped radials. The metapterygoid is rod-shaped and seems to articulate with a smaller rod-like element.

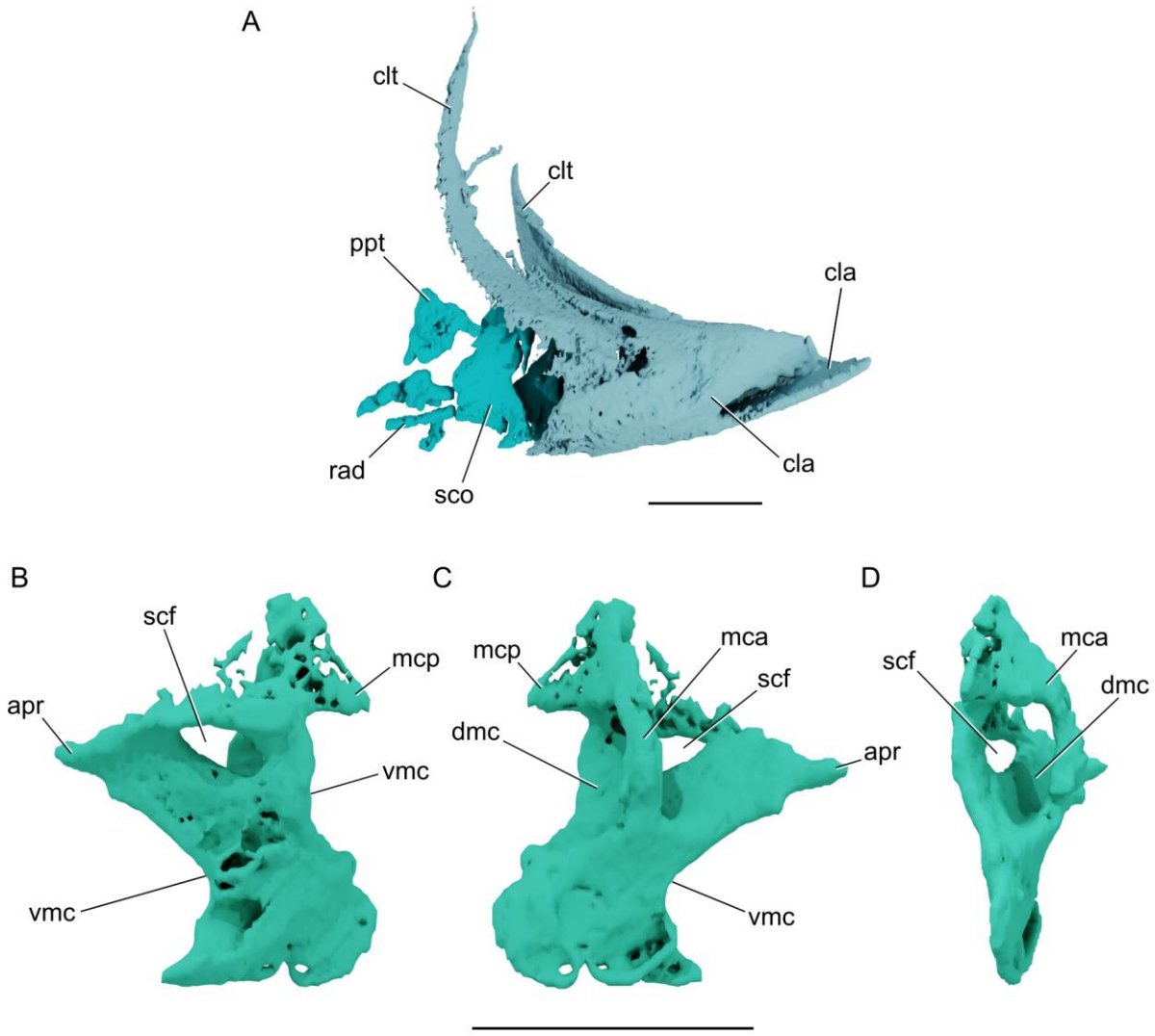

Figure 3.10 – Render of the pectoral girdle of Actinopterygii gen. et sp. nov. 1. (A) Shoulder girdle of the holotype (CP 065) in right lateral view. (B-D) Scapulocoracoid of CP 5073 in (B) lateral, (C) mesial, and (D) anterior views. apr, anterior process, cla, clavicle, clt, cleithrum, dmc, dorsal muscle canal, mca, mesocoracoid arch, mcp, mesocoracoid process, ppt, propterygium, rad, radials, scf, spracoracoid foramen, sco, scapulocoracoid, vmc, ventral muscle canal. Scale bar = 5 mm.

3.3.1.9 Vertebral column

Vertebral elements are present in the holotype (CP 065) but are preserved in greater detail in CP 5073. The first vertebral segment is composed of individualized basidorsal and interdorsal elements forming the neural arch and spine, whereas the ventral portion is formed by a robust basiventral. The first basiventral almost completely encloses the aortic canal, which is only open dorsomesially. CP 5073 shows the basidorsal elements bearing well-developed lateral basidorsal

processes, but there is no evidence of foramen for the intersegmental artery. Basidorsal lateral processes are visible in CT sections of the holotype, but cannot be segmented due to lack of consistent contrast. The second basiventral is much smaller than the first and is formed by paired robust elements. Subsequential basiventrals are also paired but less robust than the two anteriormost basiventrals. A few of the vertebral segments of CP 5073 show a median element distal to the neural spine of the basidorsal. These represent supraneurals.

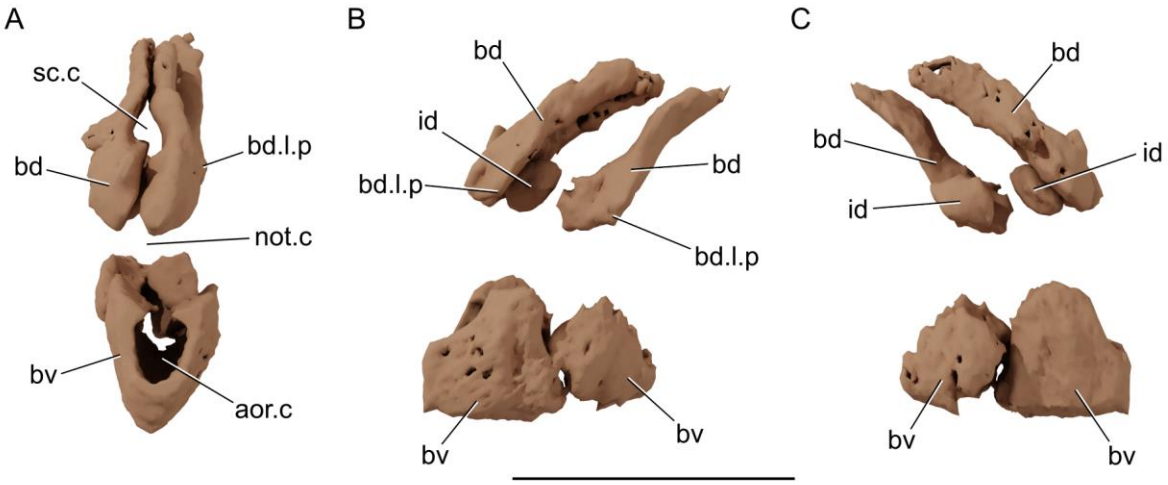

Figure 3.11 – Render of anteriormost vertebral elements of Actinopterygii gen. et sp. nov. 1 (CP 065) in (A) anterior, (B) left lateral and (C) right lateral views. aor.c, basiventral aortic canal, bd, basidorsal, bd.l.p, basidorsal lateral process, bv, basiventral, id, interdorsal, not.c, notochord canal, sc.c, spinal chord canal. Scale bar = 5 mm.

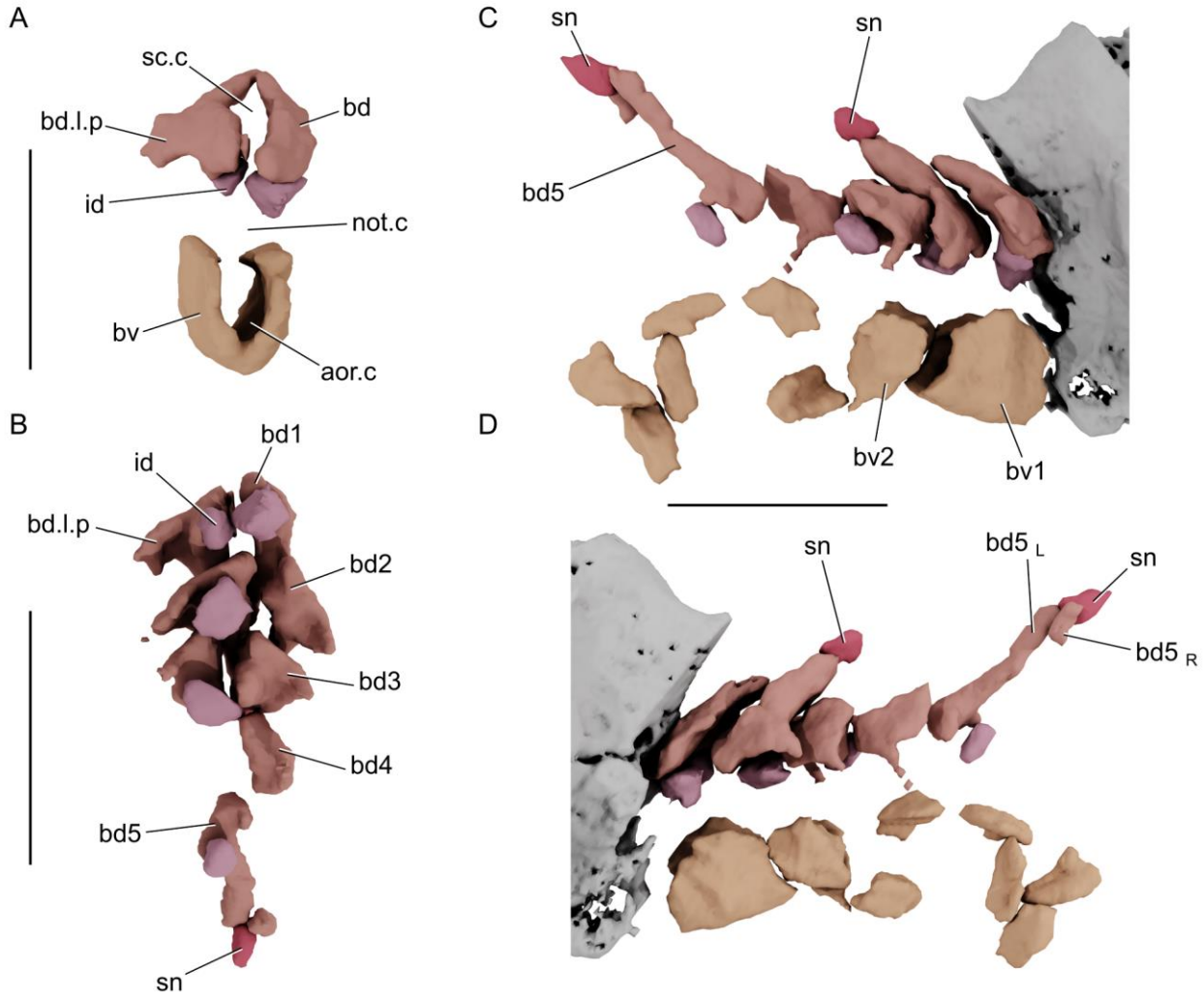

Figure 3.12 – Renders of the vertebral column of CP 5073 in (A) anterior, (B) ventral, (C) right lateral and (D) left lateral views. aor.c, basiventral aortic canal, bd, basidorsal, bd.l.p, basidorsal lateral process, bd1-5, basidorsals 1 through 5, bdL-R, basidorsal left and right, bv, basiventral, id, interdorsal, not.c, notochord canal, sc.c, spinal chord canal, sn, supraneural. Scale bar = 5 mm (A); 5 mm (B); 5 mm (C-D).

3.3.1.10 Scales

Only the scale rows closely associated with the skull and shoulder girdle are preserved. These scales show the typical rhomboid shape and are ornamented with transverse ridges. The posterior border of the scales seems to be serrated, but this feature is more clearly distinguishable in the ventral flank scales. The posterodorsal flank scales bear a different ornament, formed by thinner ridges that are parallel to the anterior margin of the scale before curving posteriorly on the scale

ventral portion. It is not possible to determine the absence or presence of peg-and-socket articulation.

3.3.2 Actinopterygii gen. et sp. nov. 2

Type material: CP 584 (holotype), a three-dimensionally preserved skull and anteriormost portion of the body preserved in a concretion.
Additional material: CP 084, CP 242, CP 508, CP 577, CP 916, CP 1239

Diagnosis: Actinopterygian defined by the following combination of features. An inclined suspensorium; broad spatulate end of the hyomandibula; one ceratohyal ossification; two or more interhyal elements; one interhyal element contributes to hyoid articulation; dermohyal closely associated with the hyomadibula but not fused to it; short uncinate processes on the first and second epibranchials; well-developed fossa bridge; diverging olfactory canal; short horizontal semicircular canal; ellipsoid anterodorsal fontanelle; straight parasphenoid; large basipterygoid processes of sphenoid with a dermal component contributed by the parasphenoid; basipterygoid fenestra on the palatoquadrate; multiple ossification centers within the palatoquadrate; first basiventral not roofing the aortic canal.

Description:

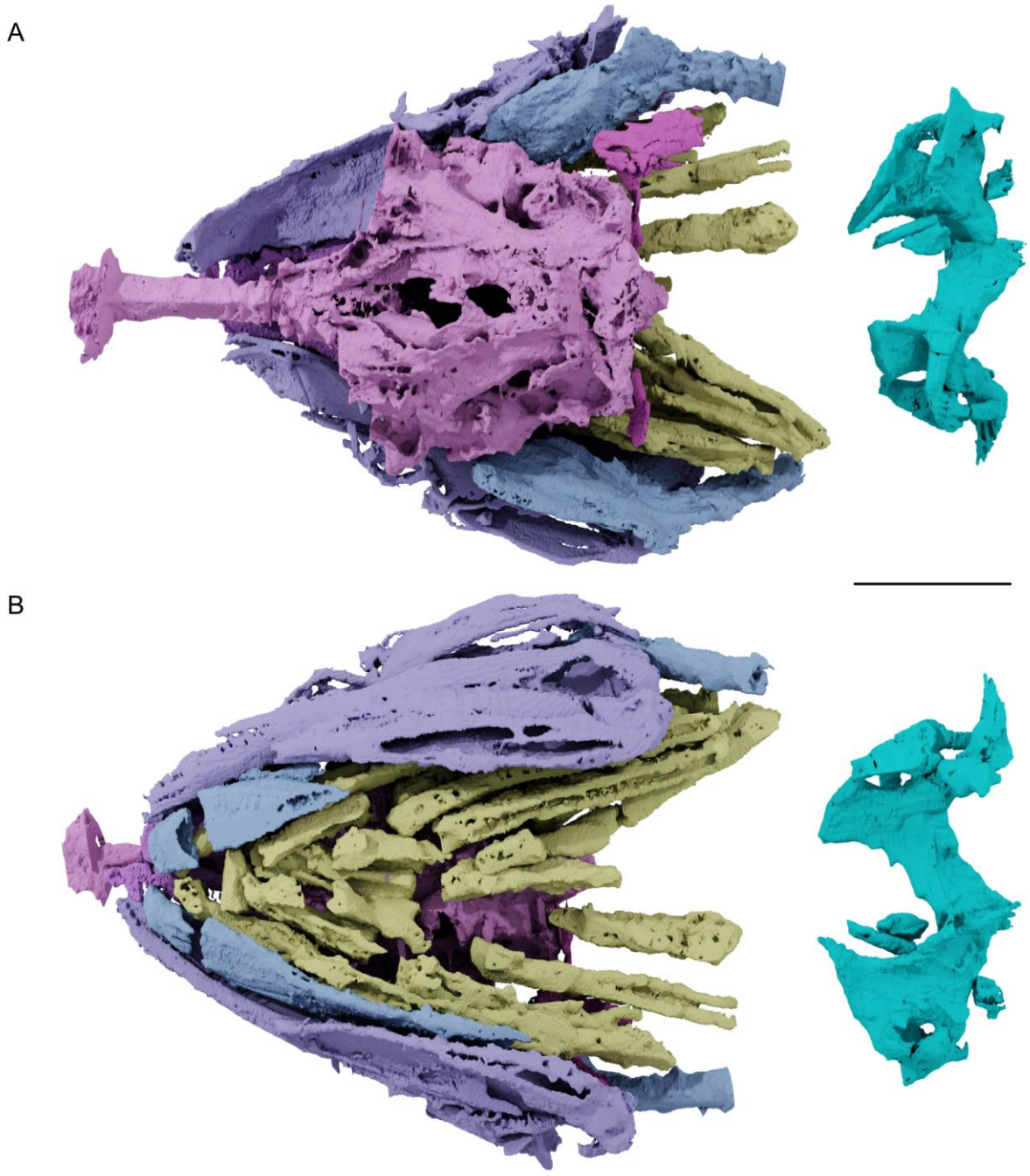

Figure 3.13 – Renders of the holotype of Actinopterygii gen. et sp. 2 (CP 584) in (A) dorsal and (B) ventral views. Scale bar = 10 mm.

3.3.2.1 Skull roof

The skull roof of CP 584 is poorly preserved, and the boundaries between individual bones are not clearly visible. Posteriorly the bones of the skull roof are not preserved, exposing the braincase. Anteriorly it is possible to see the passage of the supraorbital sensory canal coming from the snout. This canal arches laterally after the orbit before disappearing in the missing part of the skull roof. In CP 577 the skull roof is preserved as an impression in the matrix, showing the same arrangement of canals observed in CP 585. Unfortunately, given poor preservation it is not possible to determine sutures between individual components of the skull roof. In CP 577 large postemporals are visible. Anteriorly to these there is a canal perpendicular to the body midline which would mark the position of the extrascapulars. CP 916 shows large posttemporal bones marking the posterior margin of the skull roof.

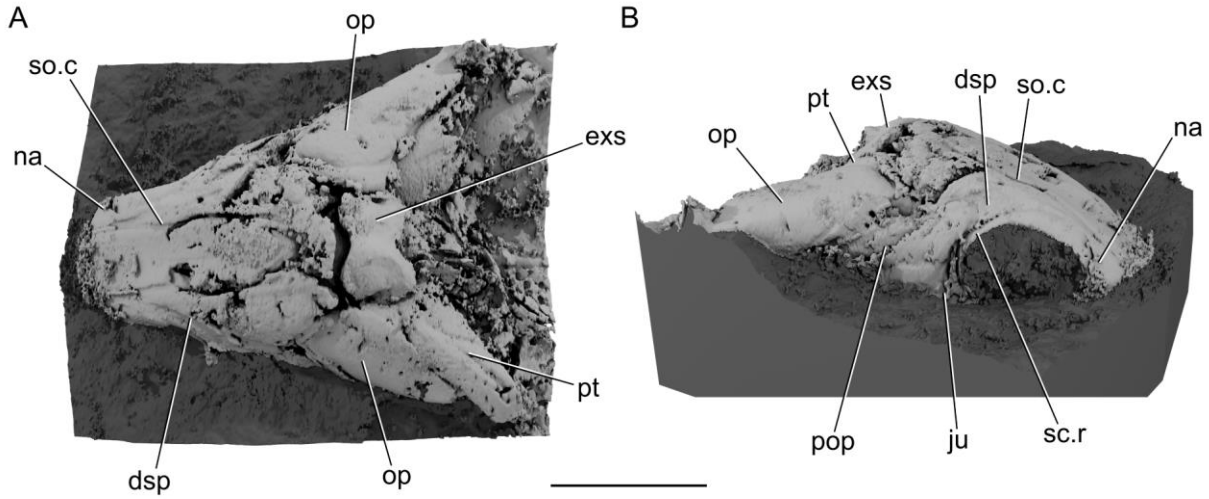

Figure 3.14 – Render of the positive model of CP 577 in (A) dorsal and (B) anterolateral views.
dsp, dermosphenotic, exs, extrascapular, ju, jugal, na, nasal, op, opercle, pop, preopercle, pt, posttemporal, sc.r, sclerotic ring, so.c, supraorbital canal. Scale bar = 10 mm.

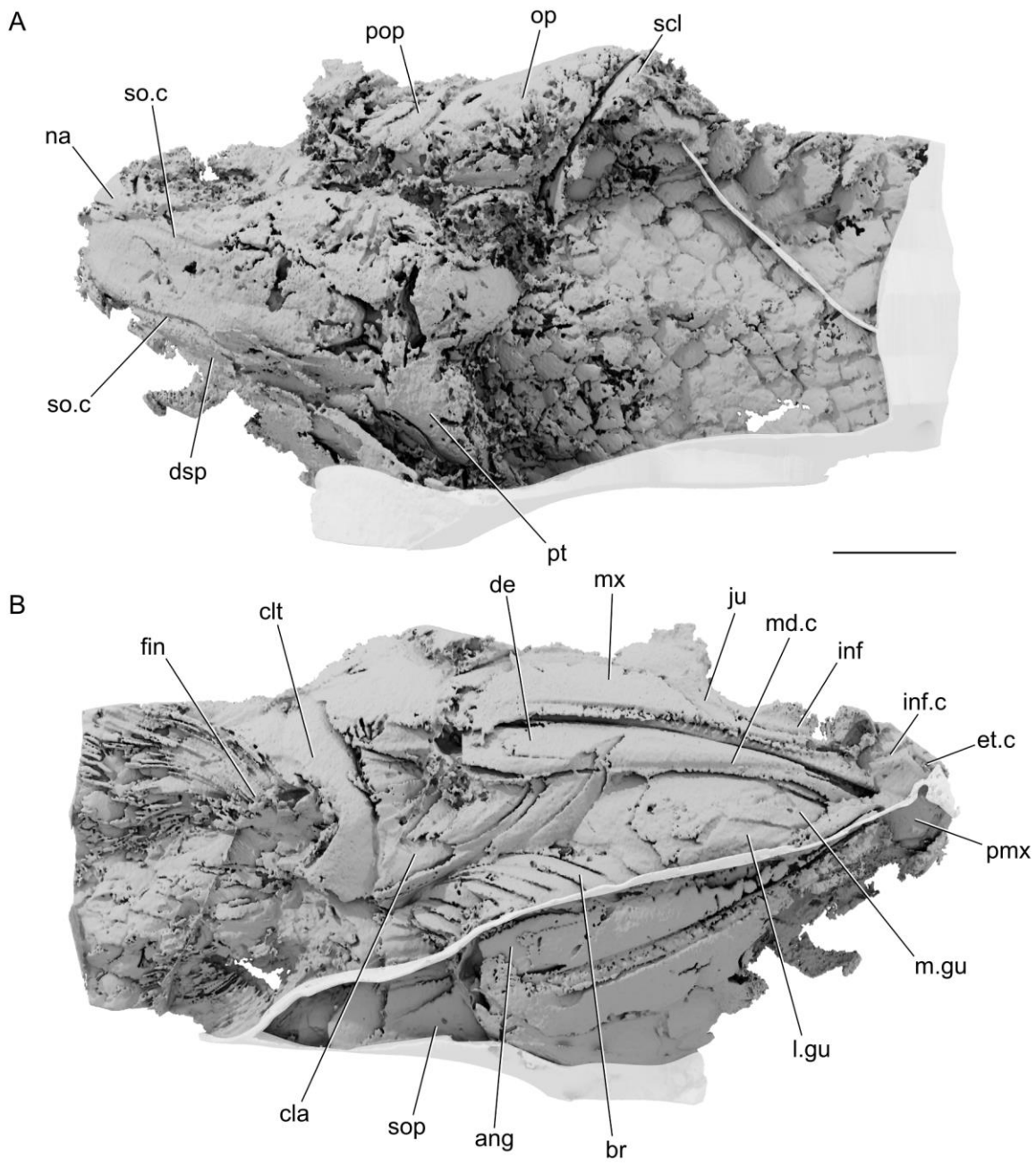

Figure 3.15 – Renders of the positive model of CP 916 showing the impression of dermal bones of the skull, pectoral girdle and squamation. ang, angular, br, branchiostegal rays, cla, clavicle, clt, cleithrum, de, dentary, dsp, dermosphenotic, et.c, ethmoidal commisure, inf, infraorbital, inf.c, infraorbital canal, ju, jugal, l.gu, lateral gular, m.gu, median gular, md.c, mandibular canal, mx, maxilla, na, nasal, op, opercle, pmx, premaxilla, pop, preopercle, pt, postemporal, scl, supracleithrum, so.c, supraorbital canal sop, subopercle. Scale bar = 10 mm.

3.3.2.2 Jaws and palate

The lateral surface of the maxilla and dentary are apparent in a positive model of the void space within the concretion and do not seem to show any ornamentation. The maxilla exhibits a long postorbital blade and rounded tooth sockets posteroventrally. The dentary is long and with a straight dorsal margin, with the ventral margin tapering anteriorly. CP 084, CP 242 and CP 1239 provide additional information on the jaws and palate.

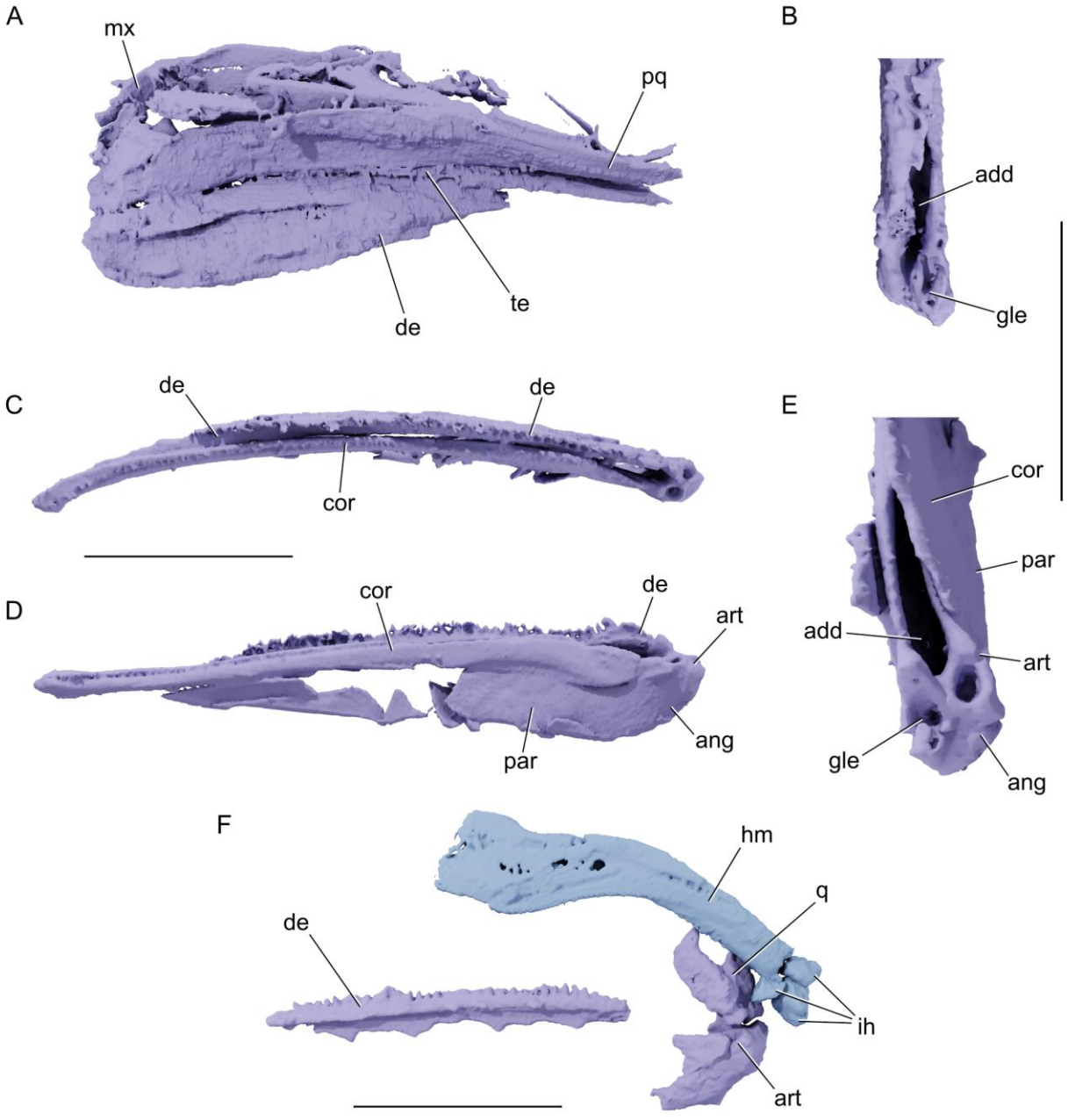

Figure 3.16 – Renders of the jaws of selected specimens of Actinopterygii gen. et sp. nov. 2. (A) Upper and lower jaws of CP 584 in mesial view. (B) Proximal end of right lower jaw of CP 584 in dorsal view. Right lower jaw of CP 916 in (C) dorsal and (D) mesial views. (E) Proximal end of left lower jaw of CP 916 in dorsal view. (F) Right jaws of CP 242 in mesial view. add, adductor fossa, ang, angular, art, articular, cor, coronoid, de, dentary, gle, glenoid, hm, hyomandibula, ih, interhyal, mx, maxilla, par, prearticular, pq, palatoquadrate, te, teeth. Scale bar = 10 mm (A, C, D); 10 mm (B,E); 10 mm (F).

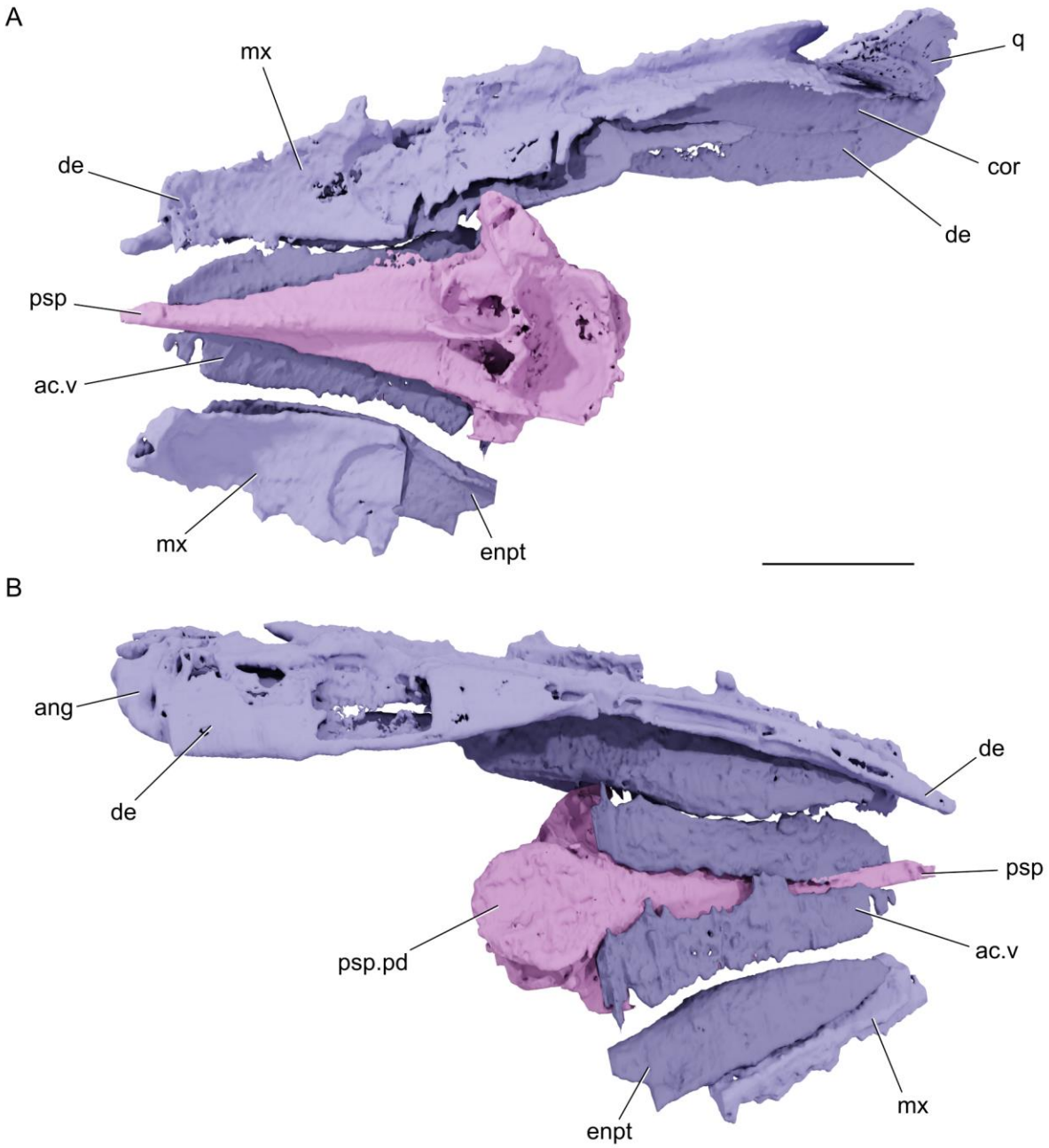

Figure 3.17 – Renders of the jaws, palate and paraspheonoid of CP 1239 in (A) dorsal and (B) ventral views. ac.v, accessory vomer, ang, angular, cor, coronoid, de, dentary, enpt, entopterygoid, mx, maxilla, psp, parasphenoid, psp.pd, posterior dermal expansion of the parasphenoid, q, quadrate. Scale bar = 10 mm.

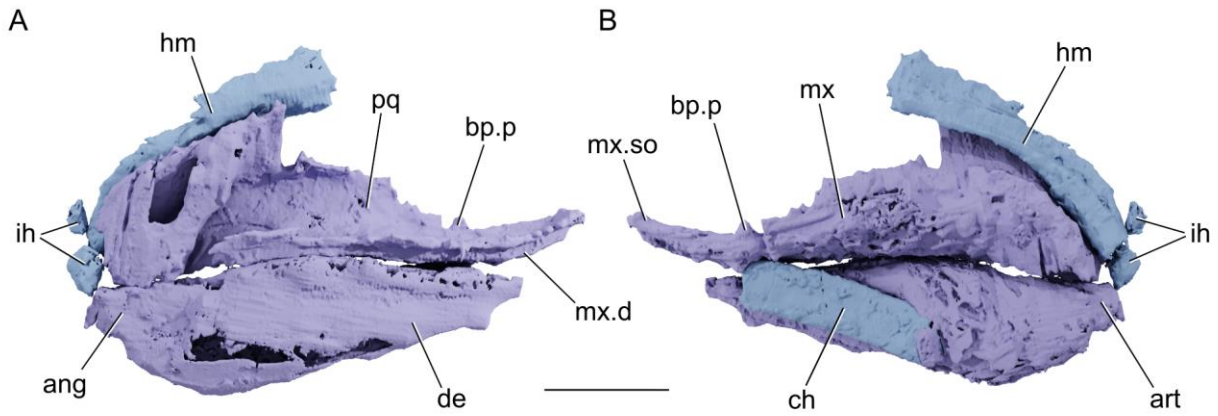

Figure 3.18 – Renders of the right jaws and hyoid arch of CP 084 in (A) lateral and (B) mesial views. ang, angulur, art, articular, bp.p, basipterygoid process, ch, ceratohyal, de, dentary, hm, hyomandibula, ih, interhyal, mx.d, dentigeous margin of maxilla, mx.so, suborbital process of maxilla, pq, palatoquadrate complex. Scale bar = 10 mm.

The palatoquadrate seems to have two ossification centers, one in the metapterygoid region and one in the entopterygoid region. The metapterygoid ossification lies dorsolaterally on the dermal bones of the palate, being almost completely hidden in mesial view. The articulation of the palate with the neurocranium is made through an articulation facet that is dorsally open. The margins of this facet are formed by two processes that extend from the metapterygoid region of the palatoquadrate. Anterior to this metapterygoid process the autopalatine region of the palatoquadrate tapers anteriorly and is bordered mesially by a thin and seemingly edentulous accessory vomer, which completes the roof of the mouth between the palate and the parasphenoid. The ventrolateral border of the palatoquadrate is bordered by a thin dermopalatine region, with minute conical teeth along its entire length. It is not possible to determine the number of dermopalatine ossifications. The palatoquadrate is separated from the parasphenoid anterior process by a long accessory vomer that goes all the way towards the parasphenoid body posteriorly. There is no evidence of a vomer due to poor preservation of the snout region.

The lower jaw is incompletely preserved on both sides of the holotype. As indicated above, the lateral surface of the dentary is only clear in the positive cast of the void space inside the concretion. The mesial surface, although incomplete, shows a robust prearticular forming the mesial border of the adductor fossa, which is bound anteriorly by a poorly preserved coronoid ossification showing evidence of dentition. There is a single row of conical teeth on the dentary. A thick artcular bone wall completes the gap between the prearticular/coronoids and the ventral margin of the lower jaw mesially. The articular is poorly preserved but shows the rounded

glenoid fossa. Ventrally below the adductor fossa in mesial view there is a thick bone extension forming the ventral wall of the lower jaw and seemingly fused to the articular. However, it is not possible to determine if this is part of the articular or angular ossifications.

In CP 916 the lower jaw is preserved in exquisite detail. The external surface of the dentary is obscured by direct contact with the matrix, making it difficult to determine presence of ornamentation. Dorsally the dentary is also poorly preserved but show the presence of small conical teeth. In mesial view the lower jaw shows the posterior border of the articular, with the remaining portion being covered by the large prearticular that forms almost the entire posteromesial surface of the lower jaw. Dorsally the prearticular is overlaid by the single coronoid, that is independent from the remaining jaw bones and extend towards the jaw symphysis. The dorsal surface of the coronoid contributes to the dentigerous margin of the jaw and is covered in small conical teeth of similar size to those of the dentary. The glenoid fossa is well preserved and biconcave, with the external cotyle being slightly more posterior and larger in diameter. The adductor fossa is formed by the dentary laterally, the articular posteriorly and the prearticular plus coronoid mesially. It is laterally compressed and elongated anteriorly. On the posterior margin of the adductor fossa, in front of the external glenoid fossa there is a small tubercle-like coronoid process that extends dorsally.

3.3.2.3 Circumorbital series

Most of the circumorbital series is too poorly preserved to permit description. The infraorbital sensory canal is visible through the anteroventral half of the orbital margin, but it is not possible to determine the extent of the dermal bones or sutures between them. The jugal seems to be missing from both sides of the skull in the holotype but a small incomplete lunate jugal is present in CP 1239, bearing the passage of the infraorbital sensory canal and no evidence of posterior rami. The supraorbital series is also too poorly preserved to allow a description in the holotype.

3.3.2.4 Neurocranium

The neurocranium of CP 584 is well preserved and threedimensional, with the exception of the dorsal sphenotic portion, which seems to be missing. Additionally, the ventral surface of

the neurocranium is partially affected by the compression contacting the underlying branchial arches and jaw bones. Thus, details of the anatomy of the ventral surface of the neurocranium are partially based on CP 577.

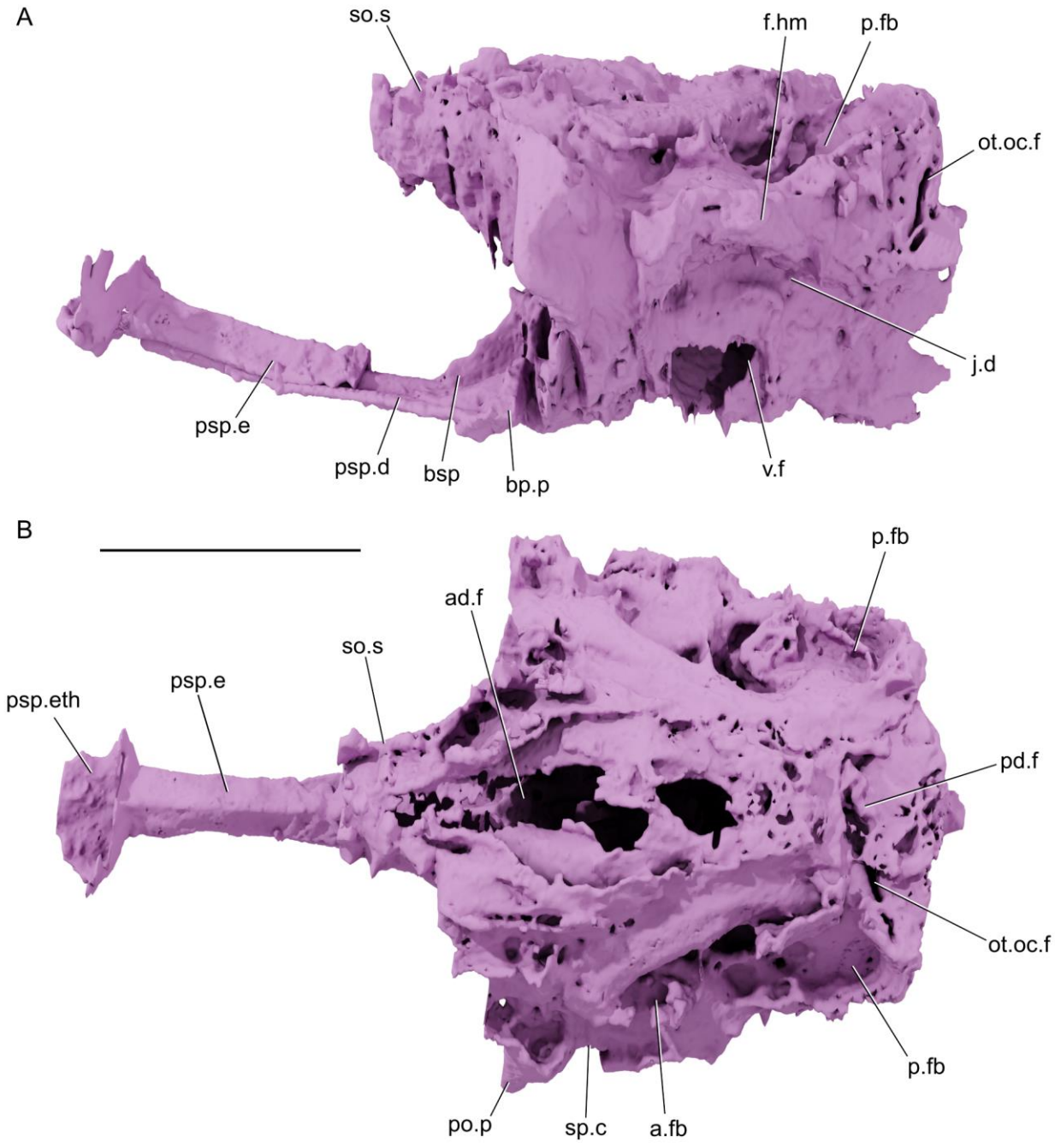

Figure 3.19 – Render of the neurocranium of the holotype of Actinopterygii gen. et sp. nov. 2 (CP 065) in (A) left lateral and (B) dorsal views. a.fb, anterior fossa bridgei, ad.f, anterodorsal fontanelle, bp.p, basipterygoid process, bsp, basisphenoid, f.hm, hyomandibular facet, j.d, jugal depression, ot.oc.f, otico-occipital fissure, p.fb, posterior fossa bridgei, pd.f, posterodorsal fontanelle, po.p, postorbital process, psp.d, dermal parasphenoid, psp.e, ventral

sphenoid, psp.eth, ethmoidal region of parasphenoid, so.s, supraorbital shelf, sp.c, spiracular canal, v.f, vestibular fontanelle. Scale bar = 10 mm.

The sphenoid is almost complete and expands posteriorly towards the basipterygoid processes. The basipterygoid processes are broad-based and triangular in dorsal view, being separated from the neurocranium body posteriorly by a thin notch. The dermal parasphenoid body is caret-shaped in transversal cross section, due to its concave ventral surface, which becomes deeper posteriorly below the basisphenoid.

The basipteryoid processes seem to have a dermal component associated with their distal end. There is no evidence of dermal ascending processes of the parasphenoid posterior to the basipterygoid processes in any of the specimens. In CP 577 there are clear grooves for the spiracle that extend from the posterolateral margin of the parasphenoid to the top of the braincase following the postorbital blade. Both CP 577 and CP 123 bear a spoon-shaped posterior end of the dermal component of the parasphenoid that underlies the posterior myodome. In CP 584, the anterior portion of the sphenoid is displaced within the orbital area. It preserves the anterior ethmoid process and has a caret shape in cross-section. In ventral view of CP 577 and CP 1239 there is a robust and circular dermal component forming the posterior end of the parasphenoid, reaching the anterior end of the ventral occipital fissure.

Dorsal to the sphenoid body there is a small median lamina, forming the basisphenoid. Laterally to the basisphenoid there is a shallow groove for the passage of the internal carotid arteries. This same groove seems to be slightly expanded ventrally, possibly for the insertion of the superior, inferior and internal rectus muscles. Posterior to the basisphenoid there is a single median posterior myodome. Posterodorsally on the posterior myodome there is a small pair of foramina, but due to preservation it is not possible to determine whether it was for the pituitary vein or the abducens nerve (VI). There is no evidence of a buccohypophyseal foramen in any of the specimens. A large foramen putatively interpreted as the palatine branch of the facial nerve (VIIpal) and the orbital artery is visible lateroventral to the posterior myodome in CP 577.

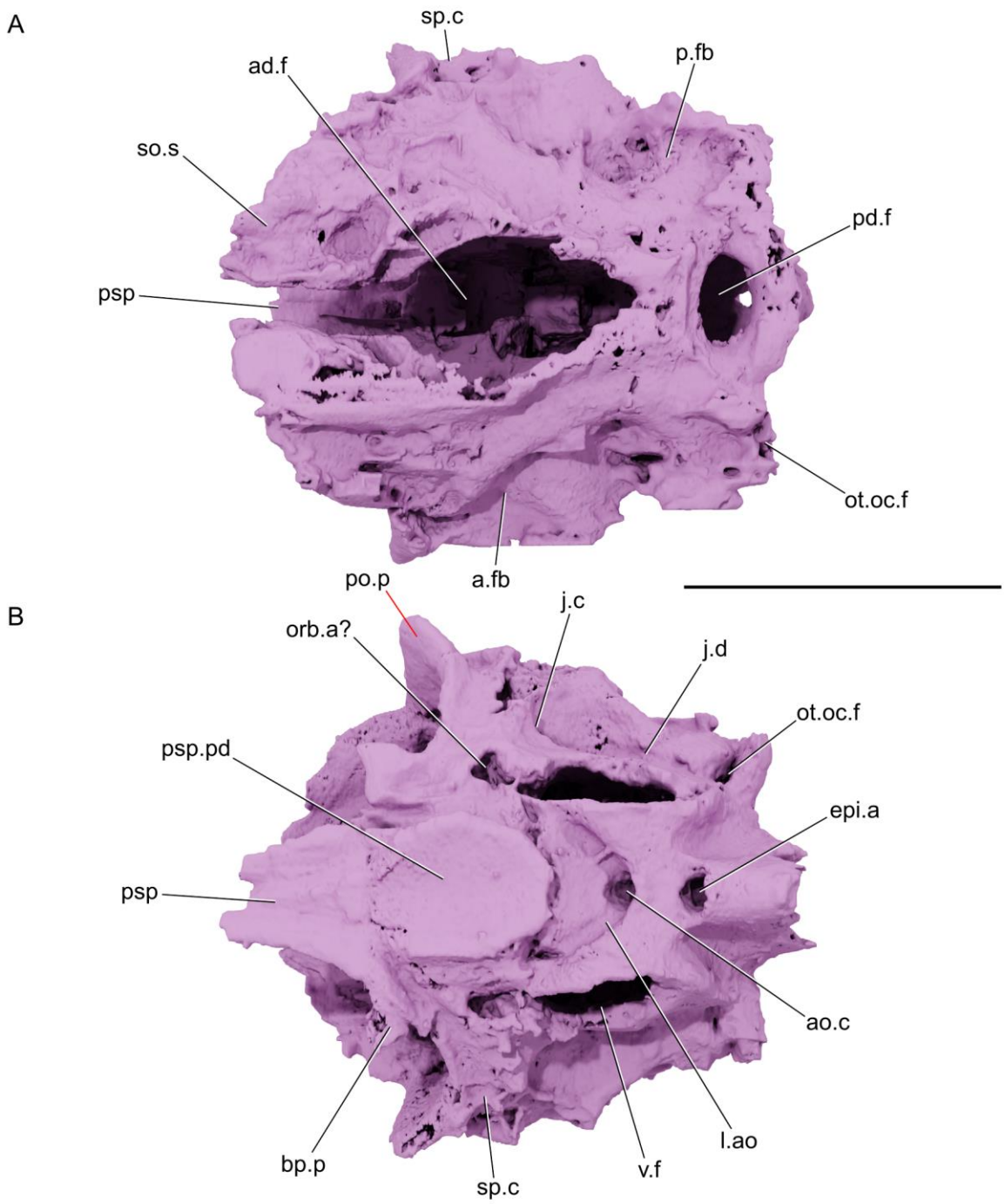

Figure 3.20 – Renders of the neurocranium of CP 577 in (A) dorsal and (B) ventral views. a.fb, anterior fossa bridgei, ad.f, anterodorsal fontanelle, bp.p, basipterygoid process, epi.a, foramen for the epibranchial arteries j.c, jugal canal, j.d, jugal depression, l.ao, lateral aortae, orb.a, foramen for the orbital artery, ot.oc.f, otico-occipital fissure, p.fb, posterior fossa bridgei, pd.f, posterodorsal fontanelle, po.p, postorbital process, psp, parasphenoid, psp.pd, posterior dermal expansion of the parasphenoid, so.s, supraorbital shelf, sp.c, spiracular canal, v.f, vestibular fontanelle. Scale bar = 10 mm.

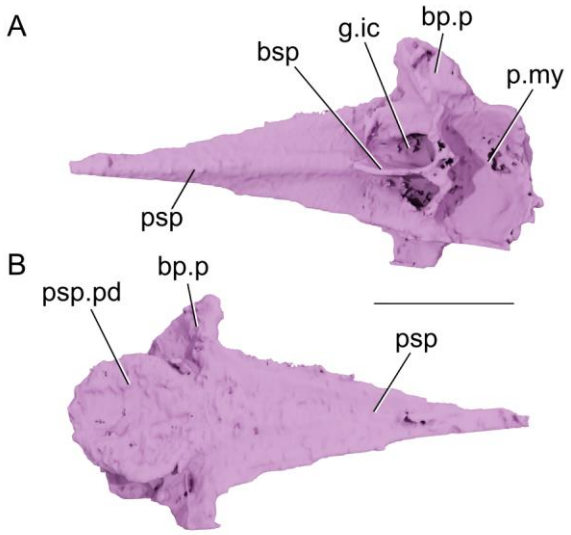

Figure 3.21 – Renders of the parasphenoid of CP 1239 in (A) dorsal and (B) ventral views. bp.p, basipterygoid process, bsp, basisphenoid, g.ic, groove for the internal carotid arteries, p.my, posterior myodome, psp, parasphenoid, psp.pd, posterior dermal expansion of the parasphenoid. Scale bar = 10 mm.

The orbital tectum is partially incomplete, but part of the supraorbital ridge is visible posterodorsally. Dorsal to the supraorbital ridge there are two delicate lateral ridges that would go toward the ethmoid portion of the braincase roof. A large, robust postorbital process defines the posterodorsal corner of the orbital recess. Between the postorbital process and the posterior myodome it is possible to see the anterior opening of the jugal canal in anterior view. At the mouth of this opening there is a small foramen for the passage of trigeminal nerve (V). The anterior opening of the jugal canal is below the level of the postorbital process. The posterior opening of the jugal canal is higher than the anterior opening and located ventral to the large hyomandibular articulation facet. Posterior to this opening there is a continuation of the jugal path through a small groove.

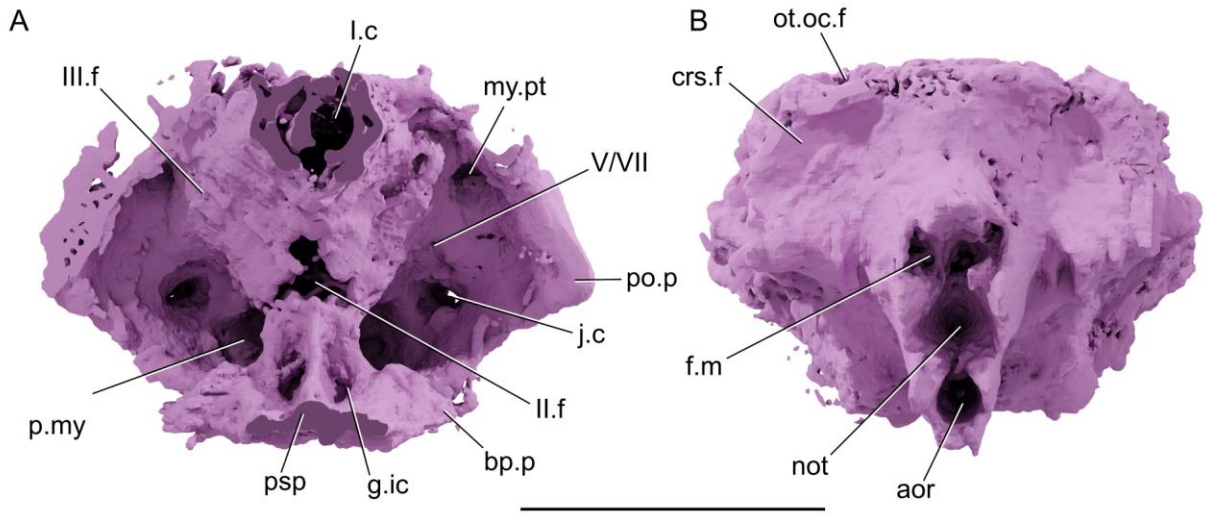

Figure 3.22 – Renders of the neurocranium of CP 065 in (A) anterior and (B) posterior views. aor, aortic canal, bp.p, basipterygoid process, crs.f, craniospinal fossa, f.m, foramen magnum, g.ic, groove for the internal carotid artery, j.c, jugal canal, my.pt, myodome for the pterygoideus muscle, not, notochord canal, ot.oc.f, otico-occipital fissure, p.my, posterior myodome, po.p, postorbital process, psp, parasphenoid, I.c, canal for the olfactory nerve (I), II.f, foramen for the optic nerves (II), III.f, foramen for the oculomotor nerve (III) V/VII, trigeminofacial foramen. Scale bar = 10 mm.

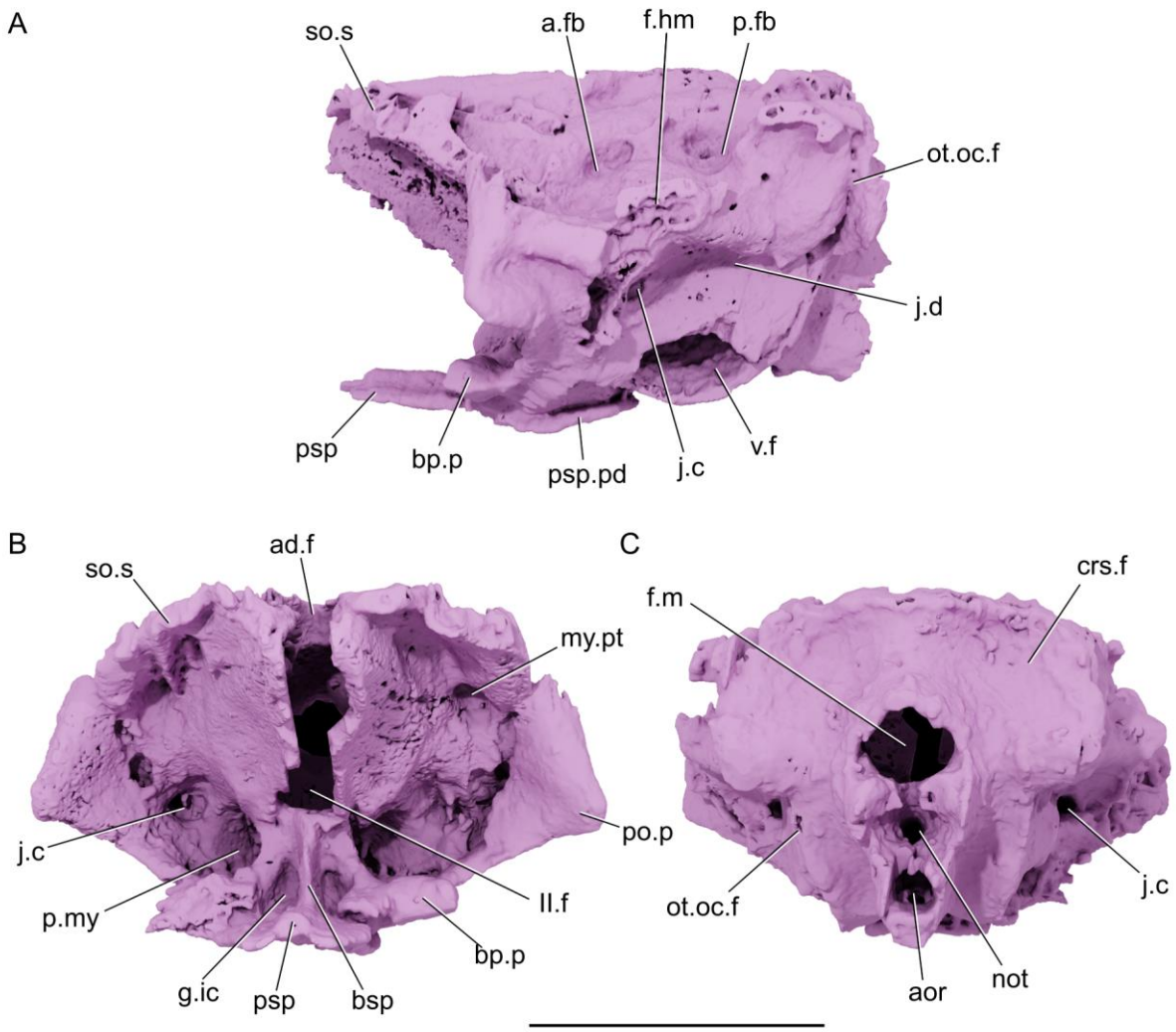

Figure 3.23 – Renders of the neurocranium of CP 577 in (A) left lateral, (B) anterior and (C) posterior views. a.fb, anterior fossa bridgei, ad.f, anterodorsal fontanelle, aor, aortic canal, bp.p,, basipterygoid process, bsp, basisphenoid, crs.f, craniospinal fossa, f.hm, hyomandibular facet, f.m, foramen magnum, g.ic, groove for the internal carotid artery, j.c, jugal canal, j.d, jugal depression, my.pt, myodome for the pterygoideus muscle, not, notochord, ot.oc.f, otico-occipital fissure, p.fb, posterior fossa bridgei, p.my, posterior myodome, psp, parasphenoid, psp.pd, posterior dermal expansion of the parasphenoid, so.s, supraorbital shelf, II.f, foramen for the optic nerve (II).
Scale bar = 10 mm.

The braincase roof has a large anterodorsal fontanelle anteriorly. It defines an elongated ellipsis in dorsal view and extends anterior up to the border between the optic tectum and telencephalon roofs. Posterodorsally on the roof of the braincase there are the large posterior fossa bridgei, bordered mesially by the posterior semicircular canal crista. This crista is poorly preserved on both sides of the braincase roof but seems to have been short. At the anterior end of these cristae there is no evidence of the striated region overhanging the posterodorsal fontanelle. The posterodorsal fontanelle is poorly preserved in the holotype but CP 577 shows a clear

ellipsoid shape with the longest axis coinciding with the otico-occipital fissure. The roof of the occipital portion of the braincase is too poorly preserve to allow description.

The wall of the occipital region of the braincase is mostly formed by the lateral prominences. These mark the external margin of the concavity of the epaxial musculature attachment. The foramen magnum protrudes from the occiput and has a circular profile. Ventral to the foramen magnum there is the conical pit for the notochord, which extends up to the posterior end of the otic portion of the braincase ventrally. At the ventralmost portion of the occiput there is the small opening for the passage of the aortic artery.

3.3.2.5 Endocast

The endocast is well-preserved with the exception of the anterior extension of the olfactory nerve canals. Unfortunately, the resolution of the scan and the preservation of the neurocranium do not permit description of most of the canals of the cranial nerves. The overall shape of the endocast agrees with that of most other late Paleozoic actinopterygians with well-ossified neurocrania.

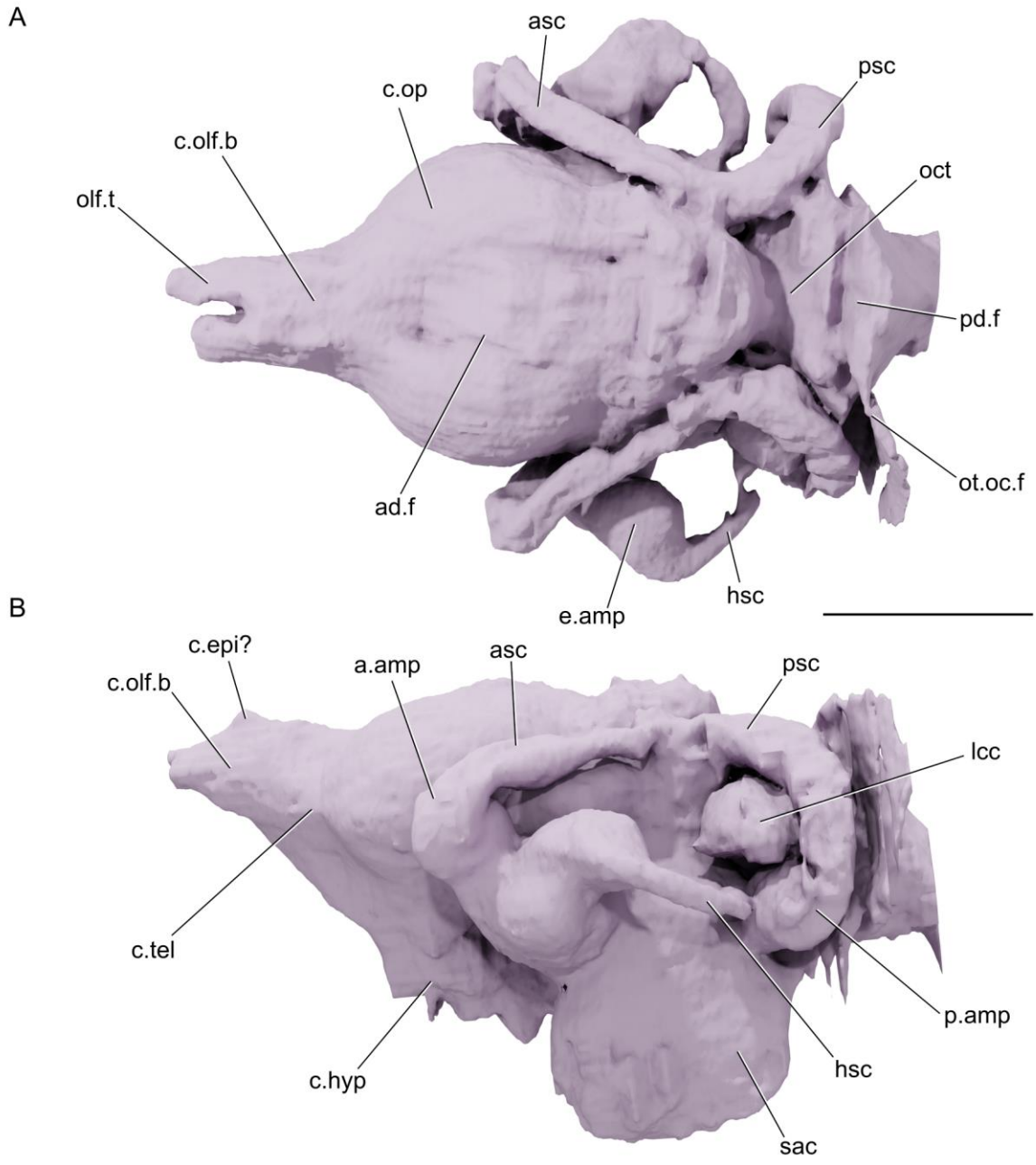

Figure 3.24 – Renders of the endocast of the holotype of Actinopterygii gen. et sp. nov. 2 (CP 584) in (A) dorsal and (B) left lateral views. c.hyp, hypophyseal chamber, c.olf.b, chamber for the olfactory bulbs, c.op, chamber for the optic lobes, c.tel, telencephalic chamber, e.amp, external ampullae, hsc, horizontal semicircular canal, lcc, lateral cranial canal, na.c, nasal capsule, nb.c, nasobasal canal, oct, area octavolateralis, ot.oc.f, otico-occipital fissure, p.amp, posterior ampullae, pd.f, posterodorsal fontanelle, psc, posterior semicircular canal, sac, saccular chamber. Scale bar = 5 mm.

The olfactory nerve canals appear to bifurcate as soon as they leave the olfactory bulb cavity. The olfactory bulbs are not directly distinguishable from the telencephalon as they seem

to form a single confluent cavity. The only demarcation between these two regions is a slight change in the concavity angle in lateral view, marking the proximal portion of the olfactory bulbs. Dorsal to the olfactory bulbs plus telencephalon complex there is a dorsal expansion defined here as an epiphyseal chamber. On the ventral portion of the forebrain region of the endocast, there is a robust ventral expansion marking the position of the hypophyseal chamber. There does not seem to be a clear differentiation of hypophyseal regions apart from a lateral concave surface which is probably associated with the hypophyseal recess. Ventrally there is the ventral expansion of the hypophyseal region towards the parasphenoid body, although it is not possible to determine if it would completely perforate the parasphenoid due to the poor preservation of the ventral surface of the braincase. Anterior to the hypophyseal chamber there is a flat surface that marks the common fenestra for the optic nerves (II). Posterior to the hypophyseal recess the hypophyseal chamber is confluent with the ventral surface of the otic region and there is no sign of a saccus vasculosus chamber.

The mesencephalic region of the endocast is formed mostly by the large optic tectum which seems to be divided in bilateral lobes separated by a narrow anterior dorsal fontanelle. Anteroventrally on the right side of the mesencephalic region it is possible to see the path of the oculomotor nerve (III) dorsal to the hypophyseal recess. The optic tectum, or mesencephalic bulbs, is round in shape and show a small prominence on its anteroventral surface that marks the passage of the trochlear nerve (IV). The posterior border of the optic tectum is marked by a depression that separates it from the cerebellar auricles.

The cerebellar auricles are small in comparison to the mesencephalic bulbs and are restricted to the area below the anterior semicircular canal. Dorsally the auricles meet at the midline and form an expanded cavity at the level of the posterior end of the anterior dorsal fontanelle. This median structure means it is not possible to observe an expansion related to the longitudinal dorsal vein. Posterior to the cerebellar auricles there is a deep depression marking the octavolateralis area, that lacks a cerebellar lobe. Posteriorly the octavolateralis area is confluent with the otico-occipital fissure and arches dorsally again to form the anterior border of the posterior dorsal fontanelle. On the space of the otico-occipital fissure it is possible to see the laterally expanded area marking the passage of the vagus nerve (X). Posterior to the otico-occipital fissure the endocast tapers towards the foramen magnum, not showing the foramina for the occipital arteries and spino-occipital nerve.

The inner ear of CP 584 is well preserved and mostly complete on both sides of the holotype. Considering its preservation, the description below is mostly based on the left inner ear. The semicircular canals are narrow and both anterior and posterior semicircular canals have a longitudinal groove extending along their dorsal surface, disappearing where they meet to form the crus commune. The crus commune lies below the level of the auricle roof but above the level of the roof of the posterior area octavolateralis. This feature is also clearly visible in the paratype CP 916. The anterior semicircular canal terminates anteriorly at a large round ampulla that connects to the anterodorsal portion of the ampulla of the horizontal semicircular canal. The horizontal semicircular canal is short and roughly half of its length is occupied by the external ampulla. Its posterior end connects directly to the anterior margin of the ampulla of the posterior semicircular canal. The posterior semicircular canal seems to be more robust that the other two and terminates ventrally at a small rounded ampulla. Posterior to the crus commune and below the posterior semicircular canal there is a large lateral cranial canal that does not seem to reconnect with the endocavity space anteriorly or bear any dorsal expansion. The saccular chamber is large shows the constriction marking the path of the otico-occipital fissure and connecting to a large oval vestibular fontanelle anteriorly.

3.3.2.6 Hyobranchial apparatus

Although incomplete and dorsoventrally flattened below the braincase, most of the hyobranchial apparatus is preserved in the holotype (CP 584). CP 1239 provides additional anatomical information.

The hyoid arch comprises a hyomandibula dorsally, and a ceratohyal and hypohyal ventrally. There is no evidence of an ossified interhyal or symplectic ventral to the hyomandibula in the holotype. An hourglass-shaped interhyal is present in CP 1239.

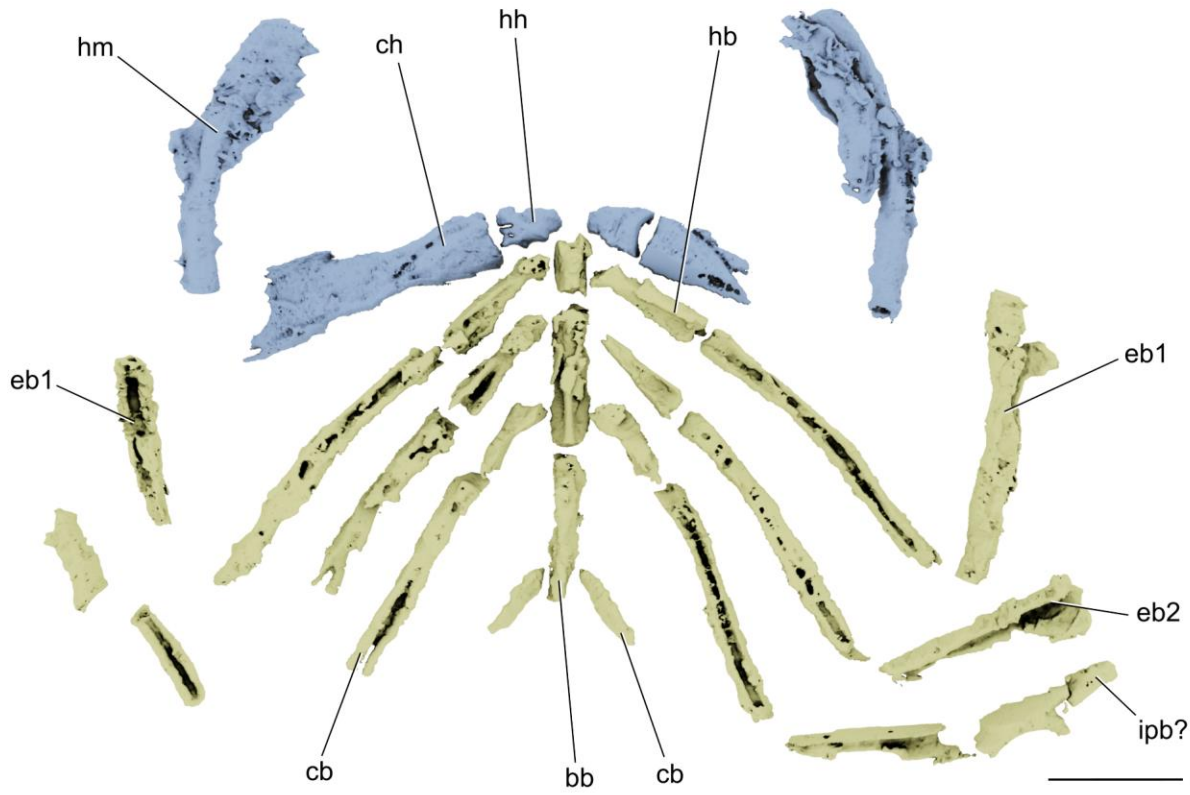

Figure 3.25 – Render of the hyobranchial apparatus of CP 065, rearticulated to interpretative position. bb, basibranchial, cb, ceratobranchial, ch, ceratohyal, eb, epibranchial, hb, hypobranchial, hh, hypohyal, hm, hyomandibula, ih, interhyal, ipb, infrapharyngobranchial. Scale bar = 10 mm.

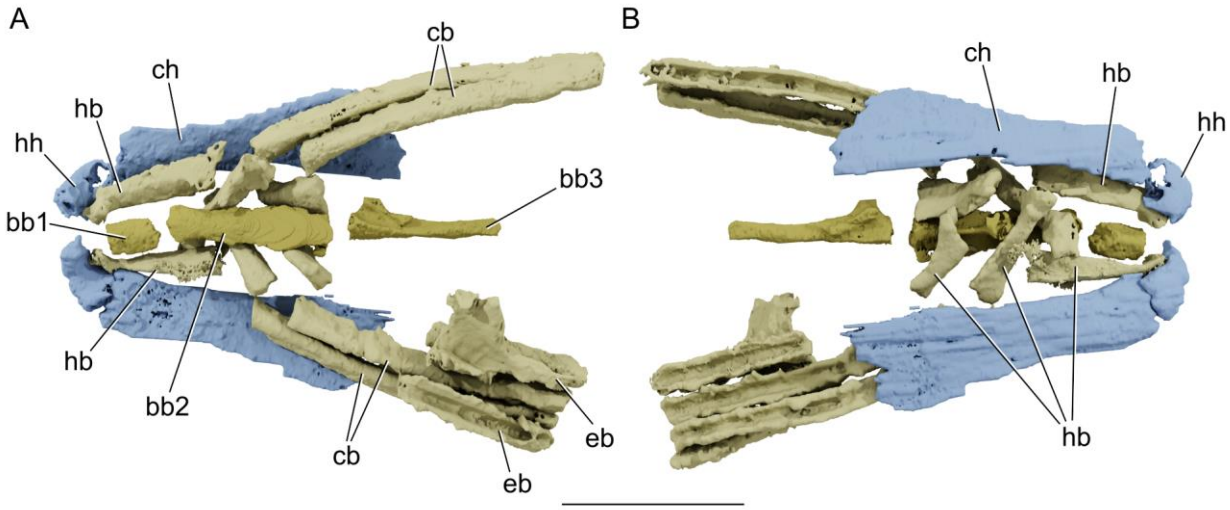

Figure 3.26 – Render of the hyobranchial apparatus of CP 1239 in (A) dorsal and (B) ventral views. bb, basibranchial, cb, ceratobranchial, ch, ceratohyal, eb, epibranchial, hb, hypobranchial, hh, hypohyal.

The branchial series is supported ventrally by three basibranchials. The anterior basibranchial is short and cylindrical, probably supporting the first hypobranchial. The second basibranchial is long and has a flat dorsal surface and a ridge ventrally, giving it a T-shape cross-section. On the ventral surface a small round projection emerging from the medial ridge. The posterior basibranchial has a differentiated anterior head, with paired small dorsal and ventral processes. Posterior to this head, the posterior basibranchial is elongated and rod-like. The hypobranchials are tube-shaped and show a slight curvature anteriorly towards the basibranchial complex and posteriorly expand at the articular surface with the ceratobranchials. A ventral groove seems to be present along the three basibranchial pairs preserved on the holotype. The ceratobranchials are undifferentiated, with the exception of posterior ones being slightly shorter than anterior ones. The anteriormost ceratobranchials possess a deep ventral groove for the passage of the branchial arteries, while the putative fifth ceratobranchial is reduced and lacks a groove. Unfortunately the epibranchials are poorly preserved due to the compression below the braincase. However, it is possible to see at least three pairs in relative detail. These epibranchials are only slightly shorter than the underlying ceratobranchials. A considerable portion of the length of the epibranchials is formed by a long anterior process expanding from the epibranchial head where the uncinate processes diverge dorsally. The uncinate processes of the first two epibranchials are broken. The process is partially preserved in the second epibranchial, bearing a broad base that indicate it could have been long in life. The third epibranchial shows a longer but still incomplete uncinate process. A flattened double-headed element is preserved anterodorsal to the second epibranchial might represent an infrapharyngobranchial, although it is too poorly preserved to permit confident identification.

3.3.2.7 Operculogular series

The operculogular series is only visible as an impression of the skull in the holotype (CP 584) and in CP 242 and CP 916. In CP 242 the opercular series is clearly visible in lateral view. The opercle is large and exhibit a rhomboidal shape, with a straight posteroventral edge. The subopercle is also rhomboidal and exhibits a rounder posteroventral edge. Its anterior margin borders the posterior end of the preopercle and its posterior margin is taller than the anterior margin. The preopercle is best preserved in CP 242, being deformed or absent in other

specimens. It shows a spatulate anterior end and an obtuse angle of the posterior process towards the jaw joint. A preopercular sensory canal is clearly visible extending through the dorsal margin of the preopercle.

In CP 242 at least eight branchiostegal rays are visible on each side of the skull, becoming taller posteriorly below the subopercle. In CP 916 the branchiostegals and gular plates are preserved in detail. Here it is possible to observe the posteriormost branchiostegal rays, giving a count of 13 rays for the whole series. The branchiostegal rays become wider anteriorly toward the gulars. There is a pair of large drop-shaped lateral gulars at the anterior end of the operculogular series, bordering the ventral margin of the dentary. In CP 916 a small ellipsoid median gular is apparent ventral to the jaw symphysis.

3.3.2.8 Shoulder girdle

The dermal shoulder girdle of Actinopterygii gen. et sp. nov. 2 is not visible in the CT-scan data of the holotype (CP 584), but the endoskeletal shoulder girdle is well-preserved. The endoskeletal girdle was partially compressed dorsoventrally so that the ventral border of each ossification contacts at midline ventrally and the dorsal borders are opposed. The ventral muscle canal seems to have been large and ellipsoid in shape, based on the extension between the dorsal and ventral extremities of the endoskeletal girdle, forming a slight concavity. The dorsal muscle canal is large and rounded, visible on both sides of the pectoral girdle. In anterior view the dorsal muscle canal is partially obscured by the curved anterior margin of the endoskeletal shoulder girdle, or anterior process (apc; Figure 3.27). The supracoracoid foramen (scf; Figure 3.27) is also well-developed and rounded in shape, being slightly oriented ventrally towards the midline of the ventral muscle canal. The coracoid plate (cop; Figure 3.27) —which forms the ventrolateral margin of the ventral muscle canal—is short and slightly curved mesially, without any evidence of foramina. The radials of the pectoral fin are still partially associated with the posterior border of the coracoid process. A robust subspherical propterygium lies dorsal to a series of axe-shaped radials. The metapterygium lies ventral to these and seems to articulated with a metapterygial process of the coracoid. The fin rays are preserved distal to the radials and show no evidence of bifurcation.

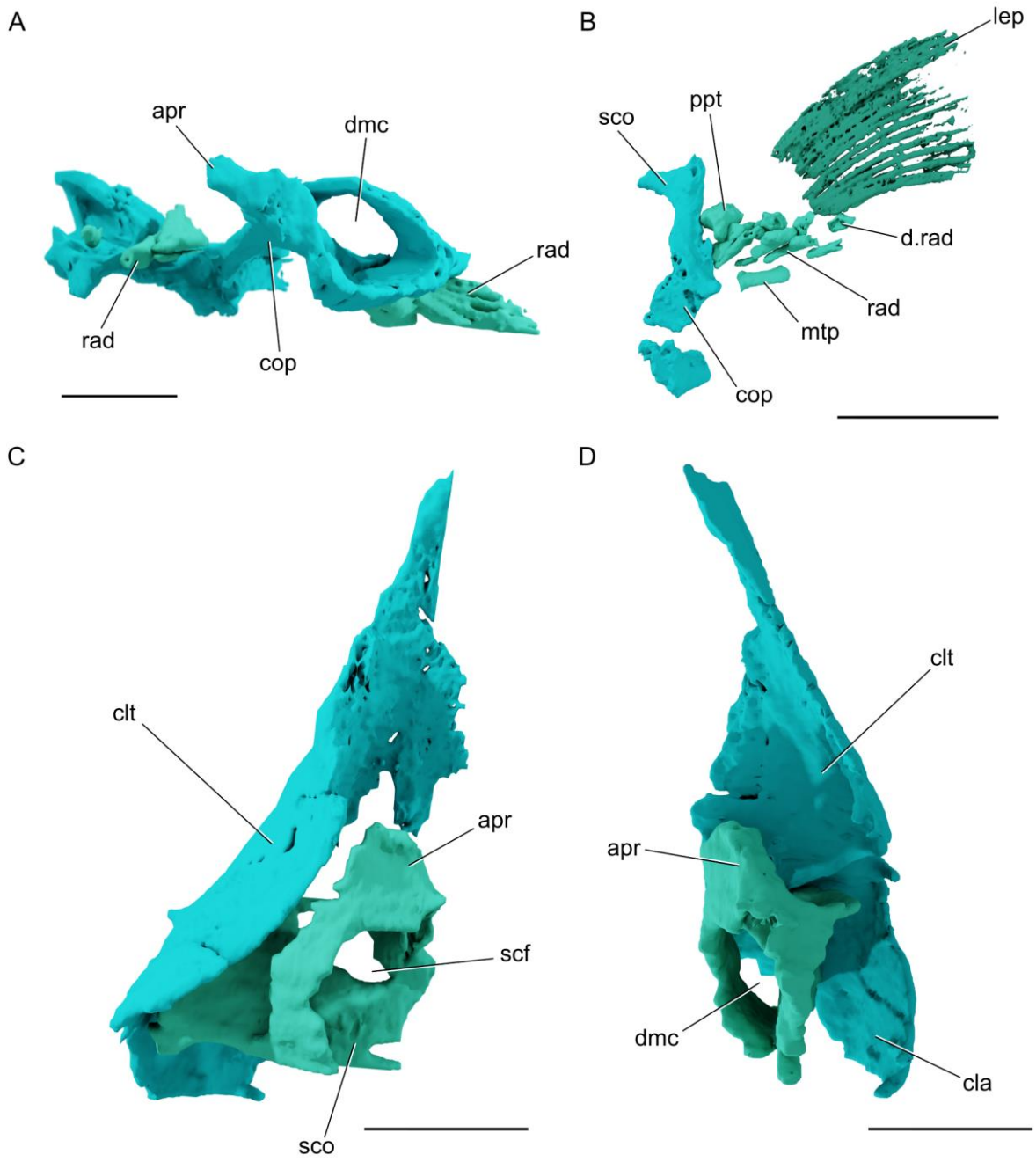

Figure 3.27 – Renders of the pectoral girdle of several specimens assigned to Actinopterygii gen. et sp. nov. 2. (A) CP 584 in anterolateral view. (B) CP 242 in mesial view. (C-D) CP 1239 in (C) mesial and (D) posterior views. apr, anterior process of the scapulocoracoid, cla, clavicle, clt, cleithrum, cop, coracoid plate, d.rad, distal radial, dmc, dorsal muscle canal, lep, lepidotrichia, mtp, metapterygoid, ppt, propterygium, rad, radial, scf, supracoracoid foramen sco, scapulocoracoid. Scale bar = 5 mm.

3.3.2.9 Vertebral column

The vertebral column of Actinopterygii gen. et sp. nov. 2 is preserved in multiple specimens. Description will focus on elements preserved in the holotype and in specimens CP 084 and CP 1239. Due to partial dorsoventral compression of the postcranium of the holotype, the vertebral elements are not preserved in detail, but there is a robust first basiventral element, which is fused ventromedially. Given the poor preservation, segmentation of vertebral elements in the holotype is not possible. In CP 1239 it is clear that the more posterior basidorsals are much smaller and more delicate than anterior members of the series, formed by paired elements with rhomboidal shape and ellipsoid cross-section. In CP 084 the dorsal portion of the vertebral segments are well-preserved. The first basidorsal is long and exhibits both an anterior and a lateral process. In more posterior basidorsal elements, there is no evidence of an anterior process, and the lateral process seems to be smaller. Filling the space between basidorsal elements ventrally there are subspherical interdorsal elements.

3.4 Discussion

3.4.1 The ray-finned fishes from the Campo Mourão Formation

The ray-finned fishes in the Permo-Carboniferous of South America are limited to a handful of examples, with many being represented by isolated or poorly diagnostic material (Mones 1986; Richter and Breitkreuz 1997; Malabarba et al. 2003; Cione et al. 2010; Figueroa and Machado 2018; Richter et al. 2022). The Paraná Basin yields the most varied late Paleozoic South American ray-finned fishes. A better understanding of these could yield important information regarding the evolution of early ray-finned fishes at high latitudes and in peri-glacial settings (Malabarba 1988; Eyles et al. 1993; Richter 2002; Figueiredo and Carvalho 2004; Hamel 2005; Mouro et al. 2020; Vesely et al. 2021; Saldanha et al. 2022; Silva et al. 2023). As mentioned above, ray-finned fishes from the latest Carboniferous to early Permian Campo Mourão Formation are poorly described in the literature, despite both known taxa (†*Santosichthys mafrensis*, †*Roslerichthys riomafrensis*) being described based on articulated and partially three-dimensional specimens. For both of these taxa, original descriptions focused on the plesiomorphic dermal skull morphology, using classical comparative work to infer the

systematic placement of these taxa along the actinopterygian stem (Malabarba 1988; Hamel 2005). However, the described morphology of these two taxa does not sufficiently differentiate them from other late Paleozoic ray-finned fishes due to the lack of endocranial characters in the holotypes and associated specimens. From examination of the holotypes of these two taxa and description and illustrations published, we agree that it is possible to differentiate these two taxa based on skull dermal bone anatomy (e.g. straight *vs* curved proximal end of the maxilla; three *vs* two infraorbitals, dorsally expanded *vs* restricted preopercle; robust *vs* delicate premaxilla).

Specimens examined here and referred to Actinopterygii gen. et sp. nov. 1 and Actinopterygii gen. et sp. nov. 2 are here considered to be new taxa because they do not show the same dermal skull features of either †*Santosichthys* or †*Roslerichthys*. None of this material shows the robust premaxilla found in †*Roslerichthys* or the expanded preopercle reaching the lateral edge of the skull roof found in †*Santosichthys*. However, given the poor preservation of external dermal bone anatomy we are cautious in our interpretations of the relationship between these new specimens and published material. Future examination of specimens identifiable to †*Santosichthys* and †*Roslerichthys* might shed light on the relationship between these to the taxa described here. However, this will only be possible using specimens that preserve sufficient details of both dermal skull and endocranium, of which we are currently unaware.

3.4.2 The morphology and systematics of early ray-finned fishes

The early evolution of ray-finned fishes has been debated for more than a century, with descriptive work dating back to the nineteenth century and interpretations of most early ray-finned fishes as ‘palaeoniscoids’, aligned to chondrostean fishes, persisting through the twentieth century (Traquair 1879, 1909; Boulenger 1902; Malabarba 1988). The study of anatomical variation of early ray-finned fishes has mostly focused on variation in dermal skull anatomy with special reference to the jaws, circumorbital series, skull roof, squamation and fin morphology (Watson 1925; White 1939; Gardiner 1967, 1984; Patterson 1982). Apart from the classic fusiform ‘palaeoniscoids’ several unique morphotypes appear in the late Paleozoic fossil record and given this morphological disparity have consistently been separated from ‘palaeoniscoids’ (Latimer and Giles 2018; Stack and Gottfried 2021; Argyriou et al. 2022; Giles et al. 2023). Using this framework several hypotheses of interrelationship have been proposed, both before

and after the emergence of phylogenetic systematics (Watson 1928; Schaeffer 1956; Gardiner 1967, 1984; Patterson 1982; Gardiner et al. 2005; Sallan 2014; Caron et al. 2023). However, these hypotheses have recovered contrasting placements for most Paleozoic ray-finned fish taxa not only in relation to each other but also to the crown. One of the main barriers for the understanding of early ray-finned fish phylogenetics is the specialized anatomy of early-diverging crown ray-finned fishes (e.g. cladistians and chondrosteans) and the absence of identifiable early representatives of these lineages in the fossil record, especially within the late Paleozoic (Friedman 2015; Friedman and Giles 2016).

Some researchers have pointed out in the past that endocranial anatomy might be an important source of additional character data useful for better understanding the interrelationships of early ray-finned fishes (Gardiner 1984; Gardiner et al. 2005; Lu et al. 2016; Giles et al. 2017, 2018; Argyriou et al. 2022). Unfortunately, most Paleozoic ray-finned fish genera lack endocranial remains or are represented by a single individual which precludes destructive work and preparation. It was only with the development of modern imaging techniques (e.g. micro-CT scanning) that researchers have been able to explore this major axis of morphological variation (Giles and Friedman 2014) and have since then reinforced the systematic value of endocranial characters bearing on the phylogenetic interrelationship of early ray-finned fishes, especially in relation to the crown (Giles et al. 2015a, 2017; Coates and Tietjen 2018; Friedman et al. 2018; Figueroa et al. 2019; Argyriou et al. 2022; Caron et al. 2023; Giles et al. 2023). This recent detailed work on endocranial anatomy of previously known and new taxa have reshaped our understanding of early ray-finned fish systematics, but the limited number of studies and specimens remains a challenge towards a more robust understanding of early ray-finned fish phylogenetics. Further complicating matters, detailed studies are generally restricted to specimens from well-known localities in North America, Europe, China and Australia (Henderson et al. 2022a), which might be problematic for sampling the true morphological—and phylogenetic—diversity of early actinopterygians.

The two taxa described herein provide important new information on unexplored aspects of early ray-finned fish endocranial morphology. Between these two taxa there is ample variation in neurocranium, hyobranchial apparatus and endoskeletal shoulder girdle that adds to the known morphological diversity of the actinopterygian stem. However, given the lack of comparative material for many of these modules of endocranial anatomy the polarity and distribution of

potential character states remains unresolved. In the most comprehensive phylogenetic matrices encompassing early ray-finned fishes (Giles et al. 2023) there are still a poor representation of hyobranchial and pectoral fin morphology characters, together representing less than 9% of the total number of characters. This lack is mostly due to the absence of well-preserved specimens for most early ray-finned taxa that show these anatomical features in detail.

3.4.2.1 Hyobranchial apparatus

The morphological diversity of the hyobranchial apparatus of early ray-finned fishes has been consistently overlooked in comparison even to other parts of the endoskeleton. This is likely due to the small number of specimens that preserve the anatomy of the hyobranchial apparatus in detail, especially when dealing with flattened specimens. However, with the advancement of imaging techniques it is now possible to extract more information from three-dimensional fossils. Thus, attention should be paid to variation in morphology of the hyoid and branchial arches when revising or describing new taxa.

Most characters used in phylogenetic analyses pertaining to the hyobranchial apparatus are related to the hyoid arch (e.g. number of ceratohyals, shape of the hyomandibula) while little attention is given to variation in morphology of the branchial arches. However, even early work on osteichthyan interrelationships have pointed out that there are useful characters within the hyobranchial apparatus (Nelson 1969; Patterson 1982). In recent analyses, branchial arch characters are present but still minimal and do not fully capture the known morphological variation within this module as in many instances these characters are limited to presence/absence or number of elements in the branchial basket.

Devonian ray-finned fishes seem to have a very conservative morphology of the hyobranchial apparatus, with a single ceratohyal, a single basibranchial, four hypobranchials, and undifferentiated epibranchials—frequently with articulation facets for the infra- and suprapharyngobranchials in the first two epibranchials (Gardiner 1984; Giles et al. 2015b). This condition is also true for the Late Devonian †*Palaeoneiros* which show otherwise more derived traits aligned to post-Devonian taxa (Giles et al. 2023). Contrastingly, post-Devonian taxa show extensive variation in hyobranchial morphology, with varying number of elements (e.g. one or two ceratohyals) and clear morphological variation (e.g. curvature of ceratobranchials,

epibranchial uncinate processes). Given the lack of detailed accounts on the hyobranchial apparatus of early ray-finned fishes, the interpretations drawn in the following paragraphs pertains to only a handful of examples (†*Mimipiscis*, Gardiner (1984); †*Raynerius*, Giles et al. (2015b); †*Palaeoneiros*, Giles et al. (2023); †*Pteronisculus*, Nielsen (1942); †*Australosomus*, Nielsen (1949); †*Brachydegma*, Argyriou et al. (2022); †*Saurichthys*, Argyriou et al. (2018)).

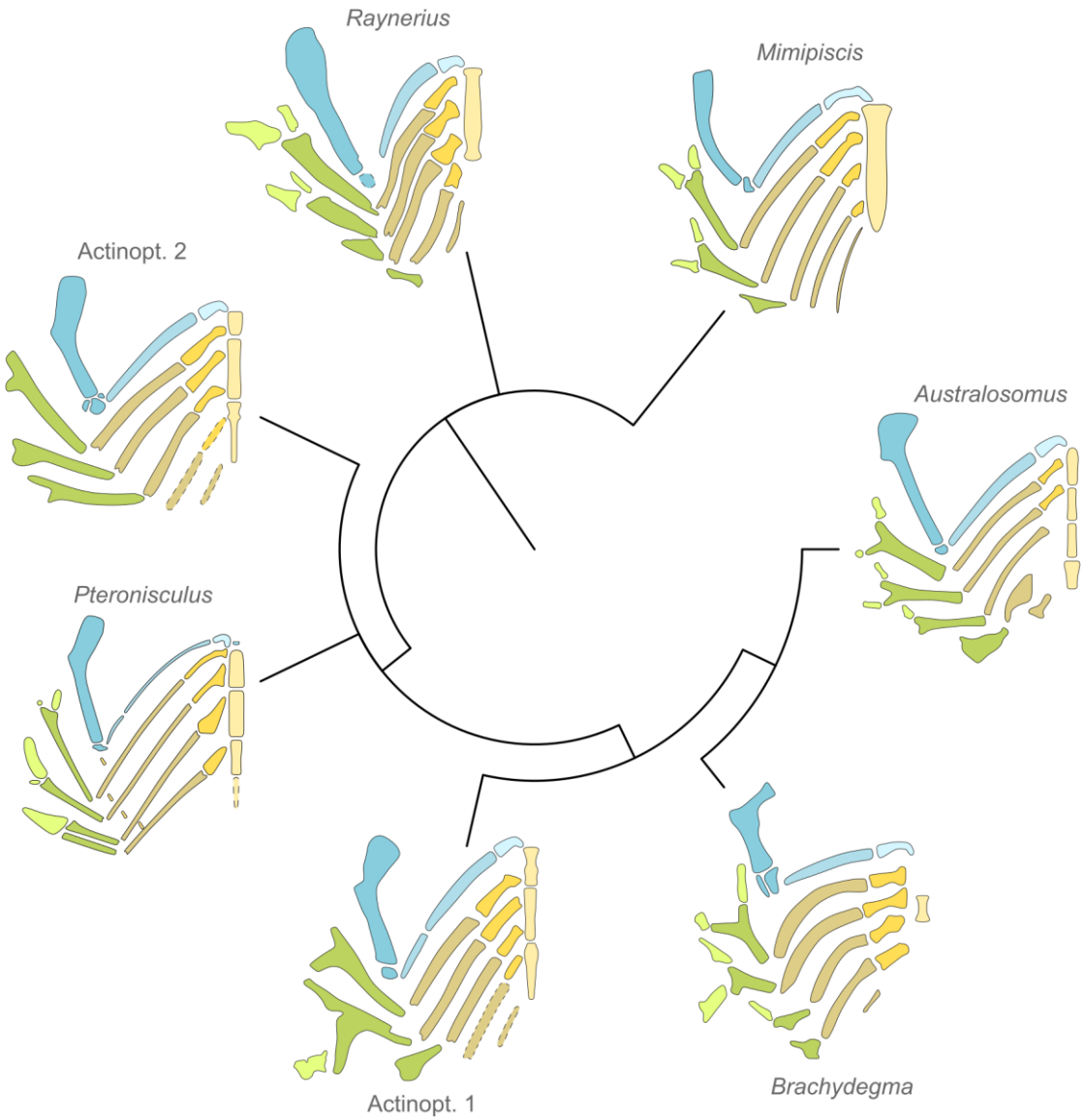

Figure 3.28 – Schematic representation of morphological diversity of selected early ray-finned fish hyobranchial elements. Tree based on hypothetical placement of the new taxa in the topology of Latimer and Giles (2018).

As exemplified in Figure 3.28 there is considerable variation in the organization of the hyobranchial apparatus in early ray-finned fishes, as well as variation in morphology of individual elements. For example, the shape of epibranchials is highly variable among taxa, with different orientations and lengths for uncinate processes and articulation facets for both infra- and suprapharyngobranchials. †*Pteronisculus* is unique among known stem ray-finned fishes in bearing interbranchial ossifications (Nielsen 1942). Variation is also present in the curvature and thickness of ceratobranchials, number and geometry of hypobranchials and basibranchials, as well as distribution of interhyals.

The two new taxa described herein add to this extensive morphological diversity as they bear a unique combination of characters. Actinopt. gen. et sp. nov. 1 bears extremely long and laterally flattened uncinate processes on the first and second epibranchials which seem to articulate with the lateral wall of the neurocranium, while the anterior ventral expansion extends below the ventral surface towards the parasphenoid. This condition more closely resembles crownward taxa such as †*Australosomus* and †*Brachydegma* where uncinate processes aid in the suspension of the branchial basket (Nielsen 1949; Argyriou et al. 2022). In stemward taxa such as †*Pteronisculus* it is common to have much smaller (or absent) uncinate processes and a more clear participation of infrapharyngobranchials in the suspension of the branchial basket (Nielsen 1942; Gardiner 1984; Giles et al. 2015b). This condition more closely resembles the organization of the branchial basket of Actinopt. gen. et sp. nov. 2, although the presence of infra- and suprapharyngobranchials could not be confirmed.

Within the hyoid arch, most of the variation between early ray-finned fish taxa pertains to the number of ceratohyals and the number of elements between the dorsal and ventral halves of the arch, such as interhyals or symplectic (Figure 3.28). In Devonian taxa only one ceratohyal is present, while crownward taxa can have one or two elements (Nielsen 1942; Gardiner 1984; Giles et al. 2015b; Figueroa et al. 2019; Argyriou et al. 2022; Giles et al. 2023). Another important variation pertains to the presence of an opercular process in the hyomandibula, which is absent in stemward forms and generally present in taxa commonly aligned to the actinopterygian crown (Patterson 1982; Gardiner 1984; Giles et al. 2017). The geometry of the hyomandibular opercular process is also variable, with stemward taxa bearing a small poorly differentiated process, while crownward forms exhibit a well-developed process that clearly connects to the opercle (Giles et al. 2017; Argyriou et al. 2022). Thus, these aspects of the dorsal

hyoid arch seem to have clear polarities established and considerable phylogenetic value. However, other axes of variation of the hyoid arch show a more confusing evolutionary history.

Given the developmental and nomenclatural difference between an ‘interhyal’ and a ‘symplectic’ (Moy-Thomas 1933; Warth et al. 2017; Argyriou et al. 2022) it is problematic to infer an accessory hyoid element as a symplectic in fossil taxa. Thus, in this work all accessory hyoid elements are considered as intehyals, without distinguishing symplectic ossifications. The variation in number of interhyals has caught the attention of researchers (Véran 1988; Argyriou et al. 2022). There does not appear to be a clear phylogenetic pattern in the distribution of interhyal elements, but with a more extensive sampling of hyoid arch morphology in early ray-finned fishes it might be possible to better establish patterns of evolution of accessory hyoid elements. In the taxa described herein Actinopt. gen. et sp. nov. 1 shows the condition similar to that of most described early ray-finned fishes, with a single robust interhyal immediately ventral to the proximal end of the hyomandibula, in some cases interacting with the jaw articulation. In Actinopt. gen. et sp. nov. 2 however, there are three interhyal elements contacting the proximal end of the hyomandibula (Figure 3.16). Two of these interhyals seem to interact directly with the hyomandibula, while a smaller one, located anterior to the jaw articulation lies relatively independent from the remaining hyoid ossifications. This condition seems unique in known Paleozoic ray-finned fishes, which tend to bear a single interhyal element (e.g. †*Pteronisculus*, †*Australosomus*, †*Boreosomus*, †*Coccocephalus*; Nielsen (1942, 1949), Poplin and Véran (1996)) or two dorsally expanded elements in †*Brachydegma* (Argyriou et al. 2022). Future work should focus on describing the interhyal morphology of additional early ray-finned fish taxa to better understand the morphological diversity and phylogenetic distribution of accessory hyoid ossifications.

3.4.2.2 Endoskeletal shoulder girdle

There is ample evidence that the pectoral fin morphology of ray-finned fishes is highly variable and fin morphology might correlate with swimming mode or capacity (Gerstner 1999; Lauder and Drucker 2004; Thorsen and Westneat 2005; Taft 2011), thus, it might be challenging to interpret how much of fin morphology might be suitable for understanding ray-finned fish interrelationships without introducing noise. Nevertheless, there is considerable variation in fin

morphology, especially in the endoskeletal portion of the fin which could provide insights into early ray-finned fish interrelationships.

The early-diverging †*Cheirolepis* seems to have a few unique characteristics of the pectoral fin endoskeleton that might hint on a hypothetical ancestral condition for the clade. In this taxon, the propterygium does not seem to be perforated, contrasting with all other known early ray-finned fishes (Giles et al. 2015c). Additionally, the fin endoskeleton does not seem to exhibit the tripartite scapulocoracoid of other actinopterygians and some sarcopterygians, more closely resembling primitive sarcopterygians such as †*Psarolepis* and †*Guiyu* (Zhu and Yu 2009; Zhu et al. 2012b). However, as noted by Giles et al. (2015c), this simple scapulocoracoid might be an artifact of poor mineralization of the fin endoskeleton or due to preservation, especially given that other early ray-finned fishes, such as †*Mimipiscis* show a tripartite scapulocoracoid (Gardiner 1984). Unfortunately, many other Devonian ray-finned fishes (e.g. †*Gogosardina*, †*Raynerius*, †*Kentuckia*, †*Howqualepis*, †*Donnrosenia*) lack a description of their pectoral endoskeletal remains (Eastman et al. 1908; Rayner 1952; Choo et al. 2009; Choo 2015; Giles et al. 2015b). In †*Palaeoneiros*, the scapulocoracoid mostly shows the horizontal plate, but there are indications of a tripartite morphology, likely not mineralized (Giles et al. 2023).

The endoskeletal shoulder girdle of post-Devonian Paleozoic ray-finned fishes is poorly known. Apart from the taxa described herein, only three other scapulocoracoids have been described for Permo-Carboniferous taxa (†*Trawdenia planti*, †*Palaeoniscus freieslebeni*, †*Pygopterus nielseni*; Coates and Tietjen (2018), Aldinger (1937)). In all these taxa, the scapulocoracoid shows a considerably similar morphology, comparable to that of Triassic taxa such as †*Australosomus*, †*Pteronisculus*, †*Boreosomus*, and †*Acrorhabdus* (Aldinger 1937; Nielsen 1942, 1949), as well as in extant taxa such as *Acipenser* and *Amia* (Grande and Bemis 1998; Hilton et al. 2011). Nevertheless, there is still considerable morphological variation between these taxa. The coracoid foramina (i.e. foramina for diazonal nerves) have varying distribution among these taxa, being small and widely separated dorsoventrally in †*Pygopterus* and †*Pteronisculus* (Aldinger 1937; Nielsen 1942), a large circular foramen dorsally (scf, supracoracoid foramen) followed by two small and horizontally spaced foramina in †*Trawdenia* (Coates and Tietjen 2018), large and ellipsoid bordering the lateral edge of the scapulocoracoid in †*Acrorhabdus* (Aldinger 1937), and seemingly absent in †*Boreosomus* (Nielsen 1942). In †*Australosomus*, there seems to be a single dorsoventrally oriented diazonal foramen (Nielsen

1949). In Actinopt gen. et sp. nov. 2 the dorsal diazonal foramen (or mesocoracoid forman) is large and similar in shape and position to that of †*Acrorhabdus*. The presence of a mesocoracoid process is also variable in early actinopterygians, being absent in most taxa but present in †*Trawdenia* and in Actinopt. gen. et sp. nov. 2.

3.4.2.3 Vertebral column

There is a lack of detailed information on vertebral elements for most early ray-finned fishes. Given that most described ray-finned fishes have robust squamation, the axial skeleton is commonly not readily observable without destructive sampling or CT scanning. Thus, vertebral elements have been consistently left from phylogenetic analyses and from detailed descriptive work. A few examples from the Triassic (i.e. †*Australosomus*, †*Pteronisculus*, †*Birgeria*, †*Saurichthys*) indicate that not only there is variation in vertebral morphology between taxa, but there is also regionalization of the vertebral column in many species (Nielsen 1942, 1949; Maxwell et al. 2021). Some Paleozoic taxa (e.g. †*Tarrasius*, †*Discoserra*, †*Wendyichthys*) also seem to show variation in vertebral morphology and vertebral column regionalization (Taverne 1996; Lund and Poplin 1997; Lund 2000). In †*Tarrasius* the vertebral column is preserved in detail, but unfortunately flattened and thus some morphology is not distinguishable. Nevertheless, regionalization of the axial skeleton is abundantly clear and similar to that of tetrapods (Sallan 2012).

In most cases the vertebral segments of early ray-finned fishes are formed by paired basidorsals and interdorsals forming the canal for the spinal cord and a ventral median basiventral forming the base of the aortic canal and notochord canal. The basiventral is normally thin and broad, forming an open semicircle in cross-section and thus not completely enclosing the aortic canal. However, in Actinopt. gen. et sp. nov. 1 the basiventral is robust and almost completely enclose the aortic canal, which is only open mesiodorsally. Further examination of the variation in elements of the vertebral column across Paleozoic and early Mesozoic ray-finned fishes is necessary to identify if there are more characters that can be added to phylogenetic analyses.

3.5 Conclusions

The two new taxa described above represent an important addition to the knowledge of early ray-finned fishes from the late Paleozoic. The majority of the well-known ray-finned fish taxa come from the paleotropical regions of North America, Europe and parts of Asia and many of the known taxa lack information on their endoskeletal anatomy. Thus, detailed description of novel well-preserved three-dimensional ray-finned fishes from neglected sites in South America and Africa are paramount for filling gaps in our knowledge of early ray-finned fish diversity. Additionally, taxa such as the ones described herein have the potential to reveal new anatomical innovations of potential phylogenetic or ecomorphological value. Until we have detailed description of endoskeletal anatomy of a larger set of early ray-finned fishes we will likely not be able to resolve the relationships along the actinopterygian stem.

Chapter 4 Exceptional Fossil Preservation and Evolution of the Ray-Finned Fish Brain

Note: The contents of this chapter have been published[1].

Abstract: Brain anatomy provides key evidence for the relationships between ray-finned fishes (Nieuwenhuys et al. 1998), but two major limitations obscure our understanding of neuroanatomical evolution in this major vertebrate group. First, the deepest branching living lineages are separated from the group's common ancestor by hundreds of millions of years, with indications that aspects of their brain morphology—like other aspects of their anatomy (Friedman 2015; Giles et al. 2017)—are specialized relative to primitive conditions. Second, there are no direct constraints on brain morphology in the earliest ray-finned fishes beyond the coarse picture provided by cranial endocasts: natural or virtual infillings of void spaces within the skull (Moodie 1915; Nielsen 1942; Edinger 1964; Giles and Friedman 2014; Lu et al. 2016). Here we report brain and cranial nerve soft-tissue preservation in *Coccocephalus wildi*, an approximately 319-million-year-old ray-finned fish. This example of a well-preserved vertebrate brain provides a window into neural anatomy deep within ray-finned fish phylogeny. *Coccocephalus* indicates a more complicated pattern of brain evolution than suggested by living species alone, highlighting cladistian apomorphies (Nieuwenhuys et al. 1998) and providing temporal constraints on the origin of traits uniting all extant ray-finned fishes (Nieuwenhuys et al. 1998; Ikenaga et al. 2022). Our findings, along with a growing set of studies in other animal groups (Ma et al. 2012; Edgecombe et al. 2015; Strausfeld et al. 2016), point to the importance of ancient soft tissue preservation in understanding the deep evolutionary assembly of major anatomical systems outside of the narrow subset of skeletal tissues (Pradel et al. 2009b; Maldanis et al. 2016; Trinajstic et al. 2022b).

Keywords: neuroanatomy, Carboniferous, Actinopterygii, soft-tissue

[1]Figueroa, R.T., Goodvin, D., Kolmann, M.A., Coates, M.I., Caron, A.M., Friedman, M., Giles, S. Exceptional fossil preservation and the evolution of the ray-finned fish brain. *Nature*, 614: 486-491.

4.1 Background

Actinopterygian (ray-finned fish) brains display anatomical innovations that are not seen in other vertebrates, most notably a forebrain that grows through eversion of the dorsal walls of the telencephalon, rather than evagination of its lateral walls (Braford 2009; Briscoe and Ragsdale 2019). This results in a forebrain comprising two solid hemispheres without a ventricle (Nieuwenhuys 2011). Brain anatomy therefore provides important evidence for the monophyly and interrelationships of ray-finned fishes, a major radiation containing around half of all vertebrate species (Nelson et al. 2016). Brain anatomy in living non-teleost ray-finned fishes is limited to a handful of examples, reflecting the low diversity of the deepest extant branches of the ray-finned fish tree of life. Fossil endocasts are thought to provide some constraints on brain structure deep in actinopterygian phylogeny, although the assumption that they reflect gross neuroanatomy (Jarvik 1980) has never been explicitly tested(although see examples of lobe-finned fishes (Clement et al. 2015, 2016; Dutel et al. 2019)). For over a century, rare natural endocasts (Moodie 1915; Coates 1999) and a handful of serial sectioning models (Nielsen 1942; Poplin 1974; Hamel and Poplin 2008) provided insights into the brain structure of early ray-finned fishes. Recent application of computed tomography has yielded more examples spanning the deepest branches of the actinopterygian tree (Lu et al. 2016) to the teleost and holostean stems (Giles et al. 2018; Latimer and Giles 2018) and several groups in between (Giles and Friedman 2014; Argyriou et al. 2018). These provide information on gross morphology and represent a source of characters for phylogenetic analysis (Coates 1999; Giles and Friedman 2014). However, there are considerable disconnects between our understanding of neural anatomy in fossil species, based on the endocavity, and living forms, based on the brain itself. This reflects two practical limitations—the low preservation potential of brain tissues in the fossil record combined with a poor understanding of endocavities in living taxa. As a consequence, key evolutionary steps preceding the origin of extant actinopterygian brains remain unclear.

Although rare, there is a growing record of fossil neural tissue. Palaeozoic arthropods provide the most examples (Ma et al. 2012; Edgecombe et al. 2015; Strausfeld et al. 2016), although a fossil brain is described in a Carboniferous chondrichthyan allied to ratfishes (Pradel et al. 2009b). Here we report an exceptionally well-preserved brain and associated cranial nerves in the type and only specimen of the Pennsylvanian (Bashkirian; around 319 million years old) ray-finned fish *C. wildi*, representing the first known fossil example for actinopterygians. Analyses place this taxon outside the group containing all living ray-finned fish species (Latimer and Giles 2018). Details of the brain structure in *Coccocephalus* therefore have implications for interpretations of neural morphology during the early evolutionary stages of a major vertebrate lineage. Using microcomputed tomography (μCT) analysis of fossils in concert with diffusible-iodine-based contrast enhanced computed tomography (diceCT) imaging of extant species (Gignac et al. 2016), we provide a revised picture of brain evolution in bony fishes.

4.2 Methods

4.2.1 Material examined

C. wildi is known from a single specimen (Manchester Museum, Wild Collection, MANCH: W.12451) from the roof of the Mountain Fourfoot Mine, Carre Heys, Trawden, Lancashire, UK. Its anatomy has been described previously (Watson 1925; Poplin and Véran 1996). Other three-dimensionally preserved actinopterygians hosted in nodules from this area include *Trawdenia planti* (Coates 1999; Coates and Tietjen 2018) and *Mesonichthys aitkeni*; these are all thought to derive from the so-called Soapstone Bed. This horizon lies within the Pennine Lower Coal Measures above the Bullion Coal (Upper Foot Coal) and the Mountain 1.2 m Coal (Lower Mountain Coal), but below the Arley Seam (Arley Coal) (Coates 1999; Hough 2004; Coates and Tietjen 2018). This is within the Langsettian regional substage, which correlates with the upper part of the Bashkirian stage of the international timescale (Waters et al. 2011).

4.2.2 Preservation of brain tissues

The brain of *Coccocephalus* appears to be preserved in a manner comparable to the younger (roughly 300 million years old) chondrichthyan brain reported (Pradel et al. 2009b; Pradel 2010). In both examples, the brain is preserved in three dimensions within an enclosed skeletal space (the braincase), potentially allowing the development of a microenvironment favorable for the preservation of certain soft-tissue structures. The failure of cranial nerves to extend beyond the outer wall of the braincase in both examples provides support for this localized model of preservation. Exposed regions of soft tissue in the iniopterygian example show that its brain was preserved as calcium phosphate (Pradel et al. 2009b; Pradel 2010). However, the sole specimen of *Coccocephalus* lacks any clear external exposures of the brain or associated nerves, and the composition of the radiodense material capturing their structure remains unclear. The preservation of brains in these Carboniferous fishes shows coarse similarities to concretion-hosted Devonian placoderms (Trinajstic et al. 2022b) and Jurassic invertebrates (Vannier et al. 2016; Cherns et al. 2021) that similarly preserve three-dimensional organs within enclosed bony, shelly or chitinous carapaces. Collectively, these examples differ from the flattened preservation of neural and other soft tissues in arthropods from Cambrian shales (Ma et al. 2012; Strausfeld et al. 2016). A more detailed discussion of modes of preservation for brain tissues is provided in Appendix D.

Pathways to preservation of brain tissues are poorly understood, especially owing to the lack of experimental focus on neuroanatomical decay (Sansom et al. 2013). Available evidence indicates a relatively rapid deterioration of brain tissues, based on controlled decay of cephalochordates and agnathans (Sansom et al. 2011, 2013; Sansom and Wills 2013). However, data are lacking for taxa in which the brain is enclosed and protected by a robust endochondral ossification, as is the case in *Coccocephalus*. As such, the timing and patterns of brain decomposition in bony fishes requires further investigation.

4.2.3 Dice-CT

Comparative specimens of *Squalus acanthias* (University of Michigan Museum of Zoology (UMMZ), 253084), *Polypterus senegalus* (UMMZ, 195008), *Amia calva* (UMMZ, 235291) and *Acipenser fulvicens* (UMMZ, 219456) were prepared for diceCT by submerging the specimens in 1.25% Lugol's solution (25 g I_2 + 50 g KI for every 2 l of water) for around 14 days before scanning. DiceCT data for a specimen of *Lepidosiren paradoxa* (UF:FISH:129826) from

the Florida Museum of Natural History Ichthyology Collection was obtained from Morphosource (ark:/87602/m4/M167969).

4.2.4 X-ray computed tomography

C. wildi and extant comparative material were scanned at the CTEES facility of the Department of Earth and Environmental Sciences, University of Michigan, using a Nikon XT H 225ST μCT scanner. The scan for *C. wildi* was set with 120 kV energy, 125 μA current and using a 0.5 mm copper filter. Eight frames were acquired for each projection, with an exposure time of 2.83 s, and the option for minimizing ring artefacts was selected. Effective pixel size was 15.35 μm with a geometric magnification of 13.031. The parameters for new scans of extant comparative material (*S. acanthias*, *P. senegalus*, *Acipenser brevirostrum* and *A. calva*) are given in Supplementary Table 1. Processing of data was conducted in Mimics v.21. A threshold encompassing the preserved neural soft tissue was determined and the resultant mask was cleared, with the threshold values retained. The soft tissue was manually segmented using the circle and livewire tools. Segmentation was performed by three authors (R.T.F., M.F. and S.G.), and the results were compared for consistency. The hard tissues were segmented using the same method. Rendering was performed in Blender 2.91 (https://www.blender.org/) using cycles rendering with the addition of custom shading and reflection attributes to the material properties (principled BSDF material), coupled with ambient occlusion for better lighting of minute structures and realistic shading of internal cavities.

4.3 Description

4.3.1 Endocast and otoliths

The endocast of *Coccocephalus*, as in other Palaeozoic actinopterygians, is differentiated into areas that appear to correspond to regions of the brain (Fig. 4.1 a). It agrees most closely with that described for *Lawrenciella* (Hamel and Poplin 2008; Pradel et al. 2016). Endocasts of both show a midline olfactory tract, narrow olfactory bulbs, slender cerebellar auricles and inclined horizontal semicircular canals. A single pair of otoliths, filling the saccular chamber, are preserved (Fig. 4.1 b,d). These are large and teardrop shaped in lateral view, similar to those

reported in some other Palaeozoic and early Mesozoic actinopterygians (Coates 1998). Their mesial and lateral surfaces are slightly convex and concave, respectively.

4.3.2 Overall preservation of the brain

The cranial cavity contains a symmetrical object that is more radiodense than the surrounding matrix (Fig. 4.2 and Appendix Figs D.1-8), extending from the level of the orbit to the oticooccipital fissure. It comprises three principal structures: a central, hollow midline body; ramifications on either side of the central body that, in some cases, are associated with endoskeletal nerve foramina; and a diamond-shaped sheet that lies posterodorsal to the other elements. The central body includes three regions: a long, narrow anterior extension; a swollen middle region comprising a horizontal plate with two dorsal hemispheres and a ventral outgrowth; and a flattened posterior tube with a slit-like opening on the dorsal midline. On the basis of this appearance (Pradel et al. 2009b) and a comparison with the neural features of extant fishes (Fig. 4.2 and Appendix Fig. D.1), we interpret the structure as a preserved brain. The three regions described above approximately correspond to the forebrain, midbrain and hindbrain.

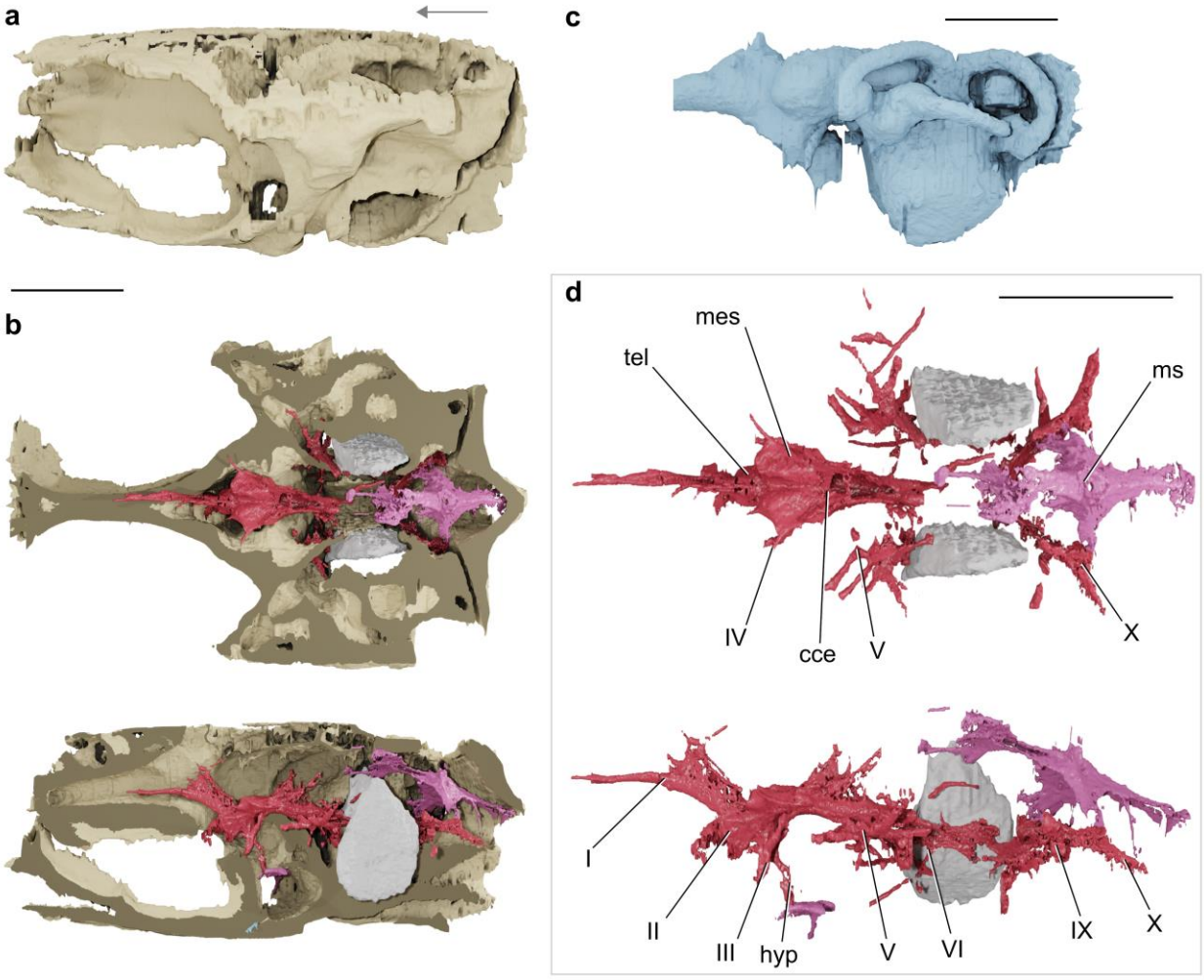

Figure 4.1 – The neurocranium, endocast, otoliths and preserved brain of *C. wildi* (MANCH: W.12451) based on micro-computed tomography. **a**, The neurocranium in left lateral view. **b**, Cutaways of the neurocranium in dorsal (top) and left lateral (bottom) views showing the brain and otoliths in situ. **c**, The endocast in lateral view. **d**, The brain and associated preserved soft tissues in dorsal (top) and lateral (bottom) views, with the left otolith removed in the latter view for clarity. Blue, endocast; cream, braincase; grey, otoliths; red, brain and cranial nerves; pink, myelencephalic sheet. cce, corpus cerebelli; hyp, hypophysis; mes, mesencephalon; ms, myelencephalic sheet; tel, telencephalon; I, olfactory nerve; II, optic nerve; III, oculomotor nerve; V, trigeminal nerve; VI, abducens nerve; IX, glossopharyngeal nerve; X, vagus nerve. The question mark indicates an unidentified midbrain feature. Scale bars, 5 mm. The arrow indicates anterior for all panels.

4.3.3 Forebrain

The forebrain—comprising the olfactory bulbs, telencephalon and diencephalon—lies anterior to, and is considerably smaller than, the midbrain (Fig. 4.1). An elongate, slender extension anterior to the telencephalic body represents the olfactory nerve, but the olfactory bulbs are difficult to identify. The olfactory nerve extends to the midpoint of the orbit before dividing anteriorly. A dorsal sheet extends into the pineal chamber posterior to the divergence of

the olfactory tract from the telencephalon. This structure may represent the remnants of the velum transversum. Thin filaments connect the anterior and posterior margins of this sheet to the endocranial walls, and paired anterior cerebral veins exit from its base. The body of the telencephalon is formed by two small, paired swellings divided by a median septum (Appendix Fig. D.2). The swellings are moderately expanded laterally, giving the telencephalon an ellipsoidal profile in horizontal section (Appendix Fig. D.2). Each swelling is hollow and encloses a large ventricular space, indicating that the forebrain is evaginated as in sarcopterygians and chondrichthyans (Nieuwenhuys et al. 1998; Smeets 1998; Braford 2009). By contrast, all living actinopterygians possess an everted telencephalon (Nieuwenhuys et al. 1998; Northcutt 2008; Braford 2009) (Fig. 4.2 b). We interpret an additional tissue layer dorsal to the telencephalon as the forebrain meningeal tissue.

No clear boundary divides the telencephalon and diencephalon. A moderate expansion posteroventral to the telencephalon corresponds with an ellipsoidal ventricle within the main body of the brain, indicating the presence of partially developed hypothalamic inferior lobes (Appendix Figs D.2-3). The lobes are visible in cross-section as small ellipsoid structures of a slightly denser material than the matrix, but less dense than the external brain wall. The right lobe is apparent externally on the right side of the brain as a low swelling. A slender and ventrally elongated hypophysis extends from behind the hypothalamus. It leads to a differentiated distal portion contacting the buccohypophysial canal, and a posterior expansion associated with the saccus vasculosus. The ventricular space within each hypothalamic inferior lobe connects with that of the hypophysis (the diencephalic ventricle) through a narrow canal: the lateral hypothalamic recess (Morona et al. 2013). The morphology of this structure in *Coccocephalus* resembles that of *Amia* (Appendix Fig. D.4).

4.3.4 Midbrain

The mesencephalic lobes, the dorsal surfaces of which comprise the optic tectum, are well-developed and oval in dorsal view (Fig. 4.1). The lobes are connected posteriorly, level with the cerebellar region, diverging anteriorly. Two nerves emerge from the surface of the mesencephalon: a narrow, anterodorsally directed trochlear (IV) nerve; and a stout, anteroventrally directed oculomotor (III) nerve, which bifurcates within the braincase wall and enters the orbit through two foramina. A feature of unclear identity leaves from the anterior

margin of the midbrain. The optic chiasma is preserved on the anteroventral surface of the mesencephalon, along with the proximal portions of the optic (II) nerves. These extend and diverge beyond the external margin of the midline optic foramen.

Sections through the midbrain reveal ventricles (Fig. 4.2 and Appendix Figs D.5-7). The second (mesencephalic) ventricle mirrors the shape of the optic tectum, and is V-shaped transversely and U-shaped horizontally. Neither a torus longitudinalis nor torus semicircularis is apparent within the second ventricle. As these intraventricular projections represent denser regions of the brain in living taxa (Nieuwenhuys et al. 1998), we would expect them to be preferentially preserved relative to other regions of the midbrain, and interpret their absence in *Coccocephalus* as genuine. This is consistent with the distribution of this feature in extant actinopterygians, in which it is absent in cladistians and present in actinopterans. Anteriorly, the mesencephalic ventricles connect to a tube-like ventricle that opens at the roof of the diencephalon. Posteriorly, the mesencephalic ventricles contact the fourth ventricle through a narrow tube-shaped connection.

4.3.5 Hindbrain

Few features of the hindbrain are preserved. The anteriormost portion is developed as small rounded cerebellar auricular lobes, separated by the posterior limits of the mesencephalic lobes (Fig. 4.1). Posterior to these lies the recessus lateralis of the fourth ventricle, which is continuous with a thin, dorsally extensive rhombencephalic tela choroidea. The cerebellar corpus is barely developed (Appendix Fig. D.7). The fourth ventricle is open dorsally, is anteroposteriorly elongate and circular in transverse section, and lies ventral to the mesencephalic ventricle (Fig. 4.2 and Appendix Figs D.5-6). A cerebral aqueduct connecting the second and fourth ventricles is present. The internal walls of the fourth ventricle lack pronounced ridges, but it is unclear whether this is original or a taphonomic artefact. Two thin, posteroventrally directed branches of the abducens (VI) nerve leave the ventral surface of the brain level with posterior margin of the fourth ventricle. More ventrally, an additional branch extends from the saccular chamber towards the posterior myodome. Owing to the position and path of this branch, we identify it as a distally diverging branch of the abducens nerve.

The trigeminofacial nucleus and associated nerves are separated from the body of the hindbrain, presumably a taphonomic artefact (Fig. 4.1). The trigeminofacial complex on the right

of the specimen appears to be associated with the alar wall of the rhombencephalon, which has pulled away from the remainder of the hindbrain. Nerve branches located at the front of this complex are enclosed within skeletal canals and can be identified by comparison with endocasts described for Palaeozoic actinopterygians (Hamel and Poplin 2008), although we caution that this nomenclature needs review in comparison to nerve patterns in extant non-teleost actinopterygians. Two stout nerves emerge anterolaterally from the front of this complex, the most anterior of which enters the canal identified as that for the trigeminal (V) nerve, and the more posterior one the canal for the lateralis branch of the facial (VIIlat) nerve (Fig. 4.1 and Appendix Fig. D.3). A third nerve, which leaves the complex anteroventrally, enters the canal for the main branch of the facial (VII) nerve. More posteriorly, a series of nerves are associated with the inner ear and otolith, and most probably correspond to branches of the octavolateralis (VIII) nerve (Fig. 4.1 and Appendix Fig. D.8). The anterior branch of the anterior ramus of the octavolateralis extends dorsally into the anterior ampulla, with the posterior branch of the anterior ramus entering the utriculus. A posteroventral branch contacts the anterior margin of the otolith. Two to three additional rami attach to the medial margin of the otolith, and further branches may be present posteriorly.

A diamond-shaped sheet lies posterodorsal to the brain, in close association with the roof of the endocavity (Fig. 4.1 and Appendix Fig. D.1). This is in a similar position to the meninx primitiva, modified to a cisterna spinobulbularis in *Polypterus* (Jarvik 1980; Bjerring 1991) and a myelencephalic gland in some other ray-finned fishes (Chandler 1911). The dorsal surface bears a medially located opening surrounded by a thin layer of tissue that extends as a tube towards the posterodorsal fontanelle of the neurocranium. The vagus (X) nerve lies ventral to this sheet, extending posterolaterally to exit from the braincase through the oticooccipital fissure. Anterior to the vagus nerve root, the glossopharyngeal nerve (IX) extends laterally towards the endocranial wall.

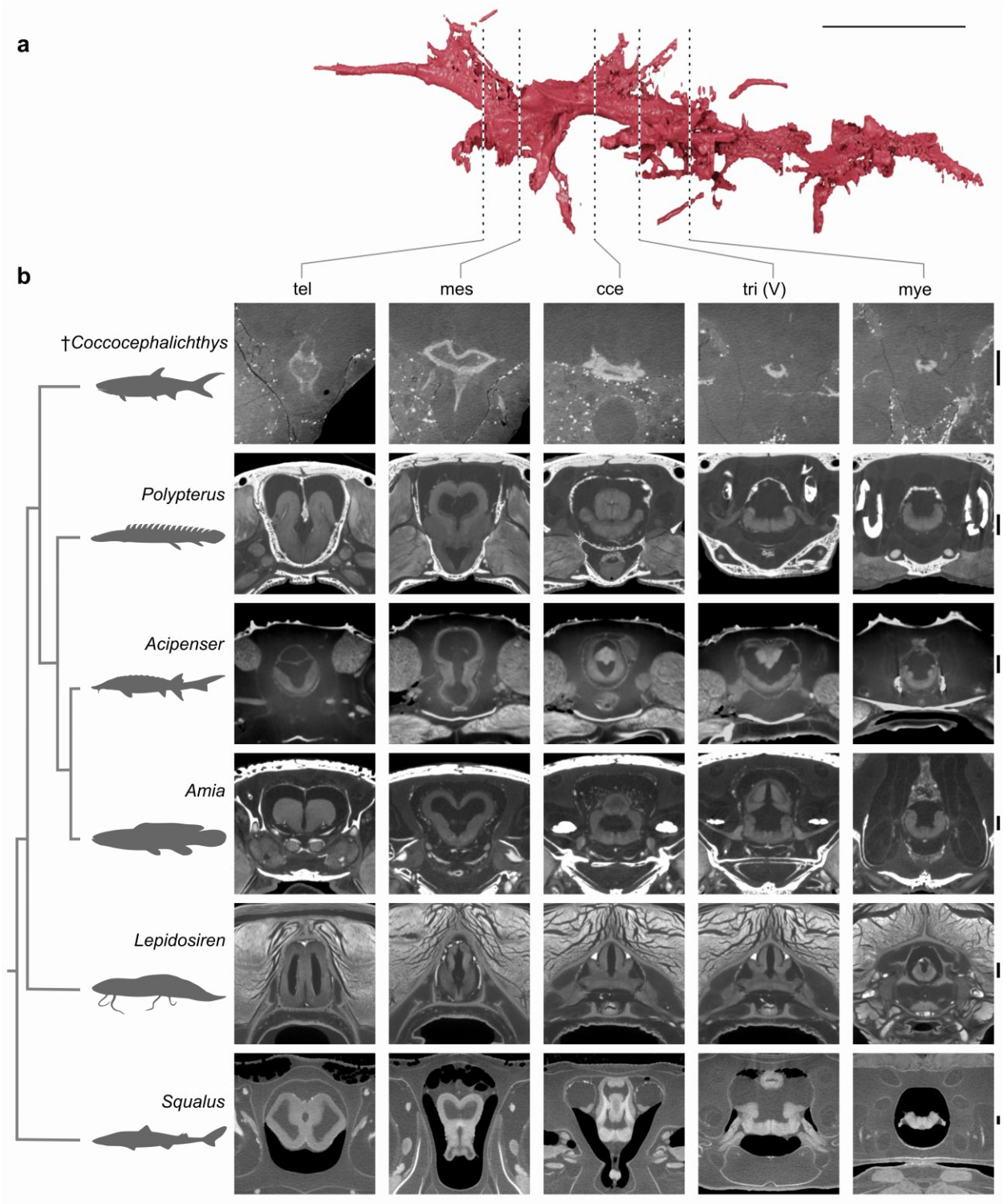

Figure 4.2 – Anatomical correspondence between the preserved brain of *C. wildi* and those of extant fishes. **a**, Three-dimensional rendering of the brain of *Coccocephalus* in left lateral view. Scale bar, 3.5 mm. **b**, Transverse sections through the brains of *Coccocephalus* and selected jawed fishes from diceCT data. mye, myelencephalon; tri (V), trigeminal nerve. Data for extant taxa are original scans from specimens in the University of Michigan Museum of Zoology (see Methods) with the exception of *Lepidosiren* (UF:FISH:129826; Morphosource

ark:/87602/m4/M167969). Silhouettes of extant taxa are adapted from PhyloPic and are available under Creative Commons 3.0 licence (https://creativecommons.org/licenses/by/3.0/) (*Squalus* and *Lepidosiren*) or in the public domain (*Acipenser*, *Amia* and *Polypterus*). Credit: *Squalus*, I. Contreras; *Lepidosiren*, R. Díaz Sibaja. The hypothetical *Coccocephalus* silhouette is based on an illustration from ref. 51. †Extinct taxon. Scale bar, 1 mm.

4.4 Discussion and conclusions

4.4.1 Correspondence between brains and endocast

It is widely assumed that there is fidelity between the shape of the brain and the endocast in early ray-finned fishes (Moodie 1915; Jarvik 1980; Coates 1999; Giles and Friedman 2014), with many brain regions corresponding with areas of the endocavity hypothesized to accommodate them. For example, the olfactory (I) nerve is housed in the olfactory tract, the tela choroidea extends towards the pineal opening and the mesencephalon is confined to the region of the optic lobes (Fig. 4.1 and Appendix Figs D.5, 8)). This indicates that endocasts can provide some accurate positional information. However, the shape of the brain in *Coccocephalus* does not closely conform to the inner surface of the endocavity (Fig 4.1 and Appendix Figs D.5, 8). The discrepancy in volume between the endocast and brain raises the possibility that the brain may have contracted during preservation. However, the fact that many cranial nerves connect with the brain itself and extend to their neurocranial foramina suggests a limit to the degree of shrinkage. Taphonomic experiments investigating soft-tissue preservation in bony fishes are in their infancy, and future research will be critical for contextualizing these interpretations. Living ray-finned fishes show varying degrees of correspondence between brain and endocast morphology (Fine et al. 1987; Herzog et al. 2017) (Fig 4.3), and perhaps rarely fill the endocavity in a manner that is comparable to lungfishes and some tetrapods (Rowe et al. 2011; Clement et al. 2015; Watanabe et al. 2019a). This does not invalidate endocasts as sources of characters or information about neuroanatomy (Coates 1999; Giles and Friedman 2014), but stresses that the features of brains and endocavities in ray-finned fishes are not interchangeable.

4.4.2 Patterns on brain evolution in bony fishes

The principal actinopterygian lineages show substantial differences in brain and endocavity structure (Fig 4.3 and Appendix Fig D.1). Living members of early-diverging groups, such as cladistians and chondrosteans, provide important clues about primitive brain anatomy but both show morphological specializations reflecting long independent evolutionary histories. As a stem

actinopterygian separated from the common ancestor of all living species by tens of millions—rather than hundreds of millions—of years (Giles et al. 2017; Latimer and Giles 2018; Figueroa et al. 2019), *Coccocephalus* provides unique information bearing on primitive ray-fin brain anatomy and sequences of change within the group. Owing to the challenges of interpreting soft-tissue preservation, we focus on features that are present and most probably reflect true morphological variability, rather than focussing on features that appear to be absent, but which may in fact have been lost during decay and preservation.

Notably, the brain of *Coccocephalus* clarifies neurological synapomorphies of the ray-finned fish total group (that is, the living radiation and all closely related fossil taxa) and crown group (that is, the living radiation only), summarized in Fig 4.3. All living ray-finned fishes display an everted telencephalon, representing the principal neuroanatomical synapomorphy of actinopterygians. However, the telencephalon of *Coccocephalus* shows the contrasting evaginated condition, as seen in non-actinopterygian fishes. This indicates that an everted forebrain originated in more crownward portions of the actinopterygian stem. The presence of an evaginated telencephalon in a Carboniferous actinopterygian also challenges the hypothesis that forebrain eversion arose due to developmental constraints associated with small body size in Devonian members of the group (Striedter and Northcutt 2006; Folgueira et al. 2012), as the forebrain region of the endocast of *Coccocephalus* is small.

Partially developed inferior lobes of the hypothalamus in *Coccocephalus* challenge the current assumption that the absence of this diencephalic outgrowth in *Polypterus* (Figs 4.2 and 4.3) represents a primitive condition for crown actinopterygians (Nieuwenhuys et al. 1998; Schmidt 2020). The presence of this feature in a stem actinopterygian suggests an alternative scenario in which it arose deep on the ray-fin stem, was lost in cladistians and retained by actinopterans, before developing fully in neopterygians (Schmidt 2020). *Coccocephalus* also provides evidence that the myelencephalic gland of holosteans and chondrosteans traces its origins to a feature present in stem actinopterygians. The myelencephalic gland, a haematopoietic (blood-generating) structure enclosed within the endocranial cavity of non-teleost actinopterans, either overlies (lepisosteids) or embraces (*Amia*, chondrosteans) the myelencephalon (Chandler 1911; van der Horst 1925). In *Polypterus*, meningeal tissue occupying the same region as the myelencephalic gland of other taxa is differentiated and highly vascularized, and is called the cisterna spinobulbaris (Jarvik 1980; Bjerring

1985). *Coccocephalus* bears a similar membranous structure overlying the rhombencephalon at the level of the vagal nerves, considered to be homologous to the cisterna spinobulbaris of *Polypterus*. On this basis, we argue that modified rhombencephalic meningeal tissues are a general feature of ray-finned fishes, with subsequent modifications in holosteans and chondrosteans towards a well-developed myelencephalic gland.

The brain of *Coccocephalus* clarifies polarities of neuroanatomical features of deeply branching crown lineages, with implications for brain evolution in more nested clades (Fig 4.3). These data provide corroboration that features of *Polypterus* such as the absence of intraventricular projections and the presence of a poorly differentiated corpus cerebelli represent primitive actinopterygian conditions. However, *Coccocephalus* suggests that a conspicuous external aspect of neuroanatomy in *Polypterus* might be apomorphic. Like lungfishes and tetrapods, *Polypterus* has a telencephalon that is much larger than the midbrain1, in contrast to the small structure in actinopterans1 and *Latimeria* (Northcutt et al. 1978). This distribution among extant bony fishes has been used to argue that a large telencephalon may be a generalized osteichthyan feature (Jarvik 1980) lost in actinopterans. However, the small telencephalon of *Coccocephalus* (Fig 4.1 d) instead suggests the convergent origin of enlarged structures in *Polypterus* and a subset of sarcopterygians. This inference is supported by outgroup comparison to chondrichthyans, many of which have a small telencephalon (White 1936). At the same time, *Coccocephalus* indicate that an apparent specialization of *Polypterus* might in fact be a more general feature of actinopterygians. *Polypterus* is unique among extant jawed vertebrates in having an invaginated corpus cerebelli, a condition that is generally interpreted as a specialization of that lineage (Nieuwenhuys et al. 1998; Ikenaga et al. 2022). However, the corpus cerebelli of *Coccocephalus* also seems to be formed as an invagination (Appendix Fig. D.7) of the dorsal surface of the rhombencephalic region, matching the arrangement of *Polypterus*. Independent gains within both lineages, or a single gain at the base of actinopterygians followed by a loss in actinopterans, represent equally parsimonious scenarios. It is not possible to select between these alternatives in the absence of additional information on brain structure in other early actinopterygians.

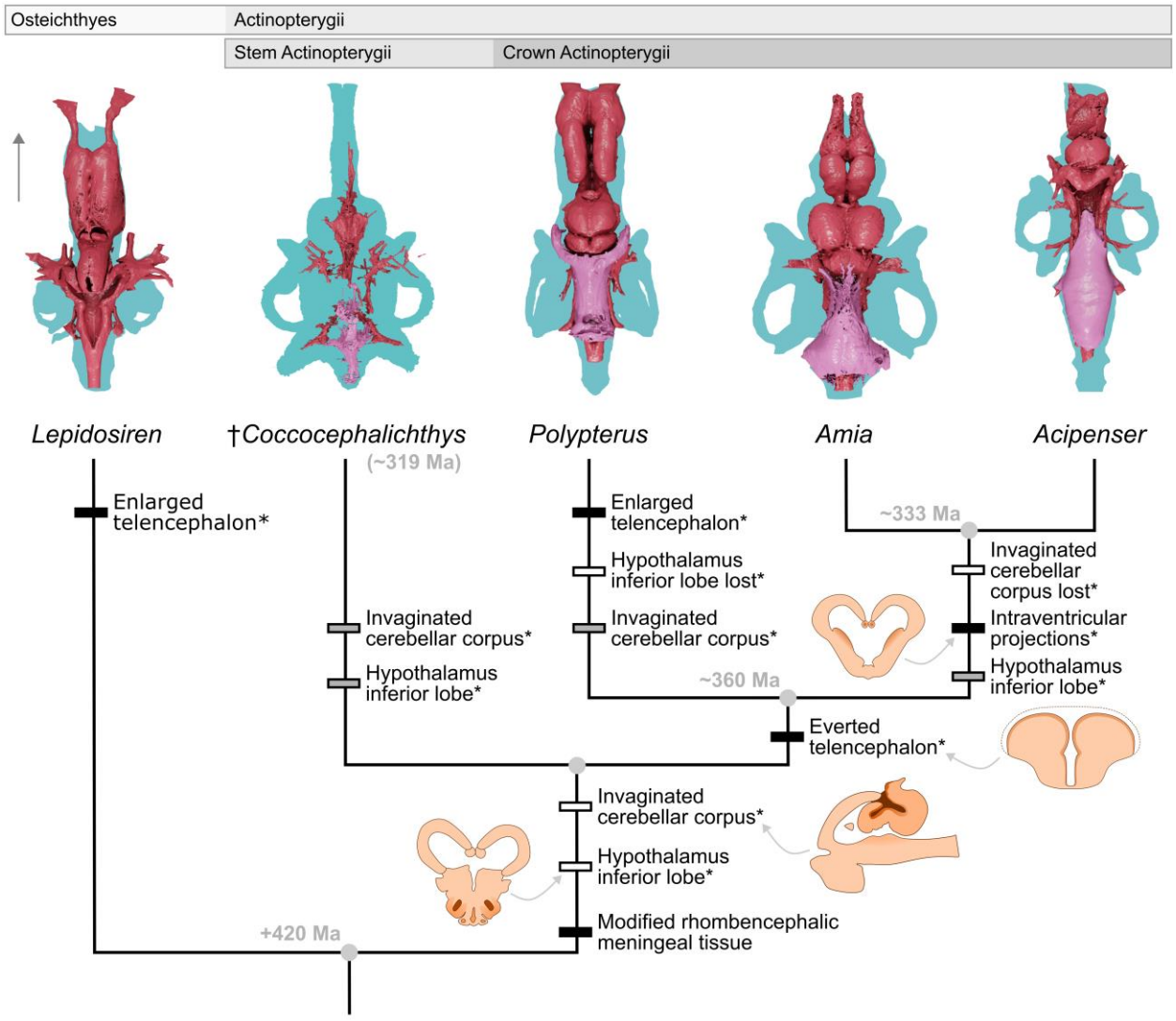

Figure 4.3 – Major anatomical transformations in actinopterygian brain structure illuminated by *Coccocephalus*. Branch labels represent character modifications. The asterisks indicate a shift in the position of a character in the cladogram due to anatomical information from *Coccocephalus*. The black bars indicate unambiguous changes; white bars indicate ACCTRAN optimizations; grey bars indicate DELTRAN optimizations. The arrow indicates the anterior direction for 3D renders. Insets: transverse and sagittal sections through the relevant portions of the brain, with darker orange shading indicating specific regions of interest. Images are not to scale. Node ages are from ref. 3. Ma, million years ago.

4.4.3 The utility of fossil brain

Coccocephalus reinforces studies of neural structures in fossil arthropods (Ma et al. 2012; Edgecombe et al. 2015; Strausfeld et al. 2016) that highlight the importance of fossil brains for patterns of neuroanatomical change in groups with deep evolutionary divergences. Beyond representing preservational curiosities, fossilized brains provide otherwise inaccessible trait data

with implications for patterns of phylogenetic relationships and character polarity. We anticipate that the preservation of neural tissue in fossil fishes is probably more common than widely thought (Coates 1999), with assumptions of non-preservation leading to potentially valuable information on the evolution of brain structural diversity being overlooked. A careful survey of fish material from taphonomically promising horizons has the potential to yield anatomical information bearing on the evolution of brain structural diversity within the principal clade of aquatic vertebrates.

Chapter 5 Soft-Tissue Fossilization Illuminates the Stepwise Evolution of the Ray-Finned Fish Brain

Note: The contents of this chapter have been published[1].

Abstract: A complex brain is central to the success of backboned animals. However, direct evidence bearing on vertebrate brain evolution comes almost exclusively from extant species, leaving substantial knowledge gaps. Although rare, soft-tissue preservation in fossils can yield unique insights on patterns of neuroanatomical evolution. Paleontological evidence from an exceptionally preserved Pennsylvanian (ca. 318 Ma) actinopterygian, *Coccocephalus,* calls into question prior interpretations of ancestral actinopterygian brain conditions. However, ordering and timing of major evolutionary innovations such as an everted telencephalon, modified meningeal tissues, and hypothalamic inferior lobes remain unclear. Here we report two distinct actinopterygian morphotypes from the latest Carboniferous-earliest Permian (~299 Ma) of Brazil that show extensive soft-tissue preservation of brains, cranial nerves, eyes and potential cardiovascular tissues. These fossils corroborate inferences drawn from *Coccocephalus*, while adding new information about neuroanatomical evolution. Skeletal features indicate that one of these Brazilian morphotypes is more closely related to living actinopterygians than the other, which is also reflected in soft-tissue features. Significantly, the more crownward morphotype shows a key neuroanatomical feature of extant actinopterygians–an everted telencephalon–that is absent in the other morphotype and *Coccocephalus*. All preserved Paleozoic actinopterygian brains show broad similarities including an invaginated cerebellum, hypothalamus inferior lobes, and a small forebrain. In each case, preserved brains are substantially smaller than the enclosing cranial chamber. The neuroanatomical similarities shared by this grade of Permo-Carboniferous actinopterygians reflect probable primitive conditions for actinopterygians, providing a revised model for interpreting brain evolution in a major branch of the vertebrate tree of life.

Keywords: Neuroanatomy, Actinopterygii, Paleozoic, telencephalon, Permo-Carboniferous

[1]Figueroa, R.T., Weinschütz, L.C., Giles, S., Friedman, M. Soft-tissue fossilization illuminates the stepwise evolution of the ray-finned fish brain. *Current Biology*, in press.

5.1 Introduction

The vertebrate brain is specialized and distinct from that of other animal groups (Nieuwenhuys et al. 1998). Jawed vertebrates (gnathostomes) show broad conservation of major brain regions (Nieuwenhuys et al. 1998; Northcutt 2002), but there is wide structural and developmental variation within the group[3] generally ascribed to differences in ecology and behavior. Among living gnathostomes, the roughly 30,000 species of ray-finned (actinopterygian) fishes display many neuroanatomical innovations (Nieuwenhuys 1982; Nieuwenhuys et al. 1998; Northcutt 2002; Striedter and Northcutt 2019) with profound variation in the size of brain regions across lineages (Northcutt and Wullimann 1988; Nieuwenhuys et al. 1998; Northcutt 2008). This diversity of brains mirrors the variety of ray-finned fishes as a whole, reflecting over 350 million years of evolution in a range of aquatic habitats (Friedman and Giles 2016; Nelson et al. 2016).

Extant animals provide abundant information about brain structure, but important gaps in our understanding remain. First, the vast majority of living ray-finned fishes belong to Teleostei, which contains roughly 98% of all extant actinopterygian species (Nelson et al. 2016). Crown teleosts are geologically young, first appearing in the fossil record (Friedman 2022; Arratia and Schultze 2024) roughly 200 million years after the origin of crown actinopterygians and nearly 300 million years after ray-finned fishes diverged from their lobe-finned sister lineage (Friedman 2022). Non-teleost actinopterygians provide critical details about neuroanatomical evolution deeper in the ray-finned fish tree, but these depauperate groups often display highly specialized morphologies. Given that early-diverging living ray-finned fishes are highly specialized (Allis 1922; Friedman 2015; Nelson et al. 2016) there are standing questions on the ordering of important morphological innovations such as the bulging of the cerebellum, hypothalamus inferior lobes and modified tela choroidea tissues. Second, while actinopterygians have a rich fossil record, few fossils provide evidence for patterns of brain evolution. Rare cranial endocasts generally represent the only evidence bearing on the neuroanatomy of extinct species, but the constraints they provide are indirect. There is evidence from several vertebrate lineages that

endocasts have a varying degree of fitting to brain anatomy (Clement et al. 2015, 2021; Fabbri et al. 2017; Dutel et al. 2019) and thus neuroanatomical evidence derived directly from fossil endocasts should be considered with care.

The recent description of a fossil brain in a late Carboniferous ray-finned fish (Figueroa et al. 2023), combined with earlier reports of a comparable preservation in a contemporary chondrichthyan (Pradel et al. 2009b; Pradel 2010), suggests that fossilized neuroanatomy might be more common than widely assumed. However, the absence of additional extinct comparators limits the impact of these known examples. Here we report new instances of three-dimensional preservation of brains and other soft tissues in ray-finned fishes from the early Permian (Cisuralian, ~298.9-272.9 Ma) Lontras Shale of Brazil, a deposit regarded as a *Konservat-Lagerstätte* (Saldanha et al. 2022). Two distinct actinopterygian morphotypes, differentiated by osteological structure, preserve brains, eyes, and other soft tissues. These specimens challenge interpretations of the evolutionary timing and sequence of innovations in the ray-finned fish brain, illustrating the significance of three-dimensionally preserved soft tissues for comparative studies.

5.2 Methods

5.2.1 Material examined

Specimens come from the Lontras Shale strata, within the uppermost Campo Mourão Formation of the Paraná Basin, Brazil. Specimens were collected at the 'campáleo' outcrop in the south of the city of Mafra, state of Santa Catarina, and are deposited in the paleontological collection of the Centro Paleontológico da Universidade do Contestado (CENPALEO-UnC).

All fossil specimens analyzed in this work (CP 065, CP.V 4364, CP.V 7053, CP.V 7227, CP 084, CP 508, CP 577, CP 584) were collected in the late Carboniferous to Early Permian Campo Mourão Formation in the surroundings of the city of Mafra, Santa Catarina, Brazil.

This study contains data acquired from ethanol preserved specimens from the University of Michigan Museum of Zoology collection. Figured specimens of *Polypterus senegalus* (UMMZ 195008), *Amia calva* (UMMZ 160805, UMMZ, 235291) and *Lepisosteus ocelatus* (UMMZ 196974).

5.2.2 Specimen visualization

The fossil specimens were scanned with the Nikon XT H 225 ST scanner of the CTEES facility in the Department of Earth and Environmental Sciences, University of Michigan. Detailed scan parameters can be found in Table S1. Segmentation of the resulting data was completed in Mimics 25.0 (Materialise, Leuven, Belgium) and further imaging of the obtained .ply 3D models was done in Blender 4.0 (Garwood and Dunlop 2014). Comparative extant species Iodine enhanced μCT data was performed following the guidelines described in Kolmann et al. (2023).

5.2.3 Geological settings

Specimens derive from the Lontras Shale sub-section of the Campo Mourão Formation in the Paraná Basin, Brazil. The age of the Lontras Shale unit is estimated between the latest Carboniferous and earliest Permian based on both radiometric dating and biostratigraphy (Holz et al. 2010; Cagliari et al. 2016; Wilner et al. 2016; Griffis et al. 2019a; Valdez Buso et al. 2019). The Lontras Shale is a stratigraphic marker within the Paraná Basin that is related to a maximum marine flooding event (França and Potter 1991). The lithology, stratigraphy and paleobiota of the Lontras Shale suggest deposition in a restricted marine setting, such as a fjord (Mouro et al. 2017). Specimens analyzed here are preserved in three dimensions and within sideritic concretions (Hamel 2005). Preservation of specimens varies as in a few examples (e.g. CP 065, CP 508, CP.V 4364) sediment is found within the fossilized skulls, while in others (e.g. CP 577, CP 584) sediment within the fossil seems to have been lost during diagenetic and post-diagenetic processes. In one specimen (CP.V 7053) the sediment within the skull seems to have been recrystallized.

5.3 Results

5.3.1 Lontras Shale ray-finned fishes

The Lontras Shale bears dark, laminated shales preserve compressed but essentially complete, articulated specimens (Malabarba 1988; Saldanha et al. 2022). Sideritic concretions within these shales contain three-dimensionally preserved skulls (Hamel 2005). These specimens show two distinct taphonomic modes where some skulls are fully perfused with matrix while others have lost the matrix infill of the skull. Micro-computed tomography (μCT) of concretions reveals skeletal anatomy plus soft-tissue structures within and around the braincase and optic capsules. Two different ray-finned fish morphotypes, distinguished on the basis of major osteological traits (Figure 5.1), show soft-tissue preservation. These forms differ in features of the mandibular, hyoid, and branchial arches, as well as the braincase (Appendix E). For each of these features, Morphotype I shows a derived state relative to Morphotype II based on comparison with well-preserved Late Devonian taxa that branch from the actinopterygian stem (Giles et al. 2015b). Osteological data suggests that Morphotype I is closely related to more crownward forms (e.g., the Triassic †*Australosomus*), while CP 584 resembles more stemward taxa from the Devonian and Carboniferous. Taken together with †*Coccocephalus wildi*, these three examples appear to represent a grade on the actinopterygian stem.

Each morphotype is represented by multiple specimens (Appendix E). However, most of our account focuses on two specimens: CP 065 for Morphotype I and CP 584 for Morphotype II (Appendix Figure E.1). Additional specimens are too incomplete to be assigned to a morphotype but display partial soft-tissue preservation (CP 1343, CP 6573). Precise taxonomic assessment of these two morphotypes is challenging. Previously described taxa from the Lontras Shale are, like many Paleozoic actinopterygians, based on poor type material (Malabarba 1988; Hamel 2005) that do not permit us to either assign the morphotypes to either existing taxa or alternatively propose new ones. We therefore leave our specimens in open nomenclature pending revision of the Lontras actinopterygian fauna.

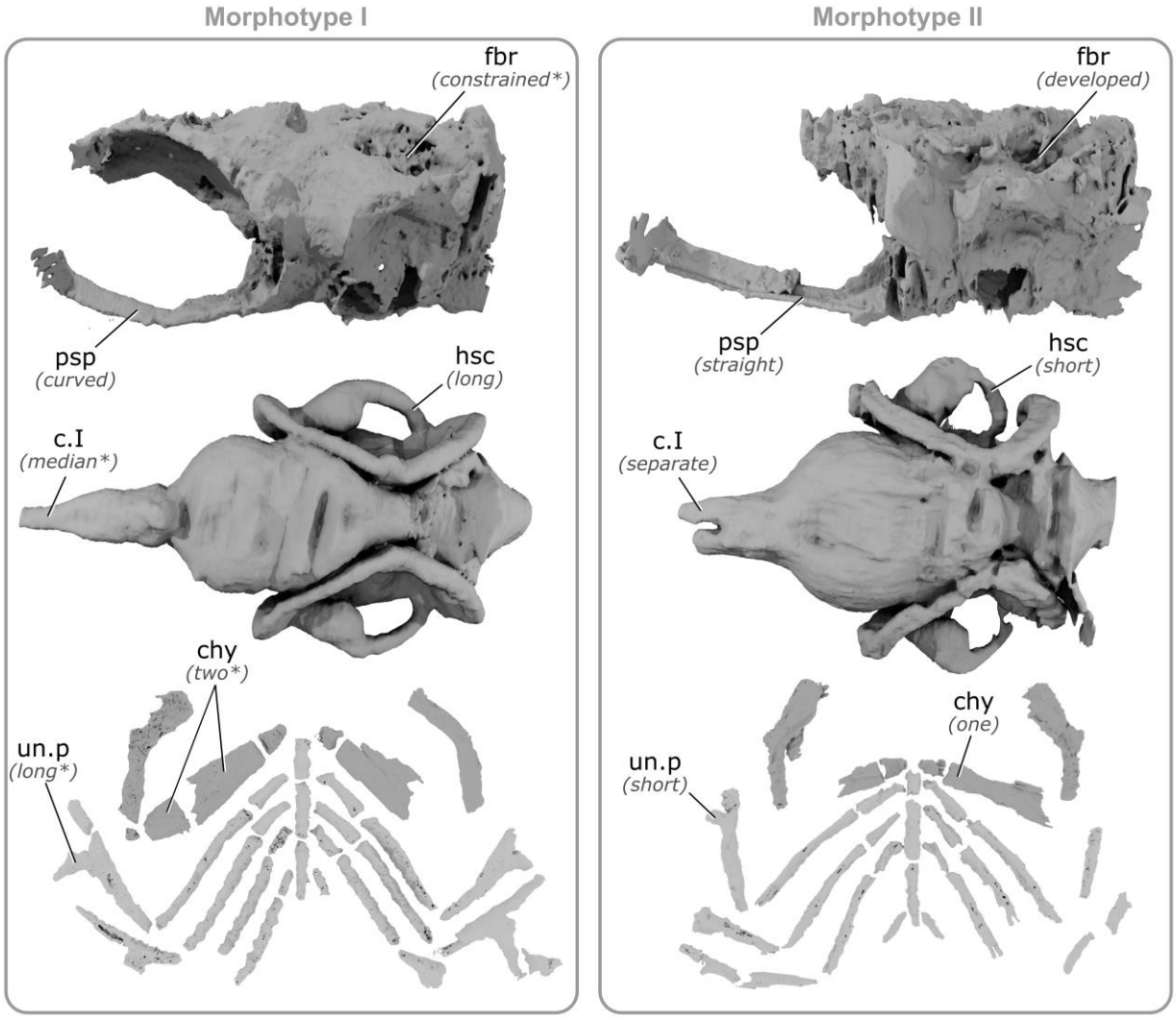

Figure 5.1 – Comparison of two morphotypes of actinopterygian fishes from the Lontras Shale, Brazil, differentiated on the basis of osteological traits, showing neurocranium (top), endocast (middle) and hyobranchial apparatus (bottom). c.I, olfactory tract, chy, ceratohyal, fbr, fossa bridgei, hsc, horizontal semicircular canal, psp, parasphenoid, un.p, uncinate processes. Panels not to scale.

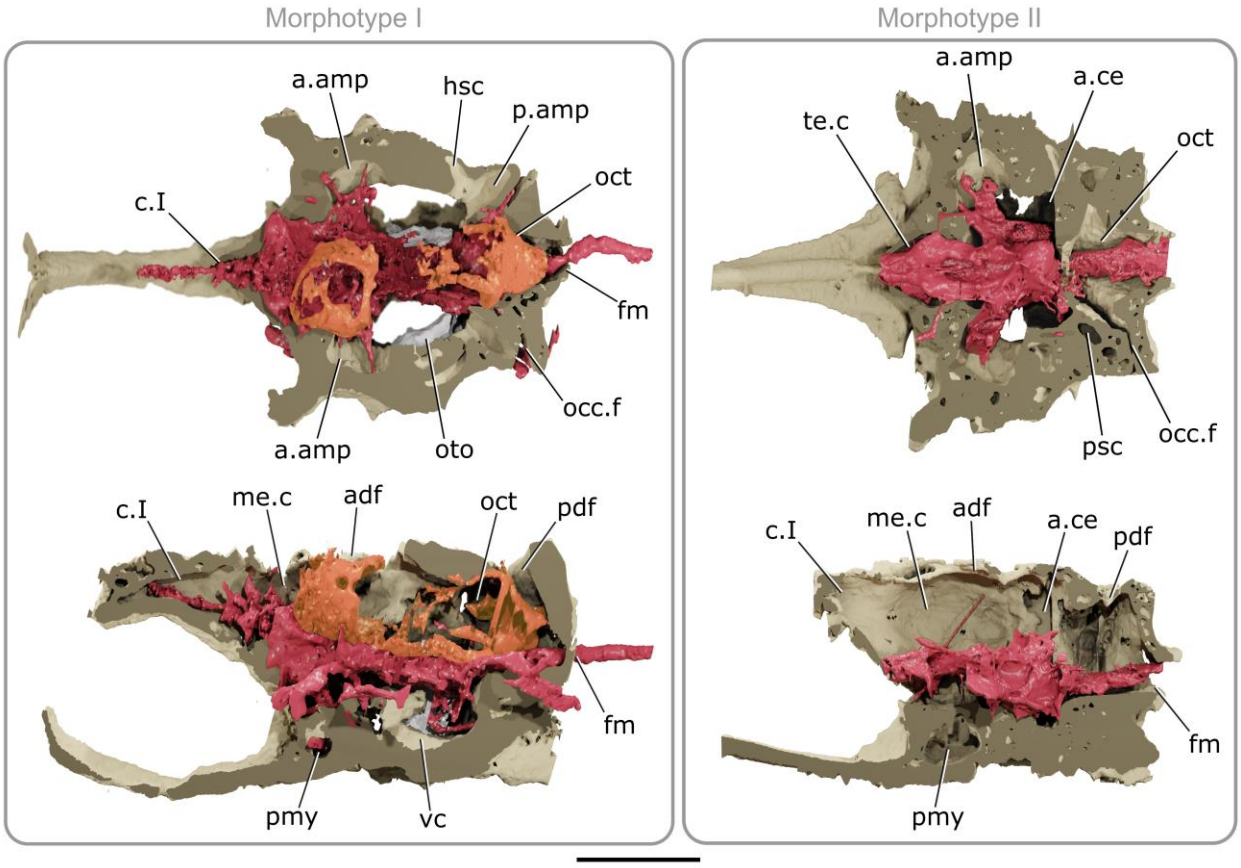

Figure 5.2 – Brain and neurocranial morphology in Permian actinopterygian fishes. Neurocranium partially removed to show position of brain within the endocavity. Morphotype I and Morphotype II in dorsal (top) and left lateral (bottom) views. Light beige = braincase, dark beige = sliced braincase plane, red = brain, orange = meningeal tissue. a.amp, anterior ampulla, a.ce, auricula cerebelli, adf, anterodorsal fontanelle, c.I, olfactory tract, fm, foramen magnum, hsc, horizontal semicircular canal, me.c, mesencephalic chamber, occ.f, occipital fissure, oct, area octavolateralis, oto, otolith, p.amp, posterior ampulla, pdf, posterodorsal fontanelle, pmy, posterior myodome, psc, posterior semicircular canal, te.c, telencephalic chamber, vc, vestibular chamber. Scale bar = 5 mm for both morphotypes.

5.3.2 Fossil brain anatomy

The brain occupies a small portion of the endocranial cavity in both morphotypes, in agreement with †*Coccocephalus* (Figueroa et al. 2023) and in contrary to widespread assumptions (Moodie 1915; Coates 1999; Giles and Friedman 2014). It appears more closely associated with the endocranial wall in Morphotype I due to the preservation of possible meningeal tissues (Figures 5.2; 5.3). Both morphotypes show clear division of the forebrain, midbrain, and hindbrain, with the midbrain representing the largest division. Cranial nerves from all three regions extend toward foramina on the endocranial wall. The gross anatomy of these

fossil brains generally corresponds with that of both extant ray-finned fishes[1] and the older stem actinopterygian †*Coccocephalus wildi* (Figueroa et al. 2023).

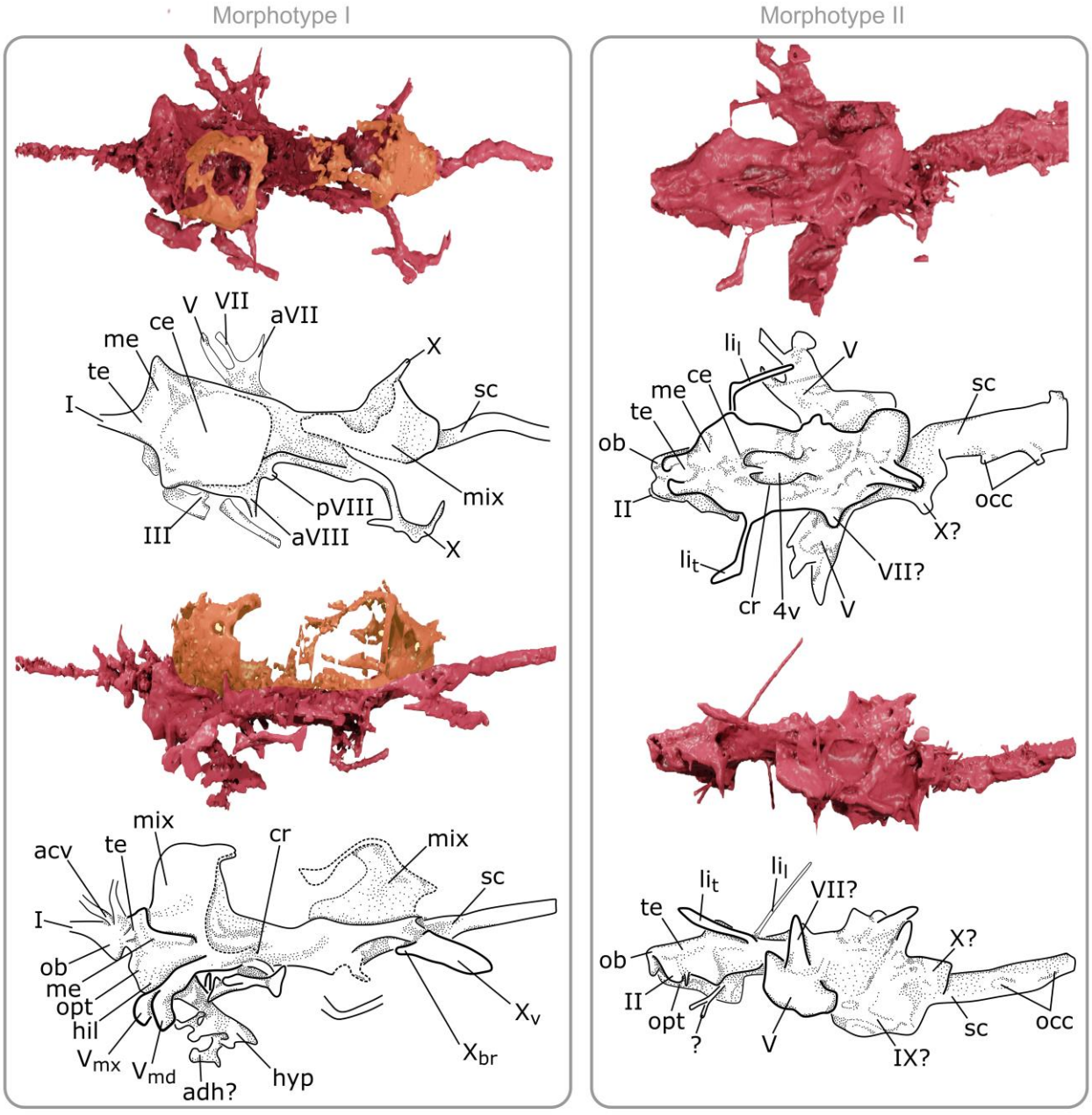

Figure 5.3 – Brain morphology in Permian actinopterygian fishes. Morphotype I (CP 065) and Morphotype II (CP 584) in dorsal (top) and left-lateral (bottom) view. Drawings are interpretative schemes based on renders. 4v, fourth ventricle, acv, anterior cerebral vein, adh, adenohypophysis, ce, cerebellum, cr, crista cerebellaris, hil, hypothamus inferor lobe, hyp, hypophysis, lil, longitudinal ligament, lit, transverse ligament, me, mesencephalon, mix, meninx, ob, olfactory bulb, occ, occipital nerves, opt, optic chiasma, sc, spinal cord, te, telencephalon, I, olfactory nerve, III, oculomotor nerve, V, trigeminal nerve, Vmd, mandibular branch of trigeminal, Vmx, maxillary branch of trigeminal, VII, facial nerve, aVII, anterior branch of facial nerve, aVIII, anterior branch of octavolateralis nerve,

pVII, posterior branch of octavolateralis nerve, IX, glossopharyngeal nerve, X, vagus nerve, Xbr, branchial branch of vagus nerve, Xv, visceral branch of vagus nerve. Scale bar = 5 mm for both morphotypes.

Morphotype I. Small, poorly preserved olfactory bulbs fused into a single median structure lie anteroventral to the telencephalon (ob, Figure 5.3). The small, V-shaped telencephalon (te, Figure 5.3) shows indications of eversion (Appendix Figure E.6). A pair of asymmetrically diverging structures extends toward the roof of the telencephalic region of the endocast, possibly representing anterior cerebral veins (acv, Figure 5.3; main choroidal veins of Weiger et al. (1988)).

The mesencephalon is well-preserved (Fig. 5.3), with the optic tectum represented as a sheet surrounding the mesencephalic ventricles (Appendix Fig. E.6). In dorsal view, the optic tectum forms diverging elliptical lobes. There is no evidence of a protrusion associated with the torus lateralis on the lateroventral wall of the diencephalon, and intraventricular projections associated with a torus longitudinalis or torus semicircularis are not apparent (Appendix Fig. E.1, me). We cannot identify a cerebral aqueduct connecting the mesencephalic ventricles to the more posterior fourth ventricle. A small internal cavity of the brain lies ventral to the fourth ventricle. This might be the extrameningeal space connected to the infundibulum (Appendix Fig. E.1, me). Small bumps posterior to the mesencephalon that seem to coalesce represent the cerebellum or corpus cerebelli (Appendix Fig. E.1). The posterior part of the hindbrain is a long stalk of circular cross-section, comprising the myelencephalon and spinal cord (sc, Figure 5.3).

The hypophysis emerges from the ventralmost portion of the diencephalon (hypothalamus) and extends ventrally towards the hypophyseal chamber of the neurocranium. The distal end of the hypophysis bears a small well-differentiated adenohypophysis (adh, Figure 5.3) that lies dorsal to the parasphenoid. The hypothalamus is elongated with large hypothalamic inferior lobes (hil, Figure 5.3).

Cranial nerves are partially visible on both sides of the brain. A single thin, poorly preserved olfactory nerve (I) extends into the olfactory canal of the endocavity. The mesencephalon bears an expansion representing the roots of the optic nerves (II; optic chiasma). At the level of the posteriormost portion of the mesencephalic bulbs, the rhombencephalon bears a nucleus that divides into three separate nerves. These appear to be, from anterior to posterior: the main motor branch of the trigeminal nerve (V), a posterior branch of the facial nerve (VII), and the octavolateralis (VIII) complex. Only two branches of the latter complex are well

preserved: one interpreted as the anterior branch of the octavolateralis (aVII) nerve, and second posteroventrally directed towards the saccular chamber and representing the posterior branch of the octavolateralis (pVII). Other branches are too poorly preserved to identify. The vagus nerve (X, Figure 5.3) extends from the hindbrain and exits the neurocranium through the otico-occipital fissure (Figure 5.3). It divides into anteriorly- and posteriorly-directed branches, which are here identified as branchial and visceral rami, respectively.

A thin sheet, closely associated with the internal surface of the endocavity, surrounds the brain (mix, Figure 5.3). It is best developed at the diencephalon-mesencephalon interface and above the rhombencephalon. The membrane connects laterally to the body of the brain, dorsal to most nerve roots, and appears to represent meningeal tissue related to the diencephalic and rhombencephalic tela choroidea.

Morphotype II. Brain anatomy for Morphotype II is less clear than for Morphotype I. The poorly preserved telencephalon consists of the left telencephalic bulb (te, Figure 5.3) and appears to be evaginated (Appendix Fig. E.6). The expanded area of the optic chiasma lies ventral to the telencephalon, immediately posterior to the median optic nerve foramen. The mesencephalon shows similar proportions to Morphotype I (CP 065), but compression of the mesencephalic ventricles suggests shrinkage or compression (me, Appendix Fig. E.1). Another specimen attributable to Morphotype II (CP 508) shows well-developed mesencephalic ventricles (Figure 5.4). A possible infundibulum extends more posteriorly than in Morphotype I. The cerebellum bears paired lobes that do not seem to coalesce (Figure 5.3). Anterodorsal and lateral bands suspend the brain within the endocranial chamber (li_l, li_t, Figure 5.3), representing possible ligaments (cf. *Polypterus*; Bjerring (1991)).

The mesencephalon shows clearly defined–but taphonomically compressed–mesencephalic bulbs forming the optic tectum (Appendix Fig. E.1). Thin separation marking the ventricular wall indicates that ventricles were present in life (Appendix Fig. E.1), but they cannot be reconstructed. The optic nerve (II) lies ventral to the mesencephalic bulbs. A small protrusion that could be the origin of the oculomotor nerve (III) is apparent on the right side of the brain near the optic chiasma.

A clearly defined crista cerebellaris (cr; Figure 5.3) from the posteriormost portion of the mesencephalic region towards the spinal cord. Small concavities posterior to the mesencephalic

bulbs represent the corpus cerebelli, which appears to be invaginated (Appendix Fig. E.8). The rhombencephalic region of the brain shows the expanded nuclei of the trigeminal nerve (V) and hyomandibular trunk of the anteroventral lateral line and facial nerves (AV + VII_{hy}; Fig. 2). These display an arrangement like Morphotype I, although they are more robust and occupy a more posterior position in Morphotype II. A nodule-like structure, likely formed from taphonomic torsion of the spinal cord, lies posterior to these nuclei. The robust spinal cord extends to reach the foramen magnum. The vagus and accessory spinal nerves are not preserved.

A large soft-tissue structure overlies the spinal cord and extends laterally towards the lateral cranial canal (Appendix Fig. E.7). We consider this structure homologous to the myelencephalic gland of chondrosteans and holosteans (van der Horst 1925; Figueroa et al. 2023).

Additional specimens. Other specimens show similar structures to the examples described above, but are less well preserved and do not generally provide additional information on brain anatomy. These include examples of Morphotype I (CP.V 4364, CP.V 7053, CP.V 7227) and Morphotype II (CP 084, CP 577).

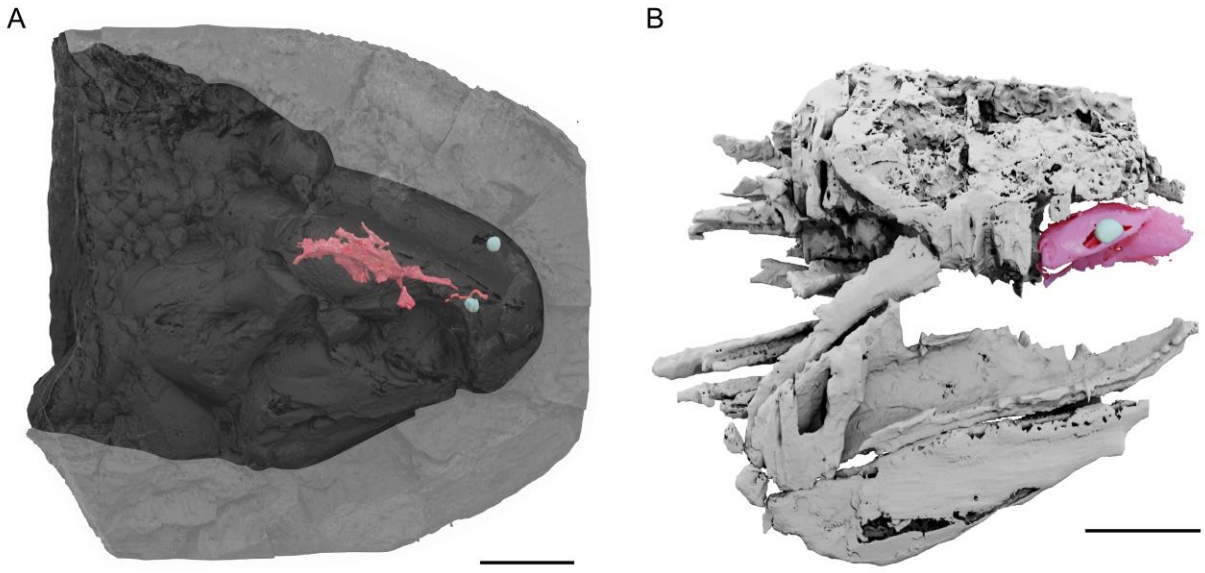

Figure 5.4 – *In situ* three-dimensional soft tissues preserved of specimens of Morphotype II. (A) Render of CP 507 showing the brain (red) and eye lenses (gray). (B) Render of the cranium of CP 084 in right-lateral view showing eye soft-tissue. Scale bar = 10 mm.

5.3.3 Other preserved soft tissues

Apart from the brains, other soft tissues are apparent to varying degrees. Many specimens preserve eye lenses (Morphotype I: CP 065, CP.V 4364; Morphotype II: CP 084, CP 508), with some showing more extensive preservation of other features. In CP 084, a thin sheet of tissue embraces the mesial half of the eye lens (Fig. 5.3), likely representing the sclera and retina (Fig 3B; Fig. S5). The mesial face of this sheet bears tuberous structure corresponding to the optic nerve. CP 4364 shows scleral tissue dissociated from the displaced eye lens, but attached to the brain via a robust optic nerve tract. Some specimens show possible evidence of extrinsic eye muscles (Appendix Fig E.3).

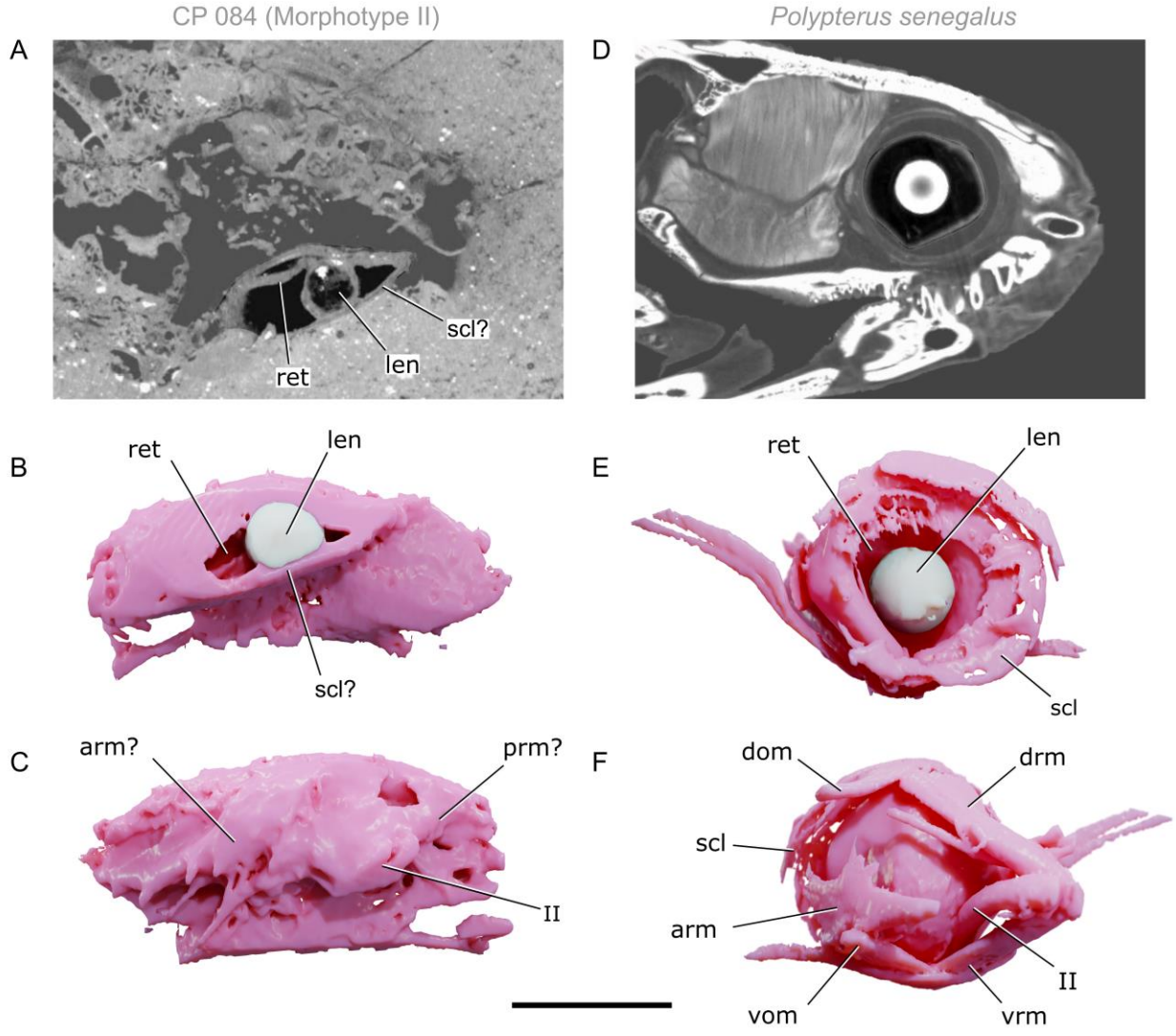

Figure 5.5 – Eye morphology in fossil and extant actinopterygians. (A-C) Morphotype II (CP 084), (D-F) *Polypterus senegalus* (UMMZ 195008). (A,D) μCT sagittal section through eye, (B,E) render of right eye in lateral view, (C-F) render of right eye in mesial view. arm, anterior rectus muscle, dom, dorsal obliquus muscle, drm, dorsal rectus muscle, len, lens, prm, posterior rectus muscle, ret, retina, scl, sclera, vom, ventral obliquus muscle, vrm, ventral rectus muscle, II, optic nerve. Scale bar = 10 mm.

Gill filaments are well preserved in several specimens (Morphotype I: CP 065; Morphotype II: CP 084; and indeterminate: CP 1343, CP 6573). The gill filaments are short and robust in both morphotypes, attaching to the lateral margin of the elongate ceratobranchials. Some filaments show the area of attachment to the branchial arch in detail (Appendix Fig E.4).

Putative cardiovascular elements are poorly preserved in all specimens, with fragments of blood vessels observed in a small number of specimens (Morphotype I: CP 4346, Morphotype II: CP 084, CP 584). However, these do not provide any valuable anatomical information (Appendix Fig. E.5).

5.4 Discussion

5.4.1 Placement and polarity of character changes

Given the osteological variation and polarity of these characters described above, we interpret these two Brazilian morphotypes to form a grade on the actinopterygian stem together with *Coccocephalus* (Figure 5.6). Thus, these fossils provide insights on the polarity of important neuroanatomical changes along the actinopterygian stem.

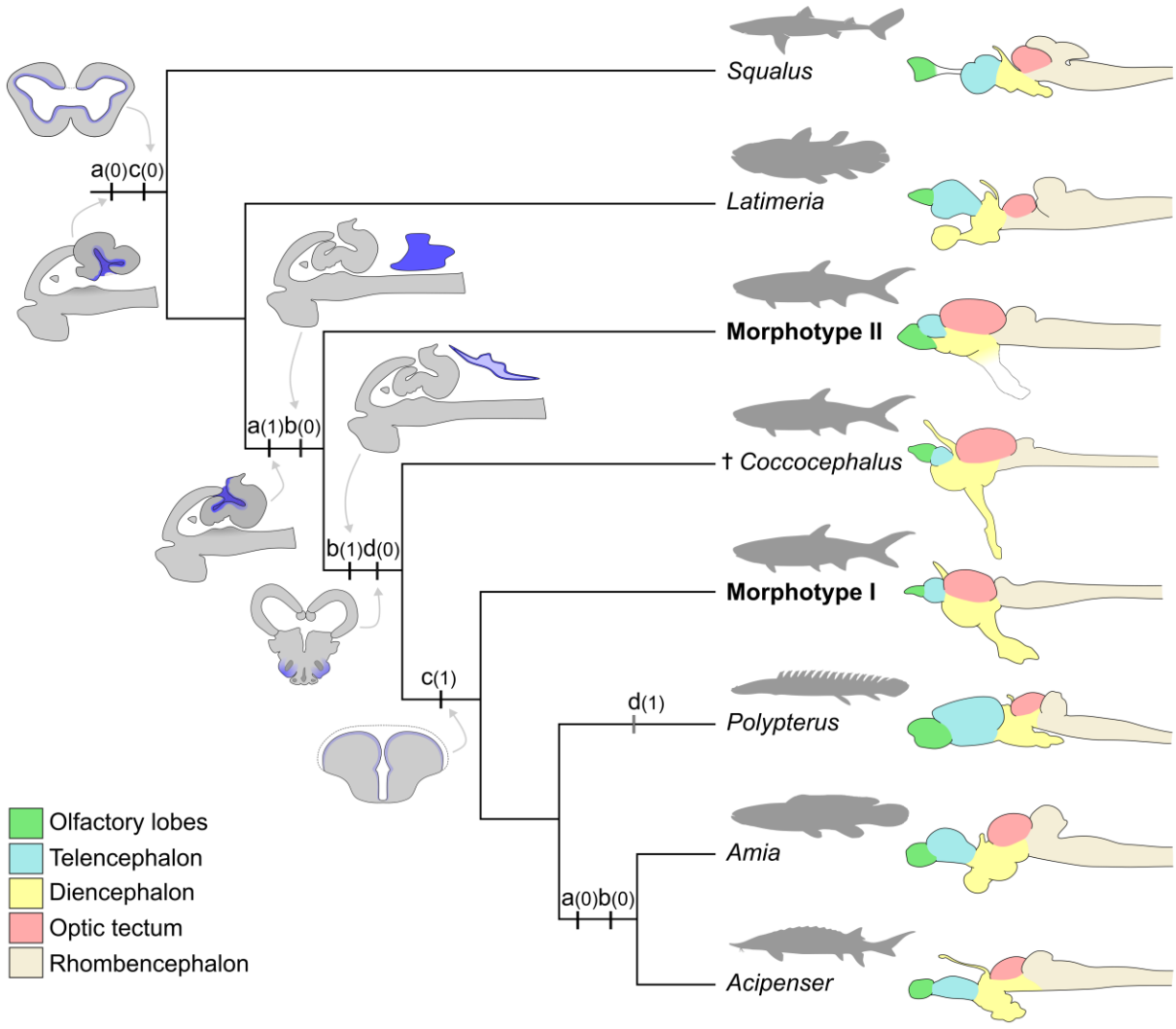

Figure 5.6 – Schematic representation of ray-finned fish brain evolution. a, corpus cerebelli (0 = evaginated; 1 = invaginated; illustrated by sagittal sections through idealized hindbrain), b, modified rhombencephalic meningeal tissue (0 = myelencephalic gland; 1 = cisterna spinobulbaris; illustrated by sagittal sections through idealized hindbrain and spinal cord), c, telencephalon (0 = evaginated, 1 = everted; illustrated by axial sections through idealized telencephalon), d, hypothalamus inferior lobes (0 = present; 1 = absent; illustrated by axial sections through idealized diencephalon). Taxon silhouettes obtained from PhyloPic (https://www.phylopic.org/). Extant taxa brain diagrams based on Nieuwenhuys et al (1998).

Telencephalon eversion versus evagination. In Morphotype I, the telencephalon displays a dorsolateral expansion and ventral compression towards the area of the optic chiasma, resulting in a V-shaped structure in cross-section (Appendix Fig E.6). This resembles the everted telencephalon geometry of all extant ray-finned fishes. Morphotype II (e.g. CP 584) and †*Coccocephalus* (Figueroa et al. 2023), show a contrasting anatomical condition. In cross-section the telencephalon of these taxa forms a symmetrical bulge with a central cavity but

lacking a ventral compression (Appendix Figures E.1, 6). This is similar to structure in living sarcopterygians and chondrichthyans, and so is interpreted here as representing a plesiomorphic evaginated telencephalon. We therefore place telencephalic eversion as a feature emerging crownward of †*Coccocephalus* but stemward of CP 065 (Figure 5.6). More information from late Paleozoic fossil brains will be essential for better understanding the timing of origin of the everted condition found in living ray-finned fishes, but current information points to a late Paleozoic origin for the development of this condition.

Hypothalamus inferior lobes. The presence of a hypothalamus inferior lobe in some specimens challenges the current hypothesis of character polarity. Since a hypothalamus inferior lobe is absent in the earliest diverging lineage of crown ray-finned fishes (i.e., cladistians) it was assumed to be a derived feature of actinopterans (crown ray-finned fishes excluding Cladistia (Rustamov 2006; Schmidt 2020)). However, its presence in some of the Brazilian specimens, as well as in the older †*Coccocephalus*, challenges this hypothesis. Conditions in these probable stem actinopterygians imply the absence of the hypothalamus inferior lobe in cladistians is a reversal within that lineage rather than retention of a primitive arrangement. The apparent absence of a hypothalamus inferior lobe in some of the Brazilian specimens (e.g. CP 584) is likely due to taphonomy and compression of the soft-tissue against the endocranial wall. Future work should investigate the relationship between the actinopterygian hypothalamus inferior lobe and other hypothalamic projections in lobe-finned fishes and chondrichthyans. This is essential to determine if these independently emerged in several lineages or if instead hypothalamic ventral projections are primitive for crown gnathostomes.

Intraventricular projections. Extant actinopterans show well-differentiated intraventricular projections (torus longitudinalis, torus semicircularis) within the second ventricle. These are unique to the group (Nieuwenhuys et al. 1998). Cladistians are unique among living ray-finned fishes in lacking a torus longitudinalis and torus semicircularis (Jarvik 1980; Nieuwenhuys et al. 1998). All known Permo-Carboniferous actinopterygian brains show no evidence for these intraventricular projections, with all examples showing a very homogeneous ventricular margin. Thus, we confirm these intraventricular projections are a derived characteristic of actinopterans.

Additional features. Discussion of meningeal tissues and brain vascularization patterns of the analyzed fossils in comparison to living taxa can be found in Appendix E.

5.4.2 Future directions in paleoneurology

The field of paleoneurology has advanced since its early days (Stensio 1906; Edinger 1964; Buchholtz and Seyfarth 1999) through the study of endocasts as proxy for brain anatomy in several vertebrate groups (Coates 1999; Giles and Friedman 2014; Zhu et al. 2021) and two-dimensional imprints of nerve tissue in some invertebrates (Ma et al. 2012; Cong et al. 2014). However, endocast data remains limited in providing an external model of the brain at best (Northcutt 2002) and only loose constraints on morphology in taxa where the volume of the brain is small in comparison to that of the endocavity (Watanabe et al. 2019a; Challands et al. 2020). The three-dimensional preservation of neural soft-tissue structures discovered in fossil fishes by past studies (Pradel et al. 2009b) and expanded upon here suggests further tomographic surveys of vertebrates are likely to yield additional examples. Geological context for each of these cases is broadly similar, with fossil skulls preserved in three-dimensions within concretions. Several Paleozoic and early Mesozoic sites yield three-dimensional heads of actinopterygians within concretions (Woodward 1910; Moodie 1915; Nielsen 1949; Schaeffer and Dalquest 1978; Pradel et al. 2016), and we are optimistic that further tomographic surveys of this material will yield additional instances of soft tissue preservation. As investigation of other fossils expands the dataset of fossil brains, it might be possible to discern which taphonomic or environmental aspects tend to covary with the preservation of neuroanatomy. This, in turn, can be used to identify material that is most likely to yield soft-tissue structures. Even modest amounts of information on ancient brain anatomy in other branches of the actinopterygian phylogeny–including deeper parts of the actinopterygian stem, the actinopteran stem, and the teleost stem–could provide important new evidence on patterns of neuroanatomical evolution in ray-finned fishes. Our results suggest that information from fossil soft tissues can have an impact on our understanding of the evolution of deeply branching lineages,helping to identify patterns of morphological change that would be otherwise impossible to interpret only from extant taxa. The fossils described herein challenge current interpretations of the origin and timing of important

morphological innovations, especially within the forebrain. This highlights biases that might arise from reconstructing the phylogenetic history of important morphological innovations based solely on extant species. We expect that with the inclusion of more information on soft tissue anatomy of early vertebrates—gathered from exceptional soft-tissue preservation—we will be able to better understand not only the placement of fossil taxa in relation to the crown, but also revise soft-tissue features of living lineages and determine how far back in geologic time many of these putative synapomorphies of extant clades emerged.

Chapter 6 The Obscure Evolutionary History of Neuroanatomical Innovation in Ray-Finned Fishes

6.1 Introduction

Ray-finned fishes are the most diverse group of extant jawed vertebrates, comprising nearly half of all living vertebrate species (Nelson et al. 2016). High anatomical disparity complements this taxonomic richness, with actinopterygians showing diverse morphological adaptations that permit species to occupy virtually all aquatic environments, from streams and ephemeral lakes to deep oceanic trenches (Nelson et al. 2016). This substantial taxonomic and morphological variety—combined with an increasingly robust phylogenetic framework (Near et al. 2012; Alfaro 2018; Hughes et al. 2018; Rabosky et al. 2018; Near and Thacker 2024)—make ray-finned fishes an ideal system for investigating evolutionary diversification. A growing number of studies demonstrate that ray-finned fishes show a myriad of different patterns of diversification, where ecology, development and phylogenetic relationships play distinct roles in shaping current diversity and distribution (Faircloth et al. 2013; Ladich and Schulz-Mirbach 2016; Hibi et al. 2017; Rabosky et al. 2018; Dornburg et al. 2021; Egan et al. 2021; Miller and Román-Palacios 2021; Peters et al. 2024). These contributions overwhelmingly focus on external aspects of anatomy like gross body form or select skeletal features like jaws and teeth (Wainwright et al. 2012; Friedman et al. 2022; Price et al. 2022). A key soft-tissue system characterized by substantial diversity and representing an important link between other anatomical features is conspicuously absent from our understanding of ray-finned fish diversification: the brain.

Given the remarkable variety of other aspects of ray-finned fish structure, it seems likely that the ray-finned fish brain is similarly diverse, representing a promising—but largely unexamined—substrate for the study of phenotypic evolution. Prior work on other vertebrate lineages indicate considerable variation in brain morphology, and link some aspects of this variation to contrasting ecologies (Finlay and Darlington 1995; Krebs et al. 1996; Barton and Harvey 2000; Gonda et al. 2013; Fabbri et al. 2017; Ksepka et al. 2020; Segall et al. 2021;

Watanabe et al. 2021). By contrast, there is virtually no information regarding detailed brain morphology for the majority of the ray-finned fish species, outside of model species like the zebrafish *Danio* (Evans 1931; Kotrschal and Palzenberger 1992; Wullimann et al. 1996; Kotrschal et al. 1998; Ullmann et al. 2010; Khan et al. 2021) and a handful of groups targeted specifically for their extreme brain morphology (Cadwallader 1975; Eastman and Lannoo 1995; Chapman and Hulen 2001; Abrahão and Shibatta 2015; Eifert et al. 2015). Although sparse, these examples indicate links between brain structure and ecology or habitat preference in ray-finned fishes. This is particularly apparent for the olfactory bulbs and the optic tectum, brain regions with clear sensory implications (Kotrschal et al. 1998). However, since these studies have focused on a small subset of taxa and lineages it is unclear whether their findings might be applicable to actinopterygian diversity more generally. Although finer details of brain structure are lacking for most groups, coarse phenotypic measures—like relative brain size in comparison to body size (Tsuboi 2021; Fischer and Jungwirth 2022) or volumetric differences between brain regions (Schmidt 2020; Schumacher and Carlson 2022)—hint at substantial variation and an important role for modularity between brain regions (Redies and Puelles 2001; Schumacher and Carlson 2022), comparable to other aspects of ray-finned fish anatomy (Larouche et al. 2018).

Here I describe patterns of neuroanatomical variation in living ray-finned fishes and associated endocranial anatomy using high-resolution diffusible-iodine contrast-enhanced micro-CT scanning. Additionally, I present a novel landmarking scheme and preliminary quantitative results describing the morphological diversity of living ray-finned fishes.

6.2 Methods

6.2.1 Comparative 3D brain data

To better understand the morphological variation among ray-finned fish brains in three dimensions, non-destructive methods such as diffusible iodine contrast enhanced μCT scanning (dice-CT) were used to maximize the number of specimens available as well as the possibility of sampling more rare taxa that might yield important morphological information. The protocol proposed by Kolmann et al. (2023) was used to stain ethanol-preserved fish specimens from the University of Michigan Museum of Zoology collection. After staining specimens were scanned

using the Nikon XT H 225ST μCT scanner at the CTEES facility of the University of Michigan Department of Earth and Environmental Sciences. Data from additional taxa was collected from MorphoSource (morphosource.org) when available. Given the exploratory nature of this work, sampling has focused on obtaining an approximately even sampling throughout the ray-finned fish tree, but also paying attention to sampling known morphological diversity. This dataset serves as a backbone for future work, which should focus on expanding this dataset to include a better representation of exceptionally diverse (morphologically and phylogenetically) lineages. The dataset used in this work includes 76 extant ray-finned fishes from 75 different families (Appendix F).

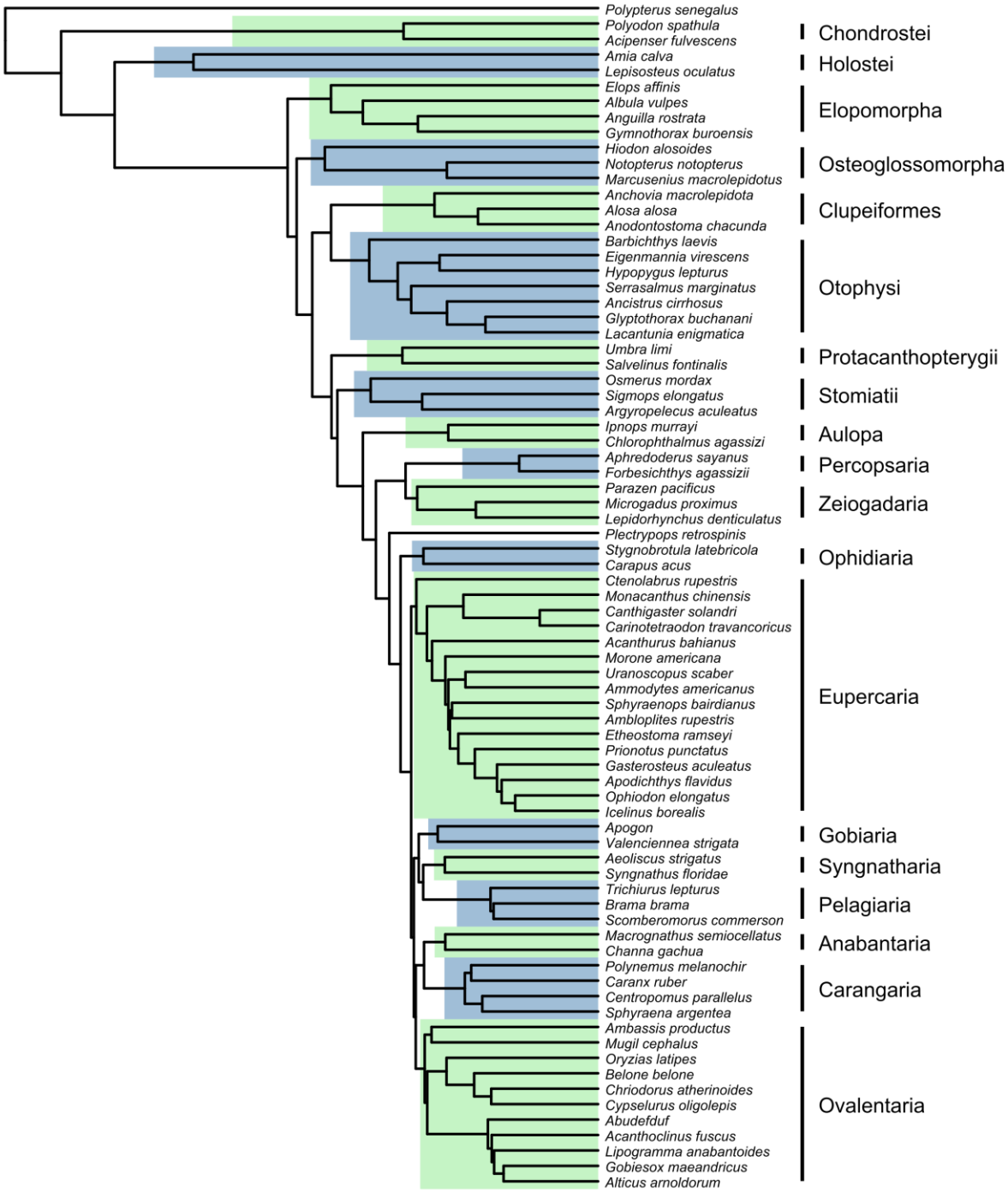

Figure 6.1 – Phylogenetic sampling used in this study based on the tree from Rabosky et al. (2018). Tips represent taxa that have been dice-CT scanned for this study. Higher level groupings are shown at right, highlighted by the two different shades on the branches.

6.2.2 Quantitative analysis

In order to explore the morphological diversity of brains in living ray-finned fishes a new geometric morphometric scheme had to be implemented. Given the known variation in ray-finned fish brain morphology in respect to different tissue layers, I had to adopt a conservative approach on devising this landmark scheme. Previous studies have focused on volumetric variation of different brain regions in teleosts (Eifert et al. 2015; Schumacher and Carlson 2022; Gebhardt and Hofmann 2023), but little attention has been given to variation in morphology, especially with respect to structures that are not discernible from surface models. Thus, I implement a new morphometric protocol for ray-finned fishes, which applies fixed landmarks directly to µCT volumes rather than surface models. This permits the inclusion of landmarks in clearly defined homologous histological features of the brain that might not be visible superficially. As cladistians (i.e. *Polypterus*, *Erpetoichthys*) are highly apomorphic and lack several features shared by other living ray-finned fishes, these have been excluded from this morphometric analysis. Landmarking was done using 3D Slicer (Fedorov et al. 2012) by importing nrrd. files of the µCT volumes converted in imageJ (Schneider et al. 2012).

The obtained landmark scheme comprises 22 fixed landmarks dispersed through the three main regions of the ray-finned fish brain (forebrain, midbrain and hindbrain):

1 – Anteriormost point of the olfactory bulb;
2 – Posteriormost point of the olfactory bulb;
3 – Anteriormost point of the telencephalon (dorsal pallium);
4 – Posteriormost point of the telencephalon (dorsal pallium);
5 – Anterior end of the hypothalamus inferior lobe;
6 – Posterior end of the hypothalamus inferior lobe;
7 – Anterior end of the hypophysis;
8 – Posterior end of the hypophysis;
9 – Intersection of optic nerves forming the optic chiasma;
10 – Anteriormost point of the optic tectum;
11 – Posteriormost point of the optic tectum;
12 – Anterior end of the torus longitudinalis;
13 – Posterior endo of the torus longitudinalis;
14 – Anterior end of the torus semicircularis;

15 – Posterior end of the torus semicircularis;

16 – Anteriormost point of the cerebellar corpus (molecular layer);

17 – Posteriormost point of the cerebellar corpus (molecular layer);

18 – Lateralmost point of the cerebellar corpus (eminentia granularis);

19 – Anterior end of the valvula cerebelli;

20 – Posterior end of the valvula cerebelli;

21 – Anterior end of the crista cerebellaris (contact with lateral wall of the corpus cerebelli);

22 – Posterior end of the crista cerebellaris.

This preliminary landmarking scheme covers important aspects of morphology in ray-finned fishes and can be expanded to include more fixed landmarks as more taxa are added to the dataset and the inclusion of sliding surface semilandmarks to cover the external surface of different brain regions.

The resulting landmarks were analyzed in the R statistical environment (R Core Team 2024). First, fcsv. coordinates exported from 3D Slicer were compiled in a single array with three dimensions (x, y, z). With this array a generalized Procrustes (GPA) was performed using the function gpagen from the package geomorph (Baken et al. 2021). Using the function gm.prcomp a principal component analysis was performed with the Procrustes-alligned coordinates. To investigate morphological disparity among different groups the function morphol.disparity was used with the groups specified being "non-teleost", "non-acanthomorph teleost" and "acanthomorph." A modification of the geomorph function shapeHulls was used to scatter plot the PC values with colored hulls separating the groups defined above.

A phylogeny including all sampled taxa was pruned from the tree of Rabosky et al. (2018). This pruned tree was obtained by a custom function which uses fishtree_phylogeny from the package fishtree (Chang et al. 2019) to read the names in the provided dataset and substitute names that do not match the tip labels of the Rabosky et al. (2018) tree. Two trees were pruned using this function: one including all the sampled taxa and one including only the taxa in the morphometric analysis. This second tree was used to perform a phylogenetic PCA using the function gm.prcomp from geomorph (Baken et al. 2021). A modification of the function fancyTree from the package phytools (Revell 2012, 2024) was used to produce a plot showing

multiple axes of variation of PC values in a composed scattergram plot colored by the specified groups.

6.3 Ray-finned fish brain morphological diversity

6.4 Brain vs endocast

Endocasts represent the infill of the space within the neurocranium where the brain is contained (Edinger 1964). Natural and reconstructed endocasts have been used as indirect evidence for brain anatomy in many fossil lineages and as important axes of morphological diversity for understanding fossil interrelationships (Moodie 1915; Stensiö 1963; Edinger 1964; Coates 1999; Janvier 2008; Giles and Friedman 2014; Zhu et al. 2021). Nevertheless, the degree to which brains conform to endocast anatomy is only known from a handful of extant examples (Neubauer 2014; Balanoff and Bever 2017; Watanabe et al. 2019a). Given the apparent complexity of the endocast of many extinct fishes, including ray-finned fishes, these remains have occasionally been considered a synonym for ‘fossil brains’ in the literature (Moodie 1915; Coates 1999). This causes confusion when brain characters are directly compared to endocast characters.

The only way to ensure the fidelity of endocast characters is through the examination of living species. Within tetrapods it seems to generally consistent that endocast volume closely approximates brain volume (Neubauer 2014; Watanabe et al. 2019a; Allemand et al. 2022) and thus it can be assumed that endocast morphology can be a reliable indicator of brain anatomy in extinct lineages (Watanabe et al. 2019b, 2021; Challands et al. 2020; Ksepka et al. 2020; Fabbri and Bhullar 2022). Problems arise when dealing with ray-finned fishes since despite the abundance of studies on brain anatomy in many ray-finned fish groups, there is virtually no information available on endocast volume—and morphology—for extant species. Studies comparing brain/body volume ratio across vertebrates have found that ray-finned fishes are among the vertebrates with the smallest ratios (Iglesias et al. 2015). Given the lack of good comparative descriptions, the extrapolation of brain morphology from osteological counterparts can be problematic for ray-finned fishes.

6.4.1 The endocast of ray-finned fishes

Important patterns of morphological diversity of ray-finned fish endocasts becomes clear when sampling taxa that have been so far overlooked. Through analyzing brain and endocast morphologies of living ray-finned fish species there seems to be important patterns that have been so far overlooked for this clade. The endocast of ray-finned fishes are much more diverse than previously thought. Given the lack of ossification of several portions of the neurocranium in many teleost lineages it was difficult to correctly determine endocast shape from skeletal specimens but given the application of dice-CT scanning techniques it is now possible to extract 3D models that accurately represent endocast morphology even when portions are unossified.

In Paleozoic stem ray-finned fish taxa, the endocasts can be divided into main regions representing regions of the brain with varying degrees of precision. The anterior end of the endocast of non-teleosts is formed by diverging olfactory lobes followed by a large area that encapsulates the forebrain and midbrain. In many Paleozoic ray-finned fishes (e.g. †*Mimipiscis*, †*Kentuckia*, †*Lawrenciella*, †*Kansasiella*) there is a margin separating the telencephalic and epiphyseal area to the broad mesencephalic area (Hamel and Poplin 2008; Giles and Friedman 2014). In living cladistians and holosteans this separation is retained, but such feature is absent in chondrosteans and teleosts. Overall, the morphology of the endocast of non-teleost ray-finned fishes is conserved and directly comparable to that of fossil stem ray-finned fishes. Unfortunately, there seems to be little correlation between endocast and brain morphology in living non-teleost ray-finned fishes, which raises question on interpretations of fossil endocasts as indirect evidence for brain anatomy in fossil ray-finned fishes.

Early-diverging teleosts (e.g. *Elops*, *Albula*, *Hiodon*) bear simple endocasts but with clearly distinguishable regions that can be directly correlated to the regions described in fossil taxa. The endocast in stem teleosteomorphs (e.g. †*Aspidorhynchus*) is like that of elopomorphs, with rounded horizontal semicircular canals and elongated endocast with a clear division between prosencephalic (olfactory + telencephalon + diencephalon) and mesencephalic (optic tectum) areas, a constricted crus-commune which separates the area for the auricula cerebelli to the area octavolateralis. The main difference in †*Aspidorhynchus* to extant elopomorphs is the extension of the lateral cranial canal within the curvature of the posterior semicircular canal. In †*Dorsetichthys* the lateral cranial canal is expanded and completely surrounds the cruss-commune embracing the inner ear (Patterson 1975; Friedman and Giles 2016; Giles et al. 2018),

whereas in other taxa (e.g. †*Pholidophorus*) the lateral cranial canal is well-developed but restricted to the area below the posterior semicircular canal (Giles et al. 2018). In most living teleosts (e.g. *Elops*, *Hiodon*) the lateral cranial canal is not noticeable. Given the similarities—but with morphological variation—in stem teleosts and living early-diverging teleosts such as elopomorphs, it is possible that a closer examination of fossil endocasts in the light of detailed anatomical work on living species might shed light on the interrelationships of early teleosts.

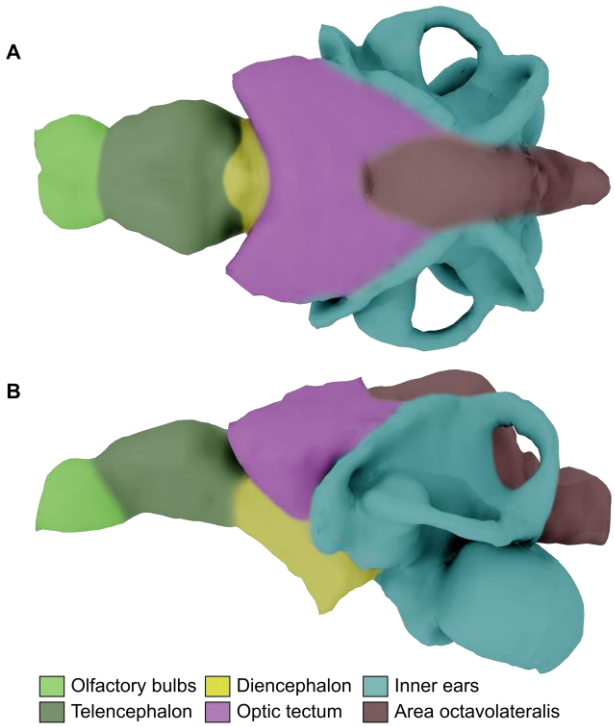

Figure 6.2 – Representation of regions of the ray-finned fish endocast. Based on *Hiodon alosoides* (UMMZ 222342)

In extant teleosts there is considerable variation in endocast morphology across lineages, as well as variation in the degree to which endocast morphology reflects brain morphology. In most analyzed teleost taxa the endocast can be divided into mains regions similar to that of non-teleosts (e.g. olfactory capsules, telencephalic area, optic tectum area, octavolateralis area, and inner ears), but in many lineages two or more of these areas lack clear boundaries (e.g. olfactory-telencephalic area; mesencephalic-octavolateralis area), while in others the endocast is formed by an undifferentiated chamber (e.g. *Ammodytes americanus*, *Canthigaster solandri*). The complexity of the endocast also seems to be highly variable across teleosts, with otophysans (e.g. *Glyptothorax*, *Barbichthys*, *Eigenmania*, *Serrasalmus*) bearing highly complex endocasts in

terms of topology of different areas than other taxa which bear simpler ‘smooth’ endocasts (e.g. *Elops*, *Caranx*, *Canthigaster*, *Alticus*, *Ophiodon*).

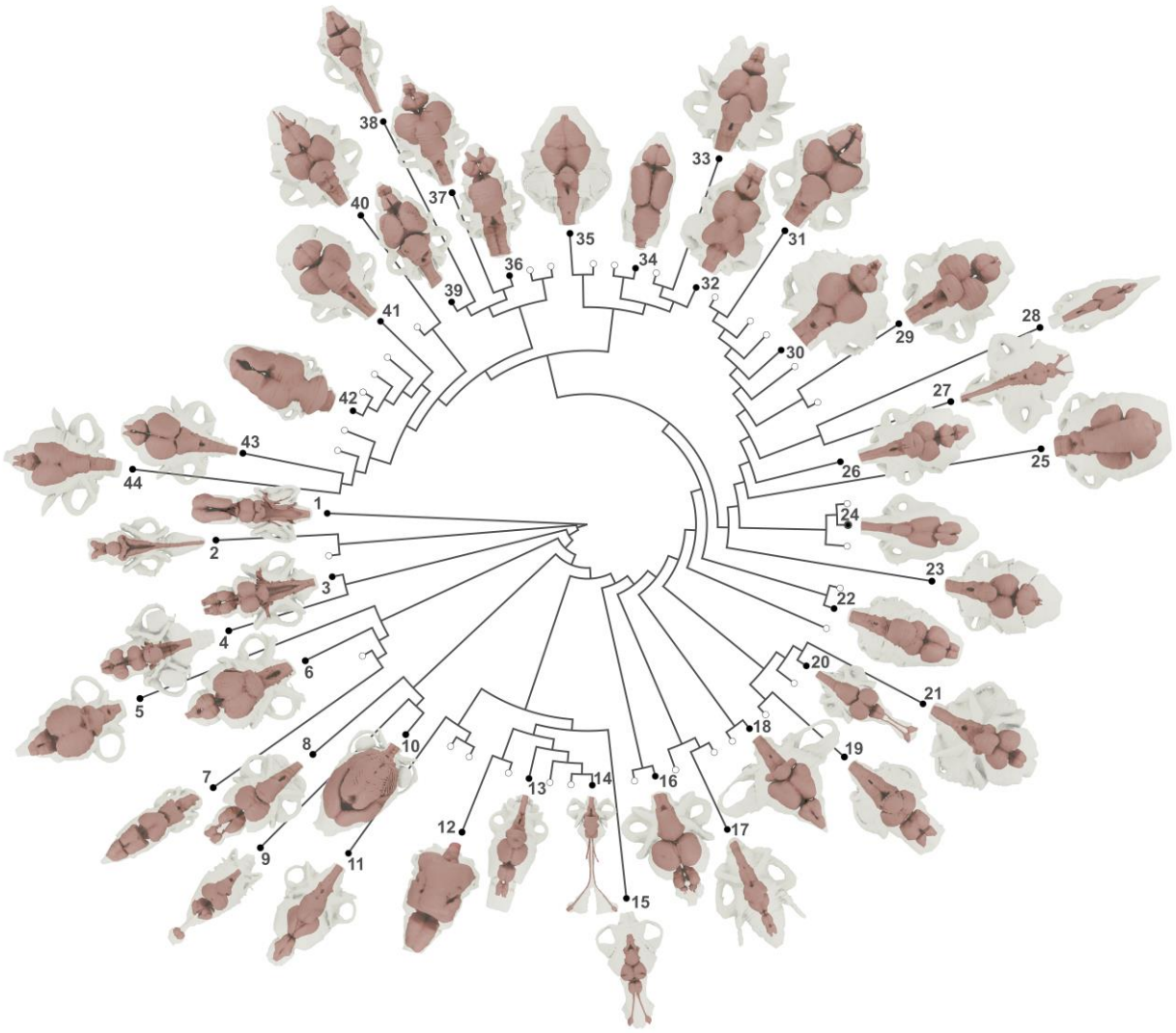

Figure 6.3 – Brain and endocast morphology across extant ray-finned fishes. 1, *Polypterus* (Polypteridae), 2, *Polyodon* (Polyodontidae), 3, *Amia* (Amiidae), 4, *Lepisosteus* (Lepisosteidae), 5, *Elops* (Elopidae), 6, *Albula* (Albulidae), 7, *Gymnothorax*, 8, *Hiodon* (Hyodontidae), 9, *Notopterus* (Notopteridae), 10, *Marcusenius* (Mormyridae), 11, *Anchovia* (Engraulidae), 12, *Eigenmannia* (Sternopygidae), 13, *Serrasalmus* (Serrasalmidae), 14, *Lacantunia* (Lacantunidae), 15, *Barbichthys* (Cyprinidae), 16, *Salvelinus* (Salmonidae), 17, *Sigmops* (Gonostomatidae), 18, *Chlorophthalmus* (Chlorophthalmidae), 19, *Forbesichthys* (Amblyopsidae), 20, *Microgadus* (Gadidae), 21, *Lepidorhynchus* (Macrouridae), 22, *Stygnobrotula* (Bythitidae), 23, *Ctenolabrus* (Labridae), 24, *Canthigaster* (Tetraodontidae), 25, *Acanthurus* (Acanthuridae), 26, *Morone* (Moronidae), 27, *Uranoscopus* (Uranoscopidae), 28, *Ammodytes* (Ammodytidae), 29, *Ambloplites* (Centrarchidae), 30, *Prionotus* (Triglidae), 31, *Ophiodon* (Hexagrammidae), 32, *Trichiurus* (Trichiuridae), 33, *Brama* (Bramidae), 34, *Aeoliscus* (Centriscidae), 35, *Valenciennea* (Gobiidae), 36, *Polynemus* (Polynemidae), 37, *Caranx* (Carangidae), 38, *Centropomus* (Centropomidae), 39, *Sphyraena* (Sphyraenidae), 40, *Ambassis* (Ambassidae), 41, *Abudefduf* (Pomacentridae), 42, *Alticus* (Bleniidae), 43, *Chriodorus* (Hemiramphidae), 44, *Cypselurus* (Exocoetidae).

Other important aspect of variation among teleosts pertains to the geometry of the semicircular canals of the inner ear. In early-diverging lineages the semicircular canals are almost rounded forming semicircles in dorsal and lateral views and bearing a horizontal semicircular canal that is slightly inclined antero-posteriorly. In aulopiforms the horizontal semicircular canal is highly compressed in the antero-posterior axis and elongated laterally, giving the inner ear a 'wing' profile in dorsal view. Another important variation is the degree to which the anterior semicircular canal is independent from the endocast body. In non-teleosts the anterior semicircular canal is almost completely independent from the endocast body, meaning that its mesial surface is separated from the endocranial cavity by bone or cartilage. In most teleosts the anterior semicircular canal is almost completely contiguous with the endocranial cavity, visible in a few taxa as a groove along the posterodorsal margin of the optic tectum area (e.g. *Elops, Hiodon, Chlorophthalmus, Caranx*). In a handful of the examined taxa, the anterior semicircular canal is not distinguishable from the endocranial wall (e.g. *Ammodytes*). Among teleosts, catfishes seem to be unique as they bear a clear separation of the anterior portion of the semicircular canal, making it independent from the endocavity (e.g. *Lacantunia*, *Glyptothorax*).

In terms of brain-to-endocast correlation index (BEC) there is little variation among taxa, with a few exceptions. For most of the 46 taxa quantified, the BEC tends to be around 0.2–0.3, with a minimum value of 0.04 and maximum of 0.66. Given the distribution of brain and endocast volume in the sample it seems that endocasts might be a good predictor of brain volume for most ray-finned fishes, but such estimates should be considered with care.

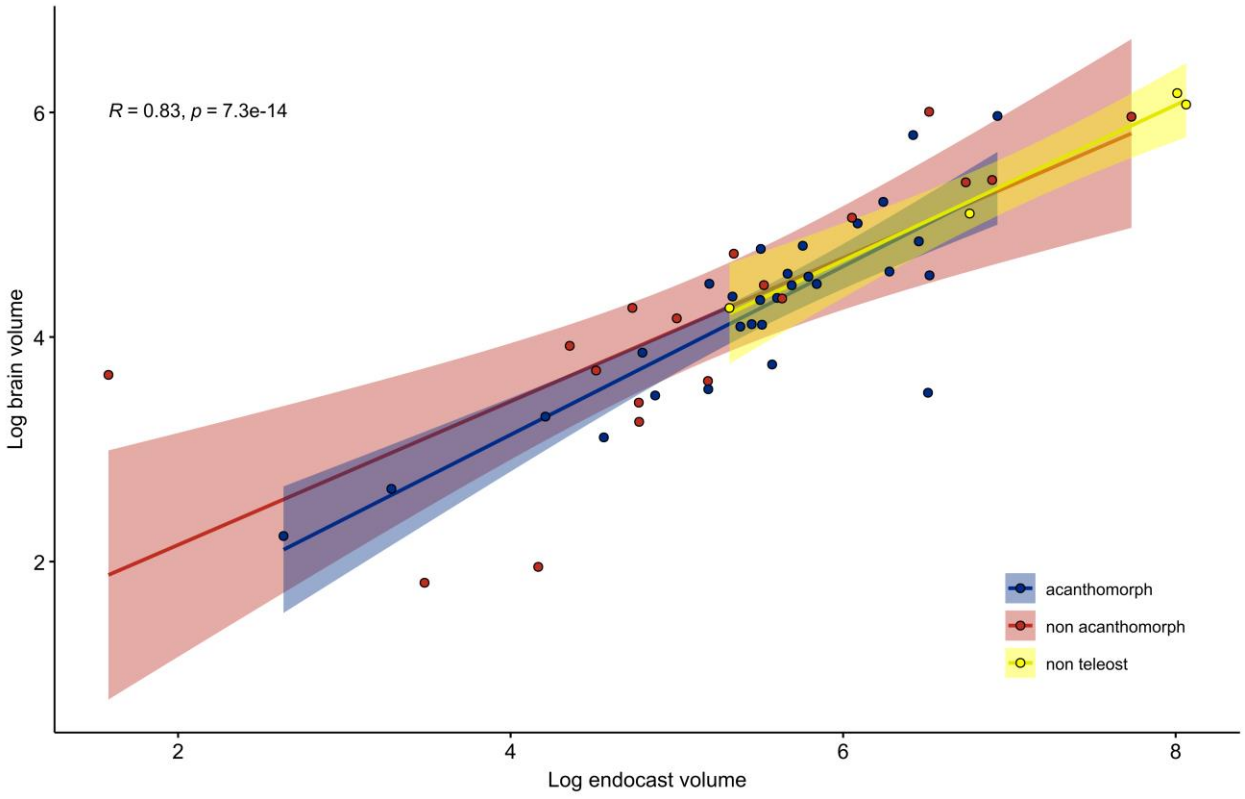

Figure 6.4 – Log bran volume versus log endocast volume of the taxa analyzed. Shaded areas represent 95% confidence intervals of regression lines.

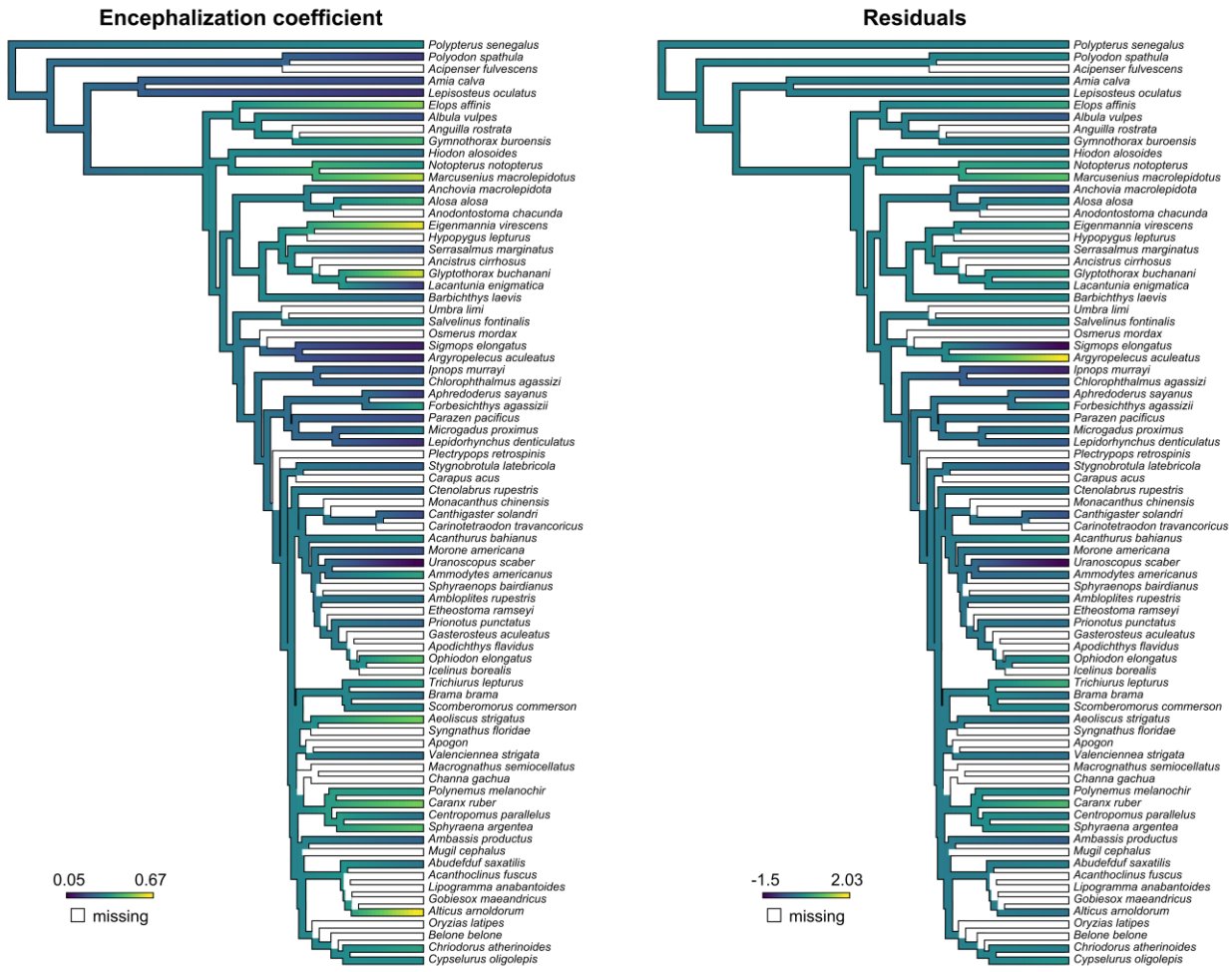

Figure 6.5 – Continuous mapping of brain-to-endocast correlation index (BEC) across the pruned phylogeny from Rabosky et al. (2018).

6.5 The myelencephalic gland

The myelencephalic gland is a hematopoietic organ found in several actinopterygians above the myelencephalic region of the brain (van der Horst 1925). This structure was first reported for *Lepisosteus osseus* (Chandler 1911) and later was found to be present in other non-teleost actinopterygians such as *Amia*, *Acipenser* and *Polyodon* (van der Horst 1925; Jarvik 1980). Although the cellular organization of this organ seems to be consistent among these fishes, the morphology of the organ is highly variable among different taxa. It has been proposed that a similar organ would be present in several Paleozoic actinopterygians given the presence of a myelencephalic expansion found in the endocast region of many of these fossil fishes (Bjerring

1978, 1984; Jarvik 1980). Thus, it has been suggested that it could be primitive for actinopterygians, although it is seemingly absent in polypterids (Chandler 1911; van der Horst 1925; Jarvik 1980). Additionally, it has been noted that a similar structure might have been present in *Eusthenopteron*, and a comparable organ is known in other sarcopterygians (e.g. the saccus endolymphaticus of lungfishes; Chandler (1911), Jarvik (1980)) and in chondrichthyans, although with a different distribution not restricted to the dorsal part of the rhombencephalon (Chiba et al. 1988). These hematopoietic organs should be relatable to the meningeal and peri-meningeal tissues of cyclostomes, chondrichthyans and teleosts, which do not seem to exhibit such hematopoietic structures (Vialli 1932).

6.5.1 Morphology

The myelencephalic gland of *Lepisosteus osseus* sits exclusively above the myelencephalic region of the brain and expands from the meningeal tissue (pia mater) of the region. In dorsal view it is boomerang-shaped, bearing paired dorsolateral expansions leading to lateral bulbs sitting within the inner ear, potentially associated with the lateral cranial canal of early actinopterygians (van der Horst, 1925; Jarvik, 1980; Bjerring, 1984). In transversal section the main body of this organ is trapezoidal with expanding lobes that lead to the lateral protrusions within the inner ear region. The main body of the organ tapers posteriorly at the level of the exit of the vagus nerve before ending in paired flattened posteriorly directed extensions. The ventral surface of the myelencephalic gland of *Lepisosteus* is marked by the dorsum of the thick pia mater that surrounds the rhombencephalic region of the brain, closely associated with the endocranial wall. Histological sections from Chandler (1911) show this organ is composed of pigment cells together with cells that resemble erythrocytes, leukocytes, and granulocytes. Additionally, this organ seems to be heavily vascularized by blood vessels and capillaries of diverse diameters (Chandler, 1911).

The blood supply of the myelencephlalic gland of *Lepisosteus* is carried through a transverse blood vessel that ramifies towards the anterolateral and posterior expansions of the myelencephalic gland. In dorsal view this main vessel exhibit the shape of an arch exiting on both posterolateral ends of the myelencephalic gland.

In *Polyodon* the myelencephalic gland shows an extremely different arrangement to that of *Lepisosteus*. In *Polyodon* it completely surrounds the posterior rhombecephalic region of the braincase, having a conical shape in lateral and dorsal views where the anterior border is broad and the organ tapers posteriorly towards the foramen magnum. In transversal section it has a round shape and is separated from the brain and spinal cord by a small gap. Furthermore, there is no evidence of the accessory paired expansions going into the lateral cranial canal. This homogeneous and large structure was first described by van der Horst (1925) who noted that in younger individuals of *Polyodon* this organ does not completely surround the brain ventrally, having a crescentic cross-section. On the analyzed specimen we find paired canal-like extensions leading to putative accessory glands on the ventral side of the brain. These small accessory structures have a kidney-like shape in lateral view and seem to be histologically similar to the main organ and surrounding blood vessels. Interestingly, van der Horst (1925) does not mention any ventral accessory structures, probably due to limitation of the dissection methods used. This structure is also not described or mentioned by Rahmat and Gilland (2014) review on brain vascularization in vertebrates.

The myelencephalic gland of *Acipenser* is different from that of *Polyodon* in several ways. In Acipenser the gland is ovoid in shape but unlike in *Polyodon* the anterior end of it extends and tapers towards the cerebellum, partially covering the crista cerebellaris and the opening of the fourth ventricle, similar to the condition in *Amia* (see below). Additionally, the gland dorsally surrounds the vagus nerves (cranial nerve X) until they reach the otic capsules area, giving the gland lateral extensions in dorsal view. Posteriorly the gland arches ventrally giving it a blunt posterior surface, terminating before the level of the foramen magnum, dorsal to the first three pairs of accessory nerves. As mentioned by Gradil et al. (2014), the myelencephalic gland of *Acipenser* bears a high percentage of heterophils, which is consistent with a mainly granulopoietic tissue.

The vascularization of the myelencephalic gland of *Acipenser* is poorly understood. From our dice-CT data it seems to be less highly vascularized than in holosteans and *Polyodon*, being irrigated by minute blood vessels and a large vessel dorsally that dichotomizes towards the lateral expansions above the vagus nerves.

The myelencephalic gland of *Amia* is poorly known compared to *Lepisosteus* and *Polyodon*. Van der Horst (1925) described it as similar in morphology and histology to

Polyodon, differing from Lepisosteus in completely surrounding the myelencephalon rather than being restricted dorsally. Van der Horst (1925) also noticed that young specimens of *Acipenser* seem to have a complete gland, whereas in larger adult specimens the myelencephalic gland is restricted dorsally forming a semi-circle shape in cross section. In dorsal view it is sub-triangular in shape as it tapers anteriorly towards the dorsum of the corpus cerebelli, where it connects to the highly vascularized connective tissue of the meninx primitiva. Posteriorly it expands following the path of the vagus nerve (cranial nerve X). In lateral view the myelencephalic gland is wide and it is possible to see how it expands both dorsally and ventrally in relation to the myelencephalon, connecting around the level of the vagus nerve (cranial nerve X). Ventrally the myelencephalic gland is thin and closely follows the inner surface of the neurocranium.

The vascularization of the myelencephalic gland of *Amia* is highly complex. The main body of the gland dorsally to the brain is permeated by an intricate network of blood vessels of various diameters. The majority of the large-diameter vessels is oriented in the antero-posterior direction, with smaller vessels and capillaries emerging from these and permeating the body of the gland towards the lateral expansions around the vagus nerves. In lateral view it is possible to note a close association between the brain blood supply and the myelencephalic gland externally. The large cerebellar branch of the cerebral carotids seems to connect to the vascularization of the myelencephalic gland at the level of the posteriormost extension of the crista cerebellaris of the brain. In this region there is a complex vascular network that connects to the myelencephalic gland and the paired basilar arteries. From this complex a series of small vessels emerges and contact the surface of the crista cerebellaris.

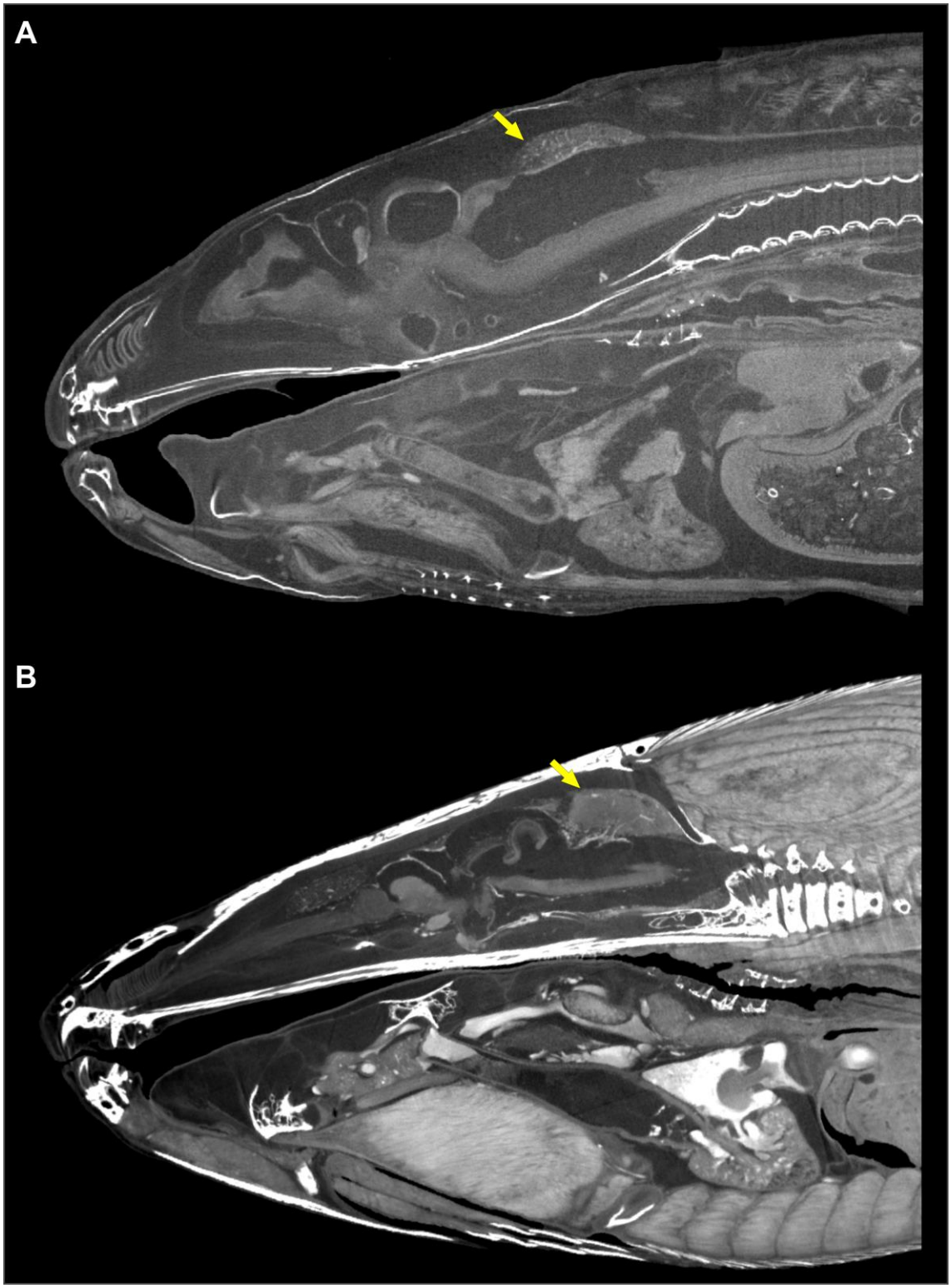

Figure 6.6 – Comparison of dice-CT slices in parasagittal section showing variation in morphology of the myelencephalic gland (yellow arrow) in (A) juvenile and (B) adult *Amia* specimens.

Although *Polypterus* apparently lacks a developed myelencephalic gland, as noted by (Van der Horst, 1925), the meninx primitiva above the rhombencephalon is highly vascularized, forming a dense sheet that covers the myelencephalon dorsally and extends up to the posterior surface of the cerebellum and laterally extending up to the level of the posterior end of the mesencephalic region. In dorsal view this structure is Y-shaped and connects to the blood supply of the rhombencephalon and mesencephalon.

As presented in previous chapters (C4, C5; Appendix E) there is direct evidence of modified meningeal tissues in fossil ray-finned fishes. Some fossils show a condition similar to cladistians where the rhombencephalic meningeal tissue is modified into two sheets encapsulating a chamber filled with intracranial fluid. This structure has been named cisterna spinobulbaris (Jarvik 1980). In other fossils, however, there is evidence of dense tissue associated to the dorsum of the myelencephalon, similar in shape and position to the myelencephalic gland of lepisosteids where lateral lobes of the myelencephalic gland extend into the inner ear (Chandler 1911; van der Horst 1925; Bjerring 1984).

Modified myelencephalic meningeal tissues are not described in teleosts and from a close examination of dice-CT scan data for 72 teleosts indicates that indeed most teleost lineages do not seem to bear any modified or expanded meningeal tissues surrounding the myelencephalon. However, in two of the analized taxa (*Serrasalmus* and *Lepidorhynchus*) there is an expanded meningeal tissue above the posteriormost portion of the myelencephalon. In *Serrasalmus* (Fig 6.7A) this structure is visible in sagittal sections as a dorsally expanded thickened area of the membranous meninges, but relatively small in comparison to the brain and to the myelencephalic gland of non-teleosts. In *Lepidorhynchus* on the other hand, this myelencephalic meningeal tissue is well-developed and highly vascularized completely covering the dorsal surface of the myelencephalon up to the opening of the fourth ventricle. Although it is still thinner than the mylencephalic gland of non-teleosts, it is very similar in terms of position, vascularization pattern and aspect in dice-CT data. Future histological work is needed to determine whether these expanded tissues bear any hematopoietic function in teleosts, but from dice-CT data it seems plausible to assume that it might—at least in *Lepidorhynchus*—as it is highly vascularized and dense.

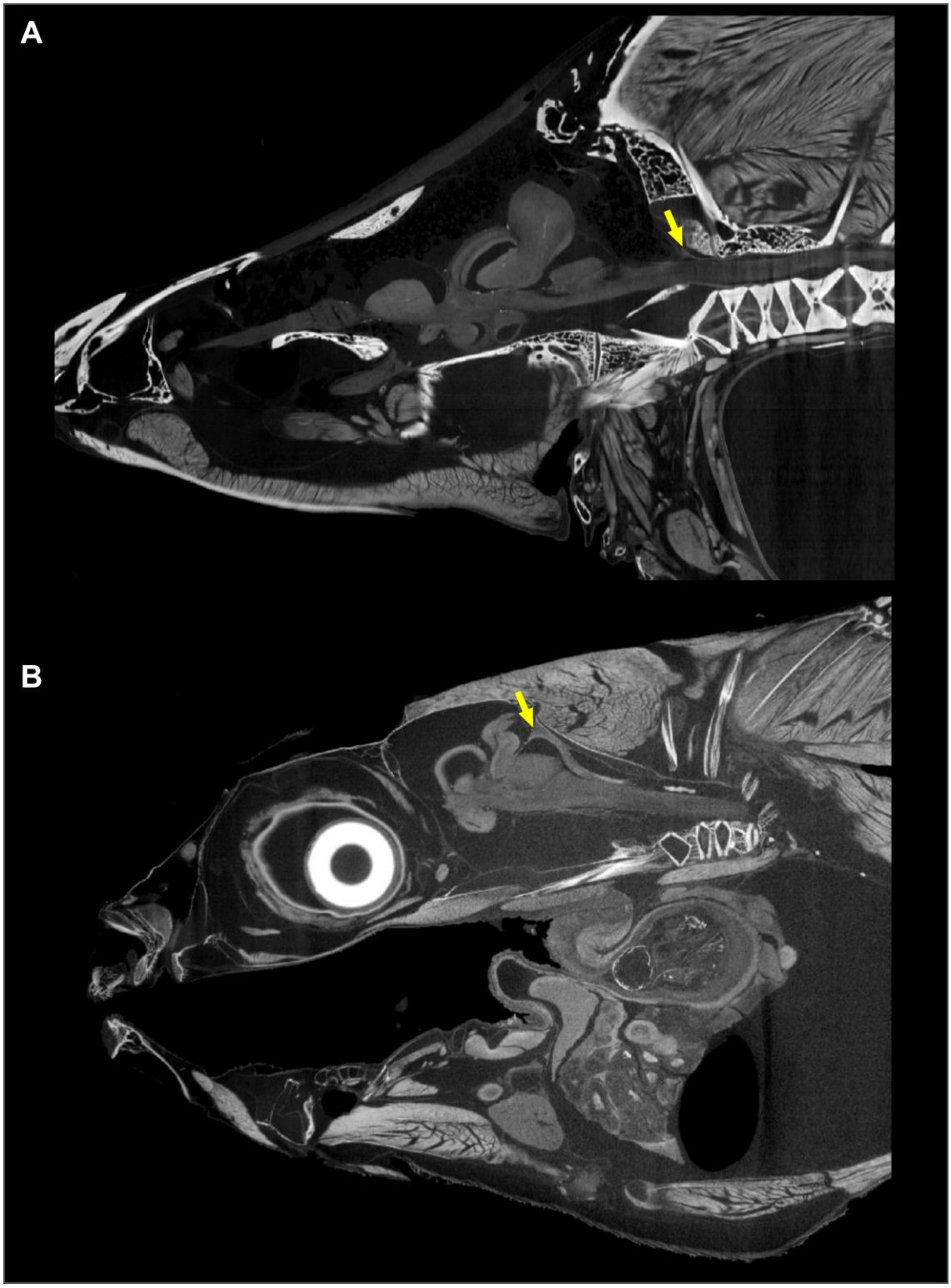

Figure 6.7 – Modified myelencephalic meningeal tissues in sagittal sections of dice-CT data in (A) *Serrasalmus* and (B) *Lepidorhynchus*.

6.5.2 Meningeal hematopoietic tissues in vertebrates

The distribution of meningeal or myelencephalic hematopoietic organs in vertebrates is still not fully understood. Outside of Actinopterygii the hematopoietic tissues in the meningeal space is restricted to scattered cell groups in the meninges of several chondrichthyans (Chiba et al. 1988). In other lineages there is evidence of organized hematopoietic tissue within the braincase of adult individuals to a smaller scale, especially during embryonic stage, which is found in all vertebrates, including humans (e.g. subcommissural organ; Rodríguez et al. (2001)). Thus, questions arise on the development and homology of hematopoietic tissues across vertebrates. In cyclostomes, although there is no braincase-confined hematopoietic tissue, there are neural crest cells that persist above the myelencephalon and spinal cord of *Eptatretus* that later differentiate into pigment cells or migrate to form nerve ganglia (Ota et al. 2007; Ota and Kuratani 2008). These cells are superficially similar to pigment cells of the myelencephalic gland of chondrosteans and holosteans. However, since there is a lack of developmental studies of the myelencephalic gland in actinopterygians, it is not possible to assume that this organ could also have originated from neural crest cells.

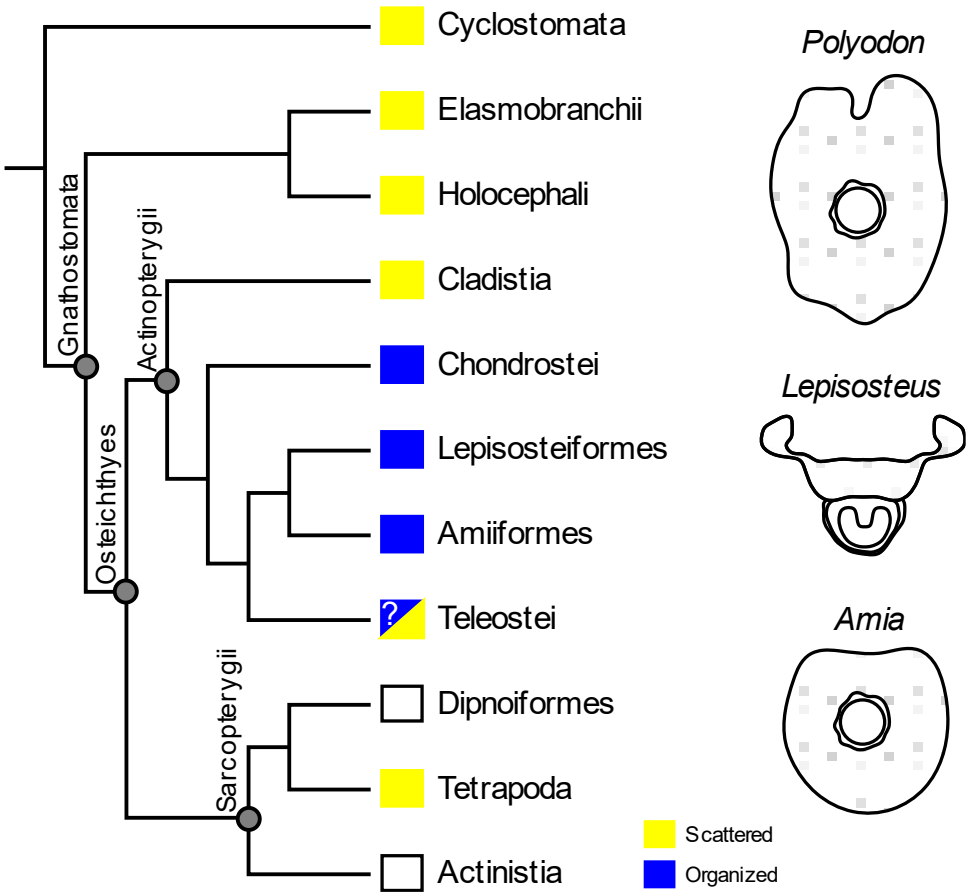

Figure 6.8 – Distribution of meningeal hematopoietic cells in the endocranial cavity of vertebrates (in adult individuals).

6.6 Unique brain adaptations and convergence

The brains of ray-finned fishes have been known to be morphologically diverse since early comparative neuroanatomy studies (Evans 1931; Nieuwenhuys 1982). However, there is still a lack of understanding on the impact of such morphological diversity to the myriad of ecomorphologies found in this hyperdiverse clade. A handful of studies have tried to address this problem by comparing brain morphology in closely related species with different ecomorphologies and propose variation of brain morphology, especially proportion between different regions, as heavily influenced by ecomorphology (Kotrschal and Palzenberger 1992; Morona et al. 2013; Sukhum et al. 2016; Saveliev 2019; Khan et al. 2021; Schumacher and Carlson 2022). Some of these studies have analyzed ray-finned fish brains on a broader scale in terms of variation of volumetric proportions or convergent morphologies (Schumacher and

Carlson 2022; Gebhardt and Hofmann 2023). Despite these, there is still a lack of understanding on the broadscale patterns of morphological diversity of ray-finned fish brains going beyond volumetric comparisons.

Polypterids have been used as a model for understanding the early evolution of the ray-finned fish brain (Allis 1922; Piotrowski and Northcutt 1996; Northcutt 2008; López et al. 2013). However, much like with its osteology and external anatomy, extant polypterids are highly apomorphic and bear little resemblance to early crown ray-finned fishes (Giles et al. 2017; Figueroa et al. 2023, 2024). This poses a challenge to understanding whether unique features of polypterids—in relation to other living clades—is indicative of the ancestral condition of ray-finned fishes or a derived condition of living polypterids.

Chondrosteans also have been used as a template for early ray-finned fishes, but as with polypterids the morphology of living chondrosteans might not directly correlate to that of early crown ray-finned fishes. As discussed in Chapters 4 and 5, the fossil brains of stem ray-finned fishes seem to indicate that the telencephalic eversion is not a feature of the total group Actinopterygii but originated at some point along the actinopteygian stem (Figueroa et al. 2023, 2024). This work also indicates that the unique combination of features found in fossils cannot be directly compared to any of the early-diverging crown ray-finned fish lineages as fossil taxa show a mosaic of features found in this set of extant taxa.

When looking at the diversity of brain morphologies in living ray-finned fishes, especially teleosts, there does not seem to be considerable variation in terms of the brain organization, but the subdivisions and tissue layers of each brain region as well as the proportion and shape of these regions varies within closely related taxa. This variation has led many researchers to investigate brain morphology as a predictor of behavior or ecology as well as studies investigating the distribution of unique brain features among living ray-finned fishes (Kotrschal et al. 1998; Northcutt 2008; Shumway 2008, 2008; Saveliev 2019; Khan et al. 2021; Kozol et al. 2023). In the sample of taxa analyzed herein there is a myriad of unique brain adaptations that can be readily observed but some of which have been overlooked in the literature so far.

For example, there seems to be a tendency of deep-bodied ray-finned fishes to have a dorsally expanded cerebellar corpus, and in some extreme cases as in *Acanthurus bahianus* the cerebellar corpus arches anterodorsally roofing the more rostral regions of the brain. Apart from

deep-bodied taxa, secondarily electroreceptive taxa such as mormyrids, gymnotiforms and some siluriforms also have a dorsally expanded corpus cerebelli, but in these the enlarged area roughly corresponds to the eminentia granularis and the electrosensory lobes, which are not directly related to the cerebellar corpus body per se. Thus, although both deep-bodied and electroreceptive taxa show enlargement of the cerebellum (or cerebellar area) the enlargement occurs independently in non-homologous tissues. One hypothesis for explaining the expanded cerebellar corpus of deep-bodied taxa is related to their swimming and preying habitus. Deep-bodied fish tend to rely on movement of paired fins, but especially pectoral fins, and require delicate balancing to keep body orientation in complex environments (Lindsey 1978; Blake 2004; Howe et al. 2021; Satterfield et al. 2023). Thus, an enlarged cerebellar corpus might be key for coping with this need for complex and intricate movement and balancing of the body. Alternatively, the dorsally-expanded cerebellar corpus of deep-bodied taxa might simply be a result of spatial constraints within the neurocranium which would force the dorsal expansion of the cerebellum. However, this hypothesis does not seem to be supported by the endocast data collected here as the brain of these taxa do not seem to fully occupy the cerebellar area of the endocranial cavity in the analyzed specimens as well as results from comparative work on brain and neurocrania of *Labeotropheus* and *Tropheops* hybrid cichlids (Conith et al. 2022).

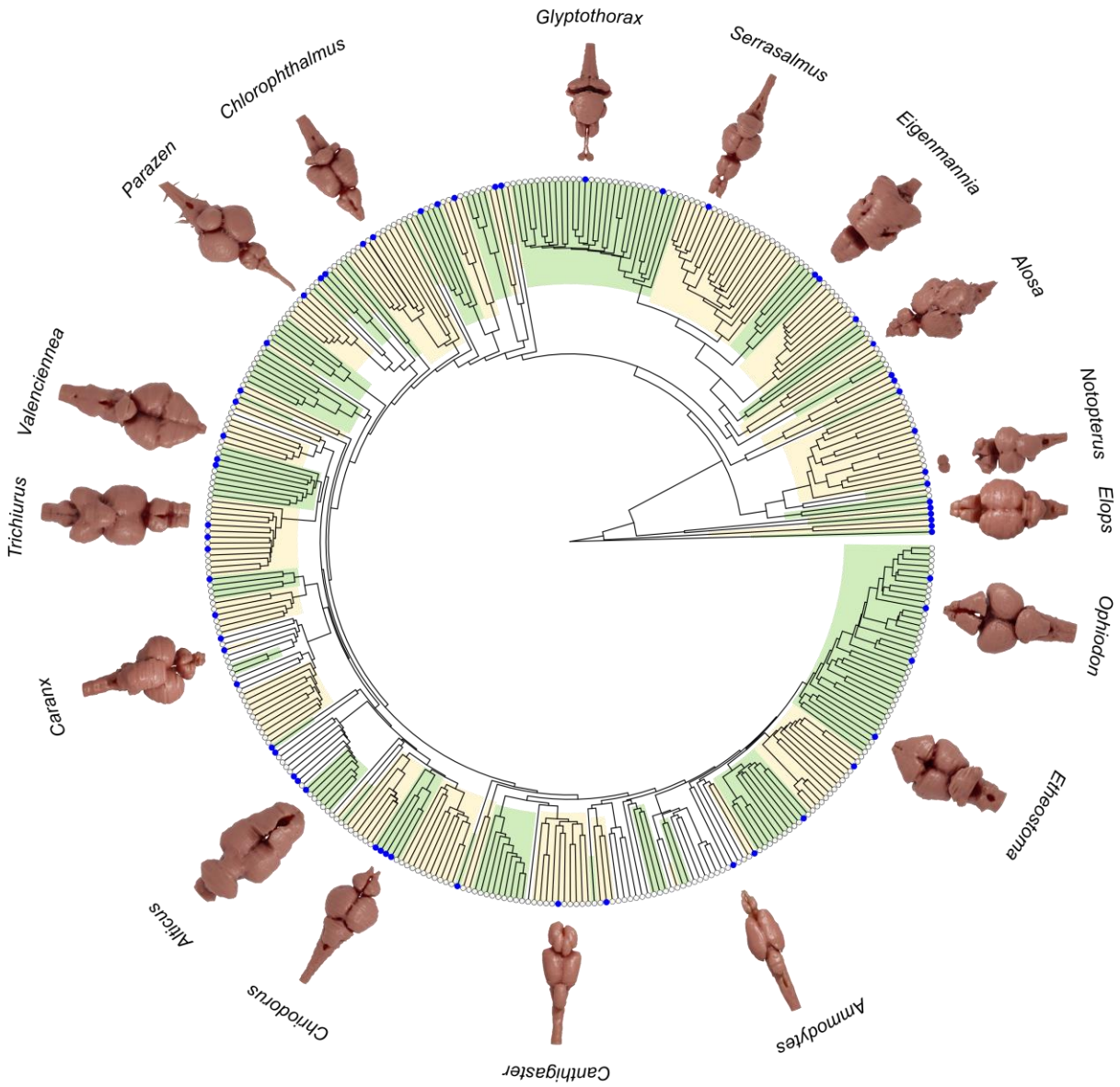

Figure 6.9 – Phylogenetic tree of ray-finned fish families showing brain morphological disparity in selected taxa. Blue tips represent families that have been sampled for this study.

Taxa with tactile fin rays such as *Prionotus* have serialized lobes on the caudal myelencephalon that are associated to controlling the movement of these specialized rays. These have been previously described as accessory spinal lobes in *Prionotus* and *Trigla* (Meek and Nieuwenhuys 1998), but there is no reference to such accessory spinal lobes in other teleost radiations apart from triglids. However, the *Polynemus* specimen analyzed for this work shows a very similar organization of accessory spinal lobes as it has been reported for triglids. Meek and Nieuwenhuis

(1998) indicated that the number of accessory spinal lobes corresponds to the number of independent fin rays or fin ray bundles in the taxa as in *Prionotus carolinus* there are four accessory spinal lobes and four independent sections of the pectoral fin, three rostroventral fin rays and a caudodorsal webbed section with multiple fin rays. However, in the specimen of *Prionotus* punctatus analyzed herein there are only three accessory spinal lobes that correspond directly to the three free pectoral fin rays of this taxon. Thus, it is likely that the identification of four accessory spinal lobes in *Prionotus* made by Meek and Nieuwenhuis (1998) is incorrect. In *Polynemus* I identified eight accessory spinal lobes which correspond to eight free pectoral fin rays. Given the phylogenetic distance between triglids and polynemids it is unlikely that the accessory spinal lobes of these two groups are homologous. Rather, these are probably result of convergence.

Different ray-finned fish lineages exhibit adaptations of the olfactory bulbs which are separated from the remainder of the forebrain by an olfactory tract. In these taxa the olfactory bulbs are more closely associated with the olfactory rosetta than the brain, while in other clades the olfactory bulbs are well-connected to the anteroventral telencephalon and connect to the olfactory capsules by long olfactory nerves. There seems to be little resemblance in terms of external morphology of taxa with stalked olfactory bulbs. In the sampled taxa such morphology is found in several siluriforms, gadids, cyprinids, and in *Notopterus*. However only siluriforms show any consistency in exhibiting this feature in different families, while others have closely related taxa with non-stalked olfactory bulbs (e.g. stalked *Microgadus* and non-stalked *Lepidorhynchus*). One possibility is that the stalked olfactory bulbs are simply a result of the olfactory capsules being distant from the remainder of the brain, but there are several taxa with differentiated olfactory capsules that do not exhibit stalked olfactory lobes (e.g. *Ammodytes*, *Centropomus*). Alternatively, the close association between the olfactory lobes and the olfactory rosetta could be controlled by an increased use of olfaction for feeding or communication, but thus far there is not enough data to support or reject this hypothesis.

6.7 Ray-finned fish brain morphometrics

From the morphometric analyses conducted for this chapter there are also interesting patterns of morphological variation that are not readily observed from comparative morphology

alone (Fig. 6.10). It seems that the morphological disparity of acanthomorph brains is relatively constrained in the morphospace with only a few taxa diverging drastically from the group centroid. This contrasts with non-acanthomorph teleosts where there is much more disparity between taxa that are spread across the morphospace, especially along PC 1 and 2. Non-teleost fishes occupy a different area of the morphospace than teleosts, but show little variation. This pattern is clearly observed when comparing PCs 1 and 2 but is also visible in other combinations (Appendix F).

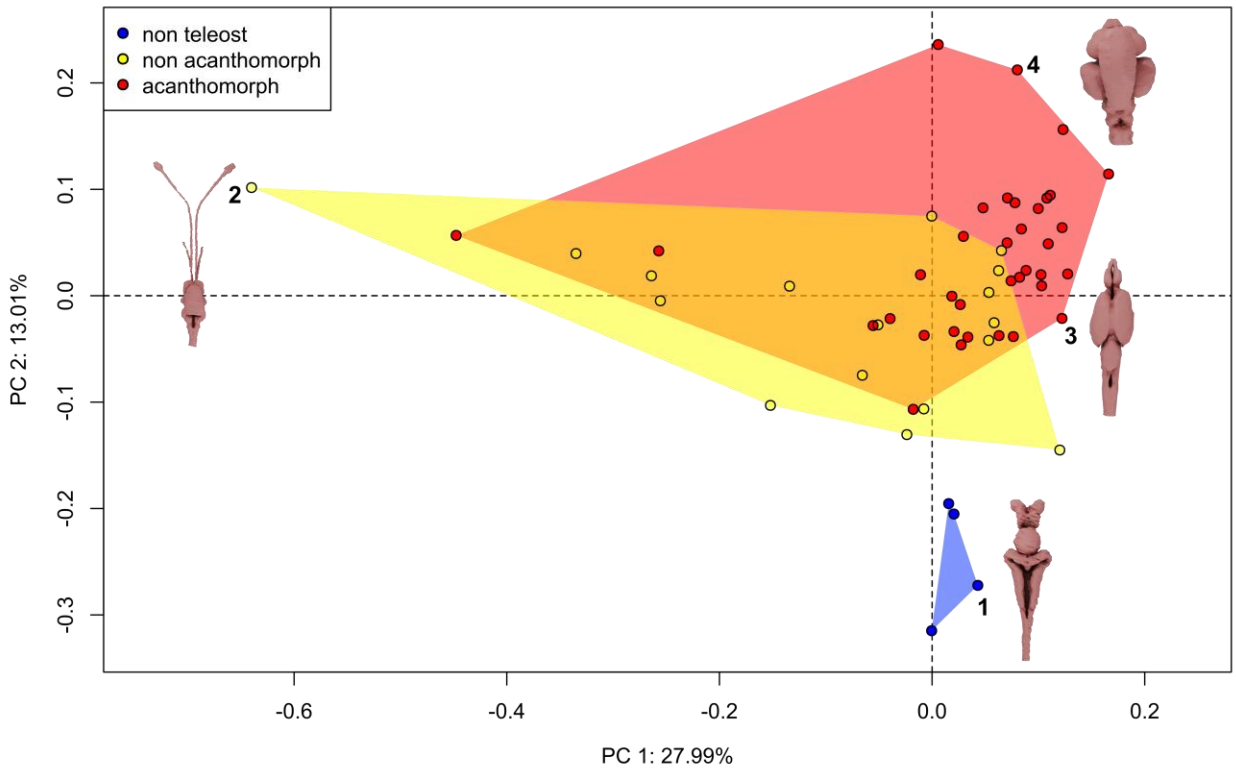

Figure 6.10 – Simplified scatterplot showing the variation in brain morphology across the sampled ray-finned fishes in PC1 and PC2.

PC 1 mostly represents variation in the distance between the anterior end of the olfactory bulbs (i.e. exit of the olfactory nerve) and the rostral end of the telencephalon (i.e. rostral end of the area ventralis). Thus, most of the PC 1 variation pertains to the heterogeneous distribution of stalked versus non-stalked olfactory lobes as well as taxa with elongated olfactory lobes. PC 2 mostly represents the variation in the antero-posterior length of the cerebellar corpus and the size of the optic tectum and torus longitudinalis within the mesencephalon. Given that non-teleost

ray-finned fishes have a small corpus cerebelli and poorly developed torus longitudinalis, these appear isolated from other ray-finned fishes in this axis. Further PCs represent less of the observed variation and are more difficult to interpret as they are more likely to encompass variation across several landmarks and brain modules.

The results of this morphometric analysis should be considered as preliminary. However, they already provide novel information regarding the morphological evolution of ray-finned fish brains. It seems that as with skeletal morphology there are important shifts separating non-teleosts, non-acanthomorph teleosts and acanthomorphs in terms of brain morphology. It is interesting to note that the variance within acanthomorphs is considerably low given the morphological and phylogenetic diversity of this clade. Future work should aim at expanding this dataset both in terms of taxonomic and phylogenetic sampling as well as potentially exploring additional landmarks that might aid in a better representation of morphological variation in ray-finned fish brains.

6.8 Future perspectives

The study of vertebrate brain evolution has advanced significantly through the past decades, shifting from directional stepwise acquisition of complexity view towards a better understanding of patterns and processes underlying brain variation in a phylogenetic context (Vernier 2017; Hall and Tropepe 2020; Schumacher and Carlson 2022). However, there is still virtually no information regarding brain morphology for the vast majority of living ray-finned fishes, which hinders our understanding of tempo and mode(s) of brain evolution in the most diverse extant vertebrate lineage.

Future endeavors should focus not only on describing brain anatomy of ray-finned fishes, but also include these in a phylogenetic framework which will provide the basis for answering a myriad of questions regarding brain evolution and correlation between neuroanatomy and ecomorphology. Recent work using advanced imaging techniques has proven valuable for quantifying brain diversity in ray-finned fishes. Examinations of intra-specific variation in brain morphology of ray-finned fishes using geometric morphometrics pointed out the potential of such methods for understanding brain shape variation in respect to ecomorphology (Kozol et al. 2023),

but an approach based on geometric morphometrics of both external and histological brain characters across ray-finned fishes more broadly is still lacking.

Chapter 7 Conclusions

This dissertation attempts to survey poorly understood aspects of early ray-finned fish diversity and how data from living species in addition to fossil data can provide reliable information on the evolution of morphology across time and space. Although this work by no means is exhaustive, I explore an important portion of the ray-finned fish evolutionary history that remains obscure.

First, by describing novel taxa and occurrences from high paleolatitude localities in South America I shorten the gap between our understanding of Paleozoic paleotropical faunas from North America, Europe and Asia to high paleolatitude and circumpolar faunas from the southern hemisphere in South America and Africa. These poorly described faunas, although mostly represented by isolated remains, still have an impact on early ray-finned fish taxonomy and biogeography. *Austelliscus ferox* described in Chapter 2 (Figueroa et al. 2021) represents the oldest occurrence of an unequivocal ray-finned fish within the Malvinohosan realm and within the Early-Middle Devonian circumpolar region. By its similarities to late Devonian predatory taxa from North America such as *Tegeolepis*, this taxon raises questions on the timing of diversification of predatory ray-finned fishes as well as implying that major morphological innovations might have taken place well-within the circumpolar circle during the Early and Middle Devonian before such morphologies appear in paleotropical areas by the Late Devonian. With this work I hope to raise awareness of the importance of describing fossil occurrences from poorly sampled regions within the southern hemisphere as these will not only help better understand how the first diversification of ray-finned fishes took place but also highlight differences between paleotropical and paleopolar ray-finned fish faunas during the Paleozoic.

The new taxa described in Chapter 3 for the Permo-Caboniferous of the Paraná Basin in southern Brazil also highlights the importance of these high-latitude faunas from the Paleozoic of South America. These two new taxa show remarkable similarities to two different sets of stem ray-finned fishes. The presence of two taxa with classically Carboniferous and putatively more derived and Triassic features in a single assemblage is remarkable. It pinpoints that some of the

evolutionary patters observed from well-sampled paleotropical ray-finned fishes might be biasing our understanding of the emergence of important morphological innovations for this clade. Additionally, by demonstrating new variation in endoskeletal characters for Paleozoic ray-finned fishes these fossils raise questions on biases in previously constructed phylogenetic matrices which focus on external dermal bone anatomy and neurocranial anatomy, with few characters pertaining to the morphology of the hyobranchial apparatus and other hidden aspects of the endoskeleton. Thus, with this study I aim to show that further morphological work is needed to better understand the hidden morphological diversity of early ray-finned fishes, as it has also been demonstrated by parallel work I have done during the development of this dissertation (Figueroa and Andrews 2022).

In chapters 4 and 5 I explore novel data that can work as a bridge between fossil and extant data on the evolution of ray-finned fishes. Given the sparsity of known occurrences of soft-tissue preservation in the fossil record and the difficulties pertaining to the accurate description of these remains and comparison to modern analogues, our knowledge of the early evolution of ray-finned fishes (and most other vertebrates) relies on skeletal data that is more readily available in the fossil record and easy to compare to data on living species. However, given that soft tissues can play an important role in the taxonomy of living species it would be expected that the same would be true for fossil taxa. By describing exceptional preservation of various soft tissues in ray-finned fish fossils from the late Paleozoic (Figueroa et al. 2023, 2024) we start to approach a more holistic understanding of the origins of the morphological diversity we observe in extant settings. The detailed anatomy of the fossilized brains presented in these two chapters not only reframe our understanding of the early evolution of the ray-finned fish brain, but also points out to morphological variation in fossil soft tissues that can play a role in better assessing taxonomic and phylogenetic interrelationship of stem ray-finned fishes.

Given the discovery of fossilized three-dimensional brains in late Paleozoic ray-finned fishes it became paramount to acquire comparative data on extant ray-finned fish brain morphology. However, upon a detailed examination of the literature I noticed a large gap in the description of brain anatomy in living ray-finned fishes, especially in terms of gross anatomy. Most of the neuroanatomical work on ray-finned fishes is restricted to a handful of lineages, as I described in Chapter 1 and 6. By compiling a large dataset of dice-CT scans of living ray-finned fishes I aim to explore hidden aspects of variation in ray-finned fish neuroanatomy. It is striking

that despite endocasts being commonly used as a proxy for brain anatomy in fossil taxa, including in ray-finned fishes, there is virtually no information regarding the endocast morphology of living ray-finned fishes. Thus, with the results described in Chapter 6 I not only provide an overview of ray-finned fish neuroanatomy but also provide the first reconstruction and regionalization of the teleost endocast. The endocast of living ray-finned fishes does not closely resemble brain anatomy in most lineages as there are large gaps in volumetric comparisons as well as in variation in size and proportion of brain regions. This raises questions on the reliability of endocasts as proxy for brains in fossil ray-finned fishes. Despite this, endocasts—of both fossil and extant taxa—can still provide important morphological information that can be used for phylogenetic analysis and maybe even ecomorphological inferences. However, it will only be possible to draw such hypotheses once we have gathered enough information on extant ray-finned fish brains and endocasts.

I hope that the results presented in this dissertation provide a basic framework for future research on the interrelationships of early ray-finned fishes integrating information from three-dimensional fossils with detailed accounts of the morphology of skeletal and soft tissue aspects of living species. I believe that a more holistic view of the early ray-finned fish fossil record is key for tackling the unstable relationships recovered in current phylogenetic analyses. Also, I want to emphasize that there is still much to discover in terms of morphological variation in living ray-finned fishes, especially for soft tissue anatomy. The frequent mismatch between phylogenetic hypotheses drawn from morphological and molecular data for ray-finned fishes can likely be influenced by a better representation of phenotypic change across extant ray-finned fishes. In this respect, the brain might represent an ideal starting point as it has clear links to ecology and phylogeny as well as information from a handful of fossils.

Appendices

Appendix A: Fossil Localities Bearing Fish Soft-Tissue Preservation

Appendix Table A.1 – List of fossil fish localities with reported or figured soft-tissue preservation worldwide.

Locality	Age	Taxa	Type of Tissue	Country	Lithology	Environment	References
Chengjiang	Early Cambrian	early chordates	muscle, gills, skin	CHN	Mudstones	Marine	Hou & Bergstrom, 2003
Burgess Shale	Mid Cambrian	early chordates	muscle, eyes, organs	CAN	Shale	Marine	Petrovich, 2001
Gleenwood shale	Middle Ordovician	Conodonta	body impression	USA	Shale	Marine	Liu et al., 2006
Soom Shale	Late Ordovician	Conodonta	body impression	ZAF	Shale	Marine	Aldridge & Theron, 1993
Eramosa	Middle Silurian	Agnatha	skin	CAN	Shale	Marine	von Bitter etal., 2007
Hunsruck Slate	Early Devonian	Placodermi		DEU	Slate	Marine	
Orcadian Basin	Middle Devonian	Agnatha, Acanthodii, Actinopterygii, Placodermi	eyes and various organs, embryos	GBR	Limestones	Marine	Davidson and Trewin, 2005
Gogo Formation	Late Devonian	Placodermi	Muscles, internal organs, nerves	AUS	Calcareous Concretions	Marine	Trinajstic et al., 2022
Escuminac Formation	Late Devonian	Placodermi	blood vessel impressions	CAN	Siltstones	Transitional	Arsenault et al., 2004
Cleveland Shale	Late Devonian	Chondrichthyes	muscle fibers	USA	Shale	Marine	Dean, 1902
Chattanooga Shale	Late Devonian	Chondrichthyes	muscles	USA	Shale	Marine	Maisey, 1989
Old Red Sandstone	Late Devonian	Acanthodii	myomers	GBR	Sandstones	Marine	Watson, 1959
Witpoort Formation	Late Devonian	Placodermi	body impression	ZAF	Shale	Marine	Gess & Trinajstic, 2017
Madene El Mrakib	Late Devonian	Chondrichthyes	skin, organs, muscles	MAR	Ferruginous Nodule	Marine	Frey et al., 2020
Granton Sandstones	Mississippian	Conodonta	muscle	GBR	Sandstones	Marine	Briggs et al., 1983

Bear Gulch Limestone	Mississippian	Chondrichthyes	skin, pigments, muscle, intestine	USA	Limestone	Marine	Grogan & Lund, 1997
Hamilton Formation	Pennsylvanian	Acanthodii	Eye rods and cones	USA	Limestone	Marine	Tanaka et al., 2014
Mazon Creek	Pennsylvanian	Chondrichthyes, Osteichthyes	body impression, eye pigment	USA	Siderite Concretions	Marine	McCoy et al., 2020
Stranger Formation	Pennsylvanian	Iniopterygia	Brain	USA	Phosphate Concretions	Marine	Pradel et al., 2009
Coffeyville Formation	Pennsylvanian	Iniopterygia	Brain	USA	Phosphate Concretions	Marine	Pradel et al., 2009
Manning Canyon Fm.	Pennsylvanian	Acanthodii	gill rakers/filaments	USA	Carbonate	Marine	Schultze, 1990
Mountain Fourfoot Mine	Pennsylvanian	Actinopterygii	brain	GBR	Phosphate Concretions	Marine	Figueroa et al., 2023
Meride Formation	Early Triassic	Actinopterygii	skin and myomers	CHE	Limestone	Marine	Maxwell et al., 2013
Monte San Giorgio	Middle Triassic	Actinopterygii	embryos	CHE	Limestone	Marine	Renesto & Stockar, 2009
Madygen	Late Triassic	Actinopterygii	body impression	KGZ	Mudstones	Lacustrine	Voigt et al., 2017
Ya Ha Tinda	Early Jurassic	Actinopterygii	gill rakers	CAN	Mudstones (calcareous)	Marine	Martindale et al., 2017
Strawberry Bank	Early Jurassic	Actinopterygii	gut impression	GBR	Calcareous Concretions	Marine	Williams et al., 2015
Osteno	Ealry Jurassic	Chondrichthyes	skin, organs?, eyes, muscles	ITA	Limestone	Marine	Duffin & Patterson, 1993
Solnhofen Limestone	Mid Jurassic	Chondrichthyes, Osteichthyes	Skin and pigments	DEU	Limestone	Marine	Petit & Khalloufi, 2012
Oxford Clay	Jurassic	Actinopterygii	indet	GBR	Mudstone	Marine	Wilby et al., 2008
Quebrada del Profeta	Late Jurassic	Actinopterygii	Muscle fibers	CHL	Shale	Marine	Schultze, 1989
Romualdo Formation	Early Cretaceous	Osteichthyes	Muscle fibers, heart, gill rakers	BRA	Concretions (Ca/P)	Lagoonal	Martill, 1988
Crato Formation	Early Cretaceous	Actinopterygii	Muscle fibers	BRA	Limestone	Marine	Osés et al., 2017
Jehol Group	Early Cretaceous	Actinopterygii	skin	CHN	Mudstone & Siltstone	Lacustrine?	Pan et al., 2013
Las Hoyas Formation	Early Cretaceous	Actinopterygii	eye pigments	ESP	Limestone	Freshwater	Gupta et al., 2008

Strzecki Group	Early Cretaceous	Actinopterygii	body impression	AUS	Mudstones & Siltstones	Fluvial?	Poropat et al., 2018
Paja Formation	Early Cretaceous	Actinopterygii	skin	COL	Limestone	Lagoonal?	Alfonso-Rojas & Cadena, 2020
Pietraroja Formation	Early Cretaceous	Actinopterygii	skin?	ITA	Limestone	Marine	Signore et al., 2005
Tlayúa Formation	Late Cretaceous	Actinopterygii	Muscle fibers, gill rakers, epitelia	MEX	Limestone	Marine	Alvarado-Ortega et al., 2007
Múzquiz	Late Cretaceous	Actinopterygii	Muscle fibers	MEX	Limestone	Marine	Riquelme et al., 2013
Kem Kem Beds	Late Cretaceous	Actinopterygii	Muscle fibers, skin, intestines	MAR	Mudstones & Limestones	Deltaic	Ibrahim et al., 2020.
En Nammura	Late Cretaceous	Actinopterygii	eyes	LBN	Limestone	Marine	Capasso et al., 2008
Hgula limestones	Late Cretaceous	Actinopterygii	eyes	LBN	Limestone	Marine	Capasso et al., 2009
Hadjula	Late Cretaceous	Agnatha	skin, heart?, liver, slime glands	LBN	Limestones	Marine	Miyashitaet al., 2019
Dinosaur Park	Late Cretaceous	Actinopterygii	blood vessels?	CAN	Sandstones	Fluvial	van der Reest & Currie, 2020
Monte Bolca	Eocene	Actinopterygii, Chondrichthyes	Muscle fibers	ITA	Limestone	Marine	Wiby & Briggs, 1997
Messel	Eocene	Actinopterygii	skin	DEU	Shale	Lacustrine	Franzen, 1985
Green River	Eocene	Actinopterygii	skin, eyes, organs	USA	Mudstones (calcareous)	Lacustrine	Meacham, 2017
Plana de Vic	Eocene	Actinopterygii	skin	ESP	Limestones	Marine	Carnavale et al., 2019
Fur Formation	Eocene	Actinopterygii	eye pigment	DNK	Diatomite	Marine	Lindgren et al., 2012
Republic, WA	Eocene	Actinopterygii	body impresson	USA	Shale (tuffaceous)	Lacustrine	Wilson, 1996
Cambay Formation	Eocene	Actinopterygii	collagen	IND	Coal? (lignite), shale	Continental	Dutta et al., 2020
Rauenberg	Oligocene	Actinopterygii	body impression	DEU	Mudstones	Marine	Maxwell et al., 2016
Aix-en-Provence	Oligocene	Actinopterygii	body impression	FRA	Limestone	Brackish	Gaudant et al., 2018

Menilite Formation	Oligocene	Actinopterygii	eye pigments	POL	Carbonate	Marine	Bienkowska-Wasiluk, 2021
Ngorora Formation	Miocene	Actinopterygii	body impression	KEN	Mudstones & Shales	Lacustrine?	Penk et al., 2019
Hindon Maar	Miocene	Actinopterygii	body impression	NZL	Gyttja	Lacustrine	Kaulfuss et al., 2018
Shiobara Group	Pleistocene	Actinopterygii	skin	JPN	Mudstones and Siltstones	Lacustrine	Allison et al., 2008

Appendix B: Chapter 2 Supplement

B.1 Specimen information

MCT890-P, consisting of part and counterpart, was collected by the late geologist Dr. Euzébio de Oliveira, who collected in the Devonian of the Ponta Grossa region, depositing several specimens in the paleontological collection of the DNPM/CPRM (pers. comm. S. Schaeffer). It was registered in the paleontological collection of DNPM/MCT on March 28, 1967. Associated information indicates the specimen was collected in the vicinity of Ponta Grossa, State of Paraná, Brazil. There is no further data on locality or horizon. A latex cast of the specimen is deposited at the American Museum of Natural History, New York, USA, under the number AMNH 19242. Geological information associated with this cast (the Permian Mafra Formation) is not supported by information associated with the original fossil, or by details of the matrix itself.

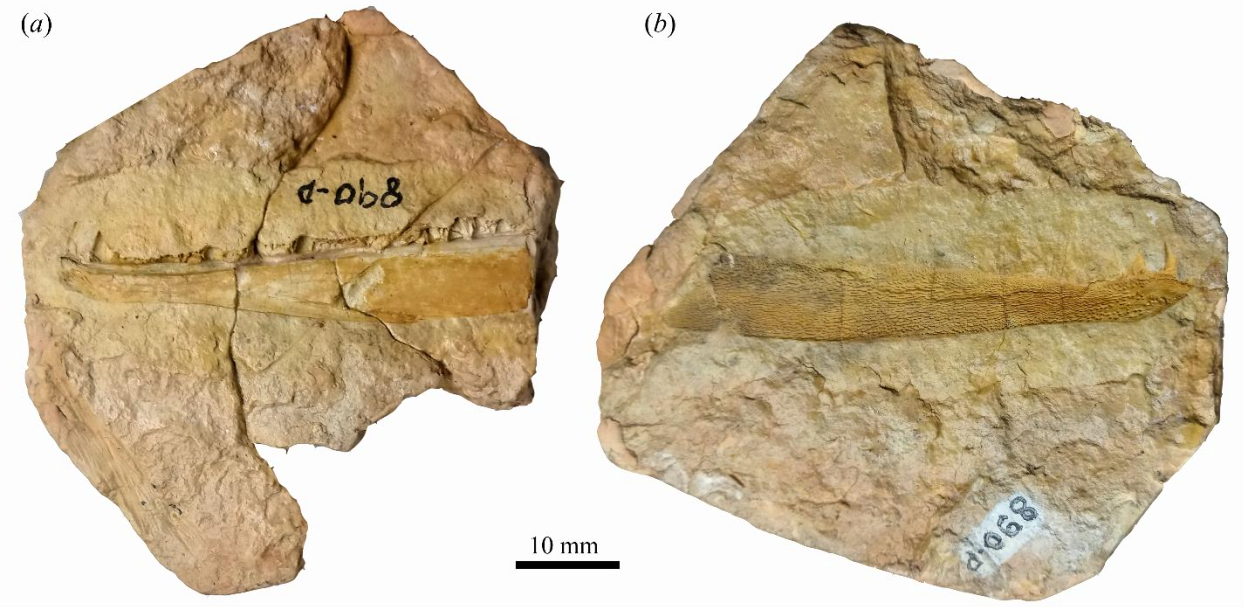

Appendix Figure B.1 - *Austelliscus ferox*, holotype, MCT890-P. Impression showing: (*a*) mesial surface of jaw; (*b*) lateral surface of jaw.

B.2 CT-scanning

Appendix Table B.1 – Specimens analyzed. Parameters for scans for specimens featured in previous studies are given by those authors. Abbreviations: AMF, Australian Museum, Sydney, Australia; CMNH, Cleveland Museum of Natural History, Cleveland, USA; IVVP, Institute of Vertebrate Paleontology and Paleoanthropology, Beijing, China; MCT, Museu de Ciências da Terra, Rio de Janeiro, Brazil; MGL, Natural History Museum of Lille, Lille, France; NHMUK, The Natural History Museum, London, UK.

	Specimen	Current	Voltage	Voxel Size
Austelliscus	MCT890-P	110 µA	120 kV	0.052 mm
Tegeolepis	CMNH 8124	60 µA	202 kV	0.072 mm
Raynerius	MGL 1245	Giles et al. (2015b)		
Meemania	IVPP V14536.5	Lu et al. (2016)		
Howqualepis	AMF 65495	Giles et al. (2015c)		
Cheirolepis	NHMUK PV P.12508	Lu et al. (2016)		

B.3 Biostratigraphic constraints for the Ponta Grossa Formation

Palynomorph biostratigraphy provides constraints on the age of the Ponta Grossa Formation (Grahn et al. 2013). The base of the formation is within the Ems Western Gondwanan Spore Zone (Grahn et al. 2013), which is correlated with the PoW Western European Spore Zone and the *sulcatus* to *kitabicus* conodont zones. This indicates a Pragian age for the base of the formation (maximum age ~411 Ma; Becker et al. (2012)). The top of the Ponta Grossa Formation (inclusive of the São Domingos Formation of some workers) is within the BMu Western Gondwanan Spore Zone (Grahn et al. 2013), which is correlated with the lower BA (= 'IV'a-b') Western European Spore Zone and the *rhenana* to *linguiliformis* conodont zones (Melo and Loboziak 2003). This places the top of the formation in the Frasnian (minimum age ~373 Ma; Becker et al. 2012). The uppermost sequence within the Ponta Grossa Formation (sequence F of Grahn et al. (2013)) is unexposed in the Ponta Grossa region, indicating that the specimen is unlikely to derive from the upper part of the unit. Base of this youngest sequence is in the Trg Western Gondwanan Spore Zone (Grahn et al. 2013), which is correlated with the TA Western European Spore Zone and the *varcus* Conodont Zone (Melo and Loboziak 2003). This indicates an early Givetian age for the base of this sequence (~387 Ma; Becker et al. (2012)), which is also a probable minimum age for MCT890-P.

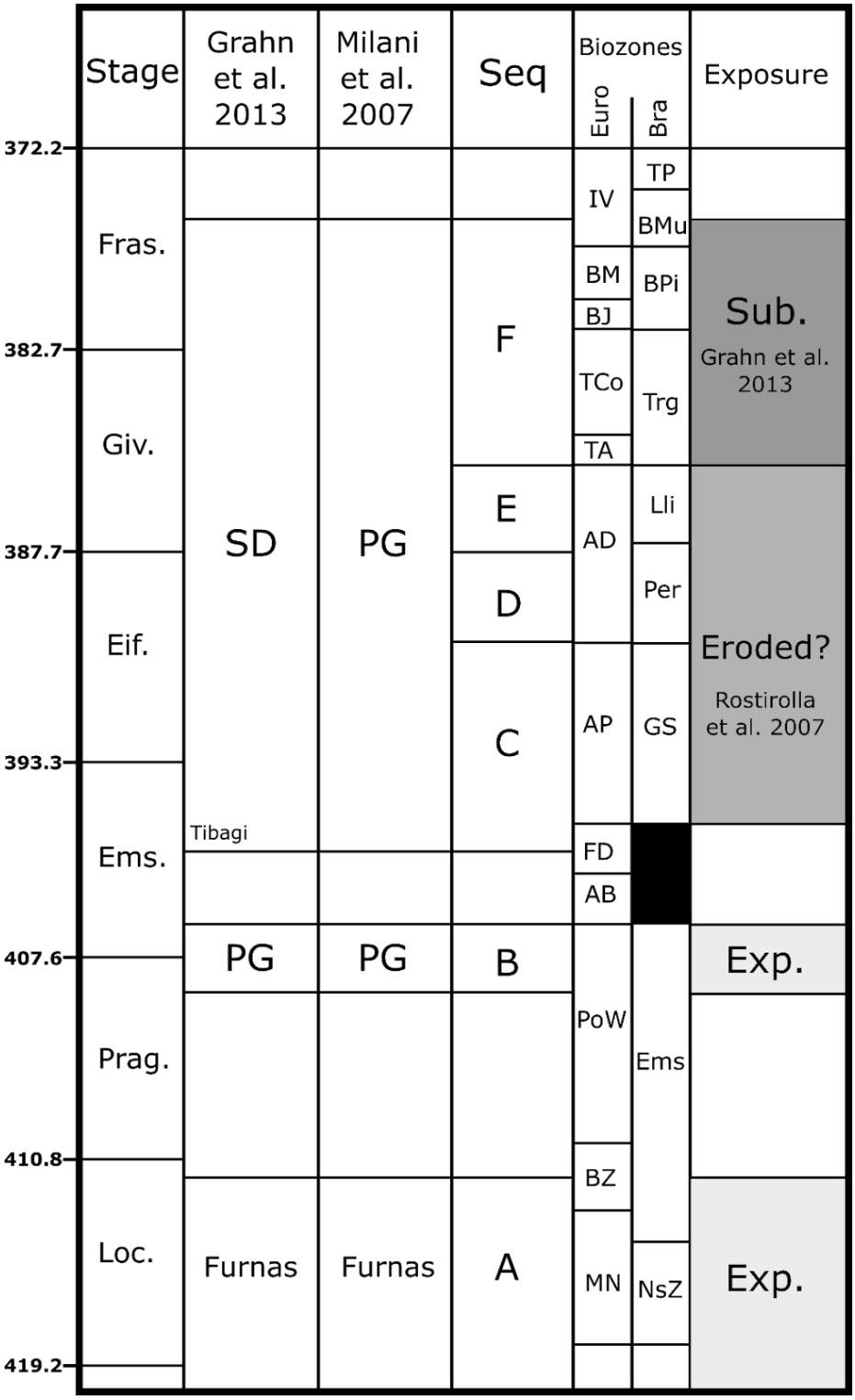

Appendix Figure B.2 – Stratigraphic column of the Ponta Grossa region. Adapted from Grahn et al. (2013) to include the alternative stratigraphic nomenclature of Milani et al. (2007) and information on exposure from Grahn et al. (2013) and Rostirolla et al. (2007) for the Ponta Grossa Region. Sub = Subsurface, Exp = Exposed.

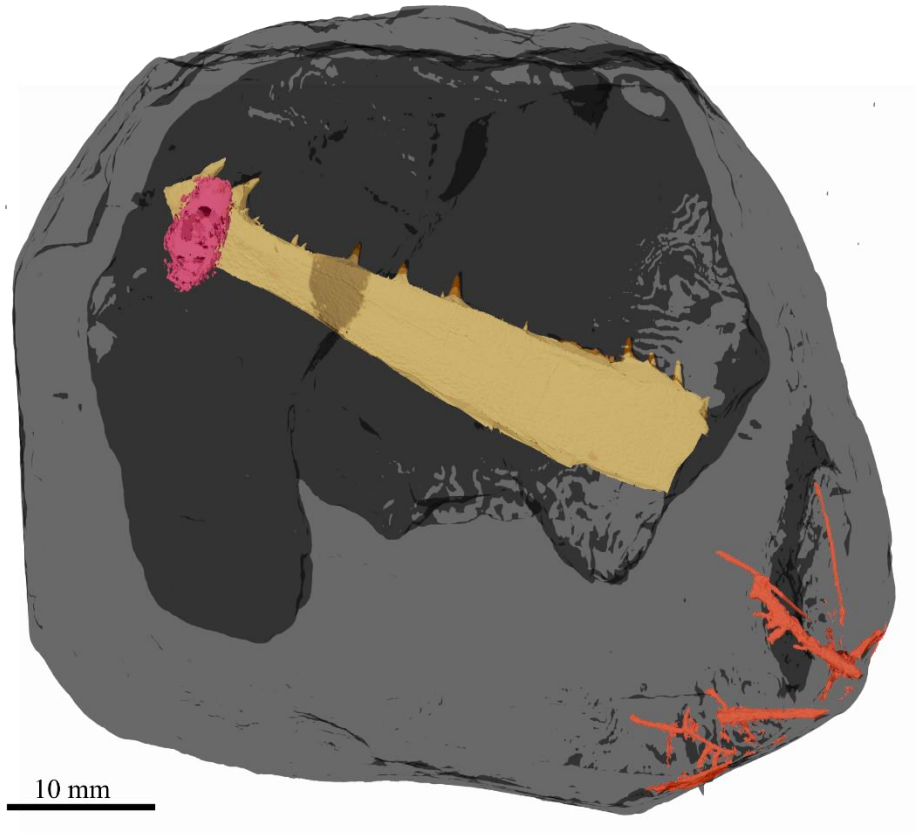

Appendix Figure B.3 – *Austelliscus ferox*, holotype, MCT890-P. Mandible (orange) shown in association with body fossil and trace fossil remains within the part and counterpart: lingulid brachiopod (magenta) and tuberous ichnofossil (red). Surrounding matrix (grey) is rendered semitransparent.

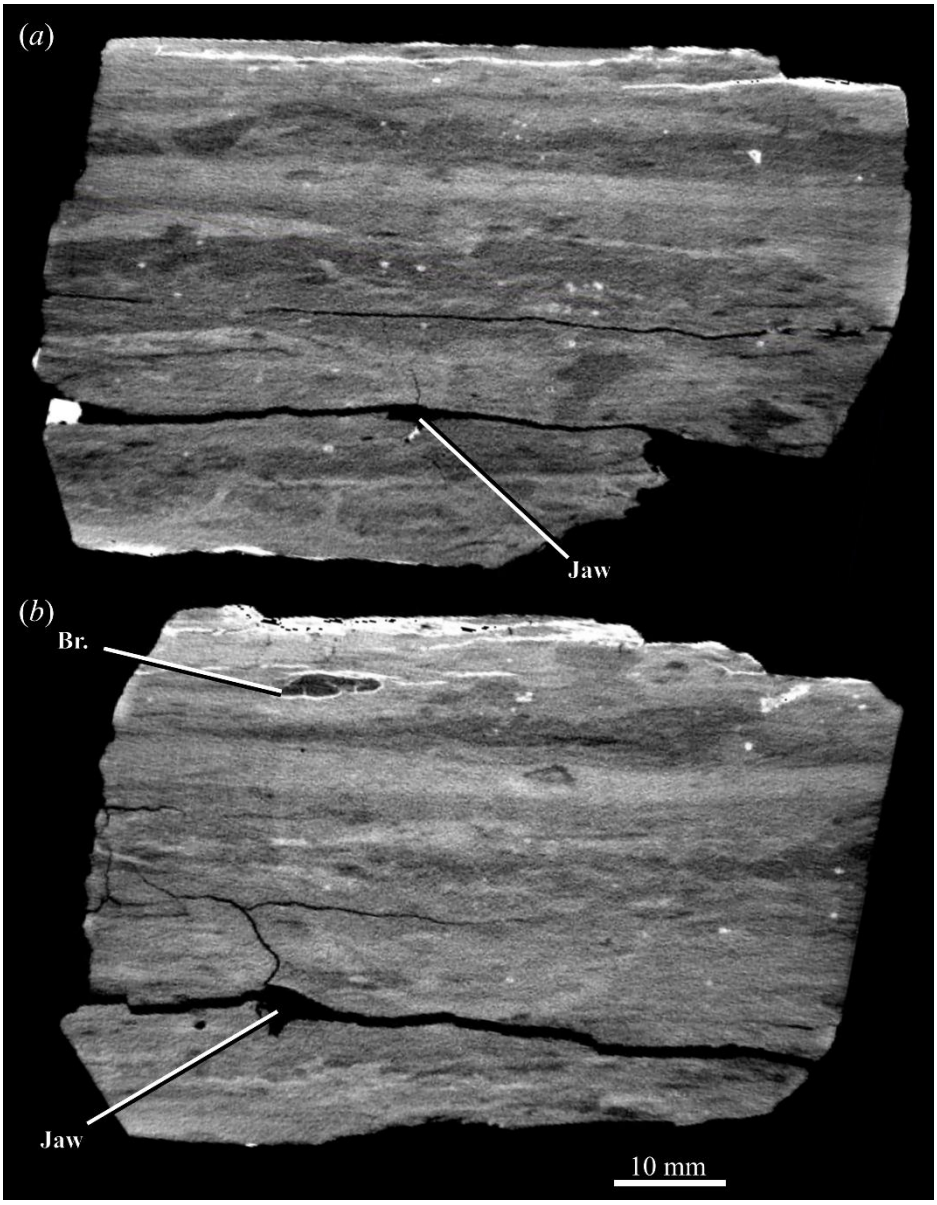

Appendix Figure B.4 – *Austelliscus ferox*, holotype, MCT890-P. Tomograms showing: (*a*) void representing jaw; (*b*) void representing jaw along with that representing lingulid brachiopod.

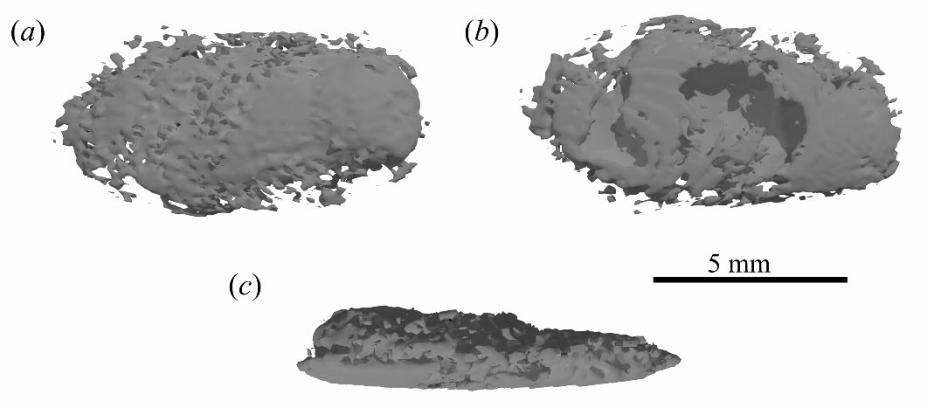

Appendix Figure B.5 – Renders of lingulid brachiopod contained within matrix of MCT890-P. (*a*) Ventral view; (*b*) dorsal view; (*c*) lateral view.

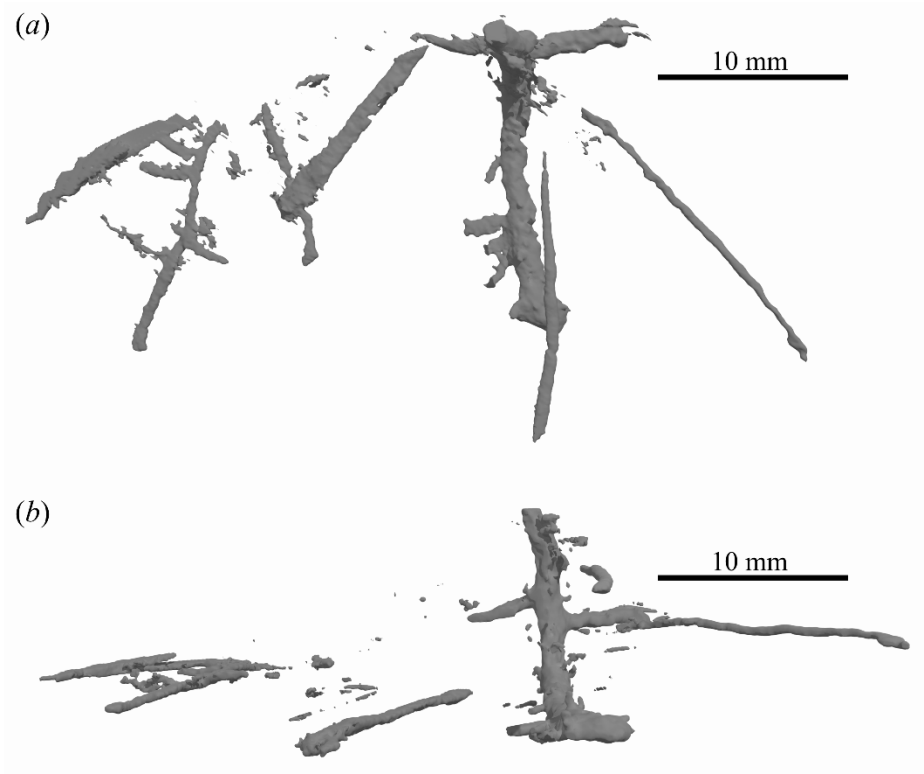

Appendix Figure B.6 – Renders models of ichnofossils preserved within the matrix of MCT890-P. (a) View perpendicular to bedding; (b) view parallel to bedding.

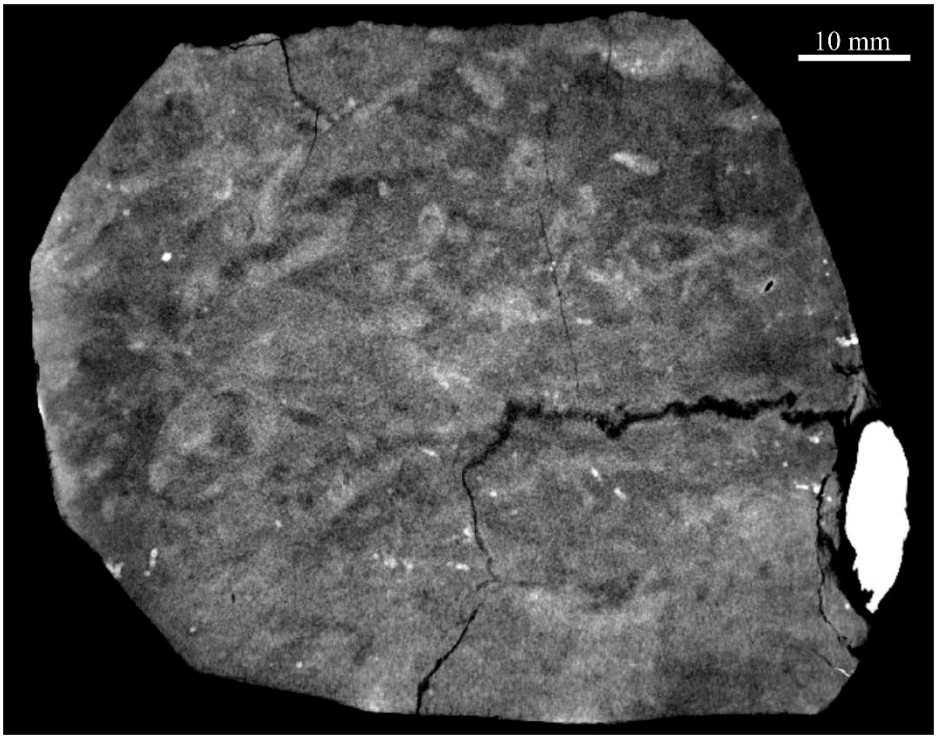

Appendix Figure B.7 – Horizontal CT slice of the sample containing the holotype of *Austelliscus ferox* (DGM 890-P) showing the abundant bioturbation.

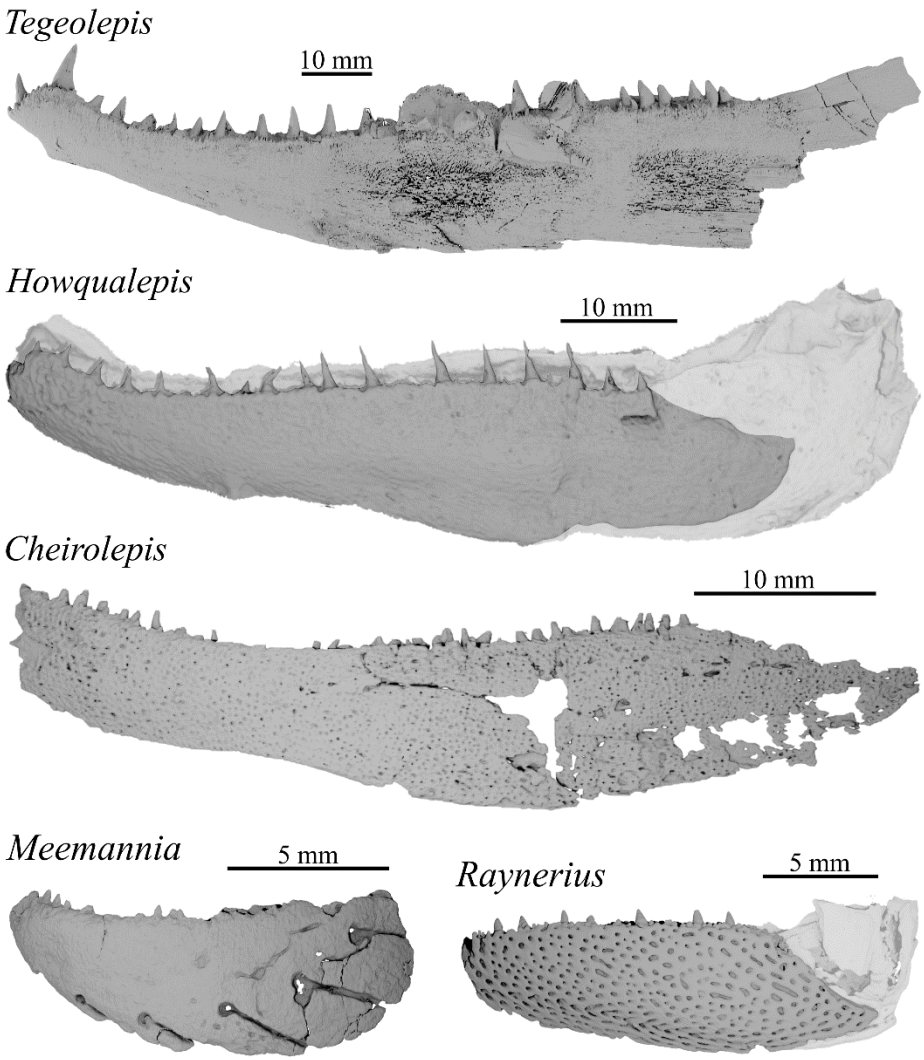

Appendix Figure B.8 – Rendered models of comparative material used in this study.

Appendix Table B.2 – Total Length/Dentary proportions in selected Devonian actinopterygians.

	TL (mm)	Dentary (mm)	Prop.	*A. ferox* TL (mm)	Reference
Cheirolepis	267	30.5	8.75	612	Pearson and Westoll (1979 fig. 16)
Mimipiscis	258	32	8.06	564	Choo (2011 fig. 19b)
Moythomasia	213	23.7	8.98	628	Choo (2015 fig. 14c)
Cuneognathus	57	7.2	7.90	553	Friedman and Blom (2006 fig. 7)
Donnrosenia	228	23.7	9.62	673	Long et al. (2008 fig. 10)
Stegotrachelus	157	18.5	8.48	594	Swartz (2009 fig. 16a)
Howqualepis	500	64.8	7.71	540	Choo (Choo 2009 fig. 6b)
Gogosardina	140	18.6	7.52	526	Choo et al. (2009 fig. 14)

B.4 Phylogenetic analysis dataset

```
#NEXUS
[written Tue Jan 12 10:39:20 EST 2021 by Mesquite  version 3.61 (build 927)
at ummp-5CD93274K8/10.0.0.158]

BEGIN TAXA;
	TITLE Taxa;
	DIMENSIONS NTAX=93;
	TAXLABELS
		Acanthodes_bronni Acipenser_brevirostrum Aesopichthys_erinaceus
Amia_calva Amphicentrum_granulosum_ Atractosteus_spatula Australosomus_kochi
Beagiascus_pulcherrimus Beishanichthys_brevicaudalis Birgeria_groenlandica
Bobosatrania_groenlandica Boreosomus_piveteaui Caturus_furcatus
Cheirolepis_canadensis Cheirolepis_schultzei Cheirolepis_trailli
Chondrosteus_acipenseroides Cladodoides_wildungensis Coccocephalichthys_wildi
Cosmoptychius_striatus Cyranorhis_bergeraci Dapedium_LIAS Dapedium_pholidotum
Dialipina_salguerioensis Dicksonosteus_arcticus Diplocercides_kayseri
Dipteronotus_ornatus Discoserra_pectinodon Donnrosenia_schaefferi
Dorsetichthys_bechei_ Ebenaqua_ritchei Elops_hawaiensis
Entelognathus_primordialis Erpetoichthys_calabaricus Eusthenopteron_foordi
Evenkia_eunoptera Fouldenia_ischiptera Fukangichthys_longidorsalis
Glyptolepis_groenlandica Gogonasus_andrewsae Gogosardina_coatesi
Guiyu_oneiros Hiodon_alosoides Howqualepis_rostridens Hulettia_americana
Ichthyokentema_purbeckensis Kalops_monophyrum Kansasiella_eatoni_
Kentuckia_deani Lawrenciella_schaefferi Lepisosteus_osseus Leptolepis_bronni
Ligulalepis Luederia_kempi Luganoia_lepidosteoides Macrepistius_arenatus
Macrosemimimus_lennieri Macrosemius_rostratus Meemannia_eos Melanecta_anneae
Mesopoma_planti Miguashaia_bureaui Mimipiscis_bartrami Mimipiscis_toombsi
Moythomasia_durgaringa Moythomasia_lineata Moythomasia_nitida
Obaichthys_decoratus Onychodus_jandemarrai Osorioichthys_marginis
Osteolepis_macrolepidotus Ozarcus_mapesae Peltopleurus_lissocephalus
Platysomus_superbus Polypterus_bichir Porolepis_sp. Propterus_elongatus
Psarolepis_romeri Pteronisculus_stensioi Raynerius_splendens
Saurichthys_madagascarensis Scanilepis_dubia Semionotus_elegans
Styloichthys_changae Styracopterus_fulcratus Tanaocrossus_kalliokoskii
```

```
Tegeolepis_clarki Tetragonolepis_semicincta Venusichthys_comptus
Watsonulus_eugnathoides Wendyichthys_dicksoni Woodichthys_bearsdeni
Austelliscus_ferox
      ;

END;


BEGIN CHARACTERS;
      TITLE  Character_Matrix;
      DIMENSIONS  NCHAR=266;
      FORMAT DATATYPE = STANDARD RESPECTCASE GAP = - MISSING = ? SYMBOLS = "
0 1 2 3 4 5 6 7 8 9";
      CHARSTATELABELS
266
Concavity_on_the_ventral_margin_of_the_dentary_forming_the_ventral_border_of_
the_lower_jaw ;
      MATRIX
      Acanthodes_bronni             0?????????????????-?????0?-?????01?-
??????-?????-?????????????1?????????????????????-????????0-?-?021?000?-?-
????-?--??0??0-????0000????00000000???1000--0-?0??????????0000--------
1???????????01?0-00--000---?0000010??0-??1010??-??-
????0000101?11100000002????00?????-?--
      Acipenser_brevirostrum        111---------00?0000-1-?010000-0101-1----
00110-00??1-001001--000--00-----------010---0-?0-1--0-0-1001011-1110020002---
011-0-0-0100000-?20020--0100--0--0--1-10?100?010-
000121112001110100001101????0----1-----01000011010-101000000-
000000101?10101110121112000110001000010
      Aesopichthys_erinaceus        1101-000000111001011100010120?0001-00110-
1111100101--1101000-
011101000000000010000120???2???120?1???????????0100101000010?11???????0??????2
?????????1???????00---------
??????????????????????????????????0110100110111?????????????100?00??????0??010
10021012???0100????????0
      Amia_calva                    1101-100012010001100000001012010101-1----
000111001100001100 00-10--
0100001111001000012 01?110101201100 1?0100001000100210101-11000?000001112021--
```

1100-00--0--1-11-0011100110112111000100011101111110010-00--010---
?1001110011110101100 0-0001110010101110100000121111011110010 00
Amphicentrum_granulosum_ 1100010100 0?110?1011?0001-020?0001-1----
01?1??000-1100000000-00--1110010000 0?1010---1-??20?-0-0-
?1200010????020010100000???0001???0????20?0010??0-
00??21011?????0?????1?01110 0?001?????????????????????????????010????0???????
??0-0??0?????????????????????????0????????0
Atractosteus_spatula 11000100-120101011000000101201011 1-1----
01211100112--3-
1011110111010010010000100001100111020120010010011000101010021 0011-0-
000100000-022020011100-00--0--1-11-0110110-
1011211100010?????????????????101?0110000110111101121010110 00-
0101110010001110100000?1111111101001100
Australosomus_kochi 111?????-??-??0??0?????01002010001-1----
01011000??0-001--0---0101111000000010100001 20??011--0-0-
10200000?000010000100000?10000100100102 2021--?101101002001001---------
0?1101012000001111102???1110-????01101001101100110-101001000-
00000110?000111010000010010??1001000010
Beagiascus_pulcherrimus 1100000000011100101110001012010001-00110-
0210-?0101003111000-?10??111?00000???00001101???????-
0?1??????????1100000000101 10???
??????????????????????????????011?10011?????????????????110?00??????1??21010011
?11????100????????0
Beishanichthys_brevicaudalis 1100?01000?0110010111000101 20?0??1-1----
00111?000-
1002100 20?00101?1100000000?10000120 1??2???1?0????????????0100000000000??????
??1?????????????????????????????01101
0?10????????0-?????????0-0?0?????????1101000001 2???1011???????0
Birgeria_groenlandica 1100110000101100101100001 0?2010001-1----
0100100010200301020000 0--0110000000001000011 01?01???110-1021000000--
0100000000001100001 00?0010?202?--010???1--???1?10-?-0????-
000121012001 1?????????????????0????11???00110000?10-101?0?000-00200100--
0013101000001200011000100001 0
Bobosatrania_groenlandica 111----1----000010111-0010120?00{0 1}1-1-
---0?0011000-2100010000-00--0100011000001010---0-??2???0-?-?0????0?0????0-1--
11000-?-0-
???10???0??????0?????????????????1????????????121??2????????????????????0
11???0110?1010?0-1????????0-0001?????????0?0100101121 0?1100??????10

Boreosomus_piveteaui 1100101100001100111110?01002010011-1----
01100-000-2003100000-1101011110000?01000110?0010300-0-
1020000101000100001000101100?1010001?120200101010011{0 1}{0 1}2111000--------
-000101010100001011111100??110???0110100110011?10-1?1??00?0-
?020011???0??1?01000101200?01000000?010
Caturus_furcatus 1100010001?110101100000001012000110-1----
000111001121O2?01200110--
0100001111???0000120??0103012011021001??00100010021O?11-1100010??0?????021--
1??0-
00????????10?00011001l??121110000?????????????11??????????0110111001111??1??1
??1000??1?0????????0100000121111110?1000000
Cheirolepis_canadensis 110?01-000000000000??010{0 1}0010?0001-
000-0-10011000-1010010000-010?1111100000101000011100??10?00-
0????????????1000000000000???0??1?
00?????????????????????????000-0?011?????????????????0-
0?00????000110101101011O???0101????????0
Cheirolepis_schultzei 1100000000O?00000000?01010020?00?1-1---
0010111?00-1010010000-
010?1111?000001010000l?00????????0??????????0??10000000000?1??0????????????
??????????????????????????????1????0?????????????????????000-
0??11?????????????????????0?00??????0??010??0?????????????????0
Cheirolepis_trailli 1100001000000000000010010{0 1}001010001-
00000-10010000-1010010000-01101111?000001010000110O??10100-0-
1010000000001000000000000001000?0??00?????0100000010O1?00--1-00---------
000100000000011l????????????1110001O1?011000????0-
????????10000000001000101011011110???0100??00??10
Chondrosteus_acipenseroides 111---------1????????-?010120????1-1----
0?2?0-?0??1?0??00?????0--00-------??01010---0-?0?1--??0-?0???1??10??02000??-
??0????????????????????000?????????????????????????????1211?20011?????????????
??----1-----?10000010?0?????????0-0?0?????????12101?00001????110??0000?10
Cladodoides_wildungensis 0?-?-??-----??-??--????-?-??-?????-?????-
-?????-?-???-???----?????-???-----????-?0??-00?????0---?0?0-0?-?---??-?---?--
?-??-??0000001?0?00010-0000-0100---0-00---------0000--------110100000---0100-
????00???????0??????0-????????--?-?---????????????????????????????--
Coccocephalichthys_wildi 11????0????11?0101010?01002010011-1----
00110-
00112000?0010?01?0?0111?00?00??100001101??1???110?1010?00000?0?101?00000?????
00?10??000?02020000?01001??2101100---------

0?0101010000??????????????????????01???????0?1????0????????????0?????????????
??????????????????????0

Cosmoptychius_striatus 110??1000?00?10010111000101 2??0001-1----
?0?1??00101002100000-
010?011100000001?10000?10???2???????1020????????10000000001?110???1?????????0?
001???1101??11111?0??00????????101?1?0000?????????????1?????011010011???????
??????????0-0?000????011110011010012???1100????0??0

Cyranorhis_bergeraci 111---------110010111-001012010001-00100-
1111100101002110000-
010101110000000?10000120?????????0???20????????000000000000110?????????????
??011?100110?1????
??????????100??0?1????1??110100101 12???0100????????0

Dapedium_LIAS 1100110000 1?1100110?000010---0-??-------
1-111100102--3-0-1000?0--
0100001101??1100012 0??0?0?01?0??????0??00??010100210101-
11???10?0001?120?0011100-00??2??1?0----------
111121?????1?011111????11011????011??0?110?1?????????????100?01?1???????210
10?????????1?1???????00

Dapedium_pholidotum 1100110000111100110100001 0---?-01-------
1-21110-102--3-0-200010--
0100001?0100110001 20???1??0??0??0?0?????0?1010000210101-
11?????????????????1?????????????0----------
??????????????????????????????011??0011?????????????????10??01?1????????10
100211121??1111???????0

Dialipina_salguerioensis 100???1000??01?0?0?????01012100001-1----
00?????????103?00????????110??00??????00?01000??0??????????????????????????0?
??000-
??1???0
11010?10?????????????????????0?0???????????0110?0001???0??1???????-

Dicksonosteus_arcticus 100??1-000000100???????00-
00000?0??1?????0010-1???10000??0??-?0???0--------?????????0????????????000-
00???--0????0?????????00000000 1?????0???0000-00??0--
0?00?????????0001000000000?101???00??????0?????????????????????????????????
??????????????????????????????????-

Diplocercides_kayseri 110?01-000??00?10??000111000010001-1----
0?010-0???100?0???00?10--00?-------
00010???00?1010?11301002 1?000?0?0000?010000-000-0?000?010???0100000010-10??0-

-1-00---------000100000000?111?0???????????????01---
0???1??????10???????????0????????????10??0??????????1????????-

Dipteronotus_ornatus 110??10000??110010010??010120?000??1----
?0??????1?0-00???1--
1?????10000000000100001201???1????0??0?1?????????100001000?1?????????????????
????1??????????????????0????????1101200???????????????????????01?0?0?11??????
?????????????0?2????????????01002?112????110?100????

Discoserra_pectinodon 11000010000101001011100010120?0000-1----
002110000-2003001100000--010000?000001000012 0???20??0-0-10?1???0?0??0-1--
120000010-????0??00??02?2?--11?0-0????????0----------
1??121?0?0???????????????????????0110?011101?00010-
????????110??1?1???00???10100201120001111?10???10

Donnrosenia_schaefferi 110?001?00001100101110000-01010001-00100-
10111?00-???0?10000-0?0?1111?000001110000110???1???0-0-
????????????1001000?0000010?0??
??????????????????????????011010011???????0-
??????????0?00??????1??11011010111????1?????????0

Dorsetichthys_bechei_ 110?0100100?1100101000001012110?11-1----
00011000102101110100000--
?101001102001000012 0???1????210?0?1?0???11?0100002101??-
11???1??1000002020011101001??0????1010000001111112100011 11?10?11?????11111???
?0110?0?1?011????1??????1??0-0?0??????10??21010000012???111011110000

Ebenaqua_ritchei 111----1----110010101-0010120?0001-1----
001011000-2?00000000-00--0100011?000??010---0-??20?00-
0?10??????????0000011000-0-
0??????????????????1????????????????????????????1?1??????????????????????????
?011??001???01?????????????11??21?????????21010021111??11101???????0

Elops_hawaiensis 1101-10010211100100000001012100111-1----
0001110010210000010001 0--1101001102001000010010021--
1200?02100101111000010210101-1100010??00???2000--1100-00--0--1-
11?01001011111120010101???????????????0-00--000--0011011111?10?11000?10-
000101001110101010000012111111001000000

Entelognathus_primordialis 100??1-100010100??0????0100?00?-
0????????0010-????10000??0??-10???100110000?001001?0?-?01?-0-0-?000-0???---
0????0?-0??00????0?0??0?????0????0?00-?0??0??0-00---------000?----?--
?0????????????????????0?????0??0??????0-??0-????0-
??0000????????11??????????????1???????-

Erpetoichthys_calabaricus 1101-11000001000000010001002011101-------
-2111000-1003000000-0101011010000000100001 20?002030100-1001101000100-1--
00000-000-000010000-000011--0001-00--
2001110???0?0000000121010001010101011000011?010??01101001000100010-101110010-
000001????0?1?100-????1-?111?11????1?00
Eusthenopteron_foordi 110001-00000000000001110-01010100100000-
0010-000-1000001100110--0100000000000000011000000200-0-1020000-
10000100010000-00101100000 10???0100100011001--0--1-00---------
000100000000111110000---1100-00--010--001011010110-100010100-1010001---
0000101010000200000110100000-
Evenkia_eunoptera 110?00100000000?00?01?0001012001111-------
-
?1??000?2002?00200001 1?01100000000????0???20???1?????0?????????????11001000000
00??
???011??0110?????????????????100?????????0??0101000?112???100?????????
Fouldenia_ischiptera 1100010100 0?1100101 0?00010110????1-1----
0?0111?00-1000?00000-?101?111?000000?10100121???20??0-
0??1?0????????0100100000000110???1?
???????0?????????????????????0110100110?????????????????0-
0?00?0??10001010100211 11???0100???????0
Fukangichthys_longidorsalis 11000?1000??11001?111?00101 20?0101-1----
011011?0????0310020?0?10101110000000???00001201001???100?100110100010010000000
000010???01???0????????1?????????????????????????????1?100000?0?????????????
?????011??00110010000?0-??11?1????000?????????1101000001 2????011????????0
Glyptolepis_groenlandica 110?-1-0000???-0?00?0111110001110010---0-
0010-010-1100000000-10--01000?0??0?0000?10?0?1????2?0-0-0020000-
10000101010000000101010 0?010???010?1?001???????????00---------
000100000000011111000?---?????????01--00?101???0?10-10011?100-
10?00?0???010?00??000?0????0001??????1-
Gogonasus_andrewsae 1100-1-0000?00-0000001110-00010100100000-
0010-0?0-1000001?00?10--0100000000000001102 0?0000200-0?1020?00-
000001000 10000?00?011000?010???0100100 0?1001--0--1-00---------
000100010000?11110000---1?00-110-010-00?1?110?01???1100??1?0-???0001---
000?1???1????????0??1???????-
Gogosardina_coatesi 1100001000000100101111000-010100?1-0010?-
1?????00-??000?0?0??0100?111100000011000011 01?020?00-0-
1010?00000?00101000000000?0?0????????????000?????????1001??0?????????????100?

?0000?????????????????????0110100110100??10-1?10?????-
000001????1??1101002101 2????10??000??00
Guiyu_oneiros 1?01-0000001000000000110-00000000001000-
0010-110-1000000100100--0111100000?00011010 0?0?0000-0-
1????0????000001000000000100010???1???????0?00?????????????0???-????-
???10000000??????????????????1?1101111001????????0-
????????100??0???????????1100111 01?????????????-
Hiodon_alosoides 1100010010011100110000001012010011-1----
100110000-2000000000-00---1001011000110000120 0?021--
12001001?0101110000000210001-0-000??000011?2010-01100-00--0----11-
010010111?11210110010????????????1110-00--010--0010111110110111001010-
000101001110111011000011111101001110000
Howqualepis_rostridens 1101-0100000110010111 1000-12010001-00100-
10111?00-1100010000-01001111?0000000100111 10??110?00-0-
1010000000000001000000000 10?0????????????1000???10????0--1-?0???-
????????10110000000?????????????????????0110100110?0????0-
????????10000000??100011101101111 1???0100?000???0
Hulettia_americana 1100010000111110100000001 0?2010001-1----
00011100102-03100200000--
0100001100 0?100?0120???10??1200?02100100?1?000100210101-0-
???????0?????020?11??-01??0--1-1000?000000?0?111101110 0?????????????????1??-
0110?00110111100101 0???1?00-0?0101????????10100101121111010100000000
Ichthyokentema_purbeckensis 1101-1001001110011010000100 2010001-1----
000110001021011012000 10--0100001101001000012 0??0204-
12101021000 01?11000100210101-1100010??0010?20?0011100-00--0--
1?11101?000111111210011 00?????????????????100-011010?110??101?10????????0-
0001011???101?10100101 1?1??1110?11??000
Kalops_monophyrum 1100010000?11100101110001-12110001-1----
00010-
0010200300020000101011100000 0?01000110???20?0??0?????????????000010000010110
??????????????????1?????????????0?---------
?????1????????????????????????????0110100110?0?????????????100?00?1????0??010
10021112???0100???????0
Kansasiella_eatoni_ 11?????????????????????00002010 0?1-1----
0??????0????????0????????????????????????????????????0???1????????0??????000
??????0??10110011 12?2001010100110111111 00-
?00000?000101010000001001111110?11110?????????????0???11?????????????0????????
??????????????????????????????0

Kentuckia_deani 110?0010000001001011100{0 1}002010001-?-
-?-?10111000-??000?000?-?10??111?00?000?1000011???02?????0-
?010?00000??10000000000011?00?100100?11102001010110100110100---------
000101?0000?0010011?100?111101????????0???011????0-
??????????????????????????0??????????????????????0
Lawrenciella_schaefferi ??????????????????????0??????????-
???????????0???0????
???????????0??10110010020020010101001111101100---------
000101?1000000100l1?11001111O?????????????0????????????????????????????????
??????????????????????
Lepisosteus_osseus 11000100-120101001010000100201011l-1----
00211100112-
0310011111011001000001000110000110011103012001001001100010101002100l1-0-
????0??????22020011101-00--0--1-11-0110110-
00112011000100011101111101110111001101001101111011210101l000-
0101110010001110100000101111111101001100
Leptolepis_bronni 11000100101111100100??0001012110011-1----
00010-000-2-01110100000--
?10001110200100001200??2???121??02100l0?11?010000210101-
11???10??0010?2??0011??0-00--
2111?10??00000111??12101?1111?????????????11?????????0100111111l?101???110-
0?0111???1?0111010000012110111001110000
Ligulalepis 11?????????????1?1???00??00000?01?00000-
0?????0???????00????????0?????????????????????????????????????-
??????????????????00?0010??0?000?0?01?01???????00---------0000--------
1101?????????????????????????0??
??????????-
Luederia_kempi
??0?????0??0??????
??????1?????????????????????????0??????????????0??10?100???2020010101001O?211?
100---?-----
0??111???000??1?????????????????????????????0????????????????????????????
????????????????????
Luganoia_lepidosteoides 11001100001011-01000??0011--11-000?1----
1-1111-00-0-
0200120?0?10101001O?000010000120l?02?????0??0?1?01???110100002000l?????????
??????????????????????????????????0????????1??0????????????????????????011010?
1?01101????????????0-0?21??001?10111010000012l??1111???????0

Macrepistius_arenatus 110??10001??10????0?0?0010120????1-00000-
10111?0112-03?01200l?0--
?100?01?0????0000120???1???1?0???????????0?0001002101O???????10??00101120?0011
?00-
00???????10100100001111121?121001?????????????????10??01???0?11???????????-
????0-0??1?????????????????????????1110???????0
Macrosemimimus_lennieri 110001000???1110110?00001012O?0???-1----
00010-?0112-?1001211?0--
0100?01100???0000120???10????0010?10000????0001002101O????????0??00???202001?
??0-00??0--1?11-0101110-
11?12110?0?10?????????????10????011??0011???????10????????0-
0?01?1????1???10100000l2?????????????0
Macrosemius_rostratus 11000100012110?01?00?0001012100?11-1----
00011010112--0-00001-?0--0101001100O?10000120??0104012O?1001?00000010001002-
1101-0-???????0????2??0011??0-00???????11-010011?-
1?01211??00?????????????????1?????011??0?1101111?1??1????1?00-
01?101000??011?0100?10121111111O?00?000
Meemannia_eos 11??????????0???????????0{0 1}002000??1-1-
---01?0????????????00????????0????????????000011???0?0?00-0-
1?????????????????????????????0???0??????1???000???1?0?????0?---------
000??????????????????00---0?0101111?????????????????0-
??0
Melanecta_anneae 1101-01000?0110010111000100l?10001-1----
0??????00-1?0?0?0000-
0?0?1111?00000??100001?0?????????0?????????????0100000000??????0?????????????
??????????????????????????????1?????????????????????????????00???0?11???????
??????????0-0?00??????1??110110111112???1100????????0
Mesopoma_planti 110?001?00??1100101110?01012010??1-1----
001?1??00-?0?1?{0 1}0000-
?1?10111??0000??100001?0?????????0?????????????0100000000l0????0??0??????1???
??????????????????0?????????????????????????0111100012?1?0????01101001l???011?
???????????0?00?????????1101001111l???000????????0
Miguashaia_bureaui 110001-0000010-10100000110000100000001000-
?010-001?1?0000110-010--00?-------000100012O?0020?113-
100???????0?00000010000-000-
??1?0?0????0?????????????????10??0
1---0010???????10????????0-0010?1????0??0101?000001???0001????0?1-

Mimipiscis_bartrami 1100001000000100101110000-01010011-00001-
10111000-1000010000-0100111110000001100001101002O?00-0-
?0100000000001010000000001000?10?00?00?00100000010O1??2001000---------
00010010000-0?11???????????1?????01101001102?00110-
1110100010000002?1?0101110100211120?0?1000000?010
Mimipiscis_toombsi 1100001000001100101111000-02010011-00001-
10111000-1000010000-0100111110000001100001101002010O-0-
1010000000000101000000000100O?10?000000001000000100100200l{0 1}00---------
00010010000-011100100---1001010100110100110100011O-
1110100010000000111010l?10100211110?011000000?010
Moythomasia_durgaringa 1101-01000?01100101110000-12010011-00010-
110??100-1110011000-0100111110000000100001101001010O-0-
1010000000000101000000100100O?10?000110101000000100100100100O---------
000101100000O??1???????????1?1?100110110110100011O-
1110100010000000111?1?11101002111102?11?00100?010
Moythomasia_lineata 1100001100011100101110000-02010??1-00000-
1101?100-1000110000-010?1111?000001010000110???1???0-
0?1???????????0001000?0010010???
??????????????????????????1010011010?11?????????????????100?00??11??10101O?0021
012???11?0???????0
Moythomasia_nitida 1100011000011100101110000-02010001-00000-
11111100-1102010000-
01001111?000001010000110???1?????0?????????????1100000000101l0??????????????
??1?10011011?11???????
??????????100?00?????01??11010021111???1100??????00
Obaichthys_decoratus 110?01000?2010?0??0???0010020?0??1-1----
001110?0??2--3-0?1111?0--
?100001100???00???2010110??120010?100?1?001000100210101-0-
???????0???????001???0-00??0--1-1?-?11?110-
???120110??1?????????????????????01101001101?110?12??1??1??0-
010011?0?000111010000011?????1?01?0?100
Onychodus_jandemarrai 1100000000000000001001110000l0?0011---
000010-010-110000-1001110101111000000000001010O0?00100-?-100-000?00--
0100010000-000-
??100?010???0??000??01?11?????1??0???????????1000000000???????????11???00--
01---001000001010-10??00??101010010---0?0??01?0000020??00110????01-
Osorioichthys_marginis 1100001000?0110010110100100111O?01-00000-
?1010000-1001010000-

```
010?1111?00?00101000011O???1?????????????????????0100000000100102?0??0???0??0???
??????????????????????????????????????????11?????????????????0110100111???????
???????????0-0?00?0?11000111O??02?????????????????0
      Osteolepis_macrolepidotus     110011-000-000000?-001110-00010100100000-
0010-010-1000001000-?0--0100000000000000001?00???0200-0-
?0???0????000100010000100101???0?01???????????0?1????????????00---------
000????????0?????????????????????????010101?101??????0-???????00-
1?10??????0??0101010000 2???0001????0?1-
      Ozarcus_mapesae               0?-?-??-----??-??--?????????-??????????-
-???????-???-???----?????-???-----????-?0??-????????---?0?0-00??---??-?------
?-??-??0000001???0001??0?00-01??---0-00---------0000--------
1?????????????????????????????????00000000-10100000??-?-?---
????????????????????????????????--
      Peltopleurus_lissocephalus    110?00110001110010110000101201000 1-1----
00010-000-
100200020010 10?0100010000?100001201???0????0??0??????????0100001000 01???????
??????????????????????????????????0????????????????????????????????????01???
0?11???????????????-????0-0021?1????1??1101000011 2???1000???????0
      Platysomus_superbus           111--10?----010010111-001012010001-1----
001111000-1000000000-00--
01110?0000001 0?0012????2?????0?????????????0100001000001?????????????????0?1?
??????????????????????????12100?001?????????????????????011010?11???????????
??????0-0?00??????0??0?0100000 12???110????????0
      Polypterus_bichir             1100011000001000000010001002011101-------
-2111000-10030000---0101011010000000100001201002030100-
100110100010000 1000000-000-00001??00-000011--0001-
00????????10????0?000000012101000 1?10101011000?????10100110100 1000100010-
101110010-0000010000001010100000120111011010010 00
      Porolepis_sp.                 1100100000-00000??-?0111110001110010---0-
0010-010-1000000000-10--0100000000000?000102001??0200-0-?000?00-
?000010001000000010101 00??10???0100000 0?10????0--1-00---------
000100001000?111?000?---?????110-01110101011000010-?00???100-
1010??0???0???0010?00001???100????????-
      Propterus_elongatus           11000100???1101?1100?00?1002110101-1----
00????1?112--0-002010?0--0101001100 0?1000012 0?????????0??0?1?0?0??0?0001002-
1001-0-
??????????????0?1?????????????????????0????????1?????????????????????????0
11????11???11???01????????0-00?0110??0?011?0100???02?111110?1??1000
```

Psarolepis_romeri 1101-1-000?0??-0???001?10-
120100??????????0??0-??0-????????00?0?--??111000000000011010010000000-
??1????0???0000?0??00?00?????00100??11???0?10000????01???????00---------
000100000000?????????????????1111011111?????????????????????0?0??0?????1??1
??????????????????????-
Pteronisculus_stensioi 1100001000011107101110?01012010001-1----
011110001020021000000-010?0?111000001010000110?0010200-0-
102000000000110000000000011000?10?100110202001010110101201100---------
000101010000011111111100111107???01101001101101110-
111010001000000117101??0101001111200001000000?010
Raynerius_splendens 11?????????????????1????00-01?10001-000??-
?111?00????1001?????1101111?0000?001000011010010?00-0-
101000000??7000000010000117??0100000???101000000100100100100---------
000100?000000???0010????100101???011011???010001?0-
111010001000?000?????????????????????????????????0
Saurichthys_madagascarensis 111--000----11-010100-00?-02100??1-1----
0?0011?00-?0?1?00100001 0?011100000007100001201?01?????0?10000000??000-1--
00000-1-0-00010?000???2021-0?100-00???????0----------
??0121?00???00110111?????????????010-00011?????????????????0-
0020011?100011101002111101111117??0??10
Scanilepis_dubia 110??010????11??1?0???00100001???1-1----
01111??0??1?0310-
20?0?10?0111?00?00???00???20??????????0????????????1100?00000000?????????????
??1010011010110???
??????????????0-0?????????????0100???12????0??????????
Semionotus_elegans 1100010001211-1-110100001012000?11-1----
00011100112-01000211?0--
0100000101001000012010?10?0120010?1?0?00001000100210101-0-
??????????????????1?????????????1??01?111?-
??1111100001?????????????????101001????011011?10110111011000-
010111000??0111010020112111111101001000
Styloichthys_changae 1???-????0????-??0??????0-
0?0100?0????????0?????????????????????????010000000??0010???200???0??0-
010????0???0?0?????0000??????1?100??11???0100000??0-1???0--1-00---------
000100000000?????????????????1111?????????1??????1???????????00????1?????0??0
??????????????????????-
Styracopterus_fulcratus 111--101----11001010?-0010120????1-1----
010111?00-1000?00000-?101?111?000000?10100121 1??20??0-

0??1??????????0200100000101102???1?
???????0?????????????????????0110100110?1?????????????0-
0?00?0????0??2101002111?2??0100???????0

Tanaocrossus_kalliokoskii
??????????????????????????????????1??????1?????????????????????11??????0??
??????????????????????????????100????00?????????????????????????????????
??1??0110?????????????????????
????????????10?????????1?11????????

Tegeolepis_clarki 11000000?0?01100101???00100102?0001-00000-
1101??011?000010000-
0????111?00?000?10011110??11?????0?????????????1??0000?000110?0????????????
??????????????????????????????1?100?00?????????????????????00101???0?00????
????????????0??????????0??110??001011????1????????01

Tetragonolepis_semicincta 11000100001011001001000010020?0011-1----
000110001021030011000000--0100001100?10000120???104-
??0010?100101?1?000100210101-11?0?10??00?????20011??0-
00????????0?????????????1?1??211?0?????????????????????011??0011011?101111?????
??0-000101?11010111010020112111111?1000000

Venusichthys_comptus 11000100000111001011000010121?0??1-1----
00011?00102-03000000000--
0101000000001000012?????????0??0?????????000001110001-
1???
?011?10011?????????????????0-0?01?1????1??11010000012???1100???????0

Watsonulus_eugnathoides 1100000011111-1-100000001012000011-1----
000101001121000101001 00--
0101001111001000012??0102012011021?01010?1011100110110-
110001??000111202011??1101--0--1-
10100100000111121010000?????????????10????01???0?1?011101?10101???0?100020?
11???1??21010000012?-?1110??00?000

Wendyichthys_dicksoni 111---------11001011?-001012010001-00110-
1111100111102111000-110?0111?000000010000120??0????0-
0???2????????0000000000010110?0??????0???2????0???1??1?????????????????????10
1?????????????????????????01???1011?????????????????{0 1}-
0?00?1????1??0101001011 2???1100???????0

Woodichthys_bearsdeni 1100001000?011001011100010120100 01-00100-
1111?000-1000100000-010?1111?000000010000110???1???0-
0??000?0000???0100000000010??0?????0?????0?0?10??1001??1101100---------

```
00010100?0000?????????????????????0110110110?????????????????0-
0?00???1101??11010011112???1100????????0
      Austelliscus_ferox
11?????????????????????????????????????????????????????????????????????????????10
1001111???1?????????????????????????????????????????????????????????????????????
???????????????????????????????????????????????????????????????????????????????
??????????????????????????????????1

;

END;
```

B.5 Code for Bayesian analysis

```
begin mrbayes;

lset rates=gamma coding=variable;

outgroup Dicksonosteus_arcticus;

constraint root = Acanthodes_bronni Acipenser_brevirostrum
Aesopichthys_erinaceus Amia_calva Amphicentrum_granulosum_
Atractosteus_spatula Australosomus_kochi Beagiascus_pulcherrimus
Beishanichthys_brevicaudalis Birgeria_groenlandica Bobosatrania_groenlandica
Boreosomus_piveteaui Caturus_furcatus Cheirolepis_canadensis
Cheirolepis_schultzei Cheirolepis_trailli Chondrosteus_acipenseroides
Cladodoides_wildungensis Coccocephalichthys_wildi Cosmoptychius_striatus
Cyranorhis_bergeraci Dapedium_LIAS Dapedium_pholidotum
Dialipina_salguerioensis Diplocercides_kayseri Dipteronotus_ornatus
Discoserra_pectinodon Donnrosenia_schaefferi Dorsetichthys_bechei_
Ebenaqua_ritchei Elops_hawaiensis Entelognathus_primordialis
Erpetoichthys_calabaricus Eusthenopteron_foordi Evenkia_eunoptera
Fouldenia_ischiptera Fukangichthys_longidorsalis Glyptolepis_groenlandica
Gogonasus_andrewsae Gogosardina_coatesi Guiyu_oneiros Hiodon_alosoides
Howqualepis_rostridens Hulettia_americana Ichthyokentema_purbeckensis
Kalops_monophyrum Kansasiella_eatoni_ Kentuckia_deani Lawrenciella_schaefferi
Lepisosteus_osseus Leptolepis_bronni Ligulalepis Luederia_kempi
```

Luganoia_lepidosteoides Macrepistius_arenatus Macrosemimimus_lennieri
Macrosemius_rostratus Meemannia_eos Melanecta_anneae Mesopoma_planti
Miguashaia_bureaui Mimipiscis_bartrami Mimipiscis_toombsi
Moythomasia_durgaringa Moythomasia_lineata Moythomasia_nitida
Obaichthys_decoratus Onychodus_jandemarrai Osorioichthys_marginis
Osteolepis_macrolepidotus Ozarcus_mapesae Peltopleurus_lissocephalus
Platysomus_superbus Polypterus_bichir Porolepis_sp. Propterus_elongatus
Psarolepis_romeri Pteronisculus_stensioi Raynerius_splendens
Saurichthys_madagascarensis Scanilepis_dubia Semionotus_elegans
Styloichthys_changae Styracopterus_fulcratus Tanaocrossus_kalliokoskii
Tegeolepis_clarki Tetragonolepis_semicincta Venusichthys_comptus
Watsonulus_eugnathoides Wendyichthys_dicksoni Woodichthys_bearsdeni
Austelliscus_ferox;

constraint A= Acanthodes_bronni Ozarcus_mapesae Cladodoides_wildungensis;

constraint B= Acanthodes_bronni Acipenser_brevirostrum Aesopichthys_erinaceus
Amia_calva Amphicentrum_granulosum_ Atractosteus_spatula Australosomus_kochi
Beagiascus_pulcherrimus Beishanichthys_brevicaudalis Birgeria_groenlandica
Bobosatrania_groenlandica Boreosomus_piveteaui Caturus_furcatus
Cheirolepis_canadensis Cheirolepis_schultzei Cheirolepis_trailli
Chondrosteus_acipenseroides Cladodoides_wildungensis Coccocephalichthys_wildi
Cosmoptychius_striatus Cyranorhis_bergeraci Dapedium_LIAS Dapedium_pholidotum
Dialipina_salguerioensis Diplocercides_kayseri Dipteronotus_ornatus
Discoserra_pectinodon Donnrosenia_schaefferi Dorsetichthys_bechei_
Ebenaqua_ritchei Elops_hawaiensis Erpetoichthys_calabaricus
Eusthenopteron_foordi Evenkia_eunoptera Fouldenia_ischiptera
Fukangichthys_longidorsalis Glyptolepis_groenlandica Gogonasus_andrewsae
Gogosardina_coatesi Guiyu_oneiros Hiodon_alosoides Howqualepis_rostridens
Hulettia_americana Ichthyokentema_purbeckensis Kalops_monophyrum
Kansasiella_eatoni_ Kentuckia_deani Lawrenciella_schaefferi
Lepisosteus_osseus Leptolepis_bronni Ligulalepis Luederia_kempi
Luganoia_lepidosteoides Macrepistius_arenatus Macrosemimimus_lennieri
Macrosemius_rostratus Meemannia_eos Melanecta_anneae Mesopoma_planti
Miguashaia_bureaui Mimipiscis_bartrami Mimipiscis_toombsi
Moythomasia_durgaringa Moythomasia_lineata Moythomasia_nitida
Obaichthys_decoratus Onychodus_jandemarrai Osorioichthys_marginis
Osteolepis_macrolepidotus Ozarcus_mapesae Peltopleurus_lissocephalus

```
Platysomus_superbus Polypterus_bichir Porolepis_sp. Propterus_elongatus
Psarolepis_romeri Pteronisculus_stensioi Raynerius_splendens
Saurichthys_madagascarensis Scanilepis_dubia Semionotus_elegans
Styloichthys_changae Styracopterus_fulcratus Tanaocrossus_kalliokoskii
Tegeolepis_clarki Tetragonolepis_semicincta Venusichthys_comptus
Watsonulus_eugnathoides Wendyichthys_dicksoni Woodichthys_bearsdeni
Austelliscus_ferox;

constraint C= Acipenser_brevirostrum Aesopichthys_erinaceus Amia_calva
Amphicentrum_granulosum_ Atractosteus_spatula Australosomus_kochi
Beagiascus_pulcherrimus Beishanichthys_brevicaudalis Birgeria_groenlandica
Bobosatrania_groenlandica Boreosomus_piveteaui Caturus_furcatus
Cheirolepis_canadensis Cheirolepis_schultzei Cheirolepis_trailli
Chondrosteus_acipenseroides Coccocephalichthys_wildi Cosmoptychius_striatus
Cyranorhis_bergeraci Dapedium_LIAS Dapedium_pholidotum
Dialipina_salguerioensis Diplocercides_kayseri Dipteronotus_ornatus
Discoserra_pectinodon Donnrosenia_schaefferi Dorsetichthys_bechei_
Ebenaqua_ritchei Elops_hawaiensis Erpetoichthys_calabaricus
Eusthenopteron_foordi Evenkia_eunoptera Fouldenia_ischiptera
Fukangichthys_longidorsalis Glyptolepis_groenlandica Gogonasus_andrewsae
Gogosardina_coatesi Guiyu_oneiros Hiodon_alosoides Howqualepis_rostridens
Hulettia_americana Ichthyokentema_purbeckensis Kalops_monophyrum
Kansasiella_eatoni_ Kentuckia_deani Lawrenciella_schaefferi
Lepisosteus_osseus Leptolepis_bronni Ligulalepis Luederia_kempi
Luganoia_lepidosteoides Macrepistius_arenatus Macrosemimimus_lennieri
Macrosemius_rostratus Meemannia_eos Melanecta_anneae Mesopoma_planti
Miguashaia_bureaui Mimipiscis_bartrami Mimipiscis_toombsi
Moythomasia_durgaringa Moythomasia_lineata Moythomasia_nitida
Obaichthys_decoratus Onychodus_jandemarrai Osorioichthys_marginis
Osteolepis_macrolepidotus Peltopleurus_lissocephalus Platysomus_superbus
Polypterus_bichir Porolepis_sp. Propterus_elongatus Psarolepis_romeri
Pteronisculus_stensioi Raynerius_splendens Saurichthys_madagascarensis
Scanilepis_dubia Semionotus_elegans Styloichthys_changae
Styracopterus_fulcratus Tanaocrossus_kalliokoskii Tegeolepis_clarki
Tetragonolepis_semicincta Venusichthys_comptus Watsonulus_eugnathoides
Wendyichthys_dicksoni Woodichthys_bearsdeni Austelliscus_ferox;

prset topologypr=constraints(root, A, B, C);
```

```
lset nst=1;

mcmcp savebrlens=yes;

mcmcp filename=devjaw_bayes4;

mcmcp nchains=4 savebrlens=yes;

mcmcp nruns=2 stoprule=YES diagnfreq=1000 diagnstat=maxstddev;

mcmcp stopval=0.01 minpartfreq=0.02;

mcmcp printfreq=500 samplefreq=500;

mcmc;

sump;

sumt burninfrac=0.1;

end;
```

Appendix C: Chapter 3 Supplement

This chapter represents a preliminary account of the anatomy of two new taxa from the late Paleozoic Lontras Shale strata of the Paraná Basin in southern Brazil. Results presented in this chapter will be later submitted as a full manuscript for publication in a selected scientific journal.

Appendix D: Chapter 4 Supplement

D.1 Phylogenetic placement of †*Coccocephalus wildi*

†*Coccocephalus wildi* has been included in a number of phylogenetic analyses investigating the relationships of early ray-finned fishes (Coates 1999; Cloutier and Arratia 2004; Giles et al. 2015b, 2017; Argyriou et al. 2018; Latimer and Giles 2018; Wilson et al. 2018; Choo et al. 2019; Figueroa et al. 2019, 2021; Stack and Gottfried 2021). It was originally placed in the actinopterygian crown[1], but all subsequent analyses resolve it on the actinopterygian stem, sometimes within a large polytomy including most other late Palaeozoic ray-finned fishes. A detailed redescription of †*Coccocephalus* based on new μCT data, in conjunction with an updated phylogenetic analysis, is currently in preparation (S.G., R.F., M.F.), although we do not anticipate this leading to a change in the phylogenetic placement of the taxon.

The cranial morphology of †*Coccocephalus wildi* is comparable to other late Palaeozoic taxa that are well-within the ray-finned fish stem. The clearest comparisons are with the Carboniferous †*Kentuckia* (Rayner 1952), †*Kansasiella* (Poplin 1974), and †*Lawrenciella* (Poplin 1974; Hamel and Poplin 2008; Pradel et al. 2016), all of which preserve information on the endocranium. In common with these taxa, †*Coccocephalus* has a completely enclosed spiracular canal, a posteroventrally-directed hyoid facet, and open vestibular fontanelles continuous with the oticoocippital fissure. As in †*Kentuckia* and †*Lawrenciella*, the aortic canal of †*Coccocephalus* is pierced by a single midline opening, and as in †*Kentuckia* the divergence of the lateral dorsal aortae is not enclosed within the aortic canal and the parasphenoid is flat rather than dorsally inflected below the orbit. †*Coccocephalus* also shares other features in common with a subset of the above taxa, as well as with some Devonian and stratigraphically younger taxa.

†*Coccocephalus* is excluded from the crown by several successive nodes on the basis of the following ambiguous character optimisations (taken from Latimer and Giles (2018)):

- Character 42: bone carrying otic portion of lateral line canal extends past posterior margin of parietals
- Character 89: two infradentaries

- Character 94: coronoid process formed by suragular
- Character 100: comineralised palatoquadrate ossifications
- Character 156: braincase comprises single ossification
- Character 171: parasphenoid terminates at/anterior to ventral otic fissure
- Character 178: aortic notch absent from parasphenoid
- Character 43: two pairs of extrascapulars
- Character 69: maxilla contributes to posterior margin of cheek
- Character 153: dorsal aorta not pierced by canal/s for exit of eff.a.1
- Character 175: parasphenoid teeth small

D.2 Potential paths for the fossilization of brain tissues

The delicate soft tissues that form the brain of vertebrates are traditionally considered to be prone to rapid decomposition. However, exceptional examples from the fossil record as well as archaeological evidence and forensic material show that these tissues can survive complete obliteration under certain conditions (Tkocz et al. 1979; Brasier et al. 2017; Ortega-Hernández et al. 2019). The processes leading to fossil preservation comprise a complex system of interacting factors (Sansom et al. 2011, 2013; Naimark et al. 2018; Parry et al. 2018; Saleh et al. 2018, 2020) related to physical parameters (e.g., temperature, salinity, oxygen concentration, water composition), the depositional environment (e.g., rate of deposition, depth, granulometry, porosity) and taxon-specific aspects of biology (e.g., composition of tissues, ecology). Thus, dealing with this hyperdimensional data is a challenge for understanding modes of preservation of soft tissue in the fossil record and studies need to focus on specific environments or taxa for minimizing the number of variables involved in the process. In the following paragraphs we explore previously described modes of preservation of neural soft-tissue and compare these to the preservation of the brain of †*Coccocephalichthys wildi*.

Adipocere formation

One of the potential mechanisms through which brain material can survive is through the formation of a hard saponified fat coat called adipocere (Ubelaker and Zarenko 2011). Brain preservation through adipocere formation has been recorded for human remains to various degrees (Tkocz et al. 1979). Mähler et al. (2022) state that the preservation of soft tissues like

muscles in invertebrates occurs as pseudomorphs—the replacement of original soft tissues with minerals—and that this process might be initiated by adipocere and biofilm formation. However, examples of adipocere linked to soft-tissue preservation are not yet known described for the vertebrate fossil record, although the three-dimensional iguanodontid brain reported by Brasier et al. (2017) might be partially explained by adipocere coating. The high concentration of lipidic tissues in the brain of many vertebrates (Chavko et al. 1993; Hong et al. 2014) may facilitate the preservation through this process. Unfortunately, there is no evidence available that can securely associate the preservation of the brain described herein with adipocere coating.

Burgess Shale-style preservation

An alternative pathway for the preservation of brain tissues is that exhibited by the Cambrian faunas from the Burgess Shale. Several arthropods from these strata show preservation of flattened bilateral elements associated with the central nervous system (Ma et al. 2015; Strausfeld et al. 2016). The validity of the interpretation of these elements as central nervous systems has been amply discussed in the literature with opposing hypotheses of these elements being formed by microbial mats (Liu et al. 2018; Ortega-Hernández et al. 2019). Following the interpretation that these do indeed represent neural elements, proposed preservation pathways tend to be associated with partial decomposition of fats further suppressed by anoxic conditions causing the preservation of carbonaceous or pyritized films (Ma et al. 2015). Although we cannot refute a similar mechanism for the preservation of the elements described herein, especially due to the similar composition of fossilized remains and matrix, it is difficult to explain how this mechanism would allow for a three-dimensional preservation as seen in †*Coccocephalichthys*.

Calcium phosphate microenvironment

Finally, the three-dimensional iniopterygian brain described by Pradel (Pradel et al. 2009b; Pradel 2010) is comparable to that of †*Coccocephalichthys* in the sense that it preserves the brain body and ventricles, some nerves exit the brain body and run toward foramina on the braincase, it is visible in tomographic data as denser material than surrounding matrix, and skeletal remains are still partially articulated indicating constraints on time before burial. This iniopterygian brain seems to have been preserved through partial decay of brain fatty acids in an anoxic condition that favored the precipitation of calcium phosphate, distinguishing the fossil

brain from the surrounding calcium carbonate infill of the braincase. Pradel (2010) also argues that—since there is no evidence of other soft tissues outside the braincase and that nerves do not continue outside the braincase—the enclosed space of the cranial cavity must have played a role in the preservation of the brain tissues by creating a microenvironment that favored the preservation of the brain. Although the mechanisms that took place for this exceptional iniopterygian brain to be preserved are not clear, it is possible that a similar process permitted the preservation of the brains described here. The tomographic data from Pradel et al. (2009b) show the dense brain recrystallized tissue being surrounded by a thin halo of similar density, especially visible in less dense regions of the brain fossil. This halo is absent in our specimens, indicating that there may be differences in the mode of preservation of our specimens to that of Pradel et al. (2009b).

Bacteria-mediated phosphatization

In placoderms from the Gogo Formation (~384-382 Ma (Trinajstic et al. 2022a)) in Australia, there is ample evidence of muscle soft-tissue preservation, which is considered to have been preserved through bacteria-mediated phosphatization (Trinajstic et al. 2007, 2013, 2022b). Trinajstic et al. (2022b) report novel occurrences of placoderm organs preserved in three dimensions that, according to the authors, seem to have been preserved in the same manner as muscle tissue mentioned above. Trinajstic et al. also argues that the presence of uncrushed skeletal elements together with three-dimensional soft-tissue preservation is an indicator of rapid formation and cementation of the nodules containing these fossils. The combination of a chemocline in the water column, photic zone euxinia and bacterial activity played a major role in the preservation of soft tissues in Gogo Formation fossils (Trinajstic et al. 2007, 2022b). However, in none of the placoderm specimens reported with soft-tissue preservation is there any indication of preservation of brain tissues (although skeletal muscle innervation is present in association to muscles in some fossils (Trinajstic et al. 2007)). This, together with the higher degree of disarticulation—in comparison to †*Coccocephalichthys*—of the skeletal elements of the fossils reported by Trinajstic et al. (2022b) indicate that although preservation of internal organs is possible in various environmental conditions, neural tissue requires more precise conditions to be preserved in fossil vertebrates.

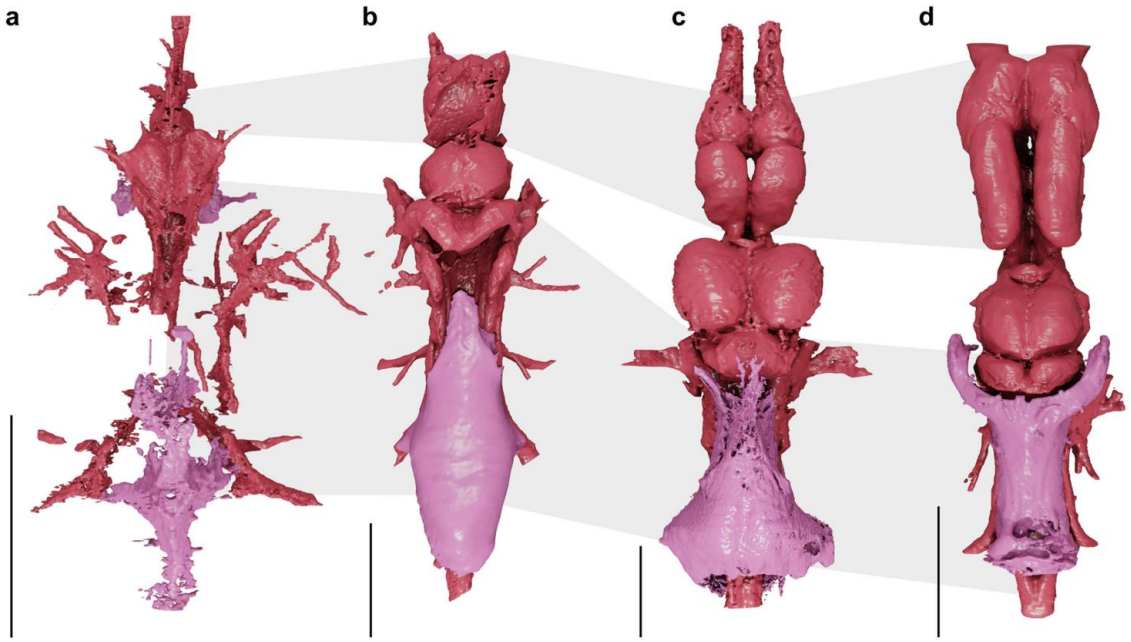

Appendix Figure D.1 – The brain (red) and myelencephalic sheet/gland (pink) of *Coccocephalus wildi* and selected extant ray-finned fishes. **a**, *Coccocephalus wildi*. **b**, *Acipenser brevirostrum*. **c**, *Amia calva*. **d**, *Polypterus senegalus*. Grey and white delimitations show margins between forebrain, midbrain and hindbrain across all taxa. Brains are shown in dorsal view and aligned at the anterior- and posteriormost points of the forebrain (olfactory bulbs, telencephalon and diencephalon) and the posteriormost point of the fourth ventricle. Scale bar = 5 mm.

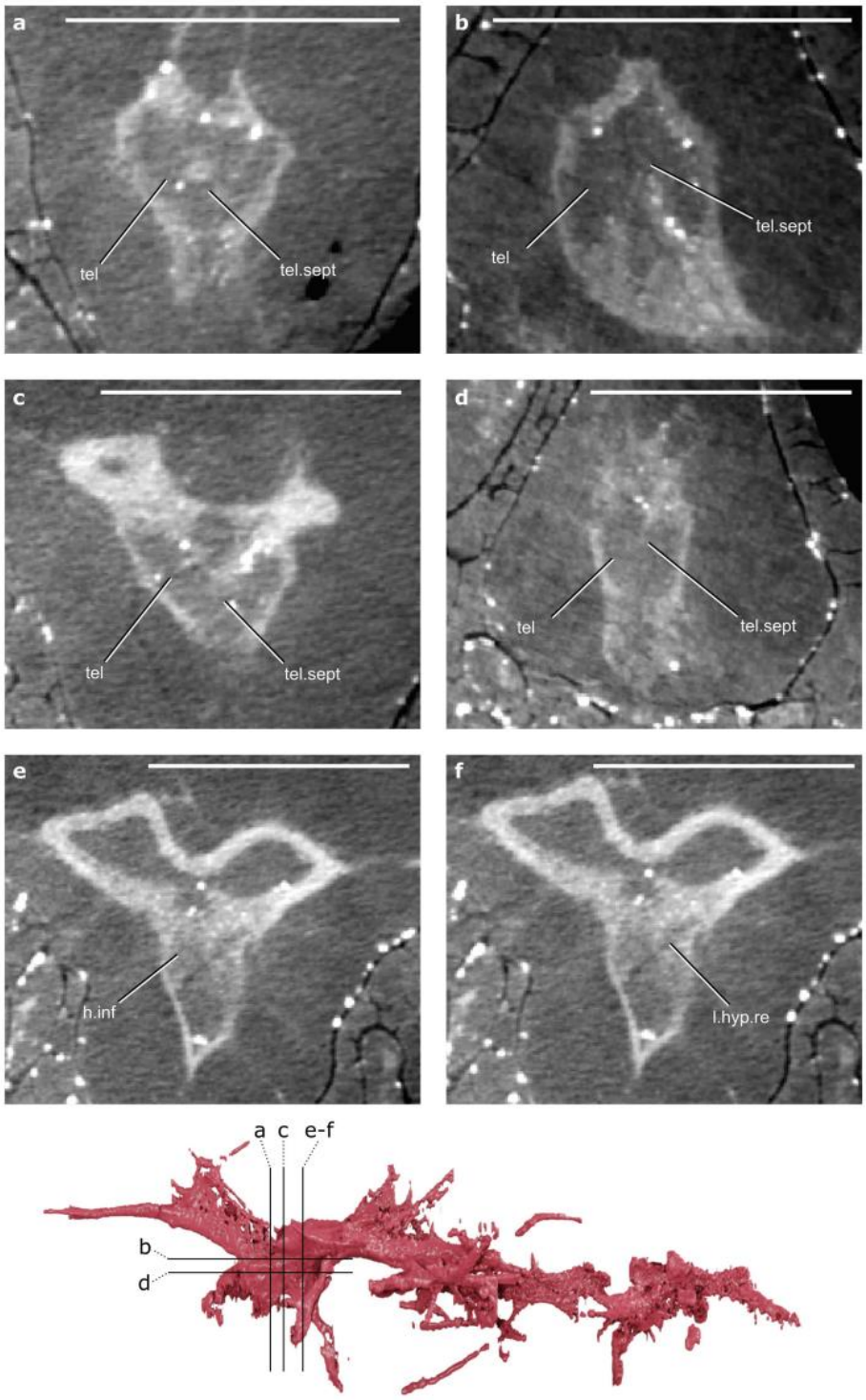

Appendix Figure D.2 – Sections through the brain of *Coccocephalus wildi*. **a**, transverse section through the anterior portion of the telencephalon. **b**, horizontal section through the ventral portion of the telencephalon. **c**, transverse section through the posterior portion of the telencephalon. **d**, horizontal section through the dorsal portion of the telencephalon. **e**, transverse section through the anterior portion of the hypothalamus inferior lobes. **f**, transverse section through the posterior portion of the hypothalamus inferior lobes. Inset shows where each of sections (a)-(e) intersect the brain. h.inf, inferior lobe of the hypothalamus; l.hyp.re, lateral hypothalamic recess; tel, telencephalon; tel.sept, telencephalic septum. Scale bar = 2 mm.

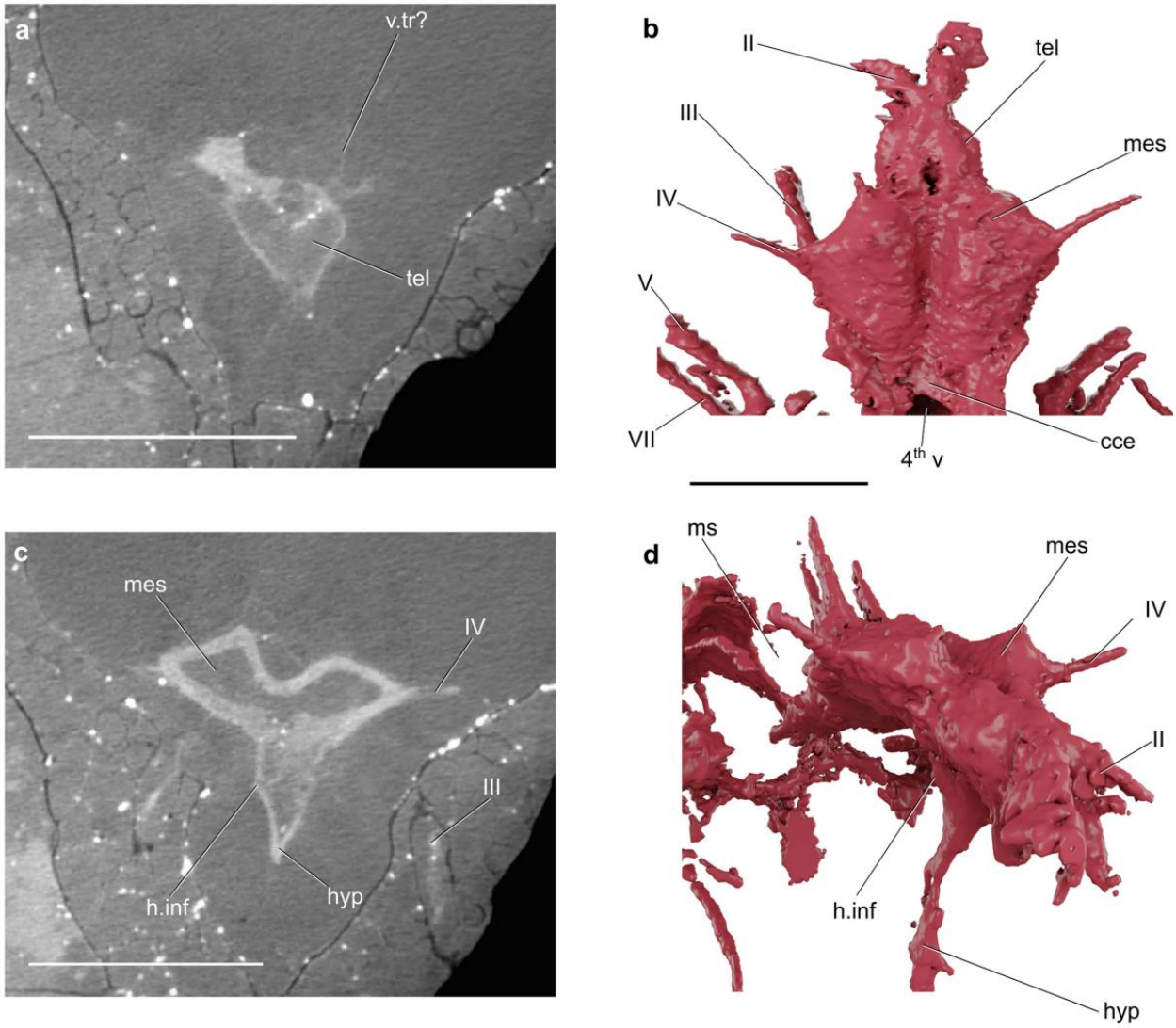

Appendix Figure D.3 – Transverse sections and renders of the brain of *Coccocephalus wildi*. **a**,**b**, the telencephalon. **c**,**d**, the mesencephalon and hypophysis. cce, corpus cerebellum; h.inf, inferior lobe of the hypothalamus; hyp, hypophysis; tel, telencephalon; mes, mesencephalon; ms, mesencephalic sheet; v. tr?, velum transversum; 4th v, fourth ventricle; II, optic nerve; III, oculomotor nerve; IV, trochlear nerve, V, trigeminal nerve; VII, facial nerve. Dorsal portion of forebrain and velum transversum digitally removed. Scale bar in a, c = 2.5 mm; scale bar in b, d = 2 mm.

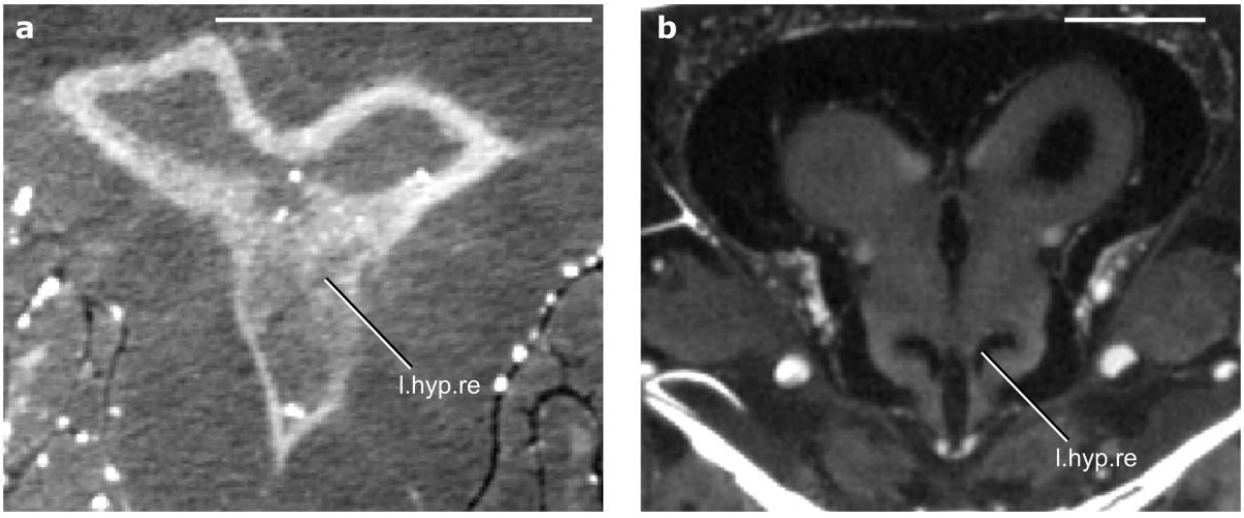

Appendix Figure D.4 – Sections through the brain of *Coccocephalus wildi* and *Amia calva*. **a**, transverse section through the diencephalon and mesencephalon of *Coccocephalus wildi*. **b**, transverse section through the diencephalon and mesencephalon of *Amia calva*. l.hyp.re, lateral hypothalamic recess. Scale bar = 2 mm.

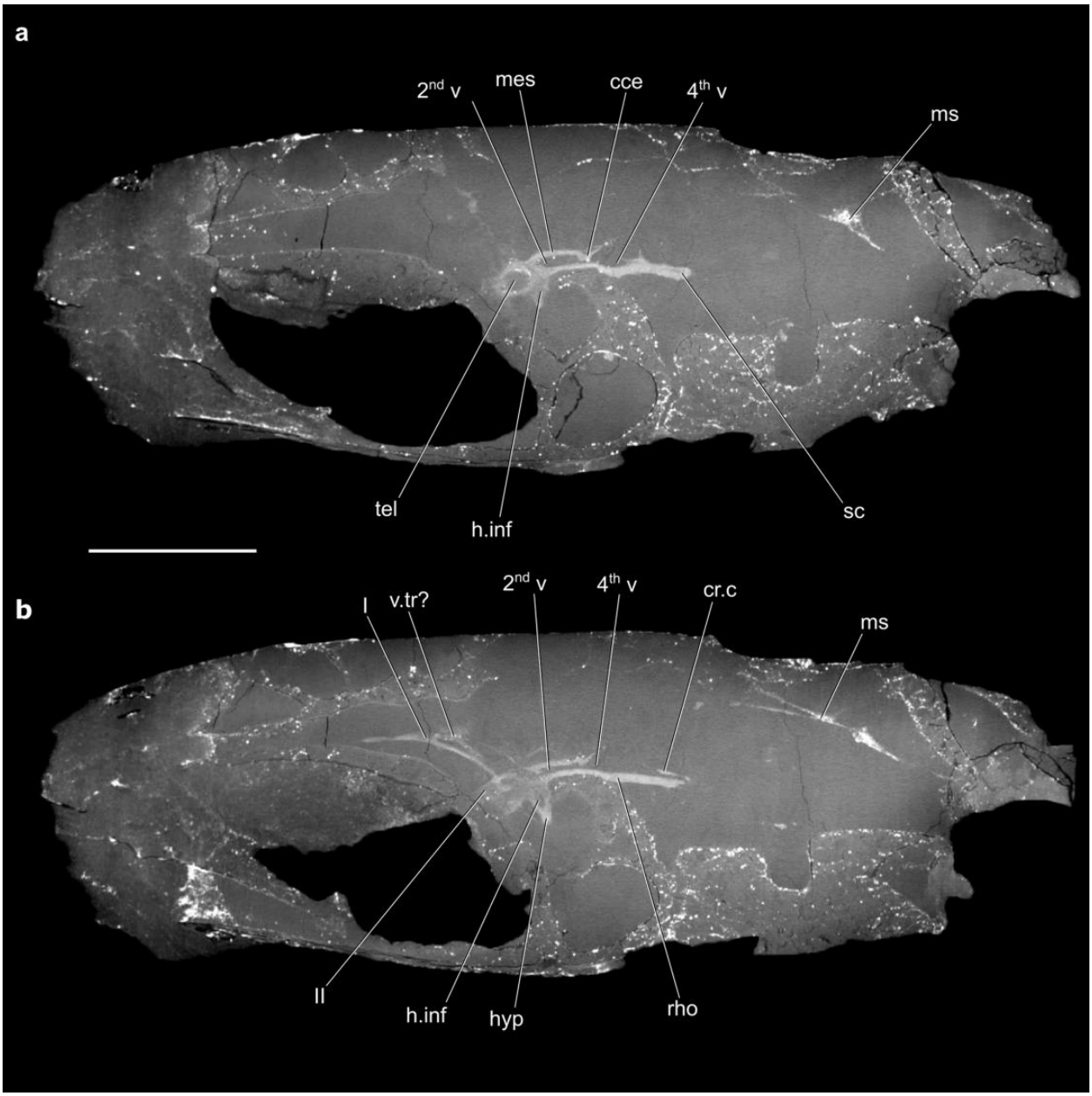

Appendix Figure D.5 – Sagittal sections through the neurocranium of *Coccocephalus wildi* showing the brain and associated structures. cce, corpus cerebelli, cr.c; crista cerebellaris, h.inf, hypothalamus inferior lobes; hyp, hypophysis; mes, mesencephalon; ms, myelencephalic sheet; rho, rhombencephalon; sc, spinal cord; tel, telencephalon; v.tr, velum transversum; 2nd v, second ventricle; 4th v, fourth ventricle; I, olfactory nerve; II, optic nerve. Scale bar = 5 mm.

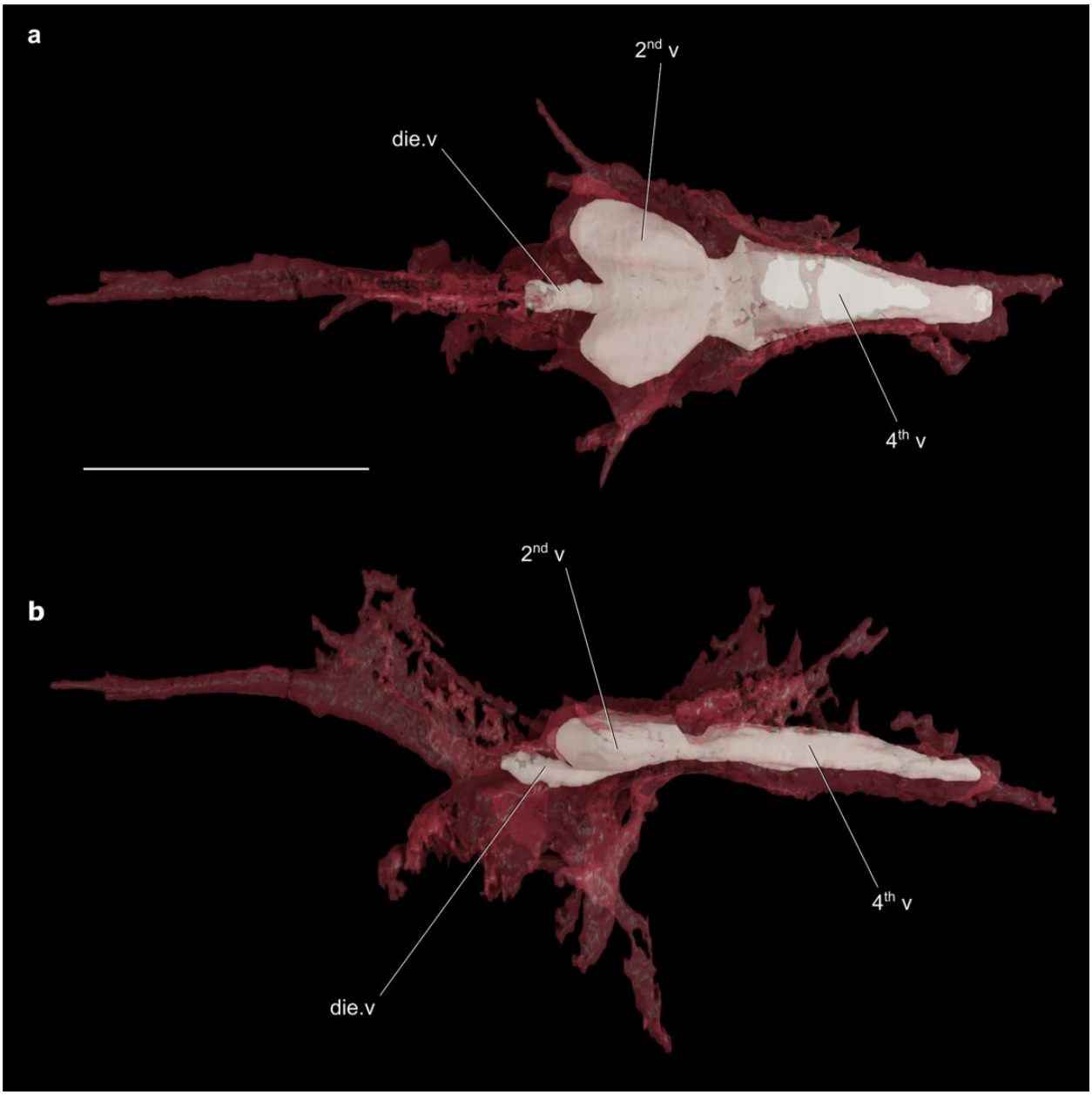

Appendix Figure D.6 – The brain of *Coccocephalus wildi* (red) rendered partially transparent to show brain ventricle configuration (white). **a**, dorsal view. **b**, left lateral view. die. v, diencephalic ventricle; 2nd v, second ventricle; 4th v, fourth ventricle. Scale bar = 5 mm.

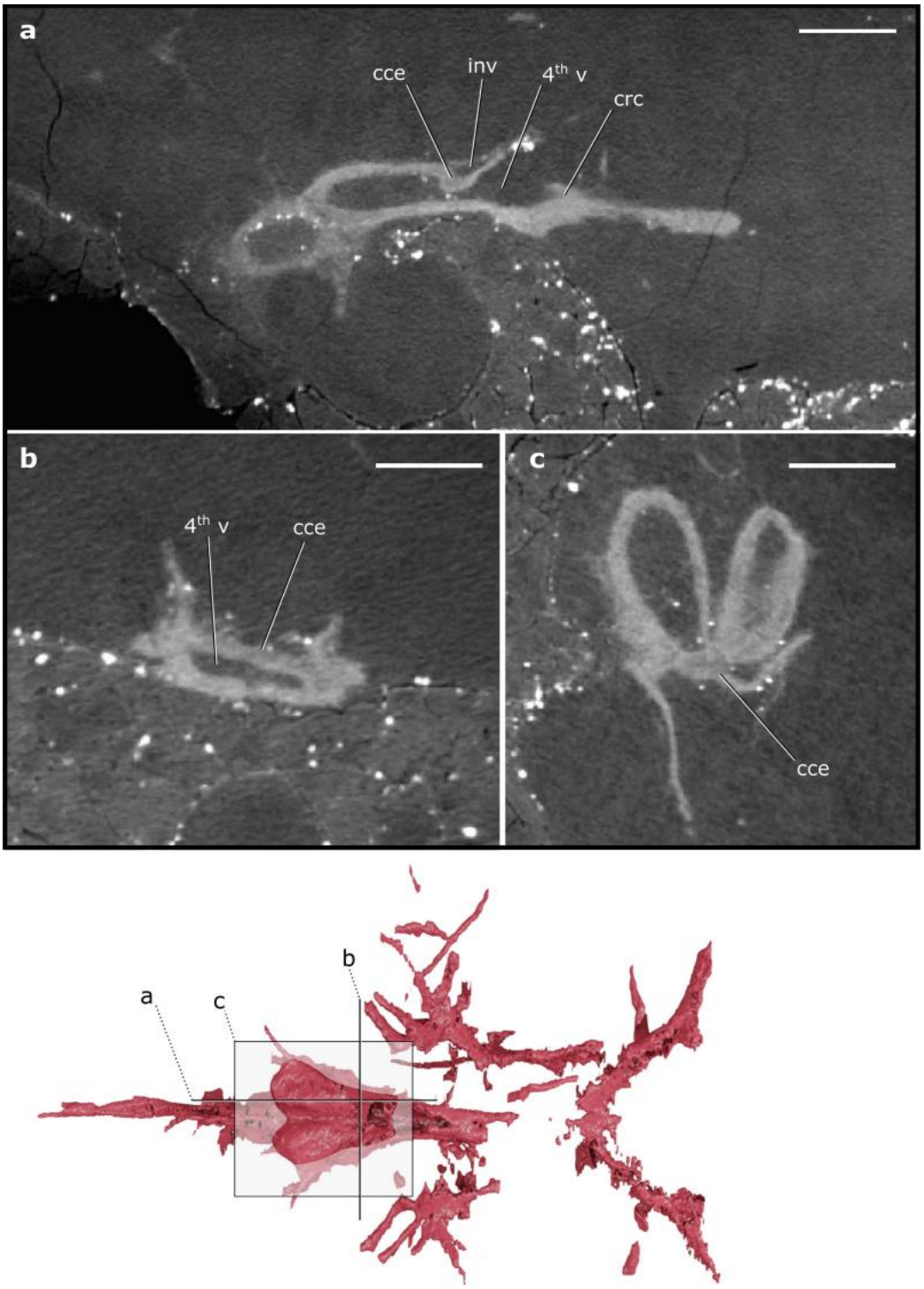

Appendix Figure D.7 – Sections through the brain of *Coccocephalus wildi* showing the rhombencephalic region. **a**, sagittal section through the brain. **b**, transverse section through the anterior portion of the rhombencephalon. **c**, horizontal section through the mesencephalic and rhombencephalic regions of the brain. cce, corpus cerebelli, crc, crista cerebellaris, inv, invagination of the cerebellum, 4th v, fourth ventricle. Scale bar = 1 mm.

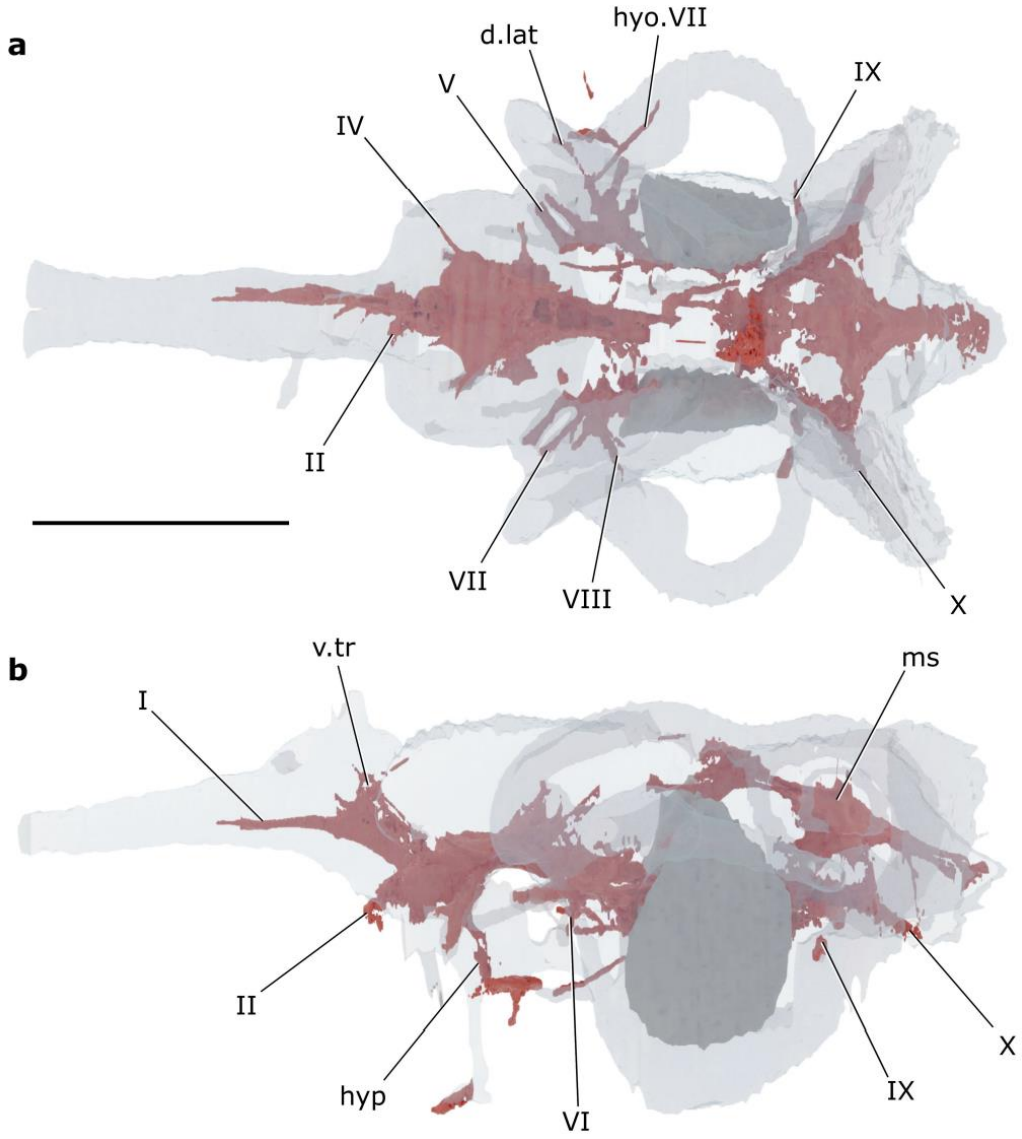

Appendix Figure D.8 – The brain of *Coccocephalus wildi* within the endocavity. **a**, dorsal view, **b**, left lateral view. d.lat, dorsal lateral line nerve, hyo.VII, hyomandibular branch of the facial nerve, hyp, hypophysis, ms, mesencephalic sheet, I, olfactory nerve, II, optic nerve, IV, trochlear nerve, V, trigeminal nerve, VI, abducens nerve, VII, facial nerve, IX, glossopharyngeal nerve, X, vagus nerve. Scale bar = 5 mm.

Appendix E: Chapter 5 Supplement

E.1 Analyzed specimens

Analyzed specimens can be divided into two morphotypes:

Morphotype I: CP 065, CP.V 4364, CP.V 7053, CP.V 7227

Morphotype II: CP 084, CP 508, CP 577, CP 584

E.2 Comparative anatomy of fossil morphotypes

The two fossil morphotypes can be differentiated on the basis of osteological features, some of which indicate that these morphotypes are likely affiliated with different parts of the actinopterygian stem. Morphotype I is distinguished by bearing two ceratohyal ossifications (anterior and posterior), a dorsomesial process on the palatoquadrate for articulation with the braincase without a notch or foramen, large and posterodorsally directed uncinate processes of the epibranchials, a fossa bridgei that is constrained above the level of the inner ear, and a common midline canal for the olfactory nerves. Morphotype II, on the other hand, shows a single ceratohyal ossification, a semilunar notch on the palatoquadrate marking the basipterygoid articulation, small and dorsally directed uncinate processes of the epibranchials, a wide and well-developed fossa bridgei that extends from the level of the posterodorsal fontanelle to the level of the anterodorsal fontanelle, and paired canals for the olfactory nerves. All the conditions found in Morphotype I are in agreement with a more crownward placement relative to both Morphotype II and *Coccocephalus wildi*, based on information from well-preserved Late Devonian and Triassic taxa (Nielsen 1949; Giles et al. 2015b, 2023). Additionally, these two morphotypes differ in several additional traits of more ambiguous polarity including parasphenoid geometry in lateral view (curved dorsally in Morphotype I versus horizontal in Morphotype II), size and shape of the anterodorsal fontanelle (large and oval in Morphotype I, smaller and slit-like in Morphotype II), and proportions of the skeletal labyrinth (external semicircular canal anteroposteriorly long with anterior and posterior limbs at an obtuse angle in Morphotype I compared to Morphotype II).

E.3 Discussion of additional brain features

Meningeal tissues. Aspects of brain suspension within the endocranial cavity are poorly documented among ray-finned fishes. Bjerring (1991) described intracranial ligaments supporting the brain of *Polypterus senegalus*, while other extant actinopterygians seem to have a well-developed meningeal tissue that suspends the brain within the neurocranial endocavity (Figueroa, pers. obs.). The Brazilian fossils show both conditions, with Morphotype I bearing a well-developed meningeal tissue above the hindbrain and forebrain while Morphotype II lacks any evidence of meningeal tissue but shows ligament-like structures connecting the brain to the endocranial wall. However, it is possible that the absence of a meningeal tissue in Morphotype II is taphonomic, as the main specimen that our description focuses on (CP 584) is preserved without matrix infill within the braincase. Thus, meningeal tissue could have been lost during either during fossilization or during dissolution and loss of the matrix infill or. The meningeal tissue preserved in Morphotype I (CP 065) differs from the brain tissue as it is a very delicate and thin sheet of tissue that attaches to the laterodorsal margins of the brain and expands dorsally following the shape of the endocranial cavity.

Meningeal tissues with associated hematopoietic organs are present in non-teleost ray-finned fishes excluding cladistians. Past work suggested that similar organs would be present in Paleozoic ray-finned fishes based on the presence of an enlarged area octavolateralis and lateral diverticula near the posterior semicircular canal (referred to as the lateral cranial canal) in some fossils (Jarvik 1980). A large mass dorsal to the rhombencephalon of Morphotype II (CP 584) is consistent with a myelencephalic gland (Fig S10). This structure is boomerang-shaped in dorsal view and extends laterally towards the lateral cranial canal. The geometry and position of this structure matches the myelencephalic gland of *Lepisosteus* (Chandler 1911). Identification of a myelencephalic gland in Morphotype II supports past inferences of its presence in early ray-finned fishes. Its lateral extension is consistent with the well-developed lateral cranial canal found in many Paleozoic ray-finned fishes and early neopterygians (Jarvik 1980; Hamel and Poplin 2008; Friedman and Giles 2016; Giles et al. 2018). This pattern suggests the myelencephalic gland of *Lepisosteus* might more closely resemble the plesiomorphic condition, with the tube-shaped gland

of chondrosteans and *Amia* being derived. A myelencephalic gland is absent in *Coccocephalus*, CP 065 and *Polypterus*, which all share a robust rhombencephalic tela choroidea modified as a cisterna spinobulbaris, following the interpretation from Jarvik (1980). We cautiously suggest the myelencephalic gland arose deep on the actinopterygian stem, with independent variations arising within the crown (Fig.7B). This agrees with the wide variability of shape and connectivity of the myelencephalic gland in extant taxa (van der Horst 1925).

Anterior cerebral vein. The anterior cerebral vein emerges at the level of the posterior end of the orbit and arches dorsomesially above the telencephalon (Bertmar 1965; Weiger et al. 1988). In ray-finned fishes, this vein tends to be well-developed during embryonic and larval stages but is sometimes absent in adults (Bertmar 1965). Allis (1897) notes that although the anterior cerebral vein is not noticeable in adult specimens of *Amia*, the paired foramina through which it would pass remain present posterodorsal on the optic capsule wall. In Paleozoic ray-finned fishes (e.g., †*Mimipiscis*, †*Mesopoma*) the canal for the anterior cerebral vein is unpaired and asymmetrical above the telencephalic region of the endocranial cavity (Gardiner 1984; Coates 1999; Hamel and Poplin 2008). In some Devonian sarcopterygians (e.g., †*Eusthenopteron*) paired canals are present, but these lay more anterior at the proximal end of the olfactory tracts (Jarvik 1980), while in others (e.g., †*Gogonasus andrewsae)* there is a single median canal (Holland 2014). Morphotype I and †*Coccocephalus* show paired but asymmetrical anterior cerebral veins that connect to the velum transversum and the orbital sinus before exiting the brain towards the left side of the skull. The asymmetry and position of these veins is consistent with the canal described in Paleozoic ray-finned fishes. However, the presence of two veins in the fossil specimens indicates that the single canal present in Paleozoic forms held two branches of this vein, which in turn agrees with the presence of paired anterior cerebral veins in living ray-finned fishes.

Appendix Table E.1 - µCT scan parameters used for fossil actinopterygians from the Lontras Shale.

	Energy (kV)	Current (uA)	Exposure (s)	Resolution (mm)	Filter	Filter (mm)	Binning	Projections	Frames/Proj.	Ring art.
CP 065	190	180	4	0.03437	Cu	3	NO	3141	4	YES
CP 584	200	180	4	0.03674	Cu	3	NO	3141	2	YES
CP 084	191	200	2	0.04509	Cu	2	NO	3141	4	YES
CP 508	200	180	4	0.03674	Cu	3	NO	3141	2	YES
CP 577	215	148	2.8	0.02638	Cu	2.5	NO	3141	4	YES
CP.V 4364	200	140	2.8	0.02966	Cu	2	NO	3141	2	YES
CP.V 7053	190	180	4	0.03432	Cu	3	NO	3141	2	YES
CP.V 7227	215	120	2.8	0.02046	Cu	2	NO	3141	4	YES
CP 1343	174	190	4	0.03691	-	-	NO	3141	2	YES
CP 6573	195	120	2.8	0.03295	Cu	2.25	NO	3141	4	YES

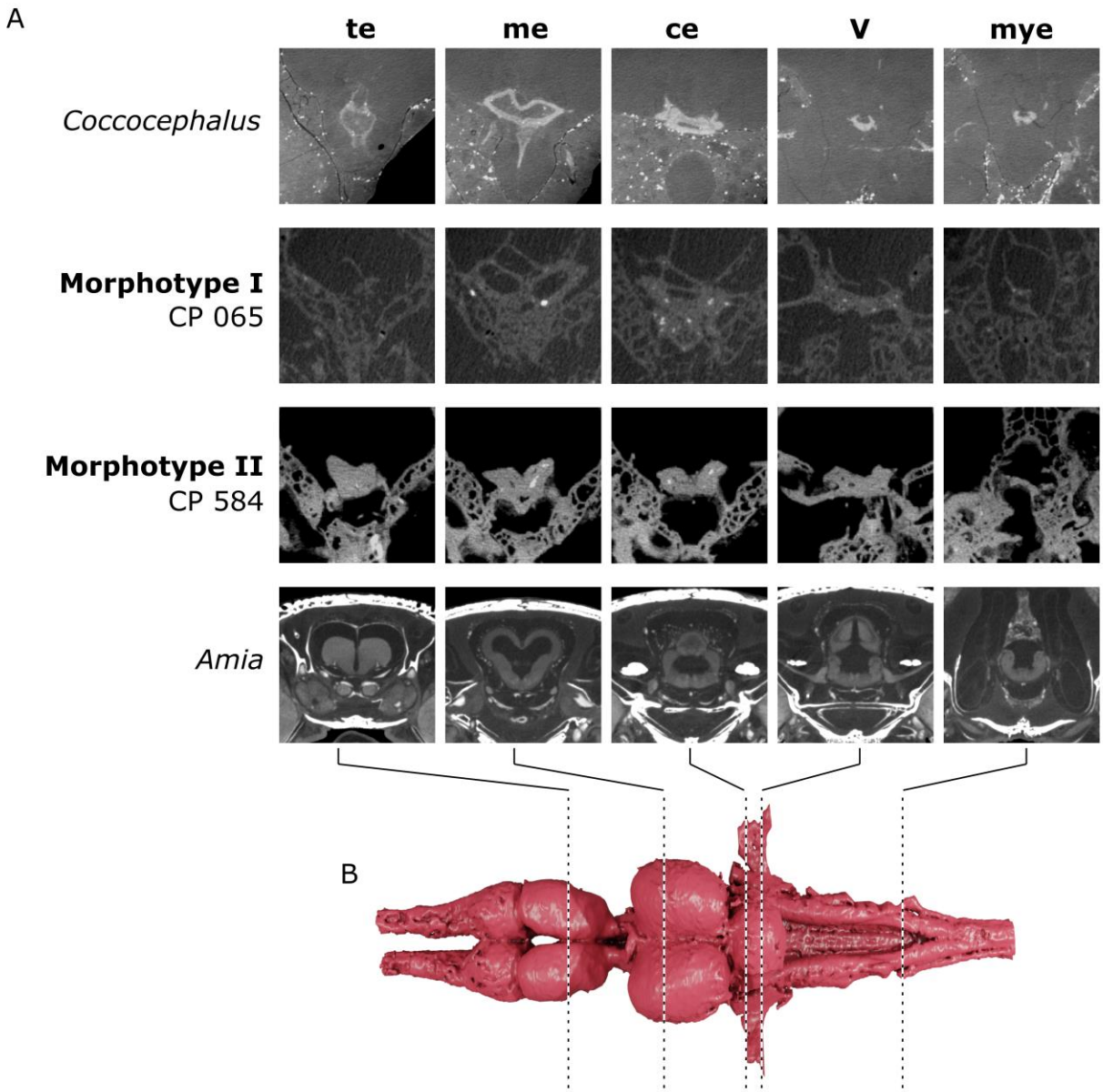

Appendix Figure E.1 - Anatomical correspondence between brains in Paleozoic actinopterygians and *Amia*. (A) axial sections from μCT, beginning with more anterior sections. (B) render of the brain of *Amia* showing approximate position of sections. Abbreviations: tel, telencephalon, mes, mesencephalon, ce, cerebellar corpus, V, trigeminal nerve, mye, myelencephalon.

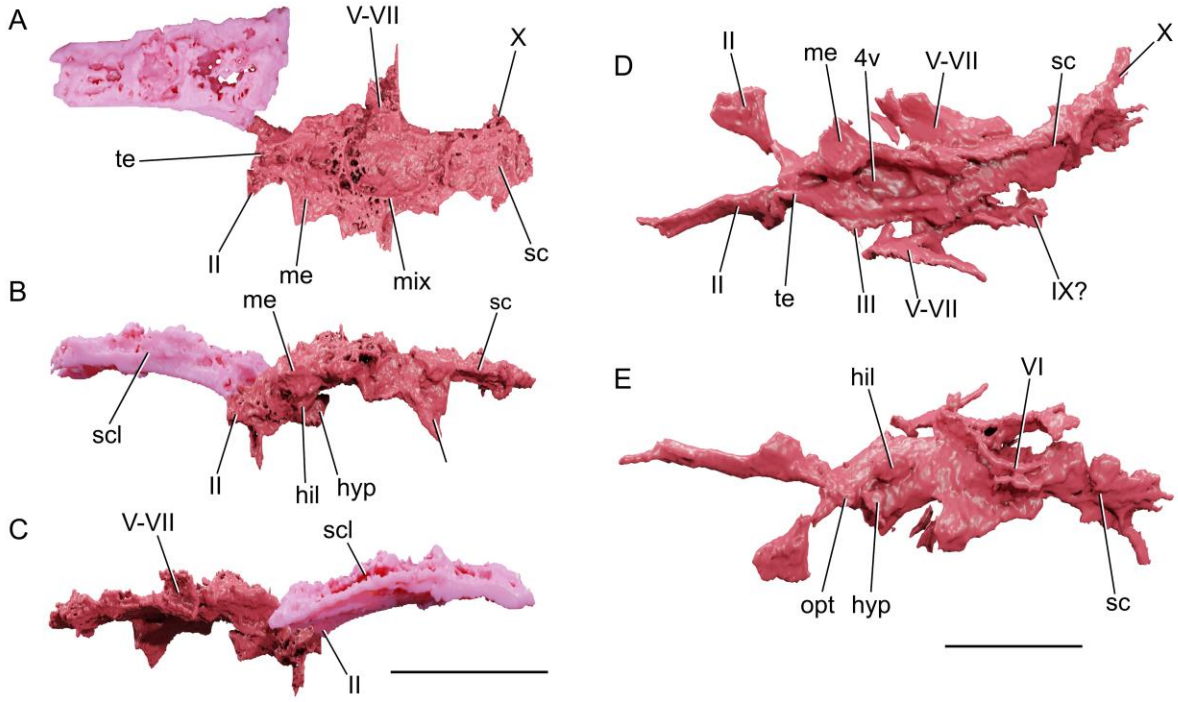

Appendix Figure E.2 – Render of selected fossil brains. (A-C) CP.V 4364 (Morphotype I) in (A) dorsal, (B) left-lateral and (C) right-lateral views; and (D-E) CP 508 (Morphotype II) in (D) dorsal and (E) ventral views. Scale bars = 5 mm.

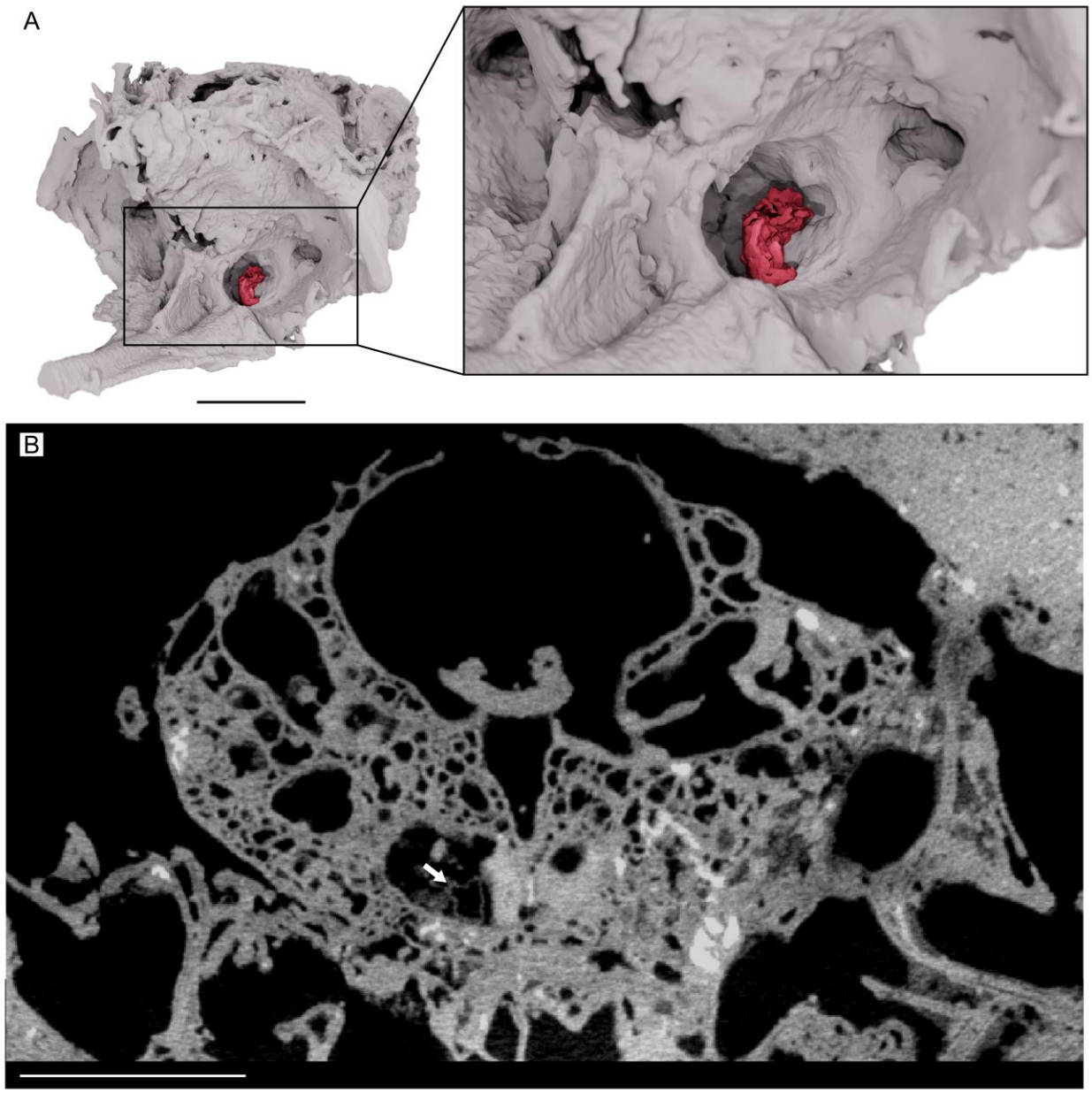

Appendix Figure E.3 – Rectus eye muscle attachment ligament within the posterior myodome of CP 584. (A) render of neurocranium (gray) and attachment ligament (red); (B) axial section from µCT showing the attachment ligament (arrow). Scale bar = 5 mm.

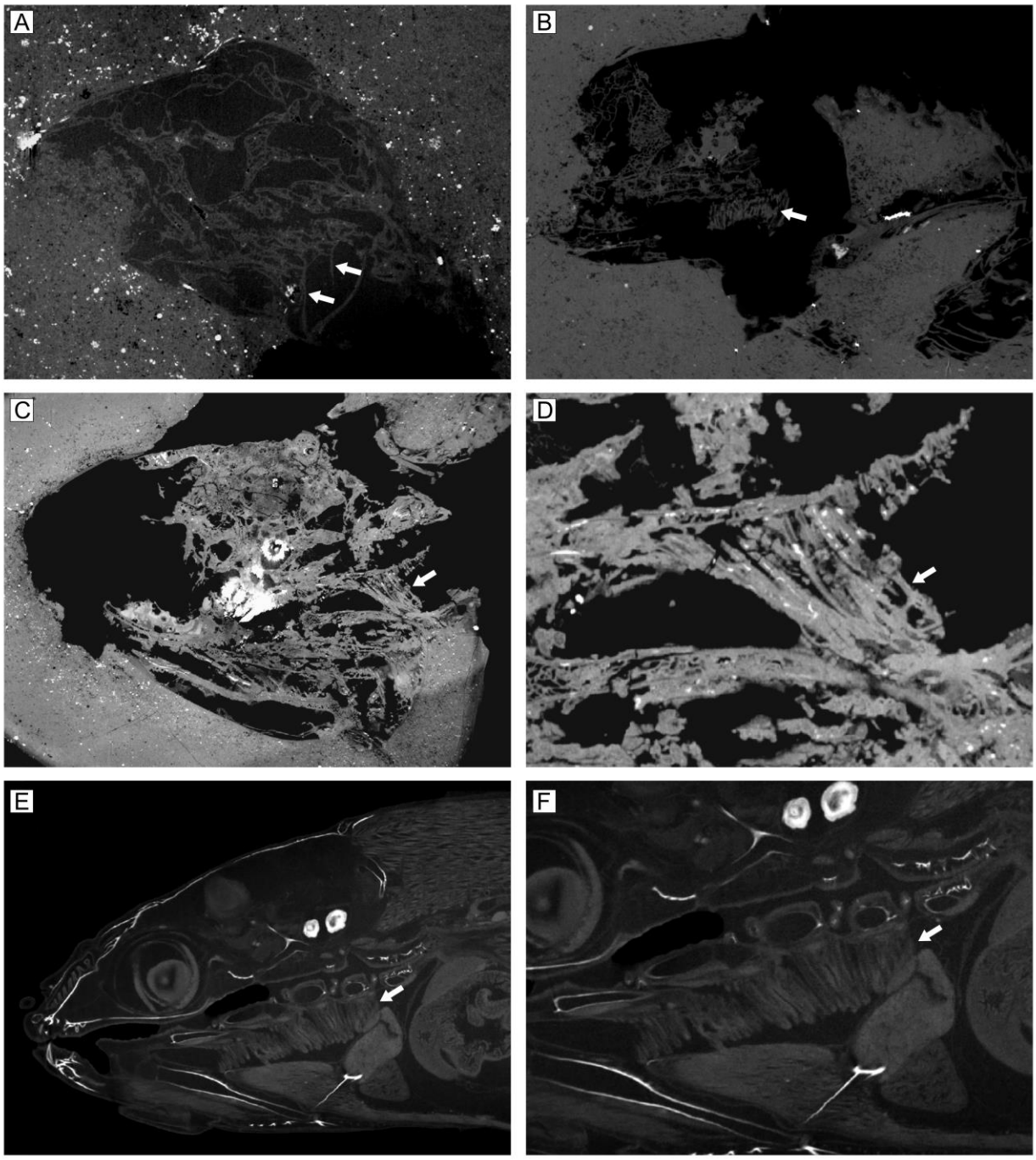

Appendix Figure E.4 – Comparison of gill filaments and lamellae in Permian actinopterygians and *Amia* sp. Based on parasagittal sections derived from μCT scans. (A) Morphotype I (CP 065). (B-D) Morphotype II (B, 7053, C-D, CP 084). E-F, *Amia* (UMMZ 160805). Arrows indicate gill filaments. Not to scale.

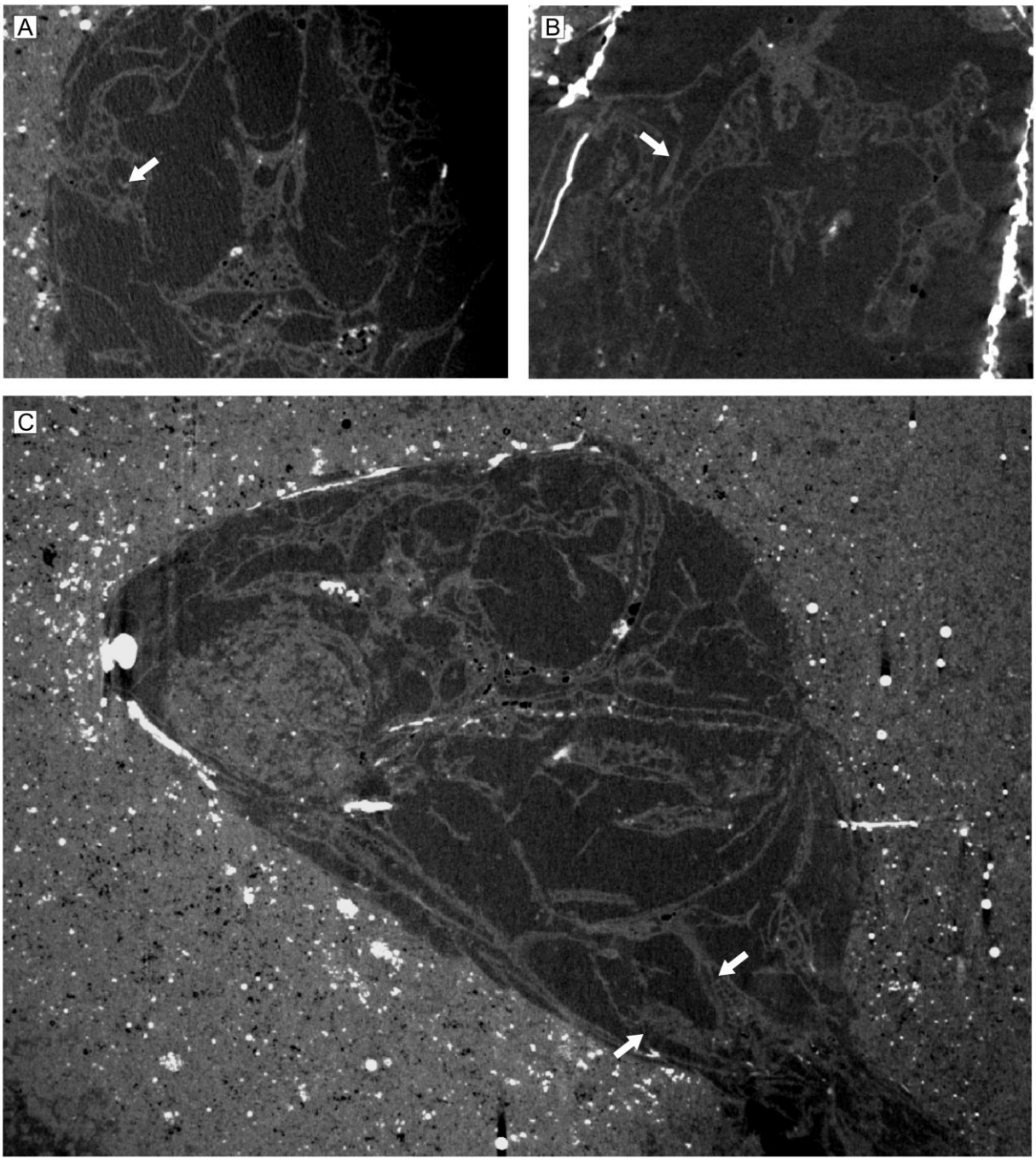

Appendix Figure E.5 – Cardiovascular elements preserved in Permian actinopterygians (Morphotype I). (A) Transverse cross-section through the neurocranium of CP 065 showing the jugal vein (arrow); (B) Horizontal section through the neurocranium of CP 4364 showing the jugal vein (arrow); (C) Sagittal section through the skull of CP 065 showing putative heart tissue preservation (arrows). Not to scale.

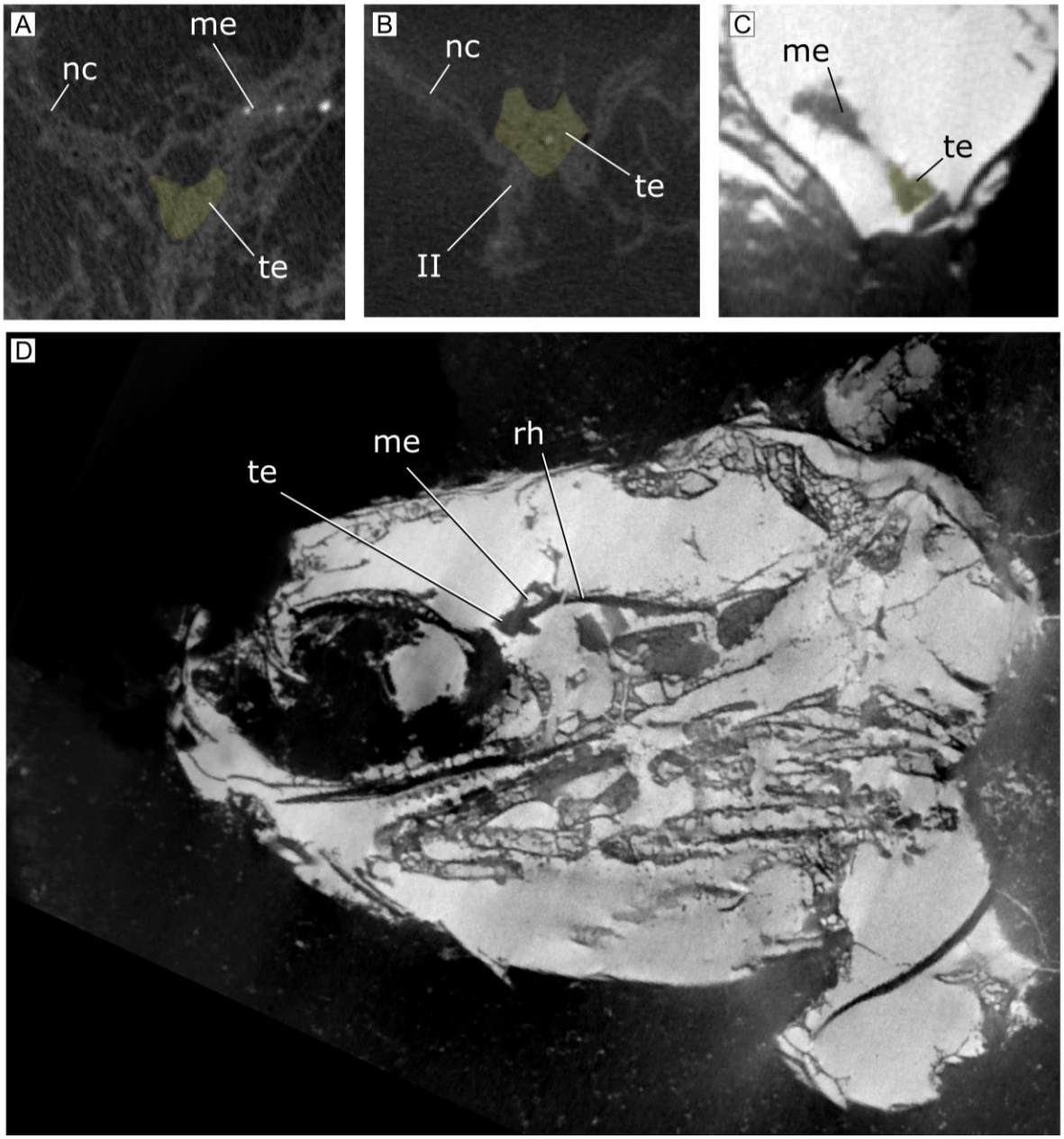

Appendix Figure E.6 – µCT sections through the forebrain of specimens assigned to Morphotype I. (A) CP 065, (B) CP.V 4364, (C) CP 7053, (D) CP 7053 in parasagittal section through the brain. me, mesencephalon, te, telencephalon, rh, rhombencephalon, nc, neurocranium, II optic nerve. Not to scale.

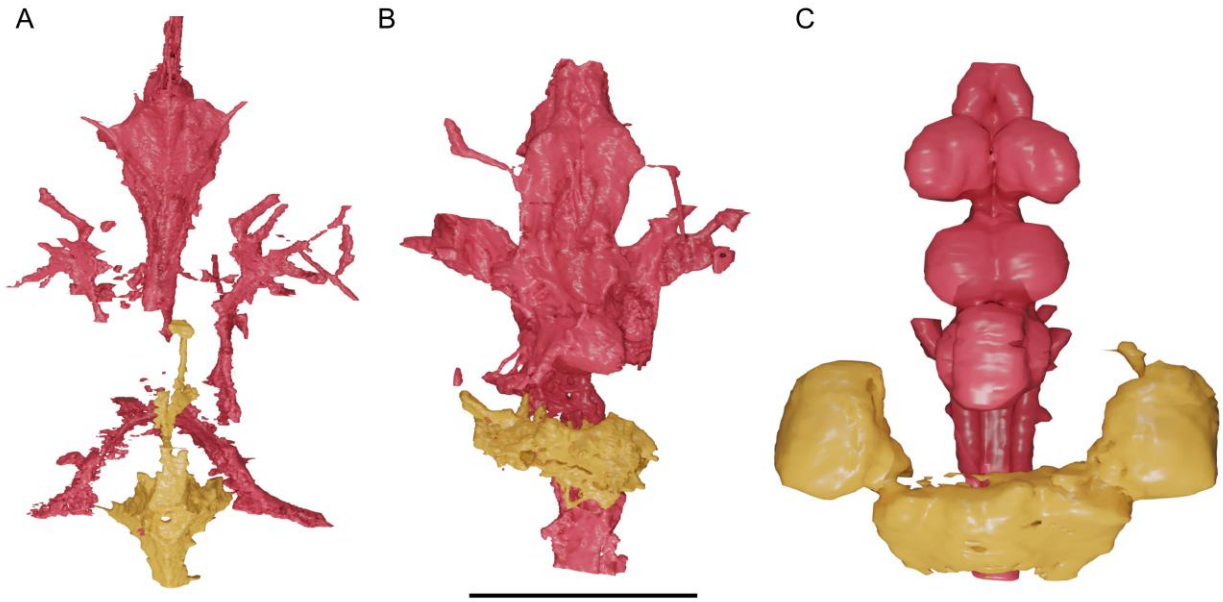

Appendix Figure E.7 – Renders of brains (red) and myelencephalic tissue (orange) in dorsal view. (A) †*Coccocephalus*, (B) CP 584 (Morphotype II), (C) Lepisosteus oculatus (UMMZ 196974). Scale bar = 5 mm (A-B) and 10 mm (C).

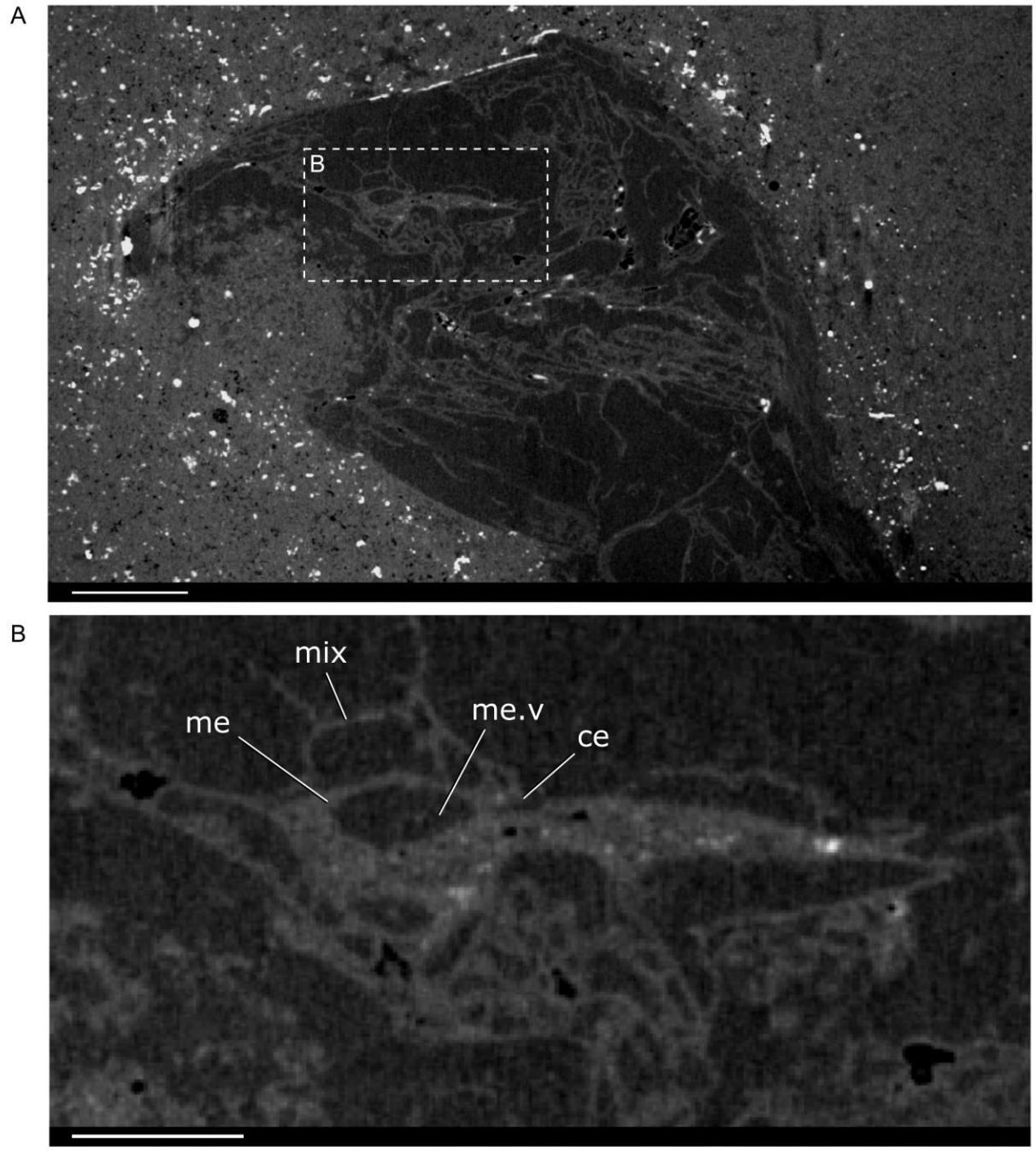

Appendix Figure E.8 – μCT through the head of Morphotype II (CP 065) in parasagittal section (A) highlighting the brain (B). ce, cerebellum, exm, extrameningeal space, me, mesencephalon, me.v, mesencephalic ventricle, mix, meningeal tissue. Scale bar = 5 mm (A); Scale bar = 2 mm (B).

Appendix F: Chapter 6 Supplement

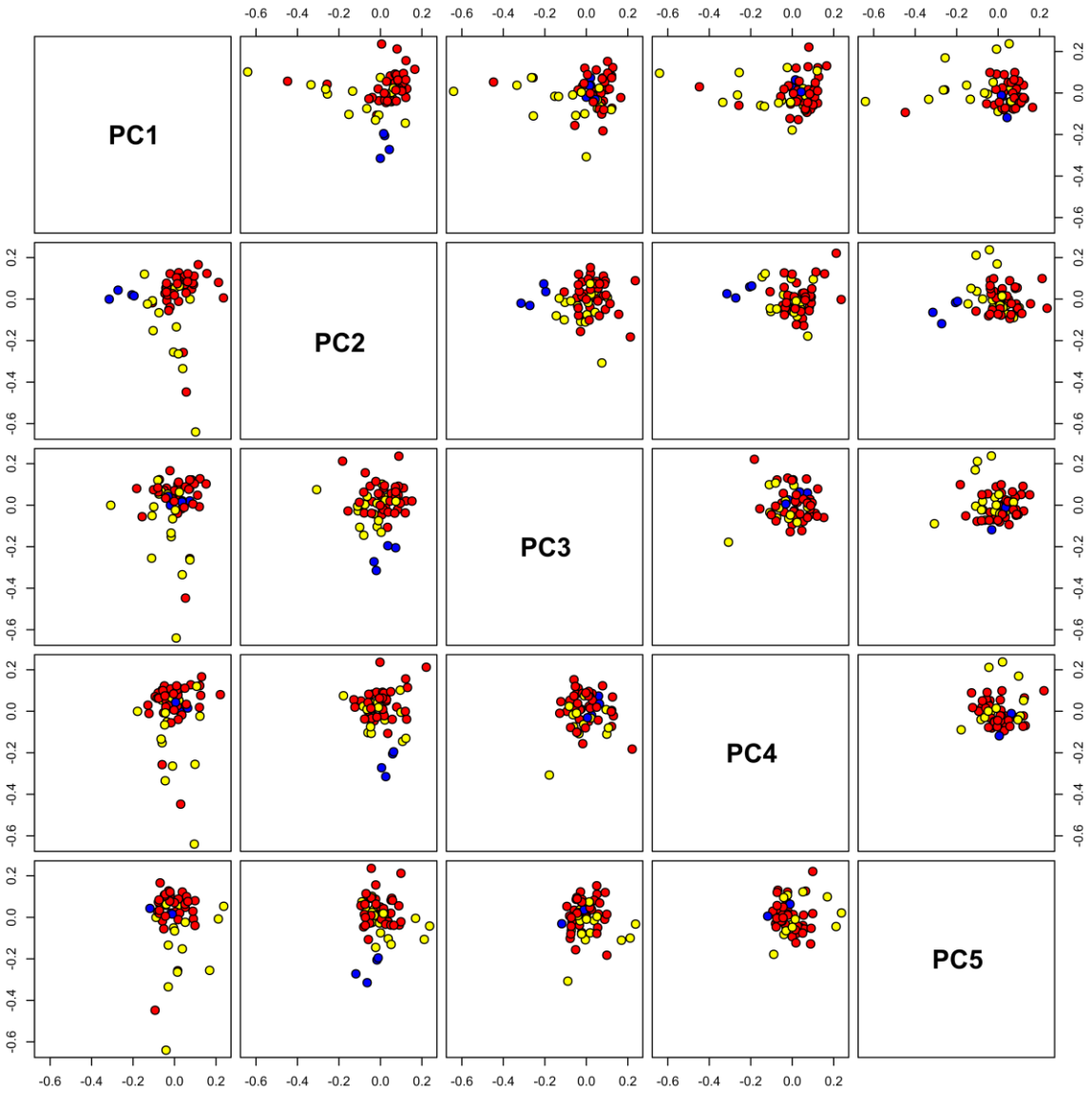

F.1 Code for morphometric analysis

```
#FIRST LETS USE THADDAEUS BUSERL SCRIPT FOR IMPORTING FCSV
SLICER LANDMARK FILES INTO R IN A
#WAY THAT GEOMORPH CAN READ IT:


#' For questions, comments, or concerns, please email me at:
#' thaddaeus.buser@gmail.com
#'
#' If you use the contents of this script in your research,
please cite:
#'
#' Taurus of the tidepool? Inferring the function of cranial
weapons in intertidal sculpins (Pisces: Cottoidea:
Oligocottinae)
#'
#' Thaddaeus J. Buser1, Victoria E. Kee1, Rebecca C. Terry2,
Adam P. Summers3, and Brian L. Sidlauskas1

library("geomorph")
library("Morpho")
library("abind")
library("rfishbase")
library("fishtree")
library("phytools")
setwd("C:\\Users\\rtfig\\Dropbox (University of
Michigan)\\Brain_morphometrics\\slicer_data")
sp_data <- read.csv("taxa_names_enc4.csv")

#taxon.labels <- read.csv(file = "G:\\My
Drive\\taxon_labels.csv",
#                   header = T, row.names = 1)

########## Whole skull, with symmetry and sliding semilandmark
curves

###################
#coordinate keeper function to grab coordinates from Slicer
output .fcsv files
keep.coordinates.only <- function (input) {
  input = as.matrix(input [, 2:4])
  return(input)
}
#'

#' Here, I'll direct R to the folder that contains all the
specimen-specific
```

```
#' folders
path.to.coords <- "G:\\My Drive\\Main Projects\\Soft Tissue
Paper\\Morpho_things"
#
#' I'll save the list of folder names contained in my folder to
an object, "f"
f = dir(path = path.to.coords)
print (f) #see the list of specimen-specific folder names
#'
#' We'll make an array to hold all of the landmark data. The
dimensions of the array
#' should be the number of landmarks x the number of dimensions
x the number of specimens:
fcsv.array <- array (dim = c(22, 3, length(f)), dimnames =
list(1:22, c("x", "y","z"), f))
fcsv.array <- array (dim = c(22, 3, length(f)), dimnames =
list(1:22, c("x", "y","z"), f))

#' Now, I'll set up a loop to populate my array. The loop with
go into each
#' specimen-specific folder (one at a time), read in the
landmarks data from
#' each .fcsv file and collate them, then fill the collated
landmark dataset
#' for that specimen into the corresponding space in the array.
#

#j <- 1
for (j in 1:length(f)){
  f.2 <- paste(path.to.coords,"/", f[j], sep = "") #pathway to
specimen-specific folder
  f.3 <- dir (patt='fcsv',  path = f.2) #list of .fcsv files
within that folder
  #f.3 <- f.3[32:35] # read-in only subset of landmarks
  landmark <- c() #create an object to hold the data from a
single .fcsv file
  LMs.working <- c() #create an object to hold the landmark data
from that file
  #' Here's the loop that reads-in the the .fcsv file, extracts
the landmark data,
  #' and collates all those landmark data for the specimen.
  for(i in 1:length(f.3)){
    landmark <- read.csv (file = paste(f.2, f.3[i], sep = '/'),
skip = 2, header = TRUE)
    working.coords <- keep.coordinates.only(landmark)
    LMs.working <- abind(LMs.working, working.coords, along = 1)
  }
```

```
  # Now populate the appropriate space in the array
  fcsv.array[,,f[j]] <- LMs.working
}

#'
###### to preview material, just type 'fcsv.array'##########

############################################################
###DATA EXCLUDING DUPLICATE TAXA AND/OR ONTOGENETIC SERIES

flag <- logical(length = length(dimnames(fcsv.array)[[3]]))
#creating logical array
flag[1:length(flag)] <- TRUE #setting all values to 'TRUE'
flag[dimnames(fcsv.array)[[3]] %in%
       c("Channa_limbata_small", "Channa_limbata_medium")] <-
FALSE #set to false if ontogenetic sample
data_nONT <- fcsv.array[,,flag] #dropping ontogenetic samples

#PERFORMING PCA
gpa<-gpagen(data_nONT) #performing procrustes analysis
coord <- gpa$coords
pca<-gm.prcomp(gpa$coords) #simple PCA from procrustes-alligned
data
plot(pca$sdev)
plot(pca)
text(pca$x, labels = labels(pca$x)[[1]], cex=0.5, font=2, pos=1)

taxa_names <- labels(pca$x)[[1]]
df_taxa <- rfishbase::load_taxa()

filtered_df <- df_taxa[df_taxa$Species %in% taxa_names, ]
filtered_df <- filtered_df[order(filtered_df$Species),]

non_tel <- c("Acipenseridae", "Amiidae", "Lepisosteidae",
"Polyodontidae")
Acanth <-
fishtree::fishtree_taxonomy("Acanthomorphata")$Acanthomorphata$t
axonomy$family

taxa_group <- ifelse(filtered_df$Family %in% non_tel,
"non_teleost",
                     ifelse(filtered_df$Family %in% Acanth,
"acanthomorph", "non_acanthomorph"))
names(taxa_group) <- taxa_names

taxa_col <- ifelse(filtered_df$Family %in% non_tel, "#0000ffff",
```

```
                    ifelse(filtered_df$Family %in% Acanth,
"#ff0000ff", "#ffff0080"))

#Morphological disparity
morphdisp <- morphol.disparity(coord ~ 1,
                               taxa_group,
                               partial = FALSE,
                               iter = 100,
                               data = NULL) %>% print(morphdisp)

#Modified shapeHulls function
MOD_shapehulls <- function(x, groups = NULL, group.cols = NULL,
group.lwd = NULL, group.lty = NULL, hull.fill = FALSE) {
  y <- as.matrix(x$PC.points)
  if (NCOL(y) < 2)
    stop("Cannot generate hulls in fewer than 2 dimensions")
  if (NCOL(y) > 2)
    y <- y[, 1:2]
  n <- NROW(y)
  if (!is.null(groups) && length(groups) != n)
    stop("Different number of observations between groups factor
and PC plot.\n",
         call. = FALSE)
  if (is.null(groups))
    groups <- rep(1, n)
  groups <- as.factor(groups)
  if (length(unique(groups)) != length(levels(groups)))
    cat("Warning: the levels in the grouping factor do not match
the number of unique factor levels.\n")
  ug <- unique(groups)
  g <- length(ug)
  if (is.null(group.cols))
    group.cols <- 1:g
  if (is.null(group.lwd))
    group.lwd <- rep(1, g)
  if (is.null(group.lty))
    group.lty <- rep(1, g)
  if (length(group.cols) != g)
    stop("Number of requested group colors does not match the
number of groups")
  if (length(group.lwd) != g)
    stop("Number of requested group widths does not match the
number of groups")
  if (length(group.lty) != g)
    stop("Number of requested group line types does not match
the number of groups")
  for (i in 1:g) {
```

```
    if (hull.fill == TRUE) {
      yy <- y[groups == ug[i], ]
      chp <- chull(yy)
      chp <- c(chp, chp[1])
      polygon(yy[chp, ], lty = group.lty[i],
              lwd = group.lwd[i], col = group.cols[i])

      print(chp)
    }
    else if (hull.fill == FALSE) {
      yy <- y[groups == ug[i], ]
      chp <- chull(yy)
      chp <- c(chp, chp[1])
      points(yy[chp, ], type = "l", lty = group.lty[i],
             lwd = group.lwd[i], col = group.cols[i])

      print(chp)
    }

  }
}

svg(filename = "brainPC12.svg", width = 10, height = 7)
PC.plot <- plot(pca, pch=1, col=taxa_col)
MOD_shapehulls(PC.plot, groups = taxa_col, group.lty = rep(0,
3), hull.fill = TRUE,
               group.cols =
c("#ff000080","#0030ff80","#ffff0080"))
points(pca$x[,1:2],pch=16, col=taxa_col)
points(pca$x[,1:2],pch=1, col="black")
legend("topleft",
       legend = c("non teleost", "non acanthomorph",
"acanthomorph"), #ordering to match colors in plot
       pch = 16,
       col = c("#0000ffff","#ffff00","#ff0000ff"))
dev.off()
text(pca$x, labels=taxa_names, cex=0.5, font=2, pos=4)



#GETING PHYLOGENY WITH TAXA IN DATASET

#get tree from fish tree of life
#this will look through the CSV file "taxa_names.csv" to get the
names to use
#since taxa_names might have taxa that are not included in the
PC analysis
```

```
#it will filter these out (if any) before performing the
fishtree_phylogeny
#this requires a bit of back and forward since the rfishbase and
fishtree packages
#adopt different names for some taxa in the analysis

#Tree all taxa
x<-sp_data[order(sp_data$data_taxa),]
xd <- x$enc
names(xd) <- x$data_taxa

Substitute_Phylo <- function(xdat, xt) {
  tree <- fishtree_phylogeny(xt, type = "chronogram")
  tree$tip.label <- sub("_", " ", tree$tip.label) #changing
underscore for spaces in tip names
  tree$tip.label
  sp_names <- xdat
  names(sp_names) <- xt
  sp_names <- sp_names[c(tree$tip.label)]
  tree$tip.label <- sp_names

  return(tree)
}

tree <- Substitute_Phylo(x$data_taxa, x$tree_taxa)

length(x$data_taxa) == length(tree$tip.label) #check if all taxa
are in the tree

plot.phylo(tree)
write.tree(tree, file = "brain_tree.tre")


#Tree just PCA-included taxa
pcaNAMES <- rownames(pca$x)

pruned.tree<-drop.tip(tree,tree$tip.label[-match(pcaNAMES,
tree$tip.label)])

length(pcaNAMES) == length(pruned.tree$tip.label) #check length

plot.phylo(pruned.tree)

write.tree(pruned.tree, file = "brainPCA_tree.tre")

#Phylo-alligned PCA
```

```
PaCA_test <- gm.prcomp(gpa$coords, phy = pruned.tree,
align.to.phy = TRUE, GLS = TRUE, transform = TRUE)
plot(PaCA_test)
text(PaCA_test$x, labels = labels(PaCA_test$x)[[1]], cex=0.5,
font=2, pos=1)

taxa_names <- labels(PaCA_test$x)[[1]]
df_taxa <- rfishbase::load_taxa()

filtered_df <- df_taxa[df_taxa$Species %in% taxa_names, ]
filtered_df <- filtered_df[order(filtered_df$Species),]

non_tel <- c("Acipenseridae", "Amiidae", "Lepisosteidae",
"Polyodontidae")
Acanth <-
fishtree::fishtree_taxonomy("Acanthomorphata")$Acanthomorphata$t
axonomy$family

taxa_col <- ifelse(filtered_df$Family %in% non_tel, "#0000ffff",
                   ifelse(filtered_df$Family %in% Acanth,
"#ff0000ff", "#ffff00ff"))

PC.plot <- plot(PaCA_test, pch=1, col=taxa_col)
MOD_shapehulls(PC.plot, groups = taxa_col, group.lty = rep(0,
3), hull.fill = TRUE,
               group.cols =
c("#ff000080","#0030ff80","#ffff00ff"))
points(PaCA_test$x[,1:2],pch=16, col=taxa_col)
points(PaCA_test$x[,1:2],pch=1, col="black")
legend("topright",
       legend = c("non teleost", "non acanthomorph",
"acanthomorph"), #ordering to match colors in plot
       pch = 16,
       col = c("blue","yellow","red"))
text(PaCA_test$x, labels=taxa_names, cex=0.5, font=2, pos=4)

#Computing phylogenetic signal (k)
phyl_PCs <- data.frame(matrix(nrow = ncol(pca$x), ncol = 2))
#data frame to fill with k values
colnames(phyl_PCs) <- c("k", "lambda")
for (i in 1:ncol(pca$x)) {
  phyl_PCs[i,1] <- phylosig(pruned.tree, pca$x[,i], method =
"K") #Get k for all axes
  phyl_PCs[i,2] <- phylosig(pruned.tree, pca$x[,i], method =
"lambda") #Get lambda for all axes
}
```

```
#Density plots of K and lambda phylogenetic signal
par(mfrow = c(1,2))
k_dense <- density(phyl_PCs$k) #density of k values through PC
axes
plot(k_dense, lwd = 0, col = "red",
     main = "Bloomberg's K")
polygon(k_dense, col = "#ff80808c")

lambda_dense <- density(phyl_PCs$lambda) #density of k values
through PC axes
plot(lambda_dense, lwd = 0, col = "red",
     main = expression(lambda))
polygon(lambda_dense, col = "#ff80808c")

#Plotting 3D phylomorphospace with time axis
fancyTree(pruned.tree, X=pca$x[,c(1,2)], type="traitgram3d")
#interactive plot with time axis

#phylo scattergram using phytools::fancytree
fancyTree(pruned.tree, X=pca$x[,c(1:4)], type="scattergram",
control = list(colors = taxa_col))

#Modified function for plotting scattergram
scatter_PCA <- function(tree, pca, fsize = 0.01, bg = "black",
n) {
  # Check the dimensions of PCA
  if (n > ncol(pca)) {
    stop("n cannot be larger than the number of PC axes")
  }

  # Set up plot grid using layout
  layout_matrix <- matrix(1:(n*n), nrow = n, byrow = TRUE)
  layout(layout_matrix)

  # Set up outer margins and inner margins
  par(oma = c(5, 5, 5, 5), mar = c(2, 2, 2, 2) + 0.1)

  # Get tip labels from the tree
  tip.labels <- tree$tip.label

  # Determine the axis limits to ensure consistency across plots
  xlims <- range(pca)
  ylims <- range(pca)

  # Loop over PC pairs
  for (i in 1:n) {
    for (j in 1:n) {
```

```
      if (i == j) {
        # if i == j, map the i-th PC
        contMap(tree, pca[, i], legend = FALSE, lwd = 2, outline
= FALSE, plot = TRUE, fsize = 0.7)
        title(xlab = paste0("PC", i), ylab = "")
        box() # Add black box around the plot
      } else {
        # if i != j, plot the i-th and j-th PCs in morphospace
        plot(pca[, c(i, j)], xlim = xlims, ylim = ylims, axes =
FALSE, xlab = "", ylab = "")
        points(pca[tip.labels %in% tree$tip.label, c(i, j)], cex
= 1.4, pch = 21, bg = bg)
        box() # Add black box around the plot

        # Add axis labels and ticks only for the outer plots
        if (i == n) {
          axis(side = 1)
          mtext(paste0("PC", j), side = 1, line = 2, cex = 0.8)
        }
        if (i == 1) {
          axis(side = 3)
          mtext(paste0("PC", j), side = 3, line = 2, cex = 0.8)
        }
        if (j == 1) {
          axis(side = 2)
          mtext(paste0("PC", i), side = 2, line = 2, cex = 0.8)
        }
        if (j == n) {
          axis(side = 4)
          mtext(paste0("PC", i), side = 4, line = 2, cex = 0.8)
        }
      }
    }
  }
}


#applying the modified scatterplot function
svg(filename = "scattergram_PC1_5.svg", width = 10, height = 10)
scatter_PCA(pruned.tree, pca$x, bg = taxa_col, n = 5)
dev.off()

#
#Plotting traitgrams of PC axis using the paleotree package
library(paleotree)
par(mfrow = c(2,2))
```

```
plotTraitgram(pca$x[,1], pruned.tree, conf.int = FALSE, lwd =
1.5, main = "PC 1")
plotTraitgram(pca$x[,2], pruned.tree, conf.int = FALSE, lwd =
1.5, main = "PC 2")
plotTraitgram(pca$x[,3], pruned.tree, conf.int = FALSE, lwd =
1.5, main = "PC 3")
plotTraitgram(pca$x[,4], pruned.tree, conf.int = FALSE, lwd =
1.5, main = "PC 4")

par(mfrow = c(3,4))
plotTraitgram(olf, pruned.tree, conf.int = FALSE, lwd = 1.5,
main = "Olfactory bulb")
plotTraitgram(olf_to_tel, pruned.tree, conf.int = FALSE, lwd =
1.5, main = "Olf to Tel")
plotTraitgram(fangle, pruned.tree, conf.int = FALSE, lwd = 1.5,
main = "Forebrain angle")
plotTraitgram(tel, pruned.tree, conf.int = FALSE, lwd = 1.5,
main = "Telencephalon")
plotTraitgram(hyp, pruned.tree, conf.int = FALSE, lwd = 1.5,
main = "Hypophysis")
plotTraitgram(inf, pruned.tree, conf.int = FALSE, lwd = 1.5,
main = "Hyp. inf. lobes")
plotTraitgram(mes, pruned.tree, conf.int = FALSE, lwd = 1.5,
main = "Optic tectum")
plotTraitgram(t_long, pruned.tree, conf.int = FALSE, lwd = 1.5,
main = "Torus longitudinalis")
plotTraitgram(t_sem, pruned.tree, conf.int = FALSE, lwd = 1.5,
main = "Torus semicircularis")
plotTraitgram(cer, pruned.tree, conf.int = FALSE, lwd = 1.5,
main = "Cerebellum")
plotTraitgram(vc, pruned.tree, conf.int = FALSE, lwd = 1.5, main
= "Valvula cerebelli")
plotTraitgram(cc, pruned.tree, conf.int = FALSE, lwd = 1.5, main
= "Crista cerebellaris")


##
#Continuous mapping using phytools::contMap for PCs and for
meristic data of brain coordinates
library(calcmorph)

blue_to_red <- c("#0571b0", "#92c5de", "#f7f7f7", "#f4a582",
"#ca0020")
viridis <- c("#fde725", "#5ec962", "#21918c", "#3b528b",
"#440154")
```

```
#PC1
PC1.cont <- contMap(pruned.tree, pca$x[,1])
PC1.cont <- setMap(PC1.cont, blue_to_red)
#PC2
PC2.cont <- contMap(pruned.tree, pca$x[,2])
PC2.cont <- setMap(PC2.cont, blue_to_red)
#PC1
PC3.cont <- contMap(pruned.tree, pca$x[,3])
PC3.cont <- setMap(PC3.cont, blue_to_red)
#PC1
PC4.cont <- contMap(pruned.tree, pca$x[,4])
PC4.cont <- setMap(PC4.cont, blue_to_red)

par(mfrow = c(2,2))
plot(PC1.cont)
plot(PC2.cont)
plot(PC3.cont)
plot(PC4.cont)

#Brain Length
B_length <- LandmarkDist(gpa$coords, 1, 22, d = 3)
BLength.cont <- contMap(pruned.tree, B_length)
BLength.cont <- setMap(BLength.cont, blue_to_red)
plot(BLength.cont)

#Brain Angle (between chiasma and cerebellum)
B_angle <- LandmarkAngle(gpa$coords, 22, 9, 17, d = 3)
Bangle.cont <- contMap(pruned.tree, B_angle)
Bangle.cont <- setMap(Bangle.cont, blue_to_red)

#Optic lobe Length
Opt_length <- LandmarkDist(gpa$coords, 10, 11, d = 3)
Optlength.cont <- contMap(pruned.tree, Opt_length)
Optlength.cont <- setMap(Optlength.cont, blue_to_red)

#Optic lobe angle (hypophysis and joint)
Opt_angle <- LandmarkAngle(gpa$coords, 8, 10, 11, d = 3)
Optangle.cont <- contMap(pruned.tree, Opt_angle)
Optangle.cont <- setMap(Optangle.cont, blue_to_red)

par(mfrow = c(2,2))
plot(BLength.cont)
plot(Bangle.cont)
plot(Optlength.cont)
plot(Optangle.cont)
```

```
####PHYLOGENY IN CHRONOSTRAT
library(strap)
FAD <- rep(0, length(tree$tip.label))
LAD <- rep(0, length(tree$tip.label))
ages <- cbind(FAD, LAD)
rownames(ages) <- tree$tip.label

tree$node.label <-
c((length(tree$tip.label)+1):(tree$Nnode+length(tree$tip.label))
) #setting node numbers
tree$edge.label <- c(1:length(tree$edge.length))
tree$root.time <-  max(tree$edge.length)
geoscalePhylo(tree, ages, cex.tip = 1.1, cex.age = 0.7, cex.ts =
1)

LandmarkDist <- function(x, a, b, d) {
  #x should be your landmark coordinates
  #geomorph is required for this function to work
  #landmark coordinates can be either a 3D array of dim(x) = [N
of landmarks, N of axis, N of taxa]
  #or a 2D array of dim(x) = [N of taxa, N of landmarks * N of
axis]
  #a should be the number of your first landmark and b the last
landmark
  #d should be a numeric value of the N of dimensions of the
dataset (2 or 3)

  if (length(dim(x)) == 3) {
    x <- two.d.array(x)
  }
  else if (length(dim(x)) == 2) {
    x <- x
  }
  if (d == 3) {
    #for 3D data
    La = ((a - 1) * 3) + 1
    Lb = ((b - 1) * 3) + 1
    Ldist3D <- (sqrt(abs(x[, La] - x[, Lb])
                     + abs(x[, La + 1] - x[, Lb + 1])
                     + abs(x[, La + 2] - x[, Lb + 2])))
    return(Ldist3D)
  } else if (d == 2) {
    #for 2D data
    La = ((a - 1) * 2) + 1
    Lb = ((b - 1) * 2) + 1
    Ldist2D <- (sqrt(abs(x[, La] - x[, Lb])
                     + abs(x[, La + 1] - x[, Lb + 1])))
```

```
    return(Ldist2D)
  } else if (b > length(x)) {
    print("Error: a or b exceed N of Landmarks")
  } else if (d > 3) {
    print("Error: d must be equal to 2 or 3")
  }
}
LandmarkAngle <- function(x, a, b, c, d) {
  if(length(dim(x)) == 3) {
    x <- two.d.array(x)
  }
  else if(length(dim(x)) == 2) {
    x <- x
  }
  if(d == 3) { #for 3D data

    La = ((a - 1)*3) + 1
    Lb = ((b - 1)*3) + 1
    Lc = ((c - 1)*3) + 1

    ab <- cbind((x[,Lb] - x[,La]), (x[,Lb+1] - x[,La+1]),
(x[,Lb+2] - x[,La+2]))
    ac <- cbind((x[,Lc] - x[,La]), (x[,Lc+1] - x[,La+1]),
(x[,Lc+2] - x[,La+2]))

    dot <- (ab[,1]*ac[,1]) + (ab[,2]*ac[,2]) + (ab[,3]*ac[,3])

    v1 <- sqrt((ab[,1]^2) + (ab[,2]^2) + (ab[,3]^2))
    v2 <- sqrt((ac[,1]^2) + (ac[,2]^2) + (ac[,3]^2))

    Lang3D <- (acos(abs(dot)/(v1 * v2)))*(180/pi)

    return(Lang3D)
  } else if (d == 2) { #for 2D data
    La = ((a - 1)*2) + 1
    Lb = ((b - 1)*2) + 1

    ab <- cbind((x[,Lb] - x[,La]), (x[,Lb+1] - x[,La+1]))
    ac <- cbind((x[,Lc] - x[,La]), (x[,Lc+1] - x[,La+1]))

    dot <- (ab[,1]*ac[,1]) + (ab[,2]*ac[,2])

    v1 <- sqrt((ab[,1]^2) + (ab[,2]^2))
    v2 <- sqrt((ac[,1]^2) + (ac[,2]^2))

    Lang2D <- acos(abs(dot)/(v1 * v2))
```

```
    return(Lang2D)
  } else if (b > (ncol(x)/d)) {
    print("Error: a or b exceed N of Landmarks")
  } else if (d > 3){
    print("Error: d must be equal to 2 or 3")
  }
}
#total brain length (L1 to L22)
brain_length <- LandmarkDist(gpa$coords, 1, 22, d = 3)

#olfactory bulb length
olf <- LandmarkDist(gpa$coords, 1, 2, d = 3)

#distance between olfactory bulb and telencephalon
olf_to_tel <- LandmarkDist(gpa$coords, 2, 3, d = 3)

#forebrain angle
fangle <- LandmarkAngle(gpa$coords, 4, 2, 9, d =3)

#telencephalon length
tel <- LandmarkDist(gpa$coords, 3, 4, d = 3)

#Hypophysis
hyp <- LandmarkDist(gpa$coords, 7, 8, d = 3)

#Hypothalamus Inferior Lobe
inf <- LandmarkDist(gpa$coords, 5, 6, d = 3)

#optic tectum length
mes <- LandmarkDist(gpa$coords, 10, 11, d = 3)

#Torus longitudinalis
t_long <- LandmarkDist(gpa$coords, 12, 13, d = 3)

#Torus semicircularis
t_sem <- LandmarkDist(gpa$coords, 14, 15, d = 3)

#Cerebellar corpus length
cer <- LandmarkDist(gpa$coords, 16, 17, d = 3)

#valvula cerebelli
vc <- LandmarkDist(gpa$coords, 19, 20, d = 3)

#crista cerebellaris
cc <- LandmarkDist(gpa$coords, 21, 22, d = 3)

meristic_data <- data.frame((cbind(OLF = olf,
```

```
                                        OLF_TEL = olf_to_tel,
                                        ANG = fangle,
                                        TEL = tel,
                                        HY = hyp,
                                        IL = inf,
                                        OT = mes,
                                        TL = t_long,
                                        TS = t_sem,
                                        CER = cer,
                                        VC = vc,
                                        CC = cc,
                                        BRAIN = brain_length)))
meristic_data$Species <- rownames(meristic_data)
```

Bibliography

Abrahão, V.P., and Shibatta, O.A., 2015, Gross morphology of the brain of *Pseudopimelodus bufonius* (Valenciennes, 1840) (siluriformes: Pseudopimelodidae): Neotropical Ichthyology, v. 13, p. 255–264.

Aldinger, H., 1937, Permische Ganoidfische Aus Ostgronland: Copenhagen, Kommissionen for Videnskabelige Undersøgelser I Grøland, .

Aldridge, R.J., and Theron, J.N., 1993, Conodonts with preserved soft tissue from a new Ordovician *Konservat-Lagerstatte*: Journal of Micropalaeontology, v. 12, p. 113–117.

Alfaro, M.E., 2018, Resolving the ray-finned fish tree of life: Proceedings of the National Academy of Sciences, v. 115, p. 6107–6109.

Allemand, R., Abdul-Sater, J., Macrì, S., Di-Poï, N., Daghfous, G., and Silcox, M.T., 2022, Endocast, brain, and bones: Correspondences and spatial relationships in squamates: The Anatomical Record, v. n/a.

Allis, E.P., 1897, The cranial muscle and cranial and first spinal nerves in *Amia calva*: Journal of Morphology, v. XII, p. 487–809.

Allis, E.P., 1922, The Cranial Anatomy of *Polypterus*, with Special Reference to *Polypterus bichir*.: Journal of Anatomy, v. 56, p. 189-294.43.

Allison, P.A., and Briggs, D.E.G., 1993, Exceptional fossil record: distribution of soft-tissue preservation through the Phanerozoic: Geology, v. 21, p. 527–530.

Alvarado-Ortega, J., Espinosa-Arrubarrena, L., Blanco, A., Vega, F.J., Benammi, M., and Briggs, D.E.G., 2007, Exceptional preservation of soft tissues in Cretaceous fishes from the Tlayúa Quarry, Central Mexico: Palaios, v. 22, p. 682–685.

Alves, Y.M., 2010, Los vertebrados fósiles del Paleozoico y Mesozoico del Estado de Tocantins (Brasil): preliminar síntesis: Caminhos de Geografia, v. 11, p. 224–236.

Anderson, M.E., Almond, J.E., Evans, F.J., and Long, J.A., 1999, Devonian (Emsian-Eifelian) fish from the Lower Bokkeveld Group (Ceres Subgroup), South Africa: Journal of African Earth Sciences, v. 29, p. 179–193.

Anderson, P.S.L., Friedman, M., Brazeau, M.D., and Rayfield, E.J., 2011, Initial radiation of jaws demonstrated stability despite faunal and environmental change: Nature, v. 476, p. 206–209.

Argyriou, T., Giles, S., and Friedman, M., 2022, A Permian fish reveals widespread distribution of neopterygian-like jaw suspension: eLife, v. 11, p. e58433.

Argyriou, T., Giles, S., Friedman, M., Romano, C., Kogan, I., and Sánchez-Villagra, M.R., 2018, Internal cranial anatomy of Early Triassic species of †*Saurichthys* (Actinopterygii: †Saurichthyiformes): implications for the phylogenetic placement of †saurichthyiforms: BMC Evolutionary Biology, v. 18, p. 161.

Arratia, G., and Schultze, H.-P., 2024, The oldest teleosts (Teleosteomorpha): their early taxonomic, phenotypic, and ecological diversification during the Triassic: Fossil Record, v. 27, p. 29–53.

Baken, E.K., Collyer, M.L., Kaliontzopoulou, A., and Adams, D.C., 2021, geomorph v4.0 and gmShiny: Enhanced analytics and a new graphical interface for a comprehensive morphometric experience: Methods in Ecology and Evolution, v. 12, p. 2355–2363.

Balanoff, A.M., and Bever, G.S., 2017, The role of endocasts in the study of brain evolution, *in* Kaas, J.H., ed., Evolutionary Neuroscience (Second Edition): London, Academic Press, p. 29–49.

Barton, R.A., and Harvey, P.H., 2000, Mosaic evolution of brain structure in mammals: Nature, v. 405, p. 1055–1058.

Becker, R.T., Gradstein, F.M., and Hammer, O., 2012, Chapter 22 - The Devonian Period, *in* Gradstein, F.M., Ogg, J.G., Schmitz, M.D., and Ogg, G.M., eds., The Geologic Time Scale: Boston, Elsevier, p. 559–601.

Bell, C.C., Han, V., and Sawtell, N.B., 2008, Cerebellum-Like Structures and Their Implications for Cerebellar Function: Annual Review of Neuroscience, v. 31, p. 1–24.

Bemis, W., 2016, Species and the Fossil Record of Fishes, Species and Speciation in the Fossil Record: The University of Chicago Press, p. 312–339.

Bender, P.A., 1999, First documentation of similar Late Permian actinopterygian fish from Australia and South Africa: Records of the Western Australian Museum Supplement, v. 57, p. 183–189.

Bertmar, G., 1965, On the Development of the Jugular and Cerebral Veins in Fishes: Proceedings of the Zoological Society of London, v. 144, p. 87–129.

Betancur-R, R., Broughton, R.E., Wiley, E.O., Carpenter, K., López, J.A., Li, C., Holcroft, N.I., Arcila, D., Sanciangco, M., Ii, J.C.C., Zhang, F., Buser, T., Campbell, M.A., Ballesteros, J.A., Roa-Varon, A., Willis, S., Borden, W.C., Rowley, T., Reneau, P.C., Hough, D.J., Lu, G., Grande, T., Arratia, G., and Ortí, G., 2013, The Tree of Life and a New Classification of Bony Fishes: PLOS Currents Tree of Life,.

Bjerring, H.C., 1978, A Contribution to Structural Analysis of the Head of Craniate Animals: Zoologica Scripta, v. 6, p. 127–183.

Bjerring, H.C., 1984, The Term “Fossa Bridgei” and Five Endocranial Fossae in Teleostome Fishes: Zoologica Scripta, v. 13, p. 231–238.

Bjerring, H.C., 1985, Facts and thoughts on piscine phylogeny, *in* Foreman, R.E., Gorbman, A., Dodd, J.M., and Olsson, R., eds., Evolutionary Biology of Primitive Fishes: Boston, MA, Springer US, p. 31–57.

Bjerring, H.C., 1991, Two Intracranial Ligaments Supporting the Brain of the Brachiopterygian Fish Polypterus senegalus: Acta Zoologica, v. 72, p. 41–47.

Blake, R.W., 2004, Fish functional design and swimming performance: Journal of Fish Biology, v. 65, p. 1193–1222.

Boisvert, C.A., Mark-Kurik, E., and Ahlberg, P.E., 2008, The pectoral fin of Panderichthys and the origin of digits: Nature, v. 456, p. 636–638.

Bosetti, E.P., 2004, Tafonomia de alta resolução das fácies de offshore da sucessão devoniana da região de Ponta Grossa, Brasil [PhD Dissertation]: Porto Alegre, Universidade Federal do Rio Grande do Sul 137p.

Bosetti, E.P., Grahn, Y., Horodyski, R.S., and Mauller, P.M., 2012, The first recorded decline of the Malvinokaffric Devonian fauna in the Paraná Basin (southern Brazil) and its cause; taphonomic and fossil evidences: Journal of South American Earth Sciences, v. 37, p. 228–241.

Boucot, Rowell, Racheboeuf, Pereira, Melo, G.D., and Siqueira, D., 2001, Position of the Malvinokaffric Realm's northern boundary (Early Devonian) based on newly discovered brachiopods from the Parecis Basin (Brazil): Journal of Geosciences, v. 46, p. 109–120.
Boucot, A.J., 1988, Devonian Biogeography: An Update: p. 211–227.
Boucot, A.J., Johnson, J.G., and Talent, J.A., 1969, Early Devonian Brachiopod Zoogeography: Geological Society of America, 132 p.
Boulenger, G.A., 1902, Further remarks on the Carboniferous Ganoid , Benedenius deneensis, Traquair: Journal of Natural History Series 7, v. 10, p. 52–53.
Braford, Jr., Mark R., 2008, Comparative Aspects of Forebrain Organization in the Ray-Finned Fishes: Touchstones or Not? Brain Behavior and Evolution, v. 46, p. 259–274.
Braford, M.R., 2009, Stalking the everted telencephalon: comparisons of forebrain organization in basal ray-finned fishes and teleosts: Brain, Behavior and Evolution, v. 74, p. 56–76.
Brasier, M.D., Norman, D.B., Liu, A.G., Cotton, L.J., Hiscocks, J.E.H., Garwood, R.J., Antcliffe, J.B., and Wacey, D., 2017, Remarkable preservation of brain tissues in an Early Cretaceous iguanodontian dinosaur: Geological Society, London, Special Publications, v. 448, p. 383–398.
Brazeau, M.D., and Friedman, M., 2015, The origin and early phylogenetic history of jawed vertebrates: Nature, v. 520, p. 490–497.
Briscoe, S.D., and Ragsdale, C.W., 2019, Evolution of the chordate telencephalon: Current Biology, v. 29, p. R647–R662.
Buchholtz, E.A., and Seyfarth, E.-A., 1999, The gospel of the fossil brain: Tilly Edinger and the science of paleoneurology: Brain Research Bulletin, v. 48, p. 351–361.
Butler, A.B., and Hodos, W., 1996, Comparative Vertebrate Neuroanatomy: John Wiley & Sons, 514 p.
Butts, T., Modrell, M.S., Baker, C.V.H., and Wingate, R.J.T., 2014, The evolution of the vertebrate cerebellum: absence of a proliferative external granule layer in a non-teleost ray-finned fish: Evolution & Development, v. 16, p. 92–100.
Cadwallader, P.L., 1975, Relationship between brain morphology and ecology in New Zealand Galaxiidae, particularly Galaxias vulgaris (Pisces: Salmoniformes): New Zealand Journal of Zoology, v. 2, p. 35–43.
Cagliari, J., Philipp, R.P., Buso, V.V., Netto, R.G., Klaus Hillebrand, P., da Cunha Lopes, R., Stipp Basei, M.A., and Faccini, U.F., 2016, Age constraints of the glaciation in the Paraná Basin: evidence from new U–Pb dates: Journal of the Geological Society, v. 173, p. 871–874.
Campbell, K.S.W., and Barwick, R.E., 1990, Paleozoic Dipnoan Phylogeny: Functional Complexes and Evolution Without Parsimony: Paleobiology, v. 16, p. 143–169.
Caputo, M.V., 1985, Late Devonian glaciation in South America: Palaeogeography, Palaeoclimatology, Palaeoecology, v. 51, p. 291–317.
Caron, A., Venkataraman, V., Tietjen, K., and Coates, M., 2023, A fish for Phoebe: a new actinopterygian from the Upper Carboniferous Coal Measures of Saddleworth, Greater Manchester, UK, and a revision of Kansasiella eatoni: Zoological Journal of the Linnean Society, p. zlad011.
Chahud, A., and Petri, S., 2013, The silty shale Taquaral Member of the early Permian Irati Formation (Paraná Basin, Brazil). Paleontology and paleoenvironments: Swiss Journal of Palaeontology, v. 132, p. 119–128.

Challands, T.J., Pardo, J.D., and Clement, A.M., 2020, Mandibular musculature constrains brain–endocast disparity between sarcopterygians: Royal Society Open Science, v. 7, p. 200933.
Chandler, A.C., 1911, On a lymphoid structure lying over the myelencephalon of *Lepisosteus*: University of California Publications in Zoology, v. 9, p. 85–104.
Chang, J., Rabosky, D.L., Smith, S.A., and Alfaro, M.E., 2019, An r package and online resource for macroevolutionary studies using the ray-finned fish tree of life: Methods in Ecology and Evolution, v. 10, p. 1118–1124.
Chapman, L., Albert, J., and Galis, F., 2008, Developmental Plasticity, Genetic Differentiation, and Hypoxia-induced Trade-offs in an African Cichlid Fish: The Open Evolution Journal, v. 2.
Chapman, L.J., and Hulen, K.G., 2001, Implications of hypoxia for the brain size and gill morphometry of mormyrid fishes: Journal of Zoology, v. 254, p. 461–472.
Chavko, M., Nemoto, E.M., and Melick, J.A., 1993, Regional lipid composition in the rat brain: Molecular and Chemical Neuropathology, v. 18, p. 123–131.
Cherns, L., Spencer, A.R.T., Rahman, I.A., Garwood, R.J., Reedman, C., Burca, G., Turner, M.J., Hollingworth, N.T.J., and Hilton, J., 2021, Correlative tomography of an exceptionally preserved Jurassic ammonite implies hyponome-propelled swimming: Geology, v. 50, p. 397–401.
Chiba, A., Torroba, M., Honma, Y., and Zapata, A.G., 1988, Occurrence of lymphohaemopoietic tissue in the meninges of the stingray Dasyatis akajei (Elasmobranchii, Chondricthyes): American Journal of Anatomy, v. 183, p. 268–276.
Choo, B., 2009, Basal Actinopterygian Fish from the Middle Devonian Bunga Beds of New South Wales, Australia.: Proceedings of the Linnean Society of New South Wales, v. 130, p. 37–46.
Choo, B., 2011, Revision of the actinopterygian genus Mimipiscis(= Mimia) from the Upper Devonian Gogo Formation of Western Australia and the interrelationships of the early Actinopterygii: Earth and Environmental Science Transactions of the Royal Society of Edinburgh, v. 102, p. 77–104.
Choo, B., 2015, A new species of the Devonian actinopterygian Moythomasia from Bergisch Gladbach, Germany, and fresh observations on M. durgaringa from the Gogo Formation of Western Australia: Journal of Vertebrate Paleontology, v. 35, p. 37–41.
Choo, B., Long, J.A., and Trinajstic, K., 2009, A new genus and species of basal actinopterygian fish from the Upper Devonian Gogo Formation of Western Australia: Acta Zoologica, v. 90, p. 194–210.
Choo, B., Lu, J., Giles, S., Trinajstic, K., and Long, J.A., 2019, A new actinopterygian from the Late Devonian Gogo Formation, Western Australia: Papers in Palaeontology, v. 5, p. 343–363.
Cignoni, P., Callieri, M., Corsini, M., Dellepiane, M., Ganovelli, F., and Ranzuglia, G., 2008, MeshLab: An Open-Source Mesh Processing Tool: The Eurographics Association, .
Cione, A.L., Gouiric-Cavalli, S., Mennucci, J.A., Cabrera, D.A., and Freije, R.H., 2010, First vertebrate body remains from the Permian of Argentina (Elasmobranchii and Actinopterygii): Proceedings of the Geologists' Association, v. 121, p. 301–312.
Cisneros, J.C., Marsicano, C., Angielczyk, K.D., Smith, R.M.H., Richter, M., Fröbisch, J., Kammerer, C.F., and Sadleir, R.W., 2015, New Permian fauna from tropical Gondwana: Nature Communications, v. 6, p. 8676.

Clement, A.M., Nysjö, J., Strand, R., and Ahlberg, P.E., 2015, Brain - Endocast relationship in the Australian lungfish, *Neoceratodus forsteri*, elucidated from tomographic data (Sarcopterygii: Dipnoi): PLoS ONE, v. 10.
Clement, A.M., Challands, T.J., Long, J.A., and Ahlberg, P.E., 2016, The cranial endocast of *Dipnorhynchus sussmilchi* (Sarcopterygii: Dipnoi) and the interrelationships of stem-group lungfishes: PeerJ, v. 2016.
Clement, A.M., Mensforth, C.L., Challands, T.J., Collin, S.P., and Long, J.A., 2021, Brain Reconstruction Across the Fish-Tetrapod Transition; Insights From Modern Amphibians: Frontiers in Ecology and Evolution, v. 9.
Clements, T., and Gabbott, S., 2022, Exceptional Preservation of Fossil Soft Tissues, p. 1–10.
Cloutier, R., and Arratia, G., 2004, Early diversification of actinopterygians, The Origin and Early Radiation of Vertebrates: Honoring Hans-Peter Schultze: Verlag Dr. Friedrich Pfeil.
Coates, M., 2003, The Evolution of Paired Fins: Theory in Biosciences, v. 122, p. 266–287.
Coates, M.I., 1998, Actinopterygians from the Namurian of Bearsden, Scotland, with comments on early actinopterygian neurocrania: Zoological Journal of the Linnean Society, v. 122, p. 27–59.
Coates, M.I., 1999, Endocranial preservation of a Carboniferous actinopterygian from Lancashire, UK, and the interrelationships of primitive actinopterygians: Philosophical Transactions of the Royal Society B: Biological Sciences, v. 354, p. 435–462.
Coates, M.I., and Tietjen, K., 2018, 'This strange little palaeoniscid': a new early actinopterygian genus, and commentary on pectoral fin conditions and function: Earth and Environmental Science Transactions of The Royal Society of Edinburgh, v. 109, p. 15–31.
Cong, P., Ma, X., Hou, X., Edgecombe, G.D., and Strausfeld, N.J., 2014, Brain structure resolves the segmental affinity of anomalocaridid appendages: Nature, v. 513, p. 538–542.
Conith, A.J., Hope, S.A., and Albertson, R.C., 2022, Covariation of brain and skull shapes as a model to understand the role of crosstalk in development and evolution: Evolution & Development, v. n/a.
Cox, C.B., and Hutchinson, P., 1991, Fishes and Amphibians from the Late Permian Pedra do Fogo Formation of Northern of Brazil: Palaeontology (Oxford), v. 34, p. 13.
Crispo, E., and Chapman, L.J., 2010, Geographic variation in phenotypic plasticity in response to dissolved oxygen in an African cichlid fish: Journal of Evolutionary Biology, v. 23, p. 2091–2103.
Cummings, M.P., 2014, PAUP* (Phylogenetic Analysis Using Parsimony (and Other Methods)), Dictionary of Bioinformatics and Computational Biology: John Wiley & Sons, Ltd.
Cunningham, J.A., Donoghue, P.C.J., and Bengtson, S., 2014, Distinguishing Biology from Geology in Soft-Tissue Preservation: The Paleontological Society Papers, v. 20, p. 275–288.
Dahlgren, U., 1927, The Life History of the Fish *Astroscopus* (The "Stargazer"): The Scientific Monthly, v. 24, p. 348–365.
Datovo, A., and Rizzato, P.P., 2018, Evolution of the facial musculature in basal ray-finned fishes: Frontiers in Zoology, v. 15.
Davis, S.P., Finarelli, J.A., and Coates, M.I., 2012, *Acanthodes* and shark-like conditions in the last common ancestor of modern gnathostomes: Nature, v. 486, p. 247–250.
Dias, E.V., 2012, A new deep-bodied fossil fish (Actinopterygii) from the Rio do Rasto Formation, Paraná Basin, Brazil: Zootaxa, v. 23, p. 1–23.

Dornburg, A., Wcisel, D.J., Zapfe, K., Ferraro, E., Roupe-Abrams, L., Thompson, A.W., Braasch, I., Ota, T., and Yoder, J.A., 2021, Holosteans contextualize the role of the teleost genome duplication in promoting the rise of evolutionary novelties in the ray-finned fish innate immune system: Immunogenetics, v. 73, p. 479–497.
Dowding, E.M., and Ebach, M.C., 2018, An interim global bioregionalisation of Devonian areas: Palaeobiodiversity and Palaeoenvironments, v. 98, p. 527–547.
Dowding, E.M., and Ebach, M.C., 2019, Evaluating Devonian bioregionalization: quantifying biogeographic areas: Paleobiology, v. 45, p. 636–651.
Duffin, C.J., Richter, M., and Neis, P.A., 1996, Shark remains from the Late Carboniferous of the Amazon Basin, Brazil: Neues Jahrbuch Für Geologie Und Paläontologie - Monatshefte, p. 232–256.
Dunkle, D.H., and Schaeffer, B., 1956, Preliminary description of a paleoniscoid fish from the Late Paleozoic of Brazil: Boletim Da Faculdade de Filosofia Ciências e Letras, Universidade de São Paulo. Geologia, v. 13, p. 5–22.
Dunkle, D.H., and Schaeffer, B., 1973, *Tegeolepis clarki* (Newberry), a palaeonisciform from the Upper Devonian Ohio Shale: Palaeontographica Abteilung A, v. 143, p. 131–138.
Dutel, H., Galland, M., Tafforeau, P., Long, J.A., Fagan, M.J., Janvier, P., Herrel, A., Santin, M.D., Clément, G., and Herbin, M., 2019, Neurocranial development of the coelacanth and the evolution of the sarcopterygian head: Nature, v. 569, p. 556–559.
Eastman, C.R., Eastman, C.R., and Survey, I.G., 1908, Devonian Fishes of Iowa: Des Moines, Iowa Geological Survey, .
Eastman, J.T., and Lannoo, M.J., 1995, Diversification of Brain Morphology in Antarctic Notothenioid Fishes: Basic Descriptions and Ecological Considerations: Journal of Morphology, v. 223, p. 47–83.
Edgecombe, G.D., Ma, X., and Strausfeld, N.J., 2015, Unlocking the early fossil record of the arthropod central nervous system: Philosophical Transactions of the Royal Society B: Biological Sciences, v. 370, p. 20150038.
Edinger, T., 1964, Recent Advances in Paleoneurology: Progress in Brain Research, v. 6, p. 147–160.
Egan, J.P., Buser, T.J., Burns, M.D., Simons, A.M., and Hundt, P.J., 2021, Patterns of Body Shape Diversity and Evolution in Intertidal and Subtidal Lineages of Combtooth Blennies (Blenniidae): Integrative Organismal Biology, v. 3, p. obab004.
Eifert, C., Farnworth, M., Schulz-Mirbach, T., Riesch, R., Bierbach, D., Klaus, S., Wurster, A., Tobler, M., Streit, B., Indy, J.R., Arias-Rodriguez, L., and Plath, M., 2015, Brain size variation in extremophile fish: local adaptation versus phenotypic plasticity: Journal of Zoology, v. 295, p. 143–153.
Ekdale, A.A., 1985, Paleoecology of the marine endobenthos: Palaeogeography, Palaeoclimatology, Palaeoecology, v. 50, p. 63–81.
Evans, F.J., 1999, Palaeobiology of Early Carboniferous lacustrine biota of the Waaipoort Formation (Witteberg Group), South Africa: Palaeontologia Africana, v. 6, p. 1–6.
Evans, H.M., 1931, A comparative study of the brains in British cyprinoids in relation to their habits of feeding, with special reference to the anatomy of the medulla oblongata: Proceedings of the Royal Society of London. Series B, Containing Papers of a Biological Character, v. 108, p. 233–257.
Evans, H.M., 1936, A comparative study of the brains in Pleuronectidae: Proceedings of the Royal Society of London. Series B - Biological Sciences, v. 122, p. 308–343.

Evans, H.M., 1940, Brain and Body of Fish; a Study of Brain Pattern in Relation to Hunting and Feeding in Fish: Philadelphia, The Blakiston company, .
Eyles, C.H., Eyles, N., and Franca, A.B., 1993, Glaciation and tectonics in an active intracratonic basin: the Late Palaeozoic Itararé Group, Paraná Basin, Brazil: Sedimentology, v. 40, p. 1–25.
Fabbri, M., and Bhullar, B.-A.S., 2022, The endocast of Euparkeria sheds light on the ancestral archosaur nervous system: Palaeontology, v. 65, p. e12630.
Fabbri, M., Mongiardino Koch, N., Pritchard, A.C., Hanson, M., Hoffman, E., Bever, G.S., Balanoff, A.M., Morris, Z.S., Field, D.J., Camacho, J., Rowe, T.B., Norell, M.A., Smith, R.M., Abzhanov, A., and Bhullar, B.-A.S., 2017, The skull roof tracks the brain during the evolution and development of reptiles including birds: Nature Ecology & Evolution, v. 1, p. 1543–1550.
Faircloth, B.C., Sorenson, L., Santini, F., and Alfaro, M.E., 2013, A Phylogenomic Perspective on the Radiation of Ray-Finned Fishes Based upon Targeted Sequencing of Ultraconserved Elements (UCEs): PLOS ONE, v. 8, p. e65923.
Fallgatter, C., and Paim, P.S.G., 2019, On the origin of the Itararé Group basal nonconformity and its implications for the Late Paleozoic glaciation in the Paraná Basin, Brazil: Palaeogeography, Palaeoclimatology, Palaeoecology, v. 531, p. 108225.
Fedorov, A., Beichel, R., Kalpathy-Cramer, J., Finet, J., Fillion-Robin, J.-C., Pujol, S., Bauer, C., Jennings, D., Fennessy, F., Sonka, M., Buatti, J., Aylward, S., Miller, J.V., Pieper, S., and Kikinis, R., 2012, 3D Slicer as an Image Computing Platform for the Quantitative Imaging Network: Magnetic Resonance Imaging, v. 30, p. 1323–1341.
Figueiredo, F.J., and Carvalho, B.C.M.C., 2004, A new actinopterygian fish from the Late Permian of the Parana Basin, southern Brazil: Arquivos Do Museu Nacional, v. 62, p. 531–547.
Figueiredo, F.J., and Gallo da Silva, V., 2006, Actinopterígios paleopterígios: morfologia e taxonomia, Paleontologia de vertebrados – grandes temas e contribuições científicas, p. 1–28.
Figueroa, R.T., and Machado, D.M. da C., 2017, Paleoictiofauna da Formação Pimenteira (Devoniano), Bacia do Parnaíba, Pi, Brasil: Revista Brasileira de Paleontologia, v. 19, p. 491–504.
Figueroa, R.T., and Gallo, V., 2017, New chondrichthyan fin spines from the Pedra de Fogo Formation, Brazil: Journal of South American Earth Sciences, v. 76, p. 389–396.
Figueroa, R.T., and Machado, D.M. da C., 2018, The Paleozoic ichthyofauna of the Amazonas and Parnaíba basins, Brazil: Journal of South American Earth Sciences, v. 82, p. 122–132.
Figueroa, R.T., and Andrews, J.V., 2022, Fitting fangs in a finite face: A novel fang accommodation strategy in a 280-million-year-old ray-finned fish: Journal of Anatomy, v. 242, p. 525–534.
Figueroa, R.T., Miguel, R., and Gallo, V., 2017, New sarcopterygians from the Carboniferous Poti Formation and from the Permian Rio do Rasto Formation, Brazil: Revista Brasileira de Paleontologia, v. 19, p. 401–406.
Figueroa, R.T., Friedman, M., and Gallo, V., 2019, Cranial anatomy of the predatory actinopterygian *Brazilichthys macrognathus* from the Permian (Cisuralian) Pedra de Fogo Formation, Parnaíba Basin, Brazil: Journal of Vertebrate Paleontology, v. 39, p. e1639722.

Figueroa, R.T., Weinschütz, L.C., and Friedman, M., 2021, The oldest Devonian circumpolar ray-finned fish? Biology Letters, v. 17, p. 20200766.
Figueroa, R.T., Weinschütz, L.C., Giles, S., and Friedman, M., 2024, Soft-tissue fossilization illuminates the stepwise evolution of the ray-finned fish brain: Current Biology,.
Figueroa, R.T., Goodvin, D., Kolmann, M.A., Coates, M.I., Caron, A.M., Friedman, M., and Giles, S., 2023, Exceptional fossil preservation and evolution of the ray-finned fish brain: Nature, v. 614, p. 486–491.
Fine, M.L., Horn, M.H.H., and Cox, B., 1987, *Acanthonus armatus* , a deep-sea teleost fish with a minute brain and large ears: Proceedings of the Royal Society of London. Series B. Biological Sciences, v. 230, p. 257–265.
Finger, T.E., 1988, Organization of Chemosensory Systems Within the Brains of Bony Fishes: Sensory Biology of Aquatic Animals, p. 339–363.
Finlay, B.L., and Darlington, R.B., 1995, Linked Regularities in the Development and Evolution of Mammalian Brains: Science, v. 268, p. 1578–1584.
Fischer, S., and Jungwirth, A., 2022, The costs and benefits of larger brains in fishes: Journal of Evolutionary Biology, v. 35, p. 973–985.
Folgueira, M., Bayley, P., Navratilova, P., Becker, T.S., Wilson, S.W., and Clarke, J.D., 2012, Morphogenesis underlying the development of the everted teleost telencephalon: Neural Development, v. 7, p. 212.
França, A.B., and Potter, P.E., 1991, Stratigraphy and Reservoir Potential of Glacial Deposits on the Itararé Group (Carboniferous-Permian), Paraná Basin, Brazil: The American Association of Petroleum Geologists Bulletin, v. 75, p. 62–85.
Frey, L., Coates, M.I., Tietjen, K., Rücklin, M., and Klug, C., 2020, A symmoriiform from the Late Devonian of Morocco demonstrates a derived jaw function in ancient chondrichthyans: Communications Biology, v. 3, p. 1–10.
Friedman, M., 2015, The early evolution of ray-finned fishes: Palaeontology, v. 58, p. 213–228.
Friedman, M., 2022, The Macroevolutionary History of Bony Fishes: A Paleontological View: Annual Review of Ecology, Evolution, and Systematics, v. 53, p. 353–377.
Friedman, M., and Blom, H., 2006, A new Actinopterygian from the Famennian of East Greenland and the interrelationships of Devonian ray-finned fishes: Journal of Paleontology, v. 80, p. 1186–1204.
Friedman, M., and Coates, M.I., 2006, A newly recognized fossil coelacanth highlights the early morphological diversification of the clade.: Proceedings. Biological Sciences / The Royal Society, v. 273, p. 245–250.
Friedman, M., and Sallan, L.C., 2012, Five hundred million years of extinction and recovery: a phanerozoic survey of large-scale diversity patterns in fishes: Palaeontology, v. 55, p. 707–742.
Friedman, M., and Giles, S., 2016, Actinopterygians: the ray-finned fishes—an explosion of diversity, *in* Clack, J.A., Fay, R.R., and Popper, A.N., eds., Evolution of the Vertebrate Ear : Evidence from the Fossil Record: Cham, Springer International Publishing, p. 17–49.
Friedman, M., Pierce, S.E., Coates, M., and Giles, S., 2018, Feeding structures in the ray-finned fish *Eurynotus crenatus* (Actinopterygii: Eurynotiformes): implications for trophic diversification among Carboniferous actinopterygians: Earth and Environmental Science Transactions of The Royal Society of Edinburgh, v. 109, p. 33–47.

Friedman, S.T., Collyer, M.L., Price, S.A., and Wainwright, P.C., 2022, Divergent Processes Drive Parallel Evolution in Marine and Freshwater Fishes: Systematic Biology, v. 71, p. 1319–1330.
Gardiner, B.G., 1962, *Namaichthys schroederi* Gurich and other Palaeozoic fishes from South Africa: Palaeontology, v. 5.
Gardiner, B.G., 1967, The significance of the preopercular in actinopterygian evolution: J. Linn. Soc. London, Zool., v. 47, p. 197–209.
Gardiner, B.G., 1984, The relationship of the palaeoniscid fishes, a review based on new specimens of *Mimia* and *Moythomasia* from the Upper Devonian of Western Australia: Bulletin of the British Museum of Natural History, v. 37, p. 173–428.
Gardiner, B.G., Schaeffer, B., and Masserie, J.A., 2005, A review of the lower actinopterygian phylogeny: Zoological Journal of the Linnean Society, v. 144, p. 511–525.
Gardiner, B.S., and Schaeffer, B., 1989, Interrelationships of lower actinopterygian fishes: Zoological Journal of the Linnean Society, v. 97, p. 135–187.
Garwood, R., and Dunlop, J., 2014, The walking dead: Blender as a tool for paleontologists with a case study on extinct arachnids: Journal of Paleontology, v. 88, p. 735–746.
Gebhardt, I.C., and Hofmann, M.H., 2023, The Diversity of the Brains of Ray-Finned Fishes: Brain Behavior and Evolution, p. 1.
Gerstner, C.L., 1999, Maneuverability of four species of coral-reef fish that differ in body and pectoral-fin morphology: Canadian Journal of Zoology, v. 77, p. 1102–1110.
Gess, R.W., 2016, Vertebrate Biostratigraphy of the Witteberg Group and the Devonian-Carboniferous Boundary in South Africa, *in* Linol, B. and de Wit, M.J., eds., Origin and Evolution of the Cape Mountains and Karoo Basin: Cham, Springer International Publishing, p. 131–140.
Gess, R.W., and Whitfield, A.K., 2020, Estuarine fish and tetrapod evolution: insights from a Late Devonian (Famennian) Gondwanan estuarine lake and a southern African Holocene equivalent: Biological Reviews, v. 95, p. 865–888.
Gignac, P.M., Kley, N.J., Clarke, J.A., Colbert, M.W., Morhardt, A.C., Cerio, D., Cost, I.N., Cox, P.G., Daza, J.D., Early, C.M., Echols, M.S., Henkelman, R.M., Herdina, A.N., Holliday, C.M., Li, Z., Mahlow, K., Merchant, S., Müller, J., Orsbon, C.P., Paluh, D.J., Thies, M.L., Tsai, H.P., and Witmer, L.M., 2016, Diffusible iodine-based contrast-enhanced computed tomography (diceCT): an emerging tool for rapid, high-resolution, 3-D imaging of metazoan soft tissues: Journal of Anatomy, v. 228, p. 889–909.
Giles, S., and Friedman, M., 2014, Virtual reconstruction of endocast anatomy in early ray-finned fishes (Osteichthyes, Actinopterygii): Journal of Paleontology, v. 88, p. 636–651.
Giles, S., Friedman, M., and Brazeau, M.D., 2015, Osteichthyan-like cranial conditions in an Early Devonian stem gnathostome: Nature, v. 520, p. 82–85.
Giles, S., Rogers, M., and Friedman, M., 2018, Bony labyrinth morphology in early neopterygian fishes (Actinopterygii: Neopterygii): Journal of Morphology, v. 279, p. 426–440.
Giles, S., Xu, G.H., Near, T.J., and Friedman, M., 2017, Early members of “living fossil” lineage imply later origin of modern ray-finned fishes: Nature, v. 549, p. 265–268.
Giles, S., Darras, L., Clément, G., Blieck, A., and Friedman, M., 2015, An exceptionally preserved Late Devonian actinopterygian provides a new model for primitive cranial anatomy in ray-finned fishes: Proceedings of the Royal Society B: Biological Sciences, v. 282.

Giles, S., Feilich, K., Warnock, R.C.M., Pierce, S.E., and Friedman, M., 2023, A Late Devonian actinopterygian suggests high lineage survivorship across the end-Devonian mass extinction: Nature Ecology & Evolution, v. 7, p. 10–19.

Giles, S., Coates, M.I., Garwood, R.J., Brazeau, M.D., Atwood, R., Johanson, Z., and Friedman, M., 2015, Endoskeletal structure in Cheirolepis (Osteichthyes, Actinopterygii), An early ray-finned fish: Palaeontology, v. 58, p. 849–870.

Gonda, A., Herczeg, G., and Merilä, J., 2013, Evolutionary ecology of intraspecific brain size variation: a review: Ecology and Evolution, v. 3, p. 2751–2764.

Grahn, Y., Mauller, P.M., Bergamaschi, S., and Bosetti, E.P., 2013, Palynology and sequence stratigraphy of three Devonian rock units in the Apucarana Sub-basin (Paraná Basin, south Brazil): Additional data and correlation: Review of Palaeobotany and Palynology, v. 198, p. 27–44.

Grahn, Y., Mendlowicz, P., Breuer, P., Bosetti, E., Bergamaschi, S., and Pereira, E., 2010, The Furnas/Ponta Grossa contact and the age of the lowermost Ponta Grossa Formation in the Apucarana Sub-Basin (Paraná Basin, Brazil): integrated palynological age determination: Revista Brasileira de Paleontologia, v. 13, p. 89–102.

Grande, L., and Bemis, W.E., 1998, A Comprehensive Phylogenetic Study of Amiid Fishes (Amiidae) Based on Comparative Skeletal Anatomy. An Empirical Search for Interconnected Patterns of Natural History: Journal of Vertebrate Paleontology, v. 18, p. 1–696.

Griffis, N.P., Montañez, I.P., Mundil, R., Richey, J., Isbell, J., Fedorchuk, N., Linol, B., Iannuzzi, R., Vesely, F., Mottin, T., da Rosa, E., Keller, B., and Yin, Q.-Z., 2019, Coupled stratigraphic and U-Pb zircon age constraints on the late Paleozoic icehouse-to-greenhouse turnover in south-central Gondwana: Geology, v. 47, p. 1146–1150.

Griffis, N.P., Montañez, I.P., Fedorchuk, N., Isbell, J., Mundil, R., Vesely, F., Weinshultz, L., Iannuzzi, R., Gulbranson, E., Taboada, A., Pagani, A., Sanborn, M.E., Huyskens, M., Wimpenny, J., Linol, B., and Yin, Q.Z., 2019, Isotopes to ice: Constraining provenance of glacial deposits and ice centers in west-central Gondwana: Palaeogeography, Palaeoclimatology, Palaeoecology, v. 531.

Hall, Z.J., and Tropepe, V., 2020, Using Teleost Fish to Discern Developmental Signatures of Evolutionary Adaptation From Phenotypic Plasticity in Brain Structure: Frontiers in Neuroanatomy,.

Hamel, M., 2005, A new lower actinopterygian from the Early Permian of the Paraná Basin , Brazil: Journal of Vertebrate Paleontology, v. 25, p. 19–26.

Hamel, M.-H., and Poplin, C., 2008, The braincase anatomy of *Lawrenciella schaefferi* , actinopterygian from the Upper Carboniferous of Kansas (USA): Journal of Vertebrate Paleontology, v. 28, p. 989–1006.

Healy, S.D., and Rowe, C., 2006, A critique of comparative studies of brain size: Proceedings of the Royal Society B: Biological Sciences, v. 274, p. 453–464.

Henderson, S., Dunne, E.M., and Giles, S., 2022, Sampling biases obscure the early diversification of the largest living vertebrate group: Proceedings of the Royal Society B: Biological Sciences, v. 289, p. 20220916.

Henderson, S., Dunne, E.M., Fasey, S.A., and Giles, S., 2022, The early diversification of ray-finned fishes (Actinopterygii): hypotheses, challenges and future prospects: Biological Reviews, p. 1–32.

Herzog, H., Klein, B., and Ziegler, A., 2017, Form and function of the teleost lateral line revealed using three-dimensional imaging and computational fluid dynamics: Journal of The Royal Society Interface, v. 14, p. 20160898.
Hibi, M., Matsuda, K., Takeuchi, M., Shimizu, T., and Murakami, Y., 2017, Evolutionary mechanisms that generate morphology and neural-circuit diversity of the cerebellum: Development, Growth & Differentiation, v. 59, p. 228–243.
Hilton, E.J., Grande, L., and Bemis, W.E., 2011, Skeletal Anatomy of the Shortnose Sturgeon, *Acipenser brevirostrum* Lesueur, 1818, and the Systematics of Sturgeons (Acipenseriformes, Acipenseridae): Fieldiana Life and Earth Sciences, v. 3, p. 1–168.
Hinsbergen, D.J.J. van, Groot, L.V. de, Schaik, S.J. van, Spakman, W., Bijl, P.K., Sluijs, A., Langereis, C.G., and Brinkhuis, H., 2015, A Paleolatitude Calculator for Paleoclimate Studies: PLOS ONE, v. 10, p. e0126946.
Hoffman, R.A., 1970, The Epiphyseal Complex in Fish and Reptiles: American Zoologist, v. 10, p. 191–199.
Holland, T., 2014, The endocranial anatomy of *Gogonasus andrewsae* Long, 1985 revealed through micro CT-scanning: Earth and Environmental Science Transactions of the Royal Society of Edinburgh, v. 105, p. 9–34.
Holz, M., França, A.B., Souza, P.A., Iannuzzi, R., and Rohn, R., 2010, A stratigraphic chart of the Late Carboniferous/Permian succession of the eastern border of the Paraná Basin, Brazil, South America: Journal of South American Earth Sciences, v. 29, p. 381–399.
Hong, H., Zhou, Y., Wu, H., Luo, Y., and Shen, H., 2014, Lipid Content and Fatty Acid Profile of Muscle, Brain and Eyes of Seven Freshwater Fish: a Comparative Study: Journal of the American Oil Chemists' Society, v. 91, p. 795–804.
Horodyski, R.S., Holz, M., Grahn, Y., and Bosetti, E.P., 2014, Remarks on sequence stratigraphy and taphonomy of the Malvinokaffric shelly fauna during the KAČÁK Event in the Apucarana Sub-basin (Paraná Basin), Brazil: International Journal of Earth Sciences, v. 103, p. 367–380.
van der Horst, C.J., 1925, The myelencephalic gland of *Polyodon*, *Acipenser* and *Amia*: Koninklijke Akademie van Wetenschappen Te Amsterdam Proceedings of the Section of Sciences, v. 28, p. 432–442.
Hough, E., 2004, Geology of the Burnley Area (SD82NW and SD83SW): British Geologic Survey, .
Howe, S., Bryant, K., Duff, A., and Astley, H., 2021, Testing the effects of body depth on fish maneuverability via robophysical models: Bioinspiration & Biomimetics, v. 17, p. 016002.
Hughes, L.C., Ortí, G., Huang, Y., Sun, Y., Baldwin, C.C., Thompson, A.W., Arcila, D., Betancur-R, R., Li, C., Becker, L., Bellora, N., Zhao, X., Li, X., Wang, M., Fang, C., Xie, B., Zhou, Z., Huang, H., Chen, S., Venkatesh, B., and Shi, Q., 2018, Comprehensive phylogeny of ray-finned fishes (Actinopterygii) based on transcriptomic and genomic data: Proceedings of the National Academy of Sciences of the United States of America, v. 115, p. 6249–6254.
Iglesias, T.L., Dornburg, A., Brandley, M.C., Alfaro, M.E., and Warren, D.L., 2015, Life in the unthinking depths: energetic constraints on encephalization in marine fishes: Journal of Evolutionary Biology, v. 28, p. 1080–1090.
Ikenaga, T., Shimomai, R., Hagio, H., Kimura, S., Matsumoto, K., Kato, D., Uesugi, K., Takeuchi, A., Yamamoto, N., and Hibi, M., 2022, Morphological analysis of the

cerebellum and its efferent system in a basal actinopterygian fish, *Polypterus senegalus*: Journal of Comparative Neurology, v. 530, p. 1231–1246.
Ishikawa, Y., Yamamoto, N., and Hagio, H., 2022, Development of Diencephalon, Optic Tectum, and Cerebellum, *in* Ishikawa, Y., Yamamoto, N., and Hagio, H., eds., Brain Development of Medaka Fish: A New Concept of Brain Morphogenesis in Vertebrates: Singapore, Springer Nature, p. 149–167.
Janvier, P., 1992, The Permian and Triassic vertebrates of Bolivia: Fo Siles y Facies de Bolivia. Revista, p. 389–391.
Janvier, P., 2007, The Devonian vertebrates of South America: Malvinokaffric fishes and Gondwana-Euramerica faunal interchange: 4th European Meeting on the Paleontology and Stratigraphy of Latin America. Cuadernos Del Museo Geominero, v. 8, p. 223–227.
Janvier, P., 2008, The brain in the early fossil jawless vertebrates: Evolutionary information from an empty nutshell: Brain Research Bulletin,.
Janvier, P., and Suárez-Riglos, M., 1986, The Silurian and Devonian vertebrates of Bolivia: Bulletin de l'Institut Francais d'études Andins, v. 15.
Janvier, P., and Melo, J., 1987, Late Devonian actinopterygian scales from the Upper Amazon Basin, northwestern Brazil: Anais Da Academia Brasileira de Ciências, v. 59, p. 213–218.
Janvier, P., and Villarroel, C., 2000, Devonian vertebrates from Colombia: Palaeontology, v. 43, p. 729–763.
Janvier, P., and Maisey, J., 2010, The Devonian vertebrates of South America and their biogeographical relationships: Morphology, Phylogeny and Paleobiogeography of Fossil Fishes, p. 431–459.
Jarvik, E., 1980, Basic Structure and Evolution of Vertebrates: Academic Press, 600 p.
Jerison, H.J., 1973, Evolution of the Brain and Intelligence: New York, NY, Academic Press, 493 p.
Jones, R.C., Hall, K., and Crow, K.D., 2023, Are vertebrates constrained to two sets of paired appendages? The morphology, development, and evolution of pre-pelvic claspers in the Holocephali: Journal of Morphology, v. 284, p. e21632.
Khan, W., Khan, M.I., Hussain, S., Masood, Z., Shadman, M., Baset, A., Rahman, A., Mohsin, M., and Alfarraj, S., 2021, Comparative analysis of brain in relation to the body length and weight of common carp (*Cyprinus carpio*) in captive (hatchery) and wild (river system) populations: Brazilian Journal of Biology, v. 82.
Kiecker, C., and Lumsden, A., 2005, Compartments and their boundaries in vertebrate brain development: Nature Reviews Neuroscience, v. 6, p. 553–564.
Klug, C., Pohle, A., Roth, R., Hoffmann, R., Wani, R., and Tajika, A., 2021, Preservation of nautilid soft parts inside and outside the conch interpreted as central nervous system, eyes, and renal concrements from the Lebanese Cenomanian: Swiss Journal of Palaeontology, v. 140, p. 15.
Knapp, A., Rangel-de Lázaro, G., Friedman, M., Johanson, Z., Evans, K.M., Giles, S., Beckett, H.T., and Goswami, A., 2023, How to tuna fish: constraint, convergence, and integration in the neurocranium of pelagiarian fishes: Evolution, v. 77, p. 1277–1288.
Kolm, N., Gonzalez-Voyer, A., Brelin, D., and Winberg, S., 2009, Evidence for small scale variation in the vertebrate brain: mating strategy and sex affect brain size and structure in wild brown trout (Salmo trutta): Journal of Evolutionary Biology, v. 22, p. 2524–2531.

Kolmann, M.A., Nagesan, R.S., Andrews, J.V., Borstein, S.R., Figueroa, R.T., Singer, R.A., Friedman, M., and López-Fernández, H., 2023, DiceCT for fishes: recommendations for pairing iodine contrast agents with μCT to visualize soft tissues in fishes: Journal of Fish Biology, v. n/a.

Kotrschal, K., and Palzenberger, M., 1992, Neuroecology of cyprinids: comparative, quantitative histology reveals diverse brain patterns, *in* Wieser, W., Schiemer, F., Goldschmidt, A., and Kotrschal, K., eds., Environmental Biology of European Cyprinids: Papers from the Workshop on 'The Environmental Biology of Cyprinids' Held at the University of Salzburg, Austria, in September 1989, Developments in environmental biology of fishes: Dordrecht, Springer Netherlands, p. 135–152.

Kotrschal, K., Van Staaden, M.J., and Huber, R., 1998, Fish Brains: Evolution and Environmental Relationships: Reviews in Fish Biology and Fisheries, v. 8, p. 373–408.

Kozol, R.A., Conith, A.J., Yuiska, A., Cree-Newman, A., Tolentino, B., Banesh, K., Paz, A., Lloyd, E., Kowalko, J.E., Keene, A.C., Albertson, C., and Duboue, E.R., 2023, A brain-wide analysis maps structural evolution to distinct anatomical module: eLife, v. 12, p. e80777.

Krebs, J.R., Clayton, N.S., Healy, S.D., Cristol, D.A., Pa^{TEL}, S.N., and Jolliffe, A.R., 1996, The ecology of the avian brain: food-storing memory and the hippocampus: Ibis, v. 138, p. 34–46.

Ksepka, D.T., Balanoff, A.M., Smith, N.A., Bever, G.S., Bhullar, B.-A.S., Bourdon, E., Braun, E.L., Burleigh, J.G., Clarke, J.A., Colbert, M.W., Corfield, J.R., Degrange, F.J., De Pietri, V.L., Early, C.M., Field, D.J., Gignac, P.M., Gold, M.E.L., Kimball, R.T., Kawabe, S., Lefebvre, L., Marugán-Lobón, J., Mongle, C.S., Morhardt, A., Norell, M.A., Ridgely, R.C., Rothman, R.S., Scofield, R.P., Tambussi, C.P., Torres, C.R., van Tuinen, M., Walsh, S.A., Watanabe, A., Witmer, L.M., Wright, A.K., Zanno, L.E., Jarvis, E.D., and Smaers, J.B., 2020, Tempo and Pattern of Avian Brain Size Evolution: Current Biology, v. 30, p. 2026-2036.e3.

Ladich, F., and Schulz-Mirbach, T., 2016, Diversity in fish auditory systems: One of the riddles of sensory biology: Frontiers in Ecology and Evolution, v. 4.

Larouche, O., Zelditch, M.L., and Cloutier, R., 2018, Modularity promotes morphological divergence in ray-finned fishes: Scientific Reports, v. 8, p. 1–6.

Latimer, A.E., and Giles, S., 2018, A giant dapediid from the Late Triassic of Switzerland and insights into neopterygian phylogeny: Royal Society Open Science, v. 5, p. 180497.

Lauder, G.V., and Drucker, E.G., 2004, Morphology and experimental hydrodynamics of fish fin control surfaces: IEEE Journal of Oceanic Engineering, v. 29, p. 556–571.

Leise, E.M., 1990, Modular construction of nervous systems: A basic principle of design for invertebrates and vertebrates: Brain Research Reviews, v. 15, p. 1–23.

Leonard, R.B., and Willis, W.D., 1979, The organization of the electromotor nucleus and extraocular motor nuclei in the stargazer (Astroscopus y-graecum): Journal of Comparative Neurology, v. 183, p. 397–413.

Lindgren, J., Kaddumi, H.F., and Polcyn, M.J., 2013, Soft tissue preservation in a fossil marine lizard with a bilobed tail fin: Nature Communications, v. 4, p. 2423.

Lindgren, J., Uvdal, P., Sjövall, P., Nilsson, D.E., Engdahl, A., Schultz, B.P., and Thiel, V., 2012, Molecular preservation of the pigment melanin in fossil melanosomes: Nature Communications, v. 3.

Lindsey, C.C., 1978, 1 - Form, Function, and Locomotory Habits in Fish, *in* Hoar, W.S. and Randall, D.J., eds., Fish Physiology, Locomotion, v. 7.: Academic Press, p. 1–100.
Liu, J., Steiner, M., Dunlop, J.A., and Shu, D., 2018, Microbial decay analysis challenges interpretation of putative organ systems in Cambrian fuxianhuiids: Proceedings of the Royal Society B: Biological Sciences, v. 285, p. 20180051.
Long, J.A., and Trinajstic, K., 2010, The Late Devonian Gogo Formation Lägerstatte of Western Australia: Exceptional Early Vertebrate Preservation and Diversity: Annual Review of Earth and Planetary Sciences, v. 38, p. 255–279.
Long, J.A., Choo, B., and Young, G.C., 2008, A new basal actinopterygian fish from the Middle Devonian Aztec Siltstone of Antarctica: Antarctic Science, v. 20, p. 393–412.
López, J.M., Perlado, J., Morona, R., Northcutt, R.G., and González, A., 2013, Neuroanatomical organization of the cholinergic system in the central nervous system of a basal actinopterygian fish, the senegal bichir Polypterus senegalus: Journal of Comparative Neurology, v. 521, p. 24–49.
Lu, J., Giles, S., Friedman, M., den Blaauwen, J.L., and Zhu, M., 2016, The oldest actinopterygian highlights the cryptic early history of the hyperdiverse ray-finned fishes: Current Biology, v. 26, p. 1602–1608.
Lund, R., 2000, The new Actinopterygian order Guildayichthyiformes from the Lower Carboniferous of Montana (USA): Geodiversitas, v. 22, p. 171–206.
Lund, R., and Poplin, C., 1997, The Rhadinichthyids (Paleoniscoid actinopterygians) from the Bear Gulch limestone of Montana (USA, lower carboniferous): Journal of Vertebrate Paleontology, v. 17, p. 466–486.
Ma, X., Hou, X., Edgecombe, G.D., and Strausfeld, N.J., 2012, Complex brain and optic lobes in an early Cambrian arthropod: Nature, v. 490, p. 258–261.
Ma, X., Edgecombe, G.D., Hou, X., Goral, T., and Strausfeld, N.J., 2015, Preservational Pathways of Corresponding Brains of a Cambrian Euarthropod: Current Biology, v. 25, p. 2969–2975.
Mähler, B., Janssen, K., Tahoun, M., Tomaschek, F., Schellhorn, R., Müller, C.E., Bierbaum, G., and Rust, J., 2022, Adipocere formation in biofilms as a first step in soft tissue preservation: Scientific Reports, v. 12, p. 10122.
Maisey, J.G., Borghi, L., and Carvalho, M.G.P.D., 2002, Lower Devonian Fish Remains from the Falkland Islands: Journal of Vertebrate Paleontology, v. 22, p. 708–711.
Malabarba, M.C., Abdala, F., Weiss, F.E., and Perez, P.A., 2003, New data on the Late Permian Vertebrate Fauna of Posto Queimado, Rio do Rasto Formation, Southern Brazil: Revista Brasileira De Paleontologia, v. 6, p. 49–54.
Malabarba, M.C.L., 1988, A new genus and species of stem group actinopteran fish from the Lower Permian of Santa Catarina State, Brazil: Zoological Journal of the Linnean Society, v. 94, p. 287–299.
Maldanis, L., Carvalho, M., Ramos Almeida, M., Freitas, F.I., De Andrade, J.A.F.G., Nunes, R.S., Rochitte, C.E., Poppi, R.J., Freitas, R.O., Rodrigues, F., Siljeström, S., Alves Lima, F., Galante, D., Carvalho, I.S., Perez, C.A., de Carvalho, M.R., Bettini, J., Fernandez, V., and Xavier-Neto, J., 2016, Heart fossilization is possible and informs the evolution of cardiac outflow tract in vertebrates: eLife, v. 5.
Mansuit, R., Clément, G., Herrel, A., Dutel, H., Tafforeau, P., Santin, M.D., and Herbin, M., 2021, Development and growth of the pelvic fin in the extant coelacanth Latimeria chalumnae: The Anatomical Record, v. 304, p. 541–558.

Martin, R.E., 1999, Taphonomy: A Process Approach: Cambridge, UK, Cambridge University Press, .
Maxwell, E.E., Romano, C., and Wu, F.-X., 2021, Regional disparity in the axial skeleton of Saurichthyidae and implications for axial regionalization in non-teleostean actinopterygians: Journal of Zoology, v. 315, p. 29–41.
McCoy, V.E., 2014, Concretions as Agents of Soft-Tissue Preservation: A Review: The Paleontological Society Papers, v. 20, p. 147–162.
Meek, J., and Nieuwenhuys, R., 1998, Holosteans and Teleosts, *in* Nieuwenhuys, R., ten Donkelaar, H.J., and Nicholson, C., eds., The Central Nervous System of Vertebrates: Volume 1 / Volume 2 / Volume 3: Berlin, Heidelberg, Springer, p. 759–937.
Meek, J., Yang, J.Y., Han, V.Z., and Bell, C.C., 2008, Morphological analysis of the mormyrid cerebellum using immunohistochemistry, with emphasis on the unusual neuronal organization of the valvula: Journal of Comparative Neurology, v. 510, p. 396–421.
Melo, J.H.G., and Loboziak, S., 2003, Devonian–Early Carboniferous miospore biostratigraphy of the Amazon Basin, Northern Brazil: Review of Palaeobotany and Palynology, v. 124, p. 131–202.
Melo, J.H.G. de, 1988, The Malvinokaffric Realm in the Devonian of Brazil: p. 669–703.
Mickle, K.E., 2012, Unraveling the systematics of palaeoniscoid fishes--Lower actinopterygians in need of a complete phylogenetic revision 476p.
Miller, E.C., and Román-Palacios, C., 2021, Evolutionary time best explains the latitudinal diversity gradient of living freshwater fish diversity: Global Ecology and Biogeography, v. 30, p. 749–763.
Mones, 1986, 1986, El contenido paleontologico de las formaciónes Carbónico-Pérmicas del Uruguay: Comunicaciónes Paleontológicas Del Museo de Historia Natural de Montevideo, v. 14, p. 205–216.
Moodie, R.L., 1915, A new fish brain from the coal measures of Kansas, with a review of other fossil brains: Journal of Comparative Neurology, v. 25, p. 135–181.
Morona, R., López, J.M., Northcutt, R.G., and González, A., 2013, Comparative analysis of the organization of the cholinergic system in the brains of two Holostean fishes, the Florida gar *Lepisosteus platyrhincus* and the bowfin *Amia calva*: Brain, Behavior and Evolution, v. 81, p. 109–142.
Mouro, L.D., Rakociński, M., Marynowski, L., Pisarzowska, A., Musabelliu, S., Zatoń, M., Carvalho, M.A., Fernandes, A.C.S., and Waichel, B.L., 2017, Benthic anoxia, intermittent photic zone euxinia and elevated productivity during deposition of the Lower Permian, post-glacial fossiliferous black shales of the Paraná Basin, Brazil: Global and Planetary Change, v. 158, p. 155–172.
Mouro, L.D., Liza Alves Forancelli Pacheco, M., Ricetti, J.H., Scomazzon, A.K., Horodyski, R.S., Fernandes, A.C., Carvalho, M.A., Weinschutz, L.C., Silva, M.S., Waichel, B.L., and Scherer, C.M., 2020, Lontras Shale (Paraná Basin, Brazil): Insightful analysis and commentaries on paleoenvironment and fossil preservation into a deglaciation pulse of the Late Paleozoic Ice Age: Palaeogeography, Palaeoclimatology, Palaeoecology, v. 555, p. 109850.
Moutinho, L.P., Nascimento, S., Scomazzon, A.K., and Lemos, V.B., 2016, Trilobites, scolecodonts and fish remains occurrence and the depositional paleoenvironment of the upper Monte Alegre and lower Itaituba formations, Lower – Middle Pennsylvanian of the Amazonas Basin, Brazil: Journal of South American Earth Sciences, v. 72, p. 76–94.

Moy-Thomas, J.A., 1933, Notes on the Development of the Chondrocranium of Polypterus Senegalus: Journal of Cell Science, v. s2-76, p. 209–229.
Mueller, T., 2022, The Everted Amygdala of Ray-Finned Fish: Zebrafish Makes a Case: Brain Behavior and Evolution, v. 97, p. 321–335.
Murakami, Y., and Sugahara, F., 2021, Evolutionary and Developmental Perspectives on the Origin and Diversification of the Vertebrate Cerebellum: Cerebellum as a CNS Hub, p. 3–24.
Murray, A. m., 2000, The Palaeozoic, Mesozoic and Early Cenozoic fishes of Africa: Fish and Fisheries, v. 1, p. 111–145.
Muscente, A.D., Vinnes, O., Sinha, S., Schiffbauer, J.D., Maxwell, E.E., Schweigert, G., and Martindale, R.C., 2023, What role does anoxia play in exceptional fossil preservation? Lessons from the taphonomy of the Posidonia Shale (Germany): Earth-Science Reviews, p. 104323.
Mutter, R.J., and Richter, M., 2007, Acanthodian remains from the Middle-Late Permian of Brazil: Geological Journal, v. 42, p. 213–224.
Naimark, E., Kalinina, M., Shokurov, A., Markov, A., Zaytseva, L., and Boeva, N., 2018, Mineral composition of host sediments influences the fossilization of soft tissues: Canadian Journal of Earth Sciences, v. 55, p. 1271–1283.
Near, T.J., and Thacker, C.E., 2024, Phylogenetic Classification of Living and Fossil Ray-Finned Fishes (Actinopterygii): Bulletin of the Peabody Museum of Natural History, v. 65, p. 3–302.
Near, T.J., Eytan, R.I., Dornburg, A., Kuhn, K.L., Moore, J.A., Davis, M.P., Wainwright, P.C., Friedman, M., and Smith, W.L., 2012, Resolution of ray-finned fish phylogeny and timing of diversification: Proceedings of the National Academy of Sciences, v. 109, p. 13698–13703.
Nelson, G.J., 1969, Gill arches and the phylogeny of fishes : with notes on the classification of vertebrates. Bulletin of the AMNH ; v. 141, article 4: .
Nelson, J.S., Grande, T.C., and Wilson, M.V.H., 2016, Fishes of the World: John Wiley & Sons, 1067 p.
Neubauer, S., 2014, Endocasts: possibilities and limitations for the interpretation of human brain evolution: Brain, Behavior and Evolution, v. 84, p. 117–134.
Nielsen, E., 1942, Studies on Triassic Fishes: Glaucolepis and Boreosomus. 1: Reitzel, .
Nielsen, E., 1949, Studies on Triassic Fishes from East Greenland II. *Australosomus* and *Birgeria*: Copenhagen, C.A. Reitzels Forlag, .
Nieuwenhuys, R., 1982, An overview of the organization of the brain of actinopterygian fishes: Integrative and Comparative Biology, v. 22, p. 287–310.
Nieuwenhuys, R., 2009, The forebrain of actinopterygians revisited: Brain, Behavior and Evolution, v. 73, p. 229–252.
Nieuwenhuys, R., 2011, The development and general morphology of the telencephalon of actinopterygian fishes: synopsis, documentation and commentary: Brain Structure and Function, v. 215, p. 141–157.
Nieuwenhuys, R., ten Donkelaar, H.J., and Nicholson, C., 1998, The Central Nervous System of Vertebrates: Berlin, Heidelberg, Springer Berlin Heidelberg, .
Northcutt, R.G., 2002, Understanding Vertebrate Brain Evolution: Integrative and Comparative Biology, v. 42, p. 743–756.

Northcutt, R.G., 2008, Forebrain evolution in bony fishes: Brain Research Bulletin, v. 75, p. 191–205.
Northcutt, R.G., and Wullimann, M.F., 1988, The Visual System in Teleost Fishes: Morphological Patterns and Trends, *in* Atema, J., Fay, R.R., Popper, A.N., and Tavolga, W.N., eds., Sensory Biology of Aquatic Animals: New York, NY, Springer, p. 515–552.
Northcutt, R.G., Neary, T.J., and Senn, D.G., 1978, Observations on the brain of the coelacanth *Latimeria chalumnae*: External anatomy and quantitative analysis: Journal of Morphology, v. 155, p. 181–192.
Ortega-Hernández, J., Lerosey-Aubril, R., and Pates, S., 2019, Proclivity of nervous system preservation in Cambrian Burgess Shale-type deposits: Proceedings of the Royal Society B: Biological Sciences, v. 286, p. 20192370.
Osés, G.L., Petri, S., Voltani, C.G., Prado, G.M.E.M., Galante, D., Rizzutto, M.A., Rudnitzki, I.D., Da Silva, E.P., Rodrigues, F., Rangel, E.C., Sucerquia, P.A., and Pacheco, M.L.A.F., 2017, Deciphering pyritization-kerogenization gradient for fish soft-tissue preservation: Scientific Reports, v. 7, p. 1–15.
Ota, K.G., and Kuratani, S., 2008, Developmental biology of hagfishes, with a report on newly obtained embryos of the Japanese inshore hagfish, Eptatretus burgeri: Zoological Science, v. 25, p. 999–1011.
Ota, K.G., Kuraku, S., and Kuratani, S., 2007, Hagfish embryology with reference to the evolution of the neural crest: Nature, v. 446, p. 672–675.
Over, D.J., 2007, Conodont biostratigraphy of the Chattanooga Shale, Middle and Upper Devonian, southern Appalachian basin, eastern United States: Journal of Paleontology, v. 81, p. 1194–1217.
Park, P.J., and Bell, M.A., 2010, Variation of telencephalon morphology of the threespine stickleback (Gasterosteus aculeatus) in relation to inferred ecology: Journal of Evolutionary Biology, v. 23, p. 1261–1277.
Parry, L.A., Smithwick, F., Nordén, K.K., Saitta, E.T., Lozano-Fernandez, J., Tanner, A.R., Caron, J.-B., Edgecombe, G.D., Briggs, D.E.G., and Vinther, J., 2018, Soft-Bodied Fossils Are Not Simply Rotten Carcasses – Toward a Holistic Understanding of Exceptional Fossil Preservation: BioEssays, v. 40, p. 1700167.
Patterson, C., 1975, The braincase of pholidophorid and leptolepid fishes, with a review of the actinopterygian braincase: Philosophical Transactions of the Royal Society of London, v. 269, p. 275–579.
Patterson, C., 1982, Morphology and interrelationships of primitive actinopterygian fishes: Integrative and Comparative Biology, v. 22, p. 241–259.
Pearson, D.M., and Westoll, T.S., 1979, The Devonian actinopterygian *Cheirolepis* Agassiz: Transactions of the Royal Society of Edinburgh, v. 70, p. 337–399.
Penn-Clarke, C.R., 2019, The Malvinokaffric Realm in the Early-Middle Devonian of South Africa: Journal of African Earth Sciences,.
Penn-Clarke, C.R., and Harper, D.A.T., 2023, The rise and fall of the Malvinoxhosan (Malvinokaffric) bioregion in South Africa: Evidence for Early-Middle Devonian biocrises at the South Pole: Earth-Science Reviews, v. 246, p. 104595.
Peters, J.W., Duclos, K.K., Wilson, M.V.H., and Grande, T.C., 2024, Morphological Diversity and Evolution of Jaw Morphologies in Zeiform Fishes (Teleostei, Paracanthopterygii): Integrative Organismal Biology, v. 6, p. obae011.

Piotrowski, T., and Northcutt, R.G., 1996, The cranial nerves of the senegal bichir, *Polypterus senegalus* [Osteichthyes: Actinopterygii: Cladistia] pp. 79—102: Brain, Behavior and Evolution, v. 47, p. 79–102.
Poplin, C.M., 1974, Etude de quelques paleoniscides pennsylvaniens du Kansas.: Cahiers de Paléontologie, Editions Du CNRS, Paris.,.
Poplin, C.M., and Véran, M., 1996, A revision of the actinopterygian fish *Coccocephalus wildi* from the Upper Carboniferous of Lancashire: Special Papers in Palaeontology, v. 52, p. 7–29.
Pradel, A., 2010, Skull and brain anatomy of Late Carboniferous Sibyrhynchidae (Chondrichthyes, Iniopterygia) from Kansas and Oklahoma (USA): Geodiversitas, v. 32, p. 595–661.
Pradel, A., Maisey, J., Tafforeau, P., and Janvier, P., 2009, An enigmatic gnathostome vertebrate skull from the Middle Devonian of Bolivia: Acta Zoologica, v. 90, p. 123–133.
Pradel, A., Maisey, J.G., Mapes, R.H., and Kruta, I., 2016, First evidence of an intercalar bone in the braincase of "palaeonisciform" actinopterygians, with a virtual reconstruction of a new braincase of *Lawrenciella* Poplin, 1984 from the Carboniferous of Oklahoma: Geodiversitas, v. 38, p. 489–504.
Pradel, A., Langer, M., Maisey, J.G., Geffard-Kuriyama, D., Cloetens, P., Janvier, P., and Tafforeau, P., 2009, Skull and brain of a 300-million-year-old chimaeroid fish revealed by synchrotron holotomography: Proceedings of the National Academy of Sciences of the United States of America, v. 106, p. 5224–5228.
Price, S.A., Friedman, S.T., Corn, K.A., Larouche, O., Brockelsby, K., Lee, A.J., Nagaraj, M., Bertrand, N.G., Danao, M., Coyne, M.C., Estrada, J.R., Friedman, R., Hoeft, E., Iwan, M., Gross, D., Kao, J.H., Landry, B., Linares, M.J., McGlinn, C., Nguyen, J.A., Proffitt, A.G., Rodriguez, S., Rupp, M.R., Shen, E.Y., Susman, V., Tovar, A.J., Vary, L.L.J., Zapfe, K.L., and Wainwright, P.C., 2022, FishShapes v1: Functionally relevant measurements of teleost shape and size on three dimensions: Ecology, v. 103, p. e3829.
R Core Team, 2024, R: A Language and Environment for Statistical Computing. R Foundation for Statistical Computing, Vienna, Austria. Available at https://www.r-project.org/. Accessed July 5, 2024.
Rabosky, D.L., Chang, J., Title, P.O., Cowman, P.F., Sallan, L., Friedman, M., Kaschner, K., Garilao, C., Near, T.J., Coll, M., and Alfaro, M.E., 2018, An inverse latitudinal gradient in speciation rate for marine fishes: Nature, v. 559, p. 392–395.
Rayner, D.H., 1952, On the cranial structure of an early palaeoniscid, *Kentuckia*, gen. nov: Transactions of the Royal Society of Edinburgh, v. 62, p. 53–83.
Redies, C., and Puelles, L., 2001, Modularity in vertebrate brain development and evolution: BioEssays, v. 23, p. 1100–1111.
Revell, L.J., 2012, phytools: an R package for phylogenetic comparative biology (and other things): Methods in Ecology and Evolution, v. 3, p. 217–223.
Revell, L.J., 2024, phytools 2.0: an updated R ecosystem for phylogenetic comparative methods (and other things): PeerJ, v. 12, p. e16505.
Rezende, J.M.P., Figueroa, R.T., Ponciano, L.C.M. de O., and Gallo, V., 2021, A new late devonian fish fauna from Northeastern Brazil: Historical Biology, v. 33, p. 3444–3453.
Richter, M., 2002, A ray-finned fish (Osteichthyes) from the Late Permian of the State of Santa Catarina (Paraná Basin), Southern Brazil: Revista Brasileira de Paleontologia, v. 2002, p. 56–61.

Richter, M., 2007, First record of Eugeneodontiformes (Chondrichthyes:Elasmobranchii) from the Paraná Basin, Late Permian of Brazil, Paleontologia: Cenario de Vida, p. 151–156.
Richter, M., and Breitkreuz, C., 1997, Permian fish remains from the Peine Formation of northern Chile: Modern Geology, v. 21, p. 171–184.
Richter, M., Neis, P.A., and Smith, M.M., 1999, Acanthodian and Actinopterygian fish remains from the Itaituba Formation, Late Carboniferous of the Amazon Basin, Brazil, with a note on acanthodian ganoin: Neues Jahrbuch Für Geologie Und Paläontologie - Monatshefte, p. 728–744.
Richter, M., Bosetti, E.P., and Horodyski, R.S., 2017, Early Devonian (Late Emsian) shark fin remains (Chondrichthyes) from the Paraná Basin, southern Brazil: Anais Da Academia Brasileira de Ciências, v. 89, p. 103–118.
Richter, M., Cisneros, JuanC., Kammerer, C.F., Pardo, J., Marsicano, C.A., Fröbisch, J., and Angielczyk, K.D., 2022, Deep-scaled fish (Osteichthyes: Actinopterygii) from the lower Permian (Cisuralian) lacustrine deposits of the Parnaíba Basin, NE Brazil: Journal of African Earth Sciences, v. 194, p. 104639.
Rizzato, P.P., and Bichuette, M.E., 2024, Gross morphology of the brain and some sense organs of subterranean pencil catfishes of the genus Ituglanis Costa and Bockmann, 1993 (Siluriformes, Trichomycteridae), with a discussion on sensory compensation versus preadaptation in subterranean fishes: Journal of Fish Biology, v. n/a, p. 1–15.
Rodrigues, J.E.C., Candeiro, C.R.A., and Canile, F.M., 2023, The Mesosauridae (Parareptilia, Mesosauria) of Paleozoic Africa and South America: Geodynamics and Paleobiogeographic Distribution: .
Rodríguez, E.M., Oksche, A., and Montecinos, H., 2001, Human subcommissural organ, with particular emphasis on its secretory activity during the fetal life: Microscopy Research and Technique, v. 52, p. 573–590.
Ronquist, F., Teslenko, M., van der Mark, P., Ayres, D.L., Darling, A., Höhna, S., Larget, B., Liu, L., Suchard, M.A., and Huelsenbeck, J.P., 2012, MrBayes 3.2: Efficient Bayesian Phylogenetic Inference and Model Choice Across a Large Model Space: Systematic Biology, v. 61, p. 539–542.
Rosa, E.L.M., Vesely, F.F., Isbell, J.L., Fedorchuk, N.D., and Souza, P.A., 2019, Constraining the timing, kinematics and cyclicity of Mississippian-early Pennsylvanian glaciations in the Paraná Basin, Brazil: Sedimentary Geology, p. #pagerange#.
Rossi, V., Unitt, R., McNamara, M., Zorzin, R., and Carnevale, G., 2022, Skin patterning and internal anatomy in a fossil moonfish from the Eocene Bolca Lagerstätte illuminate the ecology of ancient reef fish communities: Palaeontology, v. 65, p. e12600.
Rostirolla, S.P., Cândido, A.G., Vesely, F.F., and Freitas, R.C., 2007, Mapeamento Geológico da Folha de Ponta Grossa (1:100.000): Secretaria de Estado da Industria do Comércio e Assuntos do Mercosul, .
Rowe, T.B., Macrini, T.E., and Luo, Z.-X., 2011, Fossil evidence on origin of the mammalian brain: Science, v. 332, p. 955–957.
Rustamov, E.K., 2006, Organization of hypothalamic area of diencephalon in the sturgeons: Journal of Evolutionary Biochemistry and Physiology, v. 42, p. 342–353.
Saidel, W.M., 2013, Nucleus Rostrolateralis: An Expansion of the Epithalamus in Some Actinopterygii: The Anatomical Record, v. 296, p. 1594–1602.

Saidel, W.M., and Butler, A.B., 1997, An atypical diencephalic nucleus in actinopterygian fishes: Visual connections and sporadic phylogenetic distribution: Neuroscience Letters, v. 229, p. 13–16.
Saldanha, J.P., Del Mouro, L., Horodyski, R.S., do Nascimento Ritter, M., and Schmidt-Neto, H., 2022, Taphonomy and paleoecology of the Lontras Shale Lagerstätte: Detailing the warming peak of a Late Paleozoic Ice Age temperate fjord: Palaeogeography, Palaeoclimatology, Palaeoecology, p. 111326.
Saleh, F., Pittet, B., Perrillat, J.-P., and Lefebvre, B., 2018, Orbital control on exceptional fossil preservation: Geology, v. 47, p. 103–106.
Saleh, F., Clements, T., Perrier, V., Daley, A.C., and Antcliffe, J.B., 2023, Variations in preservation of exceptional fossils within concretions: Swiss Journal of Palaeontology, v. 142, p. 20.
Saleh, F., Pittet, B., Sansjofre, P., Guériau, P., Lalonde, S., Perrillat, J.-P., Vidal, M., Lucas, V., El Hariri, K., Kouraiss, K., and Lefebvre, B., 2020, Taphonomic pathway of exceptionally preserved fossils in the Lower Ordovician of Morocco: Geobios, v. 60, p. 99–115.
Sallan, L.C., 2012, Tetrapod-like axial regionalization in an early ray-finned fish: Proceedings of the Royal Society B: Biological Sciences, v. 279, p. 3264–3271.
Sallan, L.C., 2014, Major issues in the origins of ray-finned fish (Actinopterygii) biodiversity: Biological Reviews, v. 89, p. 950–971.
Sallan, L.C., and Coates, M.I., 2010, End-Devonian extinction and a bottleneck in the early evolution of modern jawed vertebrates: Proceedings of the National Academy of Sciences, v. 107, p. 10131–10135.
Sallan, L.C., and Friedman, M., 2011, Heads or tails: staged diversification in vertebrate evolutionary radiations: Proceedings of the Royal Society B: Biological Sciences, v. 279, p. 2025–2032.
Sanchez, T.M., Waisfeld, B., and Benedetto, J.L., 1991, Lithofacies, taphonomy, and brachiopod assemblages in the Silurian of western Argentina: A review of Malvinokaffric Realm communities: Journal of South American Earth Sciences, v. 4, p. 307–329.
Sansom, R.S., and Wills, M.A., 2013, Fossilization causes organisms to appear erroneously primitive by distorting evolutionary trees: Scientific Reports, v. 3, p. 2545.
Sansom, R.S., Gabbott, S.E., and Purnell, M.A., 2011, Decay of vertebrate characters in hagfish and lamprey (Cyclostomata) and the implications for the vertebrate fossil record: Proceedings of the Royal Society B: Biological Sciences, v. 278, p. 1150–1157.
Sansom, R.S., Gabbott, S.E., and Purnell, M.A., 2013, Atlas of vertebrate decay: a visual and taphonomic guide to fossil interpretation: Palaeontology, v. 56, p. 457–474.
Satterfield, D.R., Claverie, T., and Wainwright, P.C., 2023, Body shape and mode of propulsion do not constrain routine swimming in coral reef fishes: Functional Ecology, v. 37, p. 343–357.
Saveliev, A.S.K., Sergei V., 2019, Morphology and Ecomorphology of the Fish Brain: The Rhombencephalon of Actinopterygians, The Histology of Fishes: CRC Press.
Schaeffer, B., 1956, Evolution in the subholostean fishes: Evolution, v. 10, p. 201–212.
Schaeffer, B., 1971, The Braincase of the Holostean Fish *Macrepistius*, with Comments on Neurocranial Ossification in the Actinopterygii: American Museum Novitates, v. 2459, p. 1–34.

Schaeffer, B., and Dalquest, W.W., 1978, A Palaeonisciform Braincase from the Permian of Texas, With Comments on Cranial Fissures and the Posterior Myodome: American Museum Novitates, v. 2658, p. 1–15.
Schemiko, D.C.B., Vesely, F.F., and Rodrigues, M.C.N. de L., 2023, Late Paleozoic glacial to postglacial stratigraphic evolution of the Rio do Sul depocenter, Itararé and Guatá groups, Pennsylvanian-Cisuralian, southern Brazil: Brazilian Journal of Geology, v. 52.
Schmidt, M., 2020, Evolution of the hypothalamus and inferior lobe in ray-finned fishes: Brain, Behavior and Evolution, v. 95, p. 302–316.
Schneider, C.A., Rasband, W.S., and Eliceiri, K.W., 2012, NIH Image to ImageJ: 25 years of image analysis: Nature Methods, v. 9, p. 671–675.
Schultze, H.-P., 2016, Scales, Enamel, Cosmine, Ganoine, and Early Osteichthyans: Comptes Rendus Palevol, v. 15, p. 83–102.
Schultze, H.-P., and Cumbaa, S.L., 2001, Dialipina and the characters of basal actinopterygians, Major Events in Early Vertebrate Evolution: CRC Press.
Schumacher, E.L., and Carlson, B.A., 2022, Convergent mosaic brain evolution is associated with the evolution of novel electrosensory systems in teleost fishes: eLife, v. 11, p. e74159.
Scotese, C., 2020, PALEOMAP PaleoAtlas for GPlates – EarthByte: .
Sedorko, D., Netto, R.G., and Savrda, C.E., 2018, Ichnology applied to sequence stratigraphic analysis of Siluro-Devonian mud-dominated shelf deposits, Paraná Basin, Brazil: Journal of South American Earth Sciences, v. 83, p. 81–95.
Sedorko, D., Netto, R.G., Savrda, C.E., Assine, M.L., and Tognoli, F.M.W., 2017, Chronostratigraphy and environment of Furnas Formation by trace fossil analysis: Calibrating the lower Paleozoic Gondwana realm in the Paraná Basin (Brazil): Palaeogeography, Palaeoclimatology, Palaeoecology, v. 487, p. 307–320.
Segall, M., Cornette, R., Rasmussen, A.R., and Raxworthy, C.J., 2021, Inside the head of snakes: influence of size, phylogeny, and sensory ecology on endocranium morphology: Brain Structure and Function, v. 226, p. 2401–2415.
Shumway, C.A., 2008, Habitat Complexity, Brain, and Behavior: Brain Behavior and Evolution, v. 72, p. 123–134.
Silva, A.F., Santos, T.P., Xavier, P.L.A., Dani, N., Schultz, C.L., Remus, M.V.D., Philipp, R.P., Rocha, R.M., Franco, D.R., and da Silva, M.A.L., 2023, Constraining the duration of the southern Gondwana Irati-Whitehill Sea through cyclostratigraphy and its relation with deep-time astronomical solutions: Palaeogeography, Palaeoclimatology, Palaeoecology, v. 629, p. 111791.
Slater, T.S., McNamara, M.E., Orr, P.J., Foley, T.B., Ito, S., and Wakamatsu, K., 2020, Taphonomic experiments resolve controls on the preservation of melanosomes and keratinous tissues in feathers: Palaeontology, v. 63, p. 103–115.
Smeets, W.J.A.J., 1998, Cartilaginous Fishes, *in* Nieuwenhuys, R., ten Donkelaar, H.J., and Nicholson, C., eds., The Central Nervous System of Vertebrates: Volume 1 / Volume 2 / Volume 3: Berlin, Heidelberg, Springer, p. 551–654.
Stack, J., and Gottfried, M.D., 2021, A new, exceptionally well-preserved Permian actinopterygian fish from the Minnekahta Limestone of South Dakota, USA: Journal of Systematic Palaeontology, v. 19, p. 1271–1302.
Stensio, V.E.A., 1906, Uber zwei Coelacanthiden aus dem Oberdevon von Wildungen: .

Stensiö, E., 1963, The brain and the cranial nerves in fossil, lower craniate vertebrates: Skriflter Ulgitt Av Det Norske Videnskaps-Akademi, p. 1–120.
Strausfeld, N.J., Ma, X., and Edgecombe, G.D., 2016, Fossils and the evolution of the arthropod brain: Current Biology, v. 26, p. R989–R1000.
Striedter, G.F., and Northcutt, R.G., 2006, Head size constrains forebrain development and evolution in ray-finned fishes: Evolution & Development, v. 8, p. 215–222.
Striedter, G.F., and Northcutt, R.G., 2019, Synthesis: Patterns and Principles, *in* Striedter, G.F. and Northcutt, R.G., eds., Brains Through Time: A Natural History of Vertebrates: Oxford University Press, p. 0.
Sukhum, K.V., Freiler, M.K., Wang, R., and Carlson, B.A., 2016, The costs of a big brain: extreme encephalization results in higher energetic demand and reduced hypoxia tolerance in weakly electric African fishes: Proceedings of the Royal Society B: Biological Sciences, v. 283, p. 20162157.
Swartz, B.A., 2009, Devonian actinopterygian phylogeny and evolution based on a redescription of *Stegotrachelus finlayi*: Zoological Journal of the Linnean Society, v. 156, p. 750–784.
Taft, N.K., 2011, Functional implications of variation in pectoral fin ray morphology between fishes with different patterns of pectoral fin use: Journal of Morphology, v. 272, p. 1144–1152.
Taverne, L., 1996, Ostéologie et position systématique des Tarrasiiformes, actinoptérygiens (pisces) du Carbonifère de l'écosse et des États-Unis: Biol. Jb. Dodonea, v. 64, p. 138–159.
Thorsen, D.H., and Westneat, M.W., 2005, Diversity of pectoral fin structure and function in fishes with labriform propulsion: Journal of Morphology, v. 263, p. 133–150.
Tkocz, I., Bytzer, P., and Bierring, F., 1979, Preserved brains in medieval skulls: American Journal of Physical Anthropology, v. 51, p. 197–202.
Toledo, C.E.V., and Bertini, R.J., 2005, Occurrences of the fossil Dipnoiformes in Brazil and its stratigraphic and chronological distributions: Revista Brasileira de Paleontologia, v. 8, p. 47–56.
Traquair, R.H., 1879, On the Structure and Affinities of the Platysomidae: Geological Magazine, v. 6, p. 343–391.
Traquair, R.H., 1909, The Ganoid Fishes of the British Carboniferous Formations. Part I, No. 4. Palæoniscidæ. Pages 107–122; Plates XXIV–XXX: Monographs of the Palaeontographical Society, v. 63, p. 107–122.
Trewin, N.H., 1986, Palaeoecology and sedimentology of the Achanarras fish bed of the Middle Old Red Sandstone, Scotland: Earth and Environmental Science Transactions of The Royal Society of Edinburgh, v. 77, p. 21–46.
Trinajstic, K., Briggs, D.E.G., and Long, J.A., 2022, The Gogo Formation Lagerstätte: a view of Australia's first great barrier reef: Journal of the Geological Society, v. 179, p. jgs2021-105.
Trinajstic, K., Marshall, C., Long, J., and Bifield, K., 2007, Exceptional preservation of nerve and muscle tissues in Late Devonian placoderm fish and their evolutionary implications: Biology Letters, v. 3, p. 197–200.
Trinajstic, K., Sanchez, S., Dupret, V., Tafforeau, P., Long, J., Young, G., Senden, T., Boisvert, C., Power, N., and Ahlberg, P.E., 2013, Fossil Musculature of the Most Primitive Jawed Vertebrates: Science, v. 341, p. 160–164.

Trinajstic, K., Long, J.A., Sanchez, S., Boisvert, C.A., Snitting, D., Tafforeau, P., Dupret, V., Clement, A.M., Currie, P.D., Roelofs, B., Bevitt, J.J., Lee, M.S.Y., and Ahlberg, P.E., 2022, Exceptional preservation of organs in Devonian placoderms from the Gogo Lagerstätte: Science, v. 377, p. 1311–1314.

Tsuboi, M., 2021, Exceptionally Steep Brain-Body Evolutionary Allometry Underlies the Unique Encephalization of Osteoglossiformes: Brain, Behavior and Evolution, v. 96, p. 49–63.

Ubelaker, D.H., and Zarenko, K.M., 2011, Adipocere: What is known after over two centuries of research: Forensic Science International, v. 208, p. 167–172.

Ullmann, J.F.P., Cowin, G., Kurniawan, N.D., and Collin, S.P., 2010, A three-dimensional digital atlas of the zebrafish brain: NeuroImage, v. 51, p. 76–82.

Valdez Buso, V., Aquino, C.D., Paim, P.S.G., de Souza, P.A., Mori, A.L., Fallgatter, C., Milana, J.P., and Kneller, B., 2019, Late Palaeozoic glacial cycles and subcycles in western Gondwana: Correlation of surface and subsurface data of the Paraná Basin, Brazil: Palaeogeography, Palaeoclimatology, Palaeoecology, v. 531, p. 108435.

Vannier, J., Schoenemann, B., Gillot, T., Charbonnier, S., and Clarkson, E., 2016, Exceptional preservation of eye structure in arthropod visual predators from the Middle Jurassic: Nature Communications, v. 7, p. 10320.

Vega-Dias, C.S., Dias, E.V., and Richter, M., 2000, Actinopterygian remains from the Rio do Rasto Formation, Upper Permian of the Paraná Basin, Brazil: Acta Geologica Leopoldensia, v. XXIII, p. 21–31.

Véran, M., 1988, Les éléments accessoires de l'arc hyoidien des poissons teléostomes (Acanthodiens et Osteichthyens) fossiles et actuels: Mémoires du Muséum National d'Histoire Naturelle, v. 54, p. 13–98.

Vernier, P., 2017, The Brains of Teleost Fishes, *in* Kaas, J.H., ed., Evolution of Nervous Systems (Second Edition): Oxford, Academic Press, p. 59–75.

Vesely, F.F., Delgado, D., Spisila, A.L., and Brumatti, M., 2021, Divisão litoestratigráfica do Grupo Itararé no estado do Paraná: Boletim Paranaense de Geociências, v. 78.

Vialli, D.M., 1932, L'organo linfomieloide mielenceialico dei ganoidi: Italian Journal of Zoology, v. 3, p. 101–102.

Wainwright, P.C., Smith, W.L., Price, S.A., Tang, K.L., Sparks, J.S., Ferry, L.A., Kuhn, K.L., Eytan, R.I., and Near, T.J., 2012, The Evolution of Pharyngognathy: A Phylogenetic and Functional Appraisal of the Pharyngeal Jaw Key Innovation in Labroid Fishes and Beyond: Systematic Biology, v. 61, p. 1001–1027.

Wang, Z., Feng, K., Yang, F., Liang, Y., Yun, X., Tihelka, E., Bai, M., Cai, C., and Lei, M., 2022, Breathing colour into fossils: A tomographic system for reconstructing the soft tissue microstructure of amber inclusions: Optics and Lasers in Engineering, v. 148, p. 106775.

Warth, P., Hilton, E.J., Naumann, B., Olsson, L., and Konstantinidis, P., 2017, Development of the skull and pectoral girdle in Siberian sturgeon, Acipenser baerii, and Russian sturgeon, Acipenser gueldenstaedtii (Acipenseriformes: Acipenseridae): Journal of Morphology, v. 278, p. 418–442.

Watanabe, A., Balanoff, A.M., Gignac, P.M., Gold, M.E.L., and Norell, M.A., 2021, Novel neuroanatomical integration and scaling define avian brain shape evolution and development: eLife, v. 10, p. e68809.

Watanabe, A., Gignac, P.M., Balanoff, A.M., Green, T.L., Kley, N.J., and Norell, M.A., 2019, Are endocasts good proxies for brain size and shape in archosaurs throughout ontogeny? Journal of Anatomy, v. 234, p. 291–305.
Watanabe, A., Fabre, A.C., Felice, R.N., Maisano, J.A., Müller, J., Herrel, A., and Goswami, A., 2019, Ecomorphological diversification in squamates from conserved pattern of cranial integration: Proceedings of the National Academy of Sciences of the United States of America, v. 116, p. 14688–14697.
Waters, C.N., Somerville, I.D., Jones, N.S., Cleal, C.J., Collinson, J.D., Waters, R.A., Besly, B.M., Dean, M.T., Stephenson, M.H., Davies, J.R., Freshney, E.C., Jackson, D.I., Mitchell, W.I., Powell, J.H., Barclay, W.J., Browne, M.A.E., Leveridge, B.E., Long, S.L., and McLean, D., 2011, A Revised Correlation of Carboniferous Rocks in the British Isles: Geological Society of London, .
Watson, D.M.S., 1925, The structure of certain palaeoniscids and the relationships of that group with other bony fish: Proceedings of the Zoological Society of London, v. 95, p. 815–870.
Watson, D.M.S., 1928, On some Points in the Structure of Palæoniscid and allied Fish.: Proceedings of the Zoological Society of London, v. 98, p. 49–70.
Weiger, T., Lametschwandtner, A., Kotrschal, K., and Krautgartner, W.-D., 1988, Vascularization of the telencephalic choroid plexus of a ganoid fish [Acipenser ruthenus (L.)]: American Journal of Anatomy, v. 182, p. 33–41.
Wen-Jin, Z., and Min, Z., 2007, Diversification and faunal shift of Siluro-Devonian vertebrates of China: Geological Journal, v. 42, p. 351–369.
White, E.G., 1936, A classification and phylogeny of the elasmobranch fishes: American Museum Novitates, v. 837, p. 1–16.
White, E.I., 1939, A new type of palaeoniscoid fish, with remarks on the evolution of the actinopterygian pectoral fins: Proceedings of the Zoological Society of London, v. B109, p. 41–61.
Wilner, E., Lemos, V.B., and Scomazzon, A.K., 2016, Associações naturais de conodontes Mesogondolella spp., Grupo Itararé, Cisuraliano da Bacia do Paraná: Gaea - Journal of Geoscience, v. 9, p. 30–36.
Wilson, C.D., Pardo, J.D., and Anderson, J.S., 2018, A primitive actinopterygian braincase from the tournaisian of Nova Scotia: Royal Society Open Science, v. 5.
Woodward, A.S., 1910, On some Permo-Carboniferous fishes from Madagascar: Annals and Magazine of Natural History, v. 5, p. 1–6.
Wright, A.M., and Hillis, D.M., 2014, Bayesian Analysis Using a Simple Likelihood Model Outperforms Parsimony for Estimation of Phylogeny from Discrete Morphological Data: PLoS ONE, v. 9, p. e109210.
Wullimann, M.F., Rupp, B., Reichert, H., and Verlag, B., 1996, Neuroanatomy of the Zebrafish Brain: A Topological Atlas.: .
Young, G.C., and Moody, J.M., 2003, A Middle–Late Devonian fish fauna from the sierra de Perija, western Venezuela, South America: Mitteilungen Aus Dem Museum Für Naturkunde in Berlin, v. Geowissens, p. 155–206.
Zhu, M., and Yu, X., 2009, Stem sarcopterygians have primitive polybasal fin articulation: Biology Letters, v. 5, p. 372–375.

Zhu, M., Wang, W., and Yu, X., 2010, Meemannia eos, a basal sarcopterygian fish from the Lower Devonian of China –expanded description and significance, Morphology, Phylogeny and Paleobiogeography of Fossil Fishes, p. 199–214.
Zhu, M., Yu, X., Choo, B., Wang, J., and Jia, L., 2012, An antiarch placoderm shows that pelvic girdles arose at the root of jawed vertebrates: Biology Letters, v. 8, p. 453–456.
Zhu, M., Zhao, W., Jia, L., Lu, J., Qiao, T., and Qu, Q., 2009, The oldest articulated osteichthyan reveals mosaic gnathostome characters: Nature, v. 458, p. 469–474.
Zhu, M., Yu, X., Choo, B., Qu, Q., Jia, L., Zhao, W., Qiao, T., and Lu, J., 2012, Fossil Fishes from China Provide First Evidence of Dermal Pelvic Girdles in Osteichthyans: PLOS ONE, v. 7, p. e35103.
Zhu, M., Yu, X., Ahlberg, P.E., Choo, B., Lu, J., Qiao, T., Qu, Q., Zhao, W., Jia, L., Blom, H., and Zhu, Y., 2013, A Silurian placoderm with osteichthyan-like marginal jaw bones: Nature, v. 502, p. 1–7.
Zhu, Y., Giles, S., Young, G.C., Hu, Y., Bazzi, M., Ahlberg, P.E., Zhu, M., and Lu, J., 2021, Endocast and Bony Labyrinth of a Devonian “Placoderm” Challenges Stem Gnathostome Phylogeny: Current Biology, v. 31, p. 1112-1118.e4.